

Copyright
by
Rammohan Narayanaswamy
2008

**The Dissertation Committee for Rammohan Narayanaswamy Certifies that this is
the approved version of the following dissertation:**

Genome-wide analyses of single cell phenotypes using cell microarrays

Committee:

Andrew D. Ellington, Supervisor

Edward M. Marcotte, or Co-Supervisor

Vishwanath R. Iyer

Arlen W. Johnson

Scott W. Stevens

Genome-wide analyses of single cell phenotypes using cell microarrays

by

Rammohan Narayanaswamy, B.S.; M.S.

Dissertation

Presented to the Faculty of the Graduate School of

The University of Texas at Austin

in Partial Fulfillment

of the Requirements

for the Degree of

Doctor of Philosophy

The University of Texas at Austin

May 2008

Dedication

To my mother, father and wife.

Acknowledgements

I am deeply indebted to the guidance of my advisors Andy Ellington and Edward Marcotte for making my experience in graduate school intellectually rewarding and instilling in me much deeper qualities that I am certain will serve me well in life. After rotating in both the Marcotte and the Ellington labs, my interest in technology development with an aspiration to explore systems level biology led me to become a student jointly advised by both Dr. Marcotte and Dr. Ellington. I am thankful to both of them for having thought me capable of undertaking challenging projects along the way and presenting me with exciting opportunities to enrich my scientific thinking and ability to conduct research. Dr. Ellington and Dr. Marcotte have been role models for me and continue to inspire, challenge and shape my scientific outlook.

I must say that Dr. Ellington's and Dr. Marcotte's enthusiastic personality traits mirrored the lab members of both labs (something I can proudly lay claim to now) and no amount of acknowledgement would ever suffice to describe all the memorable experiences I have had with them. Considering that Dr. Ellington's lab has in excess of 40 students at any point in time, the degree of cohesiveness, tolerance and understanding that I have witnessed there is a testament to all the lab members and Dr. Ellington himself. During the time I have spent in both the labs, I have had the pleasure of making friends and colleagues for life. I have spent endless periods of scientific brain storming with many of them but also at the same time have indulged in other forms of banter. I

would especially like to thank Dr. Matt Levy who has mentored me about the way experiments need to be conducted by systematically breaking them down. He has been instrumental in many of the ideas that I have based my experiments upon and I have always looked up to his opinions. My friends, Amos Yan, Angel Syrett, Gwen Stovall and others have always been there to lift up my spirits by engaging me and keeping me well fed - a no mean task. My buddies Randy Hughes, Brad Hall, Eric Davidson, Tony Hwang and Aaron Chevalier have also helped keep me stimulated and focused during my stay and I hope that our paths cross often. Yeah, buddy!

I would also like to thank members of the Marcotte lab including Zack Simpson, Insuk Lee, Traver Hart, Kris McGary, Emily Moradi, John Prince, Dan Boutz, Zhihua Li, Wei Niu and Mark Tsechansky for all the help and advice they have given me. Indeed, being a part of the cell chip team has been a privilege, with the many things I have learnt from being associated with them. It would be fair to say that without the help of my friends and colleagues in both the labs, my accomplishments and stay would not have been as rewarding and fun. Finally, I would like to thank our tireless administrators, Alisha Hall, David Parr, Sarah Caton and Hanna Kim who had helped me with admin-related and computer-related issues.

Lastly, I would like to thank both my mom and my dad for encouraging me all the way and giving me the confidence to trust in my abilities. I can attribute a large part of my desire and will to persist with my graduate studies to them and am thankful for their remarkable patience and ability to counsel me during times of need. While my parents were an important part of my graduate career, it has been my wife who over the past two years has patiently stood by me and kept me in a positive and enthusiastic frame of mind. It is in her company and care that I have managed to finally come to the finish line.

Genome-wide analyses of single cell phenotypes using cell microarrays

Publication No. _____

Rammohan Narayanaswamy, Ph. D.

The University of Texas at Austin, 2008

Supervisors: Andrew D. Ellington & Edward M. Marcotte

The past few decades have witnessed a revolution in recombinant DNA and nucleic acid sequencing technologies. Recently however, technologies capable of massively high-throughout, genome-wide data collection, combined with computational and statistical tools for data mining, integration and modeling have enabled the construction of predictive networks that capture cellular regulatory states, paving the way for 'Systems biology'. Consequently, protein interactions can be captured in the context of a cellular interaction network and emergent 'system' properties arrived at, that may not have been possible by conventional biology.

The ability to generate data from multiple, non-redundant experimental sources is one of the important facets to systems biology. Towards this end, we have established a novel platform called 'spotted cell microarrays' for conducting image-based genetic screens. We have subsequently used spotted cell microarrays for studying multi-dimensional phenotypes in yeast under different regulatory states. In particular, we studied the response to mating pheromone using a cell microarray comprised of the yeast

non-essential deletion library and analyzed morphology changes to identify novel genes that were involved in mating. An important aspect of the mating response pathway is large-scale spatiotemporal changes to the proteome, an aspect of proteomics, still largely obscure. In our next study, we used an imaging screen and a computational approach to predict and validate the complement of proteins that polarize and change localization towards the mating projection tip. By adopting such hybrid approaches, we have been able to, not only study proteins involved in specific pathways, but also their behavior in a systemic context, leading to a broader comprehension of cell function.

Lastly, we have performed a novel metabolic starvation-based screen using the GFP-tagged collection to study proteome dynamics in response to nutrient limitation and are currently in the process of rationalizing our observations through follow-up experiments. We believe this study to have implications in evolutionarily conserved cellular mechanisms such as protein turnover, quiescence and aging. Our technique has therefore been applied towards addressing several interesting aspects of yeast cellular physiology and behavior and is now being extended to mammalian cells.

Table of Contents

List of Tables	xiii
List of figures	xiv
Chapter 1: Introduction	1
Technology drivers in functional genomics.....	2
DNA microarrays.....	3
Proteomics.....	5
Techniques for performing high content phenotype screens & applications	8
High throughput phenomics.....	8
Protein microarrays	8
Transfected cell microarrays.....	9
Imaging considerations – optics, image analysis and storage.....	10
Baker’s yeast – functional genomics’ favorite hunting ground?	11
Analysis of gene function – A change in approach necessitated?	12
A probabilistic view of gene function.....	13
A Network approach to studying genetic interactions	14
Towards characterizing the spatiotemporal dynamics of a cell- Size & Morphology.....	18
Major determinants of cell size.....	18
Yeast morphology for characterizing gene function.....	20
Towards characterizing the spatiotemporal dynamics of a cell- Localization & Spatial dynamics	23
Experimental approaches for gene tagging.....	23
Correlation between protein localization and protein function.....	25
Methods for protein localization prediction.....	26
Yeast polarization states – A powerful model system for the study of spatio-temporal control	28
General mechanisms of generation of cell polarity	30
Establishment of an axis of polarity.....	31

Role of the cytoskeleton in polarity	33
Mechanisms of transport of polarized cargo.....	34
Polarized cell growth during the mating response	36
Pheromone sensing and signal transduction	36
Budding and Mating – A sharing of the polarization machinery?	38
Specific aims	39
References	40
Chapter 2: Systematic profiling of cellular phenotypes with spotted cell microarrays reveals new mating-pheromone response genes.	46
Introduction.....	46
Results.....	48
A high-throughput screen of yeast cellular morphology	48
Independent validation of mating-pheromone response genes	52
Comparison with known pathway implicates new genes in pheromone response and shmoo formation	55
Discussion	58
Conclusion	60
Materials and methods	62
Cell microarray construction and imaging.....	62
High-throughput screen for strains unresponsive to alpha factor	63
Assay of alpha-factor-induced growth arrest.....	63
Detailed experimental protocols, Controls & Evaluation of Cell Microarrays	64
Yeast deletion strains and growth conditions	64
Slide preparation	64
Printing of cell microarrays	66
Imaging of cell microarrays	67
Image annotation database.....	68
Scoring cellular morphology phenotypes	70
Analysis of morphology mutants	72
Screening for genes affecting the mating pheromone response pathway	72
Manual scoring of shmoo defects	74

Yeast growth curves +/- alpha factor	76
False positives due to presence of diploids and MAT apha strains	77
Polymerase chain reaction (PCR) validation of deleted strains	77
Deletion strain response phenotype correlate poorly with mRNA expression changes	79
References	80
Chapter 3: Systematic definition of protein constituents along the major polarization axis reveals an adaptive re-use of the polarization machinery in pheromone treated budding yeast	92
Introduction	92
Results	94
I. Organellar movement during pheromone-induced polarized growth	94
II. Identification of specific proteins and pathways contributing to polarized growth	98
a. Identifying pheromone-induced changes in protein localization using cell microarrays	98
b. Computational identification and confirmation of additional shmoo-localized proteins	102
III. Adaptive re-use of polarization machinery	104
IV. Proteins unique to the bud or shmoo tip	110
Materials and Methods	115
Manual follow-up of shmoo-tip localized proteins	116
Image Analysis	117
Classifier construction:	118
References	119
Chapter 4: Extensive formation of punctate foci by metabolic proteins under nutrient depleted conditions in budding yeast	123
Introduction	123
Stationary phase in budding yeast – salient features	124
Signaling pathways regulating stationary phase biology	126
Important cellular mechanisms operating in stationary phase	127
Mechanisms for Stationary phase survival	127
Stationary phase – A poised state for cell cycle re-entry?	128

Yeast stationary phase as a model to study aging.....	129
Evolution of asymmetry as a means of damage segregation? ..	131
Results and discussion	134
Stationary phase imaging screen.....	134
Reversibility of the punctate phenotype	138
Biochemical enrichment of Gln1-GFP punctates	139
Analysis of formation of punctates by mass spectrometry-based shotgun proteomics.....	142
Analysis of nutrient specificities towards induction and dissolution of punctates	148
Conditions for induction	148
Conditions for dissolution.....	151
Conclusions, models and future directions	153
Protein re-cycling by autophagy	154
A protein storage mechanism for keeping cells in a poised state	156
Aggregation due to compromised protein-quality-control	156
Materials and methods	158
Media, deletions, GFP tagging and imaging.....	158
Biochemical fractionation, sample preparation and mass spectrometry	159
References	159
References.....	163
Vita	180

List of Tables

Table 1-1: Examples of public repositories of yeast datasets & gene function.....	12
Figure 2-7: A custom built DNA microarray printing robot.....	67
Table 3-1: Manually verified shmoo tip localized genes identified by the cell chip.....	100
Table 3-2: Manually verified shmoo tip localized proteins identified by the classifier.	103

List of figures

- Figure 1-1: Genomic editing by a Zinc finger transcription factor- nuclease (ZFN).**
A mutated GFP gene, with an inserted in-frame stop codon and recognition sites for zinc finger nuclease is integrated as a single copy into the genome of a cell (top line). The cell is transfected with a plasmid with a nonfunctional GFP gene (tGFP) and expression plasmids for ZFN. The integrated GFP is repaired by gene targeting, and the cell becomes GFP positive. 4
- Figure 1-2: ‘Counting’ peptides in label-free quantitative proteomics.** In SAGE, a short sequence tag is sufficient to identify a transcript, quantification of which depends on the number of times a tag is observed. In proteomics, a short proteotypic peptide is sufficient to identify a protein and redundant peptide counting affords quantification. 7
- Figure 1-3: Transfected cell microarrays.** Cells are grown as a monolayer on a slide containing spots of DNA, siRNA or other molecules along with transfection reagent. Cells in the vicinity of the spot containing a GFP plasmid turn green. 9
- Figure 1-4: Predicting consensus protein function using networks containing pre-calculated functional linkage information.** With Prp43 as an example, we show its lesser known role in rRNA processing and ribosome biogenesis using different function prediction algorithms. 16
- Figure 1-5: Inter-relationship of yeast cell size with major cellular pathways.** 19
- Figure 1-6: Major MAPK signal transduction pathways in yeast.** Every pathway is associated with a distinct morphological adaptation showing the importance of morphology is cellular physiology. 21
- Figure 1-7: Split protein complementation strategy.** A tool for determining in vivo protein-protein interaction and localization by imposing a selection based on survival. 24
- Figure 1-8: A schematic of steps involved in predicting protein localization using a Bayesian classifier.** An initial prior probability is calculated for a protein of interest. Based on the properties of the protein, a posterior probability for its localization to a particular cellular compartment is arrived at. 27
- Figure 1-9: The three major polarization states in budding yeast.** 29
- Figure 1-10: Signaling events during polarized growth in budding yeast.** After budding cues are sensed, an axis of polarity is established with the activation of Cdc42-GTP. Subsequently, a polarized actin cytoskeleton is assembled culminating in successful polarized growth. 32
- Figure 1-11: A schematic of the transport of secretory vesicles along actin cables.** Actin filaments are stabilized by tropomyosin and cross-linked by fimbrin to generate cables. Myo2p and other myosin motors may move along them and deliver cargo to actin patches that are sites of plasma membrane invaginations. 35
- Figure 1-12: Model for the establishment of pheromone-induced polarized growth.** Binding of pheromone to its receptor triggers a mitogen-activated protein kinase pathway that culminates in the transcriptional activation of several genes, cell cycle arrest and mating projection formation at the site of highest pheromone

concentration. The C-terminal domain of the receptor may be involved in coupling the polarization machinery with the pheromone signaling proteins (black)..... 37

Figure 1-13: Shared signaling proteins in budding and pheromone induced 'shmooing'. Cdc42p-GTP is a shared effector in both pheromone response and budding as indicated by the same downstream machinery involved in both processes. 39

Figure 2-1 An overview of spotted cell microarrays. (a) Cell chips are constructed using slotted steel pins to print cells robotically from 96-well plates onto poly-L-lysine or Con A/Mn²⁺/Ca²⁺-coated glass slides. The sample image shows arrayed yeast cells immunostained for tubulin using fluorescein isothiocyanate (FITC)-conjugated-goat anti-rat IgG/rat anti- α -tubulin (red), overlaid on a bright field image and a DAPI-stained image (blue) of the cells' nuclei. FISH, fluorescence in situ hybridization. (b) Wide-field light scattering image of a cell microarray (approximately 2 cm \times 6 cm) containing around 4,800 viable, haploid yeast deletion strains. The bright dots arise from light scattered when scanning the array with a Genepix DNA microarray scanner. Spots are around 200 μ m in diameter, separated by 410 μ m. (c) Close-up of a typical spot from the microarray showing distinct cells at 40 \times magnification. This image was taken immediately after printing, so growth medium (YPD, 17% glycerol, 200 mg/l G418) is still visible..... 47

Figure 2-2: Characteristic yeast cell phenotypes observed on arrays. DIC images from cell chips were collected automatically at 60 \times magnification with DAPI-stained nuclei superimposed in blue pseudocolor. Each gene name indicates the corresponding deletion strain (for example, *dse2* Δ KanMX4). (a) Six phenotypic classes observed among the haploid yeast deletion strains. YIL141W overlaps the AXL2 gene, whose disruption in the deletion strain probably provides the observed morphology. (b) Changes in cell morphology observed after treating the deletion collection with mating pheromone. Many mutants, such as the *mrps5* Δ KanMX4 deletion strain (left), form 'wild-type'-like mating projections upon adding alpha factor, while cells lacking STE7 (middle) fail to form mating projections, and cells lacking KEL1 (right) form mating projections of unusual morphology..... 50

Figure 2-3: Results of a cell microarray-based genome-wide screen for genes participating in the mating-pheromone response pathway. Strains defective in the pathway fail to arrest growth when treated with alpha factor, unlike wild-type cells. The histograms report the average results of two or three replicate growth assays for (a) 28 strains containing deletions of genes known to participate in pheromone response, (b) 38 strains identified from cell microarrays as failing to shmoo properly, (c) 178 strains forming typical shmoos, and (d) 91 strains forming shmoos with a notably enhanced frequency in the cell population. The true-positive alpha factor-response pathway mutants (ASD, arrest+shmoo defective) are well separated from non-pathway mutants. Additional mutant categories identified were those defective only in the shmoo pathway (SD, shmoo defective), and those defective only in the growth arrest pathway (AD, arrest defective). Gene names indicate strains deleted for the corresponding genes. 54

Figure 2-4: Summary of cell-chip/growth assay results. With two phenotypic screens, we expected three classes of mutants: true-positive alpha factor-response pathway

mutants (ASD), those defective only in the shmoo pathway (SD), and those defective only in the growth arrest (AD). (a) The number of genes identified in each category; (b) their interpretation. Only 413 strains were tested by growth assay, so the number of strains with wild-type phenotypes (WT) is omitted.	55
Figure 2-5: Comparison of results with the known response pathway. This comparison reveals that of the 18 known genes expected to be found in this screen, 15 were recovered (red labels); three core genes were missed (gray labels). Thirteen genes are pathway inhibitors (blue labels) whose corresponding deletion strains shmoo. Ten known pathway genes are absent from the deletion collection (green labels). Of the 15 putative additional genes found, nine (black labels, boxed) could be associated with the core pathway via protein interactions or mRNA coexpression with intermediates (pink labels, boxed). Four network-implicated intermediates (orange labels, boxed) were also found in the initial cell-chip screen, though not reconfirmed. Bold arrows mark the canonical signal transduction cascade leading to transcriptional changes. Thin black arrows indicate activation; barred lines indicate inhibition; dotted lines indicate functional genomics linkages [56]. Genes with asterisks are also implicated in filamentous growth [114]......	56
Figure 2-6: Yeast cell adherence to ConA-coated cell microarray slide surface as function of Ca/Mn concentration. Cells were spotted, then washed to test adherence.	65
Figure 2-8: Screenshot of a Cellma annotation database page. Morphology phenotypes for each gene are assigned using a structured annotation scheme. Phenotypes are classified according to their severity and penetrance and are specific for a given strain in a given microarray experiment.	69
Figure 2-9: Recall/ Precision of manual grading of morphology mutant/ wild type control chip. The blue arrow represents the threshold chosen for selection of morphology mutants in the full cell chip screen.	71
Figure 2-10: Pheromone concentration and time dependence on shmooing.	73
Figure 2-11: Grader agreement on shmoo phenotypes.	75
Figure 2-12: PCR validation of the identity of the gene deleted in 42 deletion strains. 38 strains were confirmed to have the correct deletion.	78
Figure 2-13: Comparison between cell chip identified pheromone responsive genes with mRNA expression. Both the Core (closed circles) and non-core (open circles) subsets identified by the cell chip did not show significant correlation with change in expression as measured by log(probability of a significant expression change) plotted on the y-axis and pheromone responsiveness on the cell chip being determined by the growth arrest ratio plotted on the x-axis. A subset of genes of both the primary pathway components (growth arrest ratios ~1) and pathway inhibitors (growth arrest ratio > 2) show a change in expression while many of them also do not.	79
Figure 3-1: Expository figure showing the treatment and image analyses of organellar localization upon pheromone treatment. Synthetic alpha factor is added to vegetatively growing cells containing GFP tagged Fus1p and different RFP tagged organellar marker proteins. A. Image of shmoo tip marker Fus1p labeled with GFP, clathrin marker Chc1p labeled with RFP, cell nuclei stained with DAPI B.	

Binary thresholded image, C. Binary image of nuclei used to seed watershed segmentation, D. Result of watershed segmentation, E. Shmooing cells are identified and cell-by-cell thresholding on the FITC, TRITC, and DAPI images is overlaid on the DIC image, F. Result of rotating and overlaying thresholded fluorescent intensity distributions for all shmooing cells (n=324) from multiple still images.	95
Figure 3-2: Results of rotating and overlaying thresholded fluorescent intensity distributions for all shmooing cells from multiple still images. Shmoo tip marker (FUS1) labeled with GFP, indicated organelle markers labeled with RFP, cell nuclei stained with DAPI. A. actin (SAC6), B. spindle pole (SPC42), C. clathrin (CHC1), D. golgi cis-cisterna (ANP1), E. ER/golgi (SEC13), F. peroxisome (PEX3), G. lipid particle (ERG6), H. nucleolus (SIK1), I. cytoplasm / endosomal membranes (SNF7).	97
Figure 3-3: Schematic of the work flow for performing proteome-wide localization screen.	99
Figure 3-4: Representative components of cellular systems that were recovered from the cell chip after a round of manual validation. Each panel shows a few cells from one yeast strain expressing a GFP-tagged protein localized to the tip of the shmoo following pheromone response. With the exception of YMR295C, the proteins displayed are known components of the cellular processes labeled outside each panel.....	101
Figure 3-5: GO molecular functions enriched in the list of shmoo tip localized proteins.	104
Figure 3-6: Representative components of cellular systems found localized to the shmoo tip. Components of cellular systems such as exocyst, septin, polarisome and actin cortical patch were recovered almost in their entirety (Table 3-1, 3-2). Proteins that function in signaling and fusion events such as Bem1, Fus1 and Kell are also represented.	105
Figure 3-7: Interconnectedness of spatially related classes of proteins involved in vesicular transport. The images to the right show representatives of proteins showing similar spatial localization patterns relative to the shmoo tip involved in vesicular transport events such as exocytosis, endocytosis and vesicular sorting events. These spatially related ‘groups’ also are better inter-connected to themselves than to other shmoo tip proteins in the yeast network (Left: Black circle – exocytosis, Red circle- ER-golgi & TGN sorting, Yellow circle – endocytosis related proteins showing diffuse connectivities to members of the cortical patch and other transport related proteins).	108
Figure 3-8: Functional linkages of unknown proteins recovered from the screen. Proteins in green circles were the unknown shmoo tip localized proteins that we tried to connect with the help of the network. Their partners are show in yellow. Black circles enclose proteins already known to be part of the shmoo tip network. A and B show two such unknown sets of proteins that connect at different points of the shmoo tip network.....	110
Figure 3-9: Summary of re-organization of organelles and protein complexes around the shmoo tip.	113

Figure 3-10: Venn diagram summarizing the proteins recovered. A: Intersection of the cell chip, classifier and known set of shmoo tip localized proteins from SGD. B: Of the 306 strains manually tested as part of the follow-ups, 18 were unique to the bud tip, 7 to the shmoo tip and 67 to both.	114
Figure 4-1: Growth phases of a yeast culture. As carbon sources become limiting, there is a transition from fermentative to respiratory metabolism with stationary phase onset occurring at around 4 days.	124
Figure 4-2: Overview of nutrient sensing and metabolic pathways during quiescence.	126
Figure 4-3 shows the models used to study yeast aging. Replicative life is indicative of the time spent in mitotic cell cycle while chronological lifespan also takes into consideration the time in cell quiescence cycle or stationary phase. Dotted circles represent bud scars.	130
Figure 4-4: A summary of processes affecting aging in yeast and possibly higher organisms. Reactive oxygen species (ROS) build up over time as an unavoidable consequence of changes in metabolism, genotype, nutrient intake and the environment. If damages are repaired, the cell is viable or else it ages and dies. During this phase, processes such as autophagy and mRNA storage bodies may sustain and poise the cells for cell cycle re-entry upon nutrient availability. On the other hand, decreased chaperone and proteasome functions may further aging through aggregation and other mechanisms.	132
Figure 4-5: A schematic of the cell microarray experiment conducted for imaging stationary phase protein localizations. Images of cytoplasmic proteins were examined for a change in the GFP localization from a cytosolic, diffuse phenotype to a punctate phenotype.	135
Figure 4-6: Representative strains showing formation of punctate foci of cytosolic proteins under nutrient depletion. The Asn2-GFP and the Hsp42-GFP tagged strains grown in YPD for 5 days (last panel) show a punctate phenotype. Replicate cultures grown overnight in SD were re-suspended in water for 1hour (middle panel) and in minimal media with essential nutrients (left panel). Water induces punctate foci in Hsp42-GFP and to a lesser extent in Asn2-GFP. Minimal media produces a diffuse cytosolic phenotype.	136
Figure 4-7: Functional categories enriched for proteins forming punctate foci in stationary phase. Proteins fall under several categories [110] with a hypergeometric probability better than intersecting by random chance. Examples include amino acid biosynthesis, stress chaperones and nucleic acid biosynthesis.	137
Figure 4-8: Reversibility of Gln1-GFP punctates grown in YPD for 48 hours with SD media. Gln1-GFP cultures were grown to 48 hours in YPD, spun down and treated with SD complete media before time lapse imaging on a SD agar pad for 3 hours. By 120 mins, the punctate foci are almost completely dissolved.	139
Figure 4-9: Biochemical enrichment of Gln1-GFP punctates. Gln1-GFP grown to stationary phase was lysed by glass beads and the lysate clarified by centrifugation at 13,000xg. The GFP protein signal is found highly enriched in the pellet.	141
Figure 4-10: In vitro analysis of Gln1-GFP punctates. Pellet enriched Gln1-GFP punctates (-ve control) were complemented with YPD, RNaseA and protease	

- reagents. Only proteinase K and protein detergents (rapigest, SDS) were able to disassemble the punctate bodies significantly. 142
- Figure 4-11: Schematic of mass spectrometric shotgun proteomic analysis of stationary phase yeast.** Two BY4741 cultures were grown to stationary phase and lysed with one being recovered by fresh YPD before lysis. Their respective supernatants and pellet fractions were analyzed by 2D-LC-MS/MS. Red and blue colors represent insoluble and soluble cytosolic protein fractions respectively. 144
- Figure 4-12: Calculation of Z-scores as a metric for protein transitions between fractions.** The recovered and the stationary phase supernatant and pellet fractions can transition with each other and this Z-score can be calculated as shown. The real question being addressed is represented by the diagonal arrow which is whether cytosolic proteins in the stationary phase pellet transition to the supernatant in the recovered phase (please refer text). 145
- Figure 4-13: Protein functions enriched for supernatant to pellet transitions and vice versa for the two phases.** Cytosolic enrichment is evident for the supernatant fraction of the recovered phase lysate but not such for the pellet. However, the stationary phase lysate displayed strong enrichment for cytosolic functions in both fractions..... 146
- Figure 4-14: Proteins that are most likely to form stationary phase punctates as determined by mass spectrometry and the cell chip.** A: A histogram of the Z-score differences with those passing the 95% cut-off being most likely to form punctates in stationary phase. B: The intersection between the mass spectrometry derived and the cell chip derived list of proteins likely to form such punctates..... 147
- Figure 4-15: Conditions for induction of Ade4 and Gln1 GFP punctates.** Ade4 and Gln1-GFP strains were grown to log phase before re-suspension in different media for 2hours and imaging. A: removal of adenine is necessary and sufficient to induce formation of Ade4-GFP punctates as seen by the punctates formed in the SD-Ade panel. However, adenine drop-out in the presence of cycloheximide (sd-ade(+chx)) does not produce robust punctates. B: Removal of glucose is necessary and sufficient for induction of Gln1-GFP punctates with cycloheximide not affecting this transition. 149
- Figure 4-16: Summary of punctate induction in Ade4 and Gln1-GFP strains.** Percentage of cells having punctates (from three replicate images) was plotted as a function of media conditions tested. As shown in A, Ade4-GFP punctates are induced upon adenine removal and are sensitive to cycloheximide. As in B, Gln1-GFP punctates are induced upon glucose removal and are insensitive to cycloheximide treatment..... 150
- Figure 4-17: Nutrient specific dissolution of Ade4-GFP and Gln1-GFP punctates.** Reversibility of punctate formation by re-addition of adenine (or metabolically related hypoxanthine) and glucose is displayed for Ade4-GFP and Gln1-GFP strains respectively. However, the reversal is sensitive to cycloheximide for Ade4-GFP and only partially so for Gln1-GFP. 152
- Figure 4-18: Summary of nutrient specific dissolution of Ade4-GFP and Gln1-GFP punctates.** Adenine and Glucose re-addition completely dissolves Ade4 and Gln1 GFP punctates respectively (three replicates). As shown in A, however, this

dissolution is sensitive to cycloheximide (chx) addition. Addition of chx with PMSF rescues this effect to a small extent. In B, Gln1-GFP punctate dissolution is partially sensitive to cycloheximide as seen from the Glucose+chx panel while PMSF showed no effect. 153

Figure 4-19: Recapitulation of mechanisms that may be involved in the formation of punctates. Green circles represent the pathways in question. All three suggested mechanisms may also be systemically inter-connected as depicted. 154

Figure 4-20: Punctate localization tests in autophagy and vacuole defective strains.
A: Gln1 and Ade4GFP punctates appear un-affected by a deletion in atg2 that produces an autophagy defect. Vps33 deletion that results in vacuole minus cells severely impairs Gln1-GFP punctates and appears to produce Ade4-GFP punctates that are proximal to the bud tip. B: graphical summary of the observations done in three replicates. 155

Chapter 1: Introduction

The increasingly radical insights being gained over the past decade into the workings of a cell can largely be attributed to the interdisciplinary approach being employed in biology. The reductionist view conventionally adopted where a particular biological pathway or protein function was studied in isolation is giving way to global measurements of cellular parameters and context-based investigations with regard to the entire physiology of the cell. This has led to the field of Systems Biology which simply refers to a hybrid approach in unraveling the cellular circuitry using high throughput techniques combined with sophisticated mathematical and statistical tools to integrate such data to produce credible predictive models of cell function. Put differently, Systems Biology serves as a pipeline of experimental and computational tools that generate and analyze multivariate global datasets to create testable hypothesis that reflect cell behavior under different states.

Needless to say, the incredible plasticity of cellular phenotypes in many ways complicates cell biology to beyond simplistic approaches of study. Understanding the vast sea of biochemical reactions and biophysical interactions within the confines of a cell that produce many of its defining features has always been the goal of biologists. In light of the advantages of integrating global datasets, systems biologists have preferred to study cell behavior by inventorying and piecing together the component ‘parts’ and correlating the observed changes to the particular response under study. This approach has been more in line with the recent wave of technological advances sweeping the biological landscape. For example, faster sequencing has enabled genomes from several organisms to be sequenced, laying the foundation for identifying the blueprint that makes

up a cell. The most surprising outcome of the human genome sequence has been without doubt the realization that organismal complexity is disproportionate with the number of protein coding genes. Yeast, for example, has about 6000 genes and a human, in comparison, has about five times more. However, this also means that it is possible to get a fair idea of the operations of a eukaryotic cell by studying such model organisms with fewer component parts. Indeed, comparative genomics has confirmed the evolutionary conservation of several cellular systems and functionalities from yeast to man, as will be alluded to in later sections.

The ability to grapple with the deluge of sequence information and systematically catalog the contributions of every gene towards cell function has given rise to the area of functional genomics. With a focus on developing technologies for the generation of global datasets that enumerate several aspects of a cell's function, it has contributed enormously to the systems biology toolkit and aided in building predictive models. I will introduce some of the powerful techniques that form the cornerstone of functional genomics with a focus on yeast as a model system in the next few sections. I will detail our view on our understanding of the workings of the cell from a systems perspective before moving on to describe image-based screens and polarity, the topics of my study.

TECHNOLOGY DRIVERS IN FUNCTIONAL GENOMICS

As described above, a detailed inventory of the cell is crucial to understanding function. Designated as the 'omics' technologies, the post genomics era has spawned methods that measure the composition of different cellular classes of biomolecules - mRNA (transcriptome), proteins (proteome) and metabolites (metabolome) being the common ones. In addition, reverse genetic screens are now conducted with an ease that was previously not feasible after the discovery of RNA interference and other

technologies for modulating gene function, such as gene knockout and gene tagging techniques. Such methods have suddenly provided much needed data dimensionality in biology that has resulted in unprecedented insights into the genetic circuitry underlying function. Some of these methods and their applications are briefly outlined.

DNA microarrays

Since the time the first DNA microarrays were conceptualized and used [1, 2], the development of novel, parallelizable lab-on-a-chip genomic assay systems have revolutionized mainstream biology and medicine facilitating the making of accurate diagnostic, prognostic and therapeutic decisions. In one of the seminal papers, DeRisi et al. [2], in one of its first incarnations, describe DNA microarrays fabricated with PCR products representing every gene in the budding yeast, *Saccharomyces cerevisiae* on a single glass slide to study the temporal program of gene expression upon metabolic shift from respiration to fermentation. Generally, sample preparation for microarrays that perform expression profiling involves RNA isolation from cells grown under a control state and the ‘test’ state. Reverse transcription, differential fluorophore labeling and competitive hybridization on the microarray provide an array read out under the different fluorescent channels which capture the relative expression change of individual genes on the microarray. The measurement of mRNA expression and the applications therein are now mature technologies fueling efforts towards profiling disease states, drug treatments and off-target effects, and even complete body maps of expression [3]. Such data are critical to understanding, discovering and annotating new gene functions, parsing pathway relationships by co-expression analyses, determining cross talk and establishing cause-effect relationships [4].

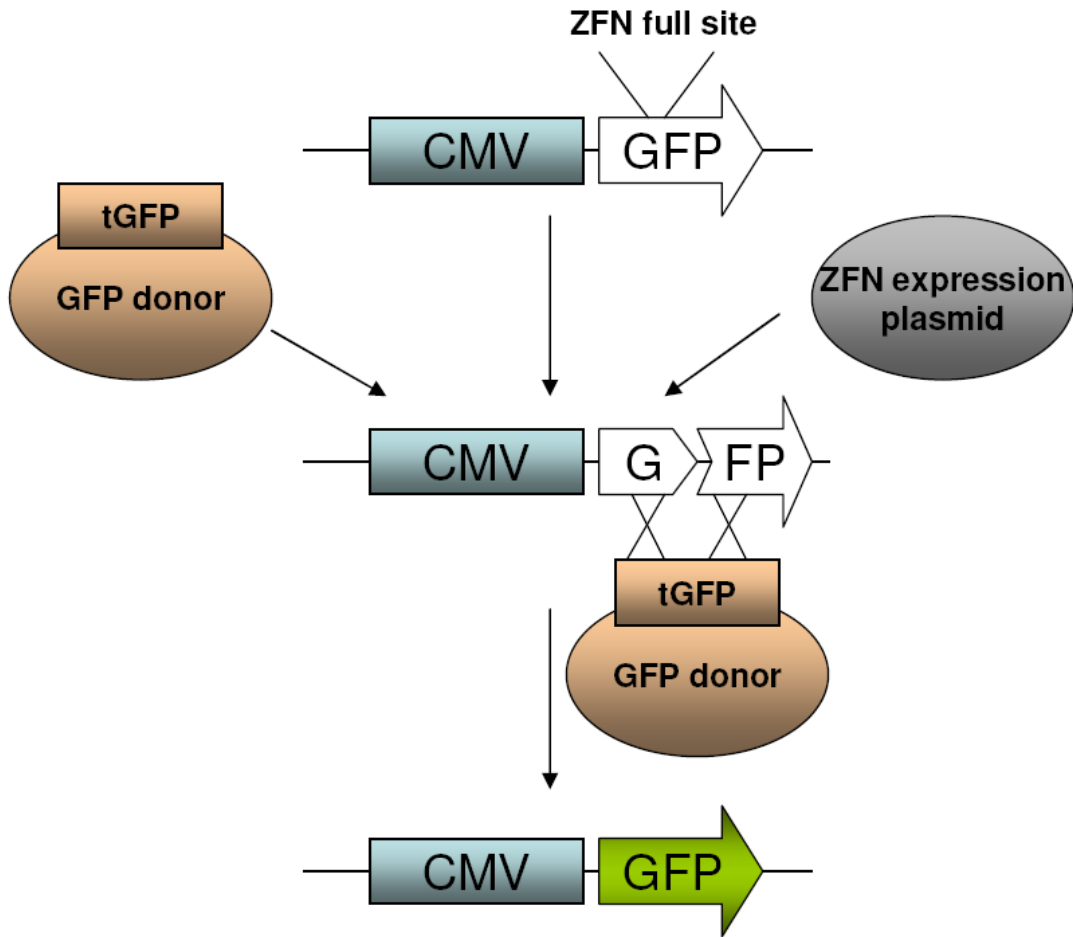


Figure 1-1: Genomic editing by a Zinc finger transcription factor- nuclease (ZFN). A mutated GFP gene, with an inserted in-frame stop codon and recognition sites for zinc finger nuclease is integrated as a single copy into the genome of a cell (top line). The cell is transfected with a plasmid with a nonfunctional GFP gene (tGFP) and expression plasmids for ZFN. The integrated GFP is repaired by gene targeting, and the cell becomes GFP positive.

In addition to expression profiling, several other insights can be gained by directly getting at the DNA sequence. Using a pooled yeast deletion library where every deleted locus bears unique bar codes and bar coded arrays to deconvolute them have helped determine the effect of these deletions under several conditions and treatments [5]. Typically, a chemogenomic profiling approach selects for strains based on their fitness to

a specific treatment enriching for their respective bar-codes, and in the process annotates gene function. Information about single nucleotide polymorphisms, mutation positions and copy number that can stratify patients based on their genotypes and also reveal disease susceptibilities can be gained through microarray-based approaches as well [6, 7]. Epigenetic markers that detect DNA methylation patterns using a modified microarray protocol have provided insights into gene silencing, genomic instabilities and the ‘cancer genome’ [8]. In recent times, massively parallel sequencing approaches [9] and advanced photolithography printing techniques [10-12] have resulted in new approaches to studying the genome. Such technologies have given rise to the ENCODE project [13] that aims to map transcription factor binding sites on the genome. **Figure 1-1** shows the ability to genomically engineer the DNA sequence using a Zinc finger nuclease, opening up possibilities of directly editing regions of a genome in diseased cells [14].

Proteomics

The transition from a completed DNA sequence to predicting actual cellular function is an as yet unsolved problem. Cells can adopt specialized functions upon differentiation in multi-cellular organisms or can undergo subtle transformations in lower organisms by switching biochemical and signaling pathways in response to diverse environmental and developmental cues. Many of these seemingly stochastic processes are directly orchestrated by protein-protein interactions inside the cell, often with exquisite temporal and spatial regulation to result in a specific phenotype or response that typifies that cellular state. It is therefore imperative to be able to profile protein expression under different cellular states, their post-translational modifications and their interactions, a

formidable task given the large and often unknown combinatorial nature of the proteome [15].

Proteins from cells under different states were traditionally compared on two-dimensional PAGE gels, generally effecting separation by pI or isoelectric point in one dimension and by molecular weight in the second dimension. Protein identification relied on even more cumbersome approaches such as Edman degradation. More recently, technological advancements in ionization procedures like time of flight (TOF) and soft ionization comprising the Matrix-associated laser desorption (MALDI) and Electro Spray Ionization (ESI) methods has enabled analyses of intact biomolecules, making mass spectrometry the method of choice for profiling the proteome [15]. Mass spectrometers can be used for simply measuring the molecular mass of a protein according to the mass by charge (m/z) ratio of their constituent peptides or to determine additional properties such as the amino acid sequence and post translational modifications.

All mass spectrometry experiments include a sample preparatory step followed by digestion, usually with a site specific protease such as trypsin. The resulting peptide mixture can be fractionated on a HPLC before analysis on a mass spectrometer. Originally, protein mixtures were separated by 1D or 2D gel electrophoresis, then in-gel-digested followed by excision of the desired protein band and its mass spectrometric identification. A MALDI-TOF instrument using simple BLAST algorithms was suitable to perform such experiments when working with systems whose genomes were fully sequenced. More recently, ESI mass spectrometry has become the method of choice for identifying proteins in complex mixtures because of higher throughput, while saving on time. Typically, tryptic digests of protein mixtures are separated in-line by employing orthogonal chromatographic procedures to reduce peptide complexity, followed by ionization and introduction into the mass spectrometer. Inside the mass spectrometer, the

peptides are resolved first according to their m/z ratios (MS1). A user specified range of peptide m/z ratios are sampled to choose specific peptide ions for a process called collision induced dissociation (CID). During this process (MS2), peptide ions are fragmented, generating a ladder of sequentially smaller peptides which allow for the deduction of the parent ion sequence and thereby the respective protein ID. In addition to its role in characterizing proteins from cellular mixtures, small molecules such as drugs and metabolites have also been identified and profiled using this technique. Proteomics analysis of complex protein mixtures is still a maturing field with several exciting avenues for improvement, such as label-free [16, 17] quantitation, and applications like protein complex mapping [18-21], personalized medicine, metabolomics [22], and biomarker discovery [23]. **Figure 1-2** shows the principle behind label-free peptide quantitation [24], a process similar to mRNA analysis using serial analysis of gene expression (SAGE).

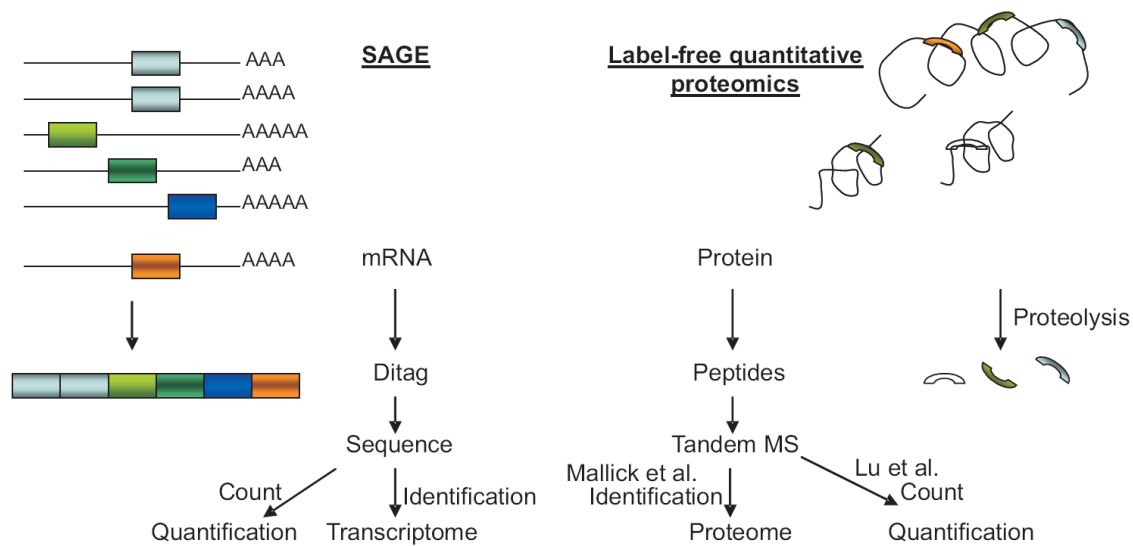


Figure 1-2: ‘Counting’ peptides in label-free quantitative proteomics. In SAGE, a short sequence tag is sufficient to identify a transcript, quantification of which depends on the number of times a tag is observed. In proteomics, a short proteotypic peptide is sufficient to identify a protein and redundant peptide counting affords quantification.

Techniques for performing high content phenotype screens & applications

High throughput phenomics

Linking genotype to cellular physiology was kick-started by the next wave of technologies aimed at adding data dimensionality through high throughput phenotype screens. Several techniques have been reported for studying phenotypes of model systems in a highly parallel manner. For example, Bochner et al. [25, 26], in their conceptualization of phenotype microarrays, used *E.coli* as a model system to perform multi-plate assays that captured respiration rates of mutant backgrounds under as many as 2000 different perturbations. Such ‘phenomics’ studies aimed at connecting genotype to phenotype have now been performed on a genome-wide scale in yeast with the availability of systematic collections of several mutant/strain libraries. The PROPHECY database now provides quantitative information about phenotypes for the complete yeast deletion collection by estimating growth rates under different environmental conditions such as salt stress and redox imbalance [27].

Protein microarrays

True high density phenotypic studies became possible when the conceptualization of microarray platforms was extended for assaying a wide variety of biologically relevant compounds (as opposed to just DNA microarrays). Michael Snyder’s and Eric Phizicky’s groups reported the first proteome array comprising the complete yeast proteome made from overexpressing and purifying ~5800 ORFs as GST tagged proteins before printing them onto glutathione coated slides [28]. These chips demonstrated broad ranging applicability in detecting *in vitro* binding events such as protein-DNA, protein-protein, protein-drug and protein-small molecule interactions, as well as in determining substrate

specificities and therefore downstream targets of purified enzymes such as kinases [29]. Antibody microarrays, a variation of the protein microarrays, have proven useful in diagnostics of diseased biofluids and validating biomarker signatures [30].

Transfected cell microarrays

The most attractive and exciting feature of such high throughput cell biology is, without doubt, the ability to quantify single cell responses such as cell growth and morphology, protein expression and localization in response to perturbations, as compared to most other systems approaches that report only population averages. Highly parallelized ‘in-cell’ assays have hit mainstream with the introduction of transfected cell microarrays [31, 32] (**Figure 1-3**).

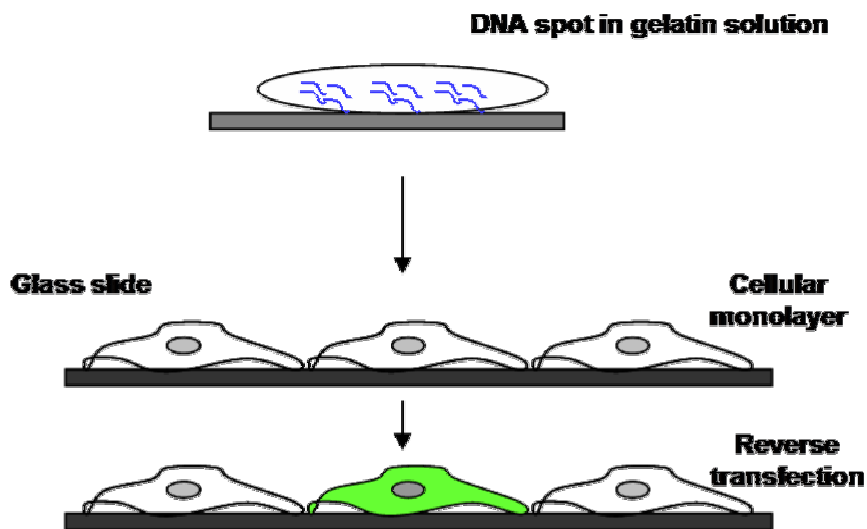


Figure 1-3: Transfected cell microarrays. Cells are grown as a monolayer on a slide containing spots of DNA, siRNA or other molecules along with transfection reagent. Cells in the vicinity of the spot containing a GFP plasmid turn green.

Transfected microarrays involve microarraying a cDNA, siRNA or other molecules of interest onto slides along with a reagent that facilitates its cellular uptake. [33, 34] An example of a reverse transfected microarray (**Figure 1-3**) is shown where

DNA spotted with a transfection reagent is taken up a monolayer of cells. Lentiviral microarrays serve as an improved version of this technique facilitating increased efficiency of uptake [35]. With the advent of RNA interference, siRNA screens have been extensively performed in this manner to silence many genes in parallel, and candidate cellular pathways examined using a reporter to study the involvement of the silenced gene. For example, apoptosis pathways can be studied by staining the cell microarray for caspase activity after siRNA uptake and imaging the slide under a microscope [36, 37].

Imaging considerations – optics, image analysis and storage

The quality of image data is pivotal to feature extraction and image analysis with minimal human intervention and a careful consideration of the optics is required to facilitate this process. The choice of objectives of the appropriate magnification and numerical aperture, for example, should be chosen depending on the size of the cells and the structures of interest [38, 39]. Digital CCD camera detectors must also be carefully considered since increased pixel numbers on a chip do not necessarily reflect an increased signal to noise ratio, due to decreased pixel sizes and therefore light sensing ability, especially in low light applications such as fluorescence microscopy. However, super-cooled CCD devices have alleviated this constraint to a large extent and high end digital cameras are now routinely utilized in high throughput microscopy applications.

Automated image analysis and storage infrastructure are essential to complete and analyze biologically meaningful information from high throughput imaging screens. Relational databases such as the PSLID (protein subcellular localization image database) and OME (open microscopy environment) have served roles in storage and analyses of the images, while phplabware and Spotfire aid in data visualization. Recently, the

development of automated image analysis methods that combine feature extraction and machine learning algorithms have proven to be an extremely sensitive and robust means of discriminating subtle variations in biologically important patterns, such as subcellular protein distribution. Ready-made software packages that are open source and free are available for high throughput image analysis such as Cell_ID, CellProfiler and ImageJ [39]. A typical automated image analysis workflow involves identifying single cells in a field by a segmentation step that divides each image into sub-regions containing individual cells from which specific features can be extracted [40]. Several features, including obvious morphological geometries such as edge pixels distinguished by regions of extreme pixel intensity variations and pixel texture across the cell that may represent unique subcellular patterns, can be obtained and statistical measurements made on them [41]. Comparisons of statistical parameters can then be performed to determine proteins that share similar localizations and therefore potentially a common pathway [42-44].

BAKER'S YEAST – FUNCTIONAL GENOMICS' FAVORITE HUNTING GROUND?

An easily tractable model system is essential for conducting the high throughput screens described above. Through the years, budding yeast *Saccharomyces cerevisiae* has become the workhorse for modern molecular and cell biological studies aided by a relatively small genome among eukaryotic model organisms and a sophisticated experimental toolbox. In addition to classical biochemical and genetic studies, yeast has proved to be the ideal foil for the maturing of several functional genomics techniques. With the recent availability of comprehensive gene deletion and epitope-tagged libraries [45-48], yeast is realizing its potential of revealing unprecedented insights into various aspects of cellular circuitry. Some of the public repositories of yeast datasets are shown in **Table 1-1**.

<u>Resource</u>	<u>Description</u>
<i>The Saccharomyces Genome Database (SGD)</i>	<i>Comprehensive database with locus pages for each gene/protein linking to a large number of other sources/data and analysis tools</i>
<i>The MIPS comprehensive yeast genome database</i>	<i>Database with entries for each gene/protein with functional information</i>
<i>Yeast GFP fusion localization database</i>	<i>Entries for each protein with localization and abundance information</i>
<i>Yeast protein localization database</i>	<i>Database with protein localization information</i>
<i>Yeast GRID</i>	<i>Information on protein-protein interactions</i>
<i>PROPHECY</i>	<i>Quantitative information about phenotypes for the complete collection of deletion strains</i>
<i>Saccaromyces cerevisiae Morphology database SCMD</i>	<i>Entries for each yeast deletion mutant with quantitative data on cell morphology</i>

Table 1-1: Examples of public repositories of yeast datasets & gene function

Analysis of gene function – A change in approach necessitated?

Yeast two hybrid screens [49, 50] produced one of the first clues about genome wide protein-protein interactions. This was followed by large scale pull down experiments [18, 20] using TAP tagged yeast strains followed by tandem mass spectrometry to identify protein interactions. Both these studies have generated enormous amounts of data with almost every protein's interacting partners being explored. Two hybrid studies, in principle, can reveal protein interactions within complexes while MS based studies cannot. In addition to physical interactions, genetic networks and epistatic relationships were identified through the construction and manipulation of comprehensive deletion libraries [51]. Such synthetic genetic analyses have provided further insights into the manifestation of phenotype from genotype.

With all this data at our disposal, it is reasonable to ask how far we are from understanding the functions of all 6000 genes in yeast and if coherent predictive models of cell function can be drawn [52]. A look at the yeast protein database (YPD) or the *Saccharomyces* genome database (SGD) shows that almost 5000 genes have been annotated to have some function showing a tremendous progress in our efforts to assign a function to genes. However, this is only true given a very liberal definition of gene function. Thus, although the number of ‘uncharacterized ORFs’ may have gone down, we still lack sufficient depth in our understanding and modeling of even well characterized genes in the context of entire systems. As a simple example, she3p, a protein annotated as being an adaptor protein that mediated mRNA transport, has a total of 33 known protein interactions identified using different methods. Its interaction with Myo4p is supported by protein complex information derived from mass spectrometry, two hybrid assays and co-purification experiments. However, its interaction with Sup45p is supported by only data derived from mass spectrometry complexes. This may therefore be a case of a novel interaction or a spurious one. In addition, the mechanism driving its interaction with such a broad of range of proteins has not been sufficiently explored. How then should we reconcile ourselves to a model of gene function given such imperfections and uncertainties in data collection and interpretation?

A probabilistic view of gene function

It is becoming clear that every experimental technique suffers from different degrees of error rates, and therefore, multiple lines of evidence implicating a particular function for a gene is required to strengthen this belief. Many frameworks are already in place for defining gene function such as the Gene Ontology (GO) project that ultimately relies heavily on manual curation to classify genes into different functional hierarchies

[53, 54]. Such hierarchical ontologies typically fall under the top-down approach to data analysis where genes are manually curated to fall under different functional categories such as ‘nitrogen metabolism’ or ‘polarized growth’ based on experimental evidence from many researchers. To its credit, this approach organizes gene function in an easy-to-comprehend manner that reflects the current view of gene function and is updated as new data is added. However, such subjectivity in classifying gene function can ultimately lead to incorrect error assessments and faulty designations of genes into categories. In the light of this problem and the explosion of data from high throughput functional genomics techniques, complementary methods adopting a bottom-up approach to providing a framework of genetic interactions have been considered.

A Network approach to studying genetic interactions

In the bottom-up approach, multiple datasets generated by several experimental techniques are weighted differently according to experimental error models and the data integrated by applying statistical methods. Such a systematic data-driven approach objectifies the entire process where new incoming data can position itself in this framework in an unbiased manner. High throughput datasets, despite their high coverage, are often associated with significant error rates. In order to estimate these rates, one can adopt ‘guilt-by-association’ strategies [55, 56] and ask how often a particular high throughput screen ‘recalls’ a known, high confidence characteristic of a specific gene or protein. These could be properties such as co-expression with other gene sets, shared localization in the same sub-cellular compartment as another protein, a shared interaction with another protein or RNA, and so forth. These ‘benchmarks’ or independently validated functional annotations form the basis for signal to noise estimations of multiple datasets and allow for the calculation of an average error rate associated with each of

them. There are many different statistical schemes for weighting the data based on their error rates, such as a Bayesian approach or other heuristic and probabilistic approaches. Irrespective of the scheme adopted, the result is the generation of networks where gene linkages are no longer binary but instead can be considered as connections whose strengths rely on the probabilistic weights of the evidence implicating them. These networks can rapidly assimilate new data coming in and can be used for bettering models of cellular function iteratively.

Although genetic interaction networks such as the one for baker's yeast are difficult to comprehend, an implicit fall-out from such probabilistic networks is the emergence of functional modules that represent highly connected gene clusters followed by a sparsely connected set. These functional modules are in fact nothing but the hierarchical functional categories identified by top-down approaches and a simple assignment of 'ribosome' or 'proteasome' give immediate relevance to all the connections identified within them. It is important to note that the boundaries of such modules are not rigid and the degree of connectedness needed to define a biological process, such as 'Splicing', is variable. For example, a set of three connected genes can be assumed to form a sub-network within a larger network of genes, and as one moves further up the complexity ladder, an entire module is encapsulated followed by many modules representing the entire cellular interactome. The interlinked nature of the modules represents the highly complex genetic circuitry that typifies the current state of molecular cell biology as we understand it. Any gene is therefore linked to any module by a relatively short path and pleiotropy is therefore implicit in such probabilistic interactomes.

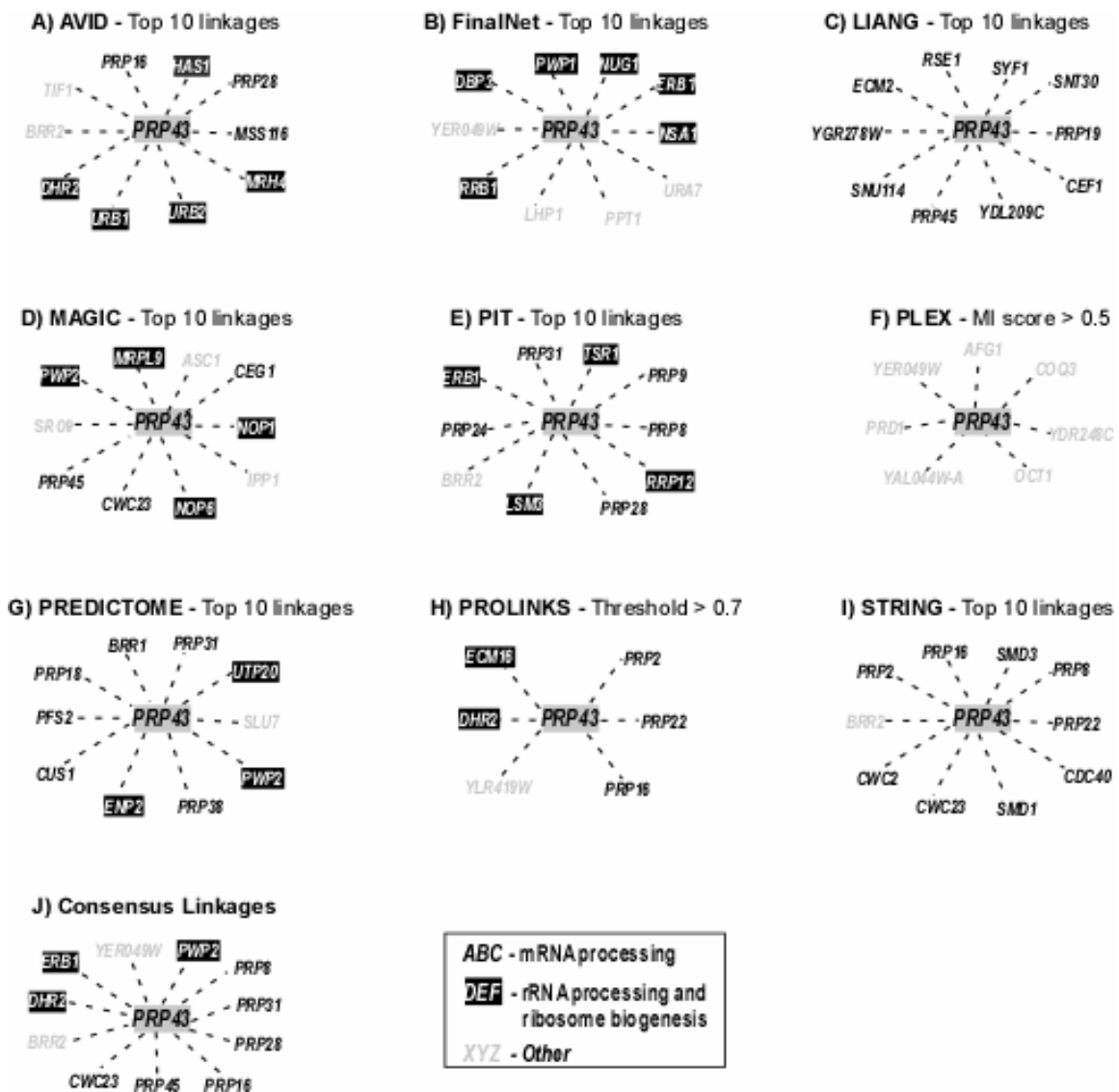


Figure 1-4: Predicting consensus protein function using networks containing pre-calculated functional linkage information. With Prp43 as an example, we show its lesser known role in rRNA processing and ribosome biogenesis using different function prediction algorithms.

Figure 1-4 shows the functional associations of *PRP43*, a gene chosen as example for function prediction by different network methods with pre-calculated linkage information. The genes linked to *PRP43* are labeled according to their broad functional categories (based upon their GO annotations and literature)—‘mRNA processing’,

including mRNA transactions, such as pre-mRNA splicing; ‘rRNA processing and biogenesis’, constituting the synthesis, processing and assembly of rRNAs into ribosomes; and ‘Other’, referring to functions besides these two categories. Several methods have been envisaged to calculate and predict yeast protein function.

For example, AVID [57] is a computational prediction framework that integrates data from high throughput experiments such as Yeast 2-hybrid, Mass Spectrometry, expression microarrays, UCSF protein localization and sequence similarity. Final Net [56], MAGIC [58], PIT [59], PREDICTOME [60] and STRING [61] are other such databases that store pre-calculated functional linkage information between yeast genes based on probabilistic guilt-by-association type approaches. As an example for demonstrating the utility of such networks, we will now take *PRP43* (YGL120C), a yeast RNA helicase through several of the functional prediction databases mentioned above (**Figure 1-4**). *PRP43* is an essential yeast DEAH box protein, a family of proteins thought to possess RNA helicase activity and that function extensively in the coordination and catalysis of the pre-mRNA splicing reaction. *PRP43* itself, although not shown to exhibit an RNA helicase activity, was implicated to function in the disassembly of the U2/U5.U6 spliceosomal complex post-catalysis and subsequent release of the lariat RNA [62]. Note that most of the apparent disagreement among the predictions of the different approaches is simply a function of including only the top 10 associations from each — as the methods include different data types and have different scoring functions, they tend to exhibit trivial differences in the ranking of associated genes. Nonetheless, although the specific predictions vary, certain linkages are identified by multiple algorithms, such as the linkages of *PRP43* to *ERB1*, *YER049W*, *CWC23*, *PWP2*, *PRP2*, *PRP28*, *DHR2*, *PRP8*, *BRR2*, *PRP31* and *PRP16*. An examination of the broad functional categories of these predicted genes shows that the majority lie in mRNA processing such

as pre-mRNA splicing, the known function of *PRP43* [63]. However, several associations are inferred with genes implicated in rRNA processing and ribosome biogenesis, in agreement with very recent data [62] that indicate that *PRP43* serves an essential role in the biogenesis of both ribosome subunits while having a non-essential role in pre-mRNA processing. Thus, the two primary functions of *PRP43* are correctly inferred by the algorithms. Although further experiments would be needed to verify the exact candidates involved in this process with *PRP43* and their manner of involvement, it is clear that integrated function prediction databases can be immensely valuable at generating new testable hypotheses.

The *S.cerevisiae* interactome probably packs the most information to date, encompassing diverse datasets and covering as many as 90% of the yeast genes. However, even this highly informative set of connections is essentially a union of all possible interactions with no spatio-temporal or conditional constraints. It is envisaged that such ‘master’ networks will, into the future, spawn sub-networks representing differential gene connectivities as more cellular states are explored and specific constraints on time and space can be imposed [64].

TOWARDS CHARACTERIZING THE SPATIOTEMPORAL DYNAMICS OF A CELL- SIZE & MORPHOLOGY

Major determinants of cell size

Size homeostasis and its inter-relationship to cell division is one of the defining characteristics of most eukaryotic cells (**Figure 1-5**). It is indeed still a mystery as to whether cells ‘sense’ cell volume, mass or biosynthetic capacity during temporal regulation of cell division [65-67]. In budding yeast and several other organisms, ploidy number has been strongly correlated with cell size in that cell volume increases with

ploidy. Although the pathways responsible for this correlation are unclear, in general, ploidy number could result in increased nuclear volume, chromatin content and the expression of an unknown number of genes, which could provide a metric against which cytosolic volume could be measured. Several studies have also shown that cell growth and cell division that are normally tightly linked are separable [66, 67].

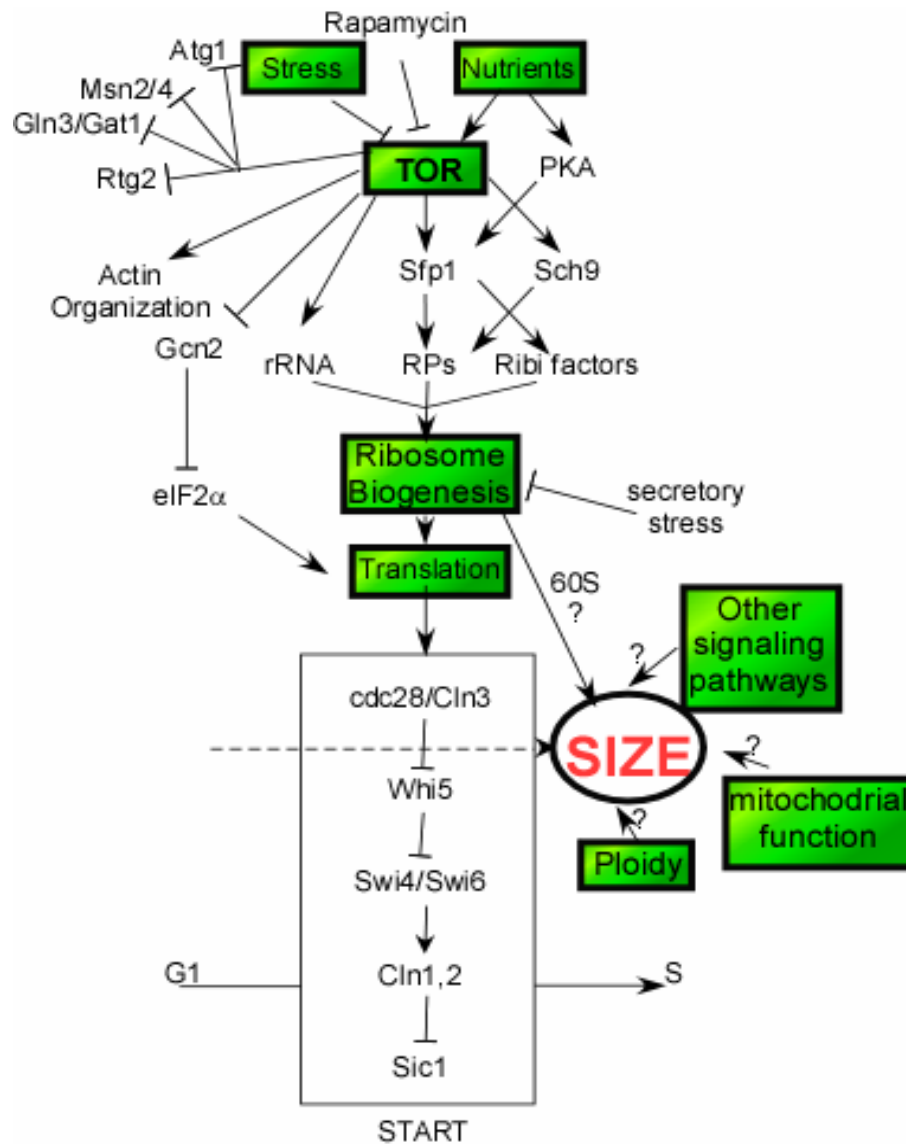


Figure 1-5: Inter-relationship of yeast cell size with major cellular pathways.

Current evidence suggests that budding yeast may assess their size based on the rate of ribosome biogenesis, judging from the close correlation between the two [68]. This model implicitly assumes that the translational capacity tends to be higher when active ribosomes are not limiting and therefore represents a state of nutrient abundance, both being necessary pre-requisites for 'Start'. The rate of ribosome biogenesis is governed by several mechanisms, such as control of nuclear localization of a master regulator of ribosome biogenesis (Ribi) called Sfp1 [69, 70]. Sfp1 is in turn modulated by the TOR (Target of Rapamycin), PKA (Protein Kinase A) and Sch9 pathways that are the primary pathways signaling the presence of nutrients. Ribosome biogenesis is hence optimally placed in the network to receive stimulus from nutrients and transmit it to downstream effectors such as Cln3 which may signal the transition to S phase. However, not all ribosomal proteins when deleted cause a smaller cell size defect. Additionally, TOR itself controls a wide array of pathways such as autophagy, P-body formation, actin organization and other metabolite triggers. Thus, despite the considerable depth to which this phenomenon has been investigated, it is far from being well understood.

Yeast morphology for characterizing gene function

The importance of morphology (**Figure 1-6**), obviously closely related to cell size, is underscored by the many signal transduction pathways that operate in yeast in response to different environmental stimuli. Shared regulatory components define all advanced eukaryotic signaling cascades without compromising on overall signal fidelity. In yeast, such pathways involve the response to pheromones, osmolarity, cell wall stress and nutrient deprivation, many of which display morphological adaptation. For example, the pheromone response polarizes the cell to result in a mating projection or 'shmoo'

morphology, while nutrient deprivation causes pseudohyphal development in a diploid yeast cell, emphasizing morphology as a recurrent theme in cell biology.

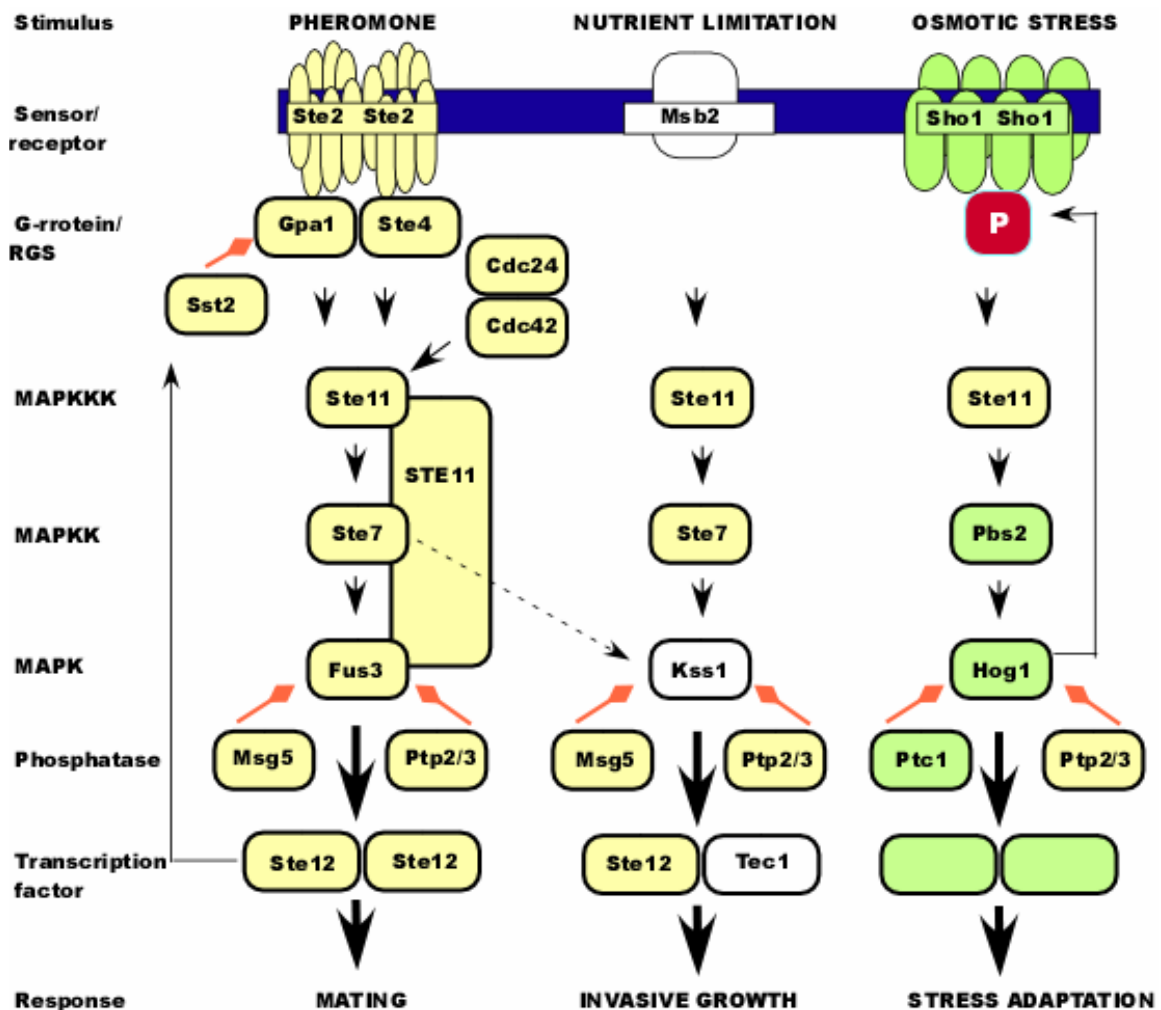


Figure 1-6: Major MAPK signal transduction pathways in yeast. Every pathway is associated with a distinct morphological adaptation showing the importance of morphology in cellular physiology.

The contribution of individual genes towards budding yeast cell morphology was qualitatively determined by visually screening the 4401 homozygous diploid mutant collection [47]. Around 15% of these deletions displayed altered morphologies from the normal ellipsoid cell shape of wild type diploid cells. The deletion mutant morphologies

were grouped into seven classes: elongated, round, small, large, pointed, clumped and other. Several deletions with similar morphological traits were categorized under the same MIPS functional category with ‘round’ mutants being defective in bud site selection and ‘small’ mutants having mitochondrial and cell cycle defects. More recently, Saito et al. [71, 72] have constructed the *Saccharomyces cerevisiae* morphology database (SCMD) that stores quantitative morphological parameters associated with every yeast deletion strain. All deletion strains were imaged in multiple channels capturing four distinct features - the DIC image, the nucleus (DAPI), cell wall (Concanavalin A) and actin (Phalloidin). Automated image processing was applied to extract ~ 500 detailed parameters describing cellular geometries such as the long axis, bud neck position, bud growth direction, nuclear size, actin localization and so forth. Of the ~4,700 strains in the non-essential deletion collection, a total of 2,378 exhibited differences from wild type cells in at least one of the 254 statistically reliable morphological parameters analyzed, indicating that around half of the non-essential yeast genes contribute towards cellular morphology. Using morphology as a means to assign gene function in known cellular pathways has been demonstrated as well [73]. For example, the ‘DNA recombination repair’ group of genes expected to have delayed or arrested mitosis are best characterized by the parameters “ratio of cells in nuclear division” and “ratio of large-budded cells to budding cells before completion of nuclear division” as determined by a control group of 14 genes. By using these query terms, a set of 19 deletions were identified in the collection with 7 of them being represented in the original set of 14 strains. Additionally, novel phenotypic attributes were identified in the genes that shared these morphological features. Such in-depth analyses of the quantitative contributions of every gene towards spatial geometries of a cell promise to add valuable dimensionality to existing functional interaction networks helping to generate better and more powerful predictive models.

TOWARDS CHARACTERIZING THE SPATIOTEMPORAL DYNAMICS OF A CELL-LOCALIZATION & SPATIAL DYNAMICS

An important goal in cell biology has been to identify the endogenous localization of biomolecules such as proteins and RNA over time in a cell, thereby, getting a handle on understanding the spatiotemporal dynamics that modulate cellular processes. Differential spatial and temporal events then become phenotypes in themselves with several genes being responsible for orchestrating these processes in a normal fashion. I will focus here on recent high throughput protein localization studies, although RNA localization has also become a topic of intense scrutiny in recent years [74].

Experimental approaches for gene tagging

Powerful techniques for cellular imaging of localization phenotypes have been developed, such as epitope tagging [75], CD-tagging [76] and chemical fluorescent strategies [77]. Comprehensive attempts to tag the proteome have only been accomplished to significant extents in budding yeast [45, 75] and fission yeast [78], although studies in fission yeast have only just begun. The first such effort at tagging the budding yeast proteome was pioneered by the Snyder lab [75] and provided the initial insights into the molecular underpinnings of cell biology. Kumar et al. used a minitransposon carrying a 3x HA epitope tag and a marker gene in the form of ‘payloads’ to insert randomly into the yeast genome. Strains possessing in-frame insertions were isolated using the marker and excess transposon elements removed from the genome via cre-lox mediated recombination. Immunofluorescence and imaging of the HA tagged strains resulted in identifying the subcellular localization of ~2700 proteins that is now accessible through the TRIPLES database. Subsequently, the O’Shea group generated an in-frame C-terminal fusion of Green fluorescent protein (GFP) with ~4200 genes in the

yeast genome by homologous recombination, making this yeast GFP collection the most extensive genome wide epitope tagged collection to date for studying intracellular proteome dynamics. More recently, novel techniques using a split protein complementation strategy have harnessed the power of protein engineering to determine protein co-localization and interactions (**Figure 1-7**). In one such instance [79], the enzyme dihydrofolate reductase is split into domains 1 & 2 and domain 3, each of which is fused to a bait and prey protein of interest. A survival selection is set up where only viable cells represent a successfully interacting pair. Such strategies have also been employed using a split GFP system for determining protein localization of a protein and of interacting proteins.

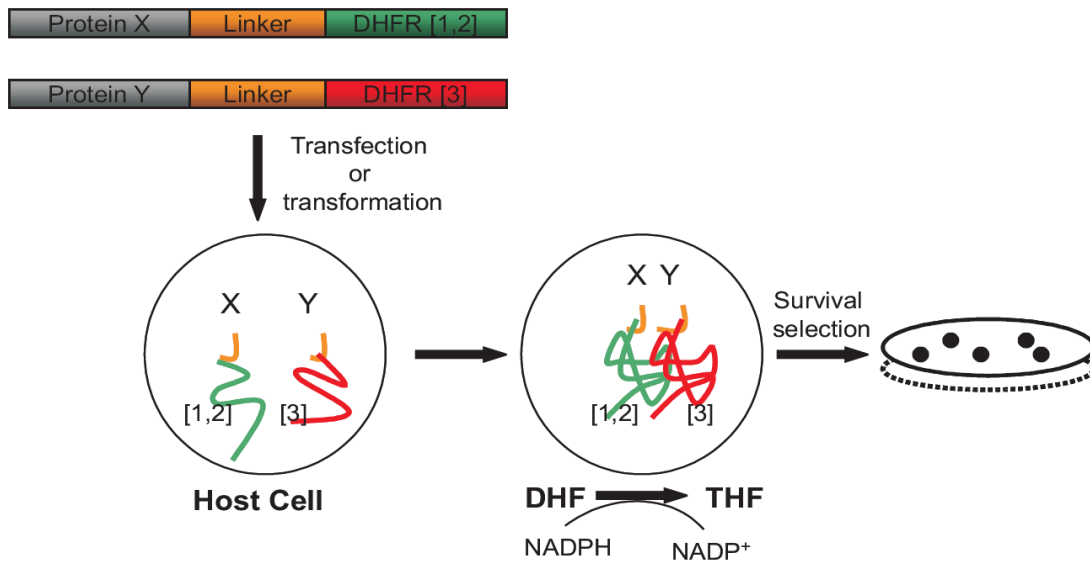


Figure 1-7: Split protein complementation strategy. A tool for determining in vivo protein-protein interaction and localization by imposing a selection based on survival.

Correlation between protein localization and protein function

This effort at systematically organizing the proteome into distinct cellular compartments is an all important aspect of functional assignment because subcellular localization has been strongly correlated to protein function. Co-localization of two proteins in the same cellular locale substantially increases the confidence for a protein-protein interaction and therefore adds valuable data dimensionality. As an example that validates this notion, the yeast proteome contains nearly 800 mitochondrial proteins, a majority of whose function is, as expected, in the process of cellular respiration. This is further emphasized when transcriptional co-regulation, a strong predictor of functional relatedness, is compared with proteome wide localization measurements. Huh et al. [45] estimated this using the 33 transcriptional modules in yeast containing sets of co-regulated genes previously identified based on > 1000 microarray datasets of mutant yeast strains under different environmental perturbations. For each module, the fraction of encoded proteins in a subcellular compartment was calculated and fold-enrichment obtained by dividing against the fraction in the whole proteome. This analysis (fold enrichments with $p < 0.05$ for 19 out of the 22 highly expressed modules tested) clearly revealed that proteins in the same transcriptional module shared subcellular compartments, such as the ‘Ergosterol’ module showing enrichment in ‘Lipid particle’ localization and ‘Histones’ showing enrichment in ‘Nuclear’ localization. Similar fold enrichments were also obtained when physical interactions were compared to co-localization, but the degree of enrichment varied between compartments. For instance, interactions between cytoplasmic proteins were 1.3-fold enriched above chance while interactions between microtubule proteins were 56-fold enriched as calculated by the sum of all genetic and physical interaction evidence reported in the GRID database. This makes intuitive sense spatially because of the potentially diverse nature of biochemical

reactions that can occur in the cytoplasm as compared to a diffusion restricted location such as the microtubule. However, statistically significant fold enrichments were also obtained between proteins in different cellular compartments that were difficult to reconcile as a consequence of experimental error rates. For example, proteins in the bud had significant chances of interacting with proteins in the cell periphery and the actin cytoskeleton in addition to bud localized proteins. Similarly, endosomal proteins had a significant chance of interacting with vacuolar proteins. Such observations establish the occurrence of dynamic protein interchanges between specific cellular compartments and underscores the importance of spatiotemporal studies as a means to understanding gene function in a cellular context.

Methods for protein localization prediction

Given the strong correlation of functional parameters with protein localization, considerable efforts have been made to enable computational prediction from other high throughput datasets. This is important for not only higher organisms such as the human proteome where systematic tagged libraries are not available, but even for systems like budding yeast where information regarding protein localization dynamics under different cellular states is relatively poor. Several predictors of protein localization have been employed. For instance, it is reasonable to expect high expression levels to be associated with cytosolic proteins and low expression levels with membrane and nuclear proteins [80, 81]. Other factors such as fluctuations of expression over time have also been used for predicting subcellular localization, with secreted proteins showing above average fluctuations while proteins in the secretory pathway but destined for the ER and golgi showing below average fluctuations. Briefly, one can estimate the probability of a protein in a particular compartment by multiplying its prior probability in that compartment with

the likelihood that it is localized to that compartment based on observations made about the protein [81]. These observations or ‘features’ could be clues such as nuclear localization signal sequences, expression levels, protein interaction partners or in fact any of the data that typically go into building an interaction network.

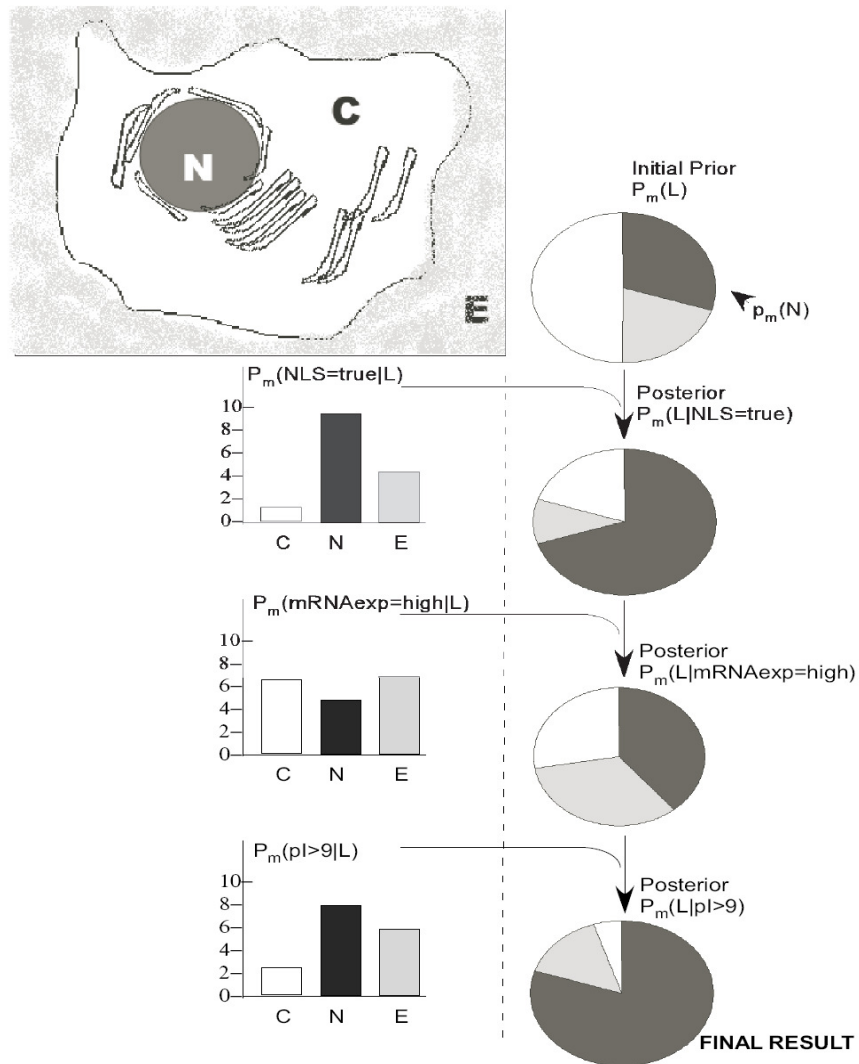


Figure 1-8: A schematic of steps involved in predicting protein localization using a Bayesian classifier. An initial prior probability is calculated for a protein of interest. Based on the properties of the protein, a posterior probability for its localization to a particular cellular compartment is arrived at.

An example of a Bayesian formalism adapted to predict protein localization is shown (**Figure 1-8**). At the onset, a prior probability of a protein ‘m’ being localized to any one of three compartments (for the sake of simplicity) is arrived at. Feature vectors that denote observations about a protein such as the presence of an NLS, its mRNA expression level or its isoelectric point are incorporated at each subsequent step to calculate the posterior probability depicted as the pie charts. The bar graphs on the left denote the probability of a feature being true given a particular localization. By adopting the proper training sets with good cross validation methods, prior probabilities, and feature vectors, one can ultimately derive the probability of finding a protein in different subcellular compartments.

Polarized cell growth pathways in yeast are an attractive model for conducting morphology and localization based studies. Therefore, in our quest toward characterizing spatiotemporal dynamics in a cell, I will focus the rest of the introduction in describing the major polarization states in yeast.

YEAST POLARIZATION STATES – A POWERFUL MODEL SYSTEM FOR THE STUDY OF SPATIO-TEMPORAL CONTROL

Mechanisms of polarization and polarized cell growth that dominate cellular life cycles essentially involve asymmetric growth from distinct regions in a cell resulting in a change in cellular structure and shape. Budding yeast *S.cerevisiae* is governed by complex polarization states that enable it to divide, mate, and forage for nutrients, and has therefore emerged as a powerful model system for studying mechanisms of eukaryotic cell polarity.

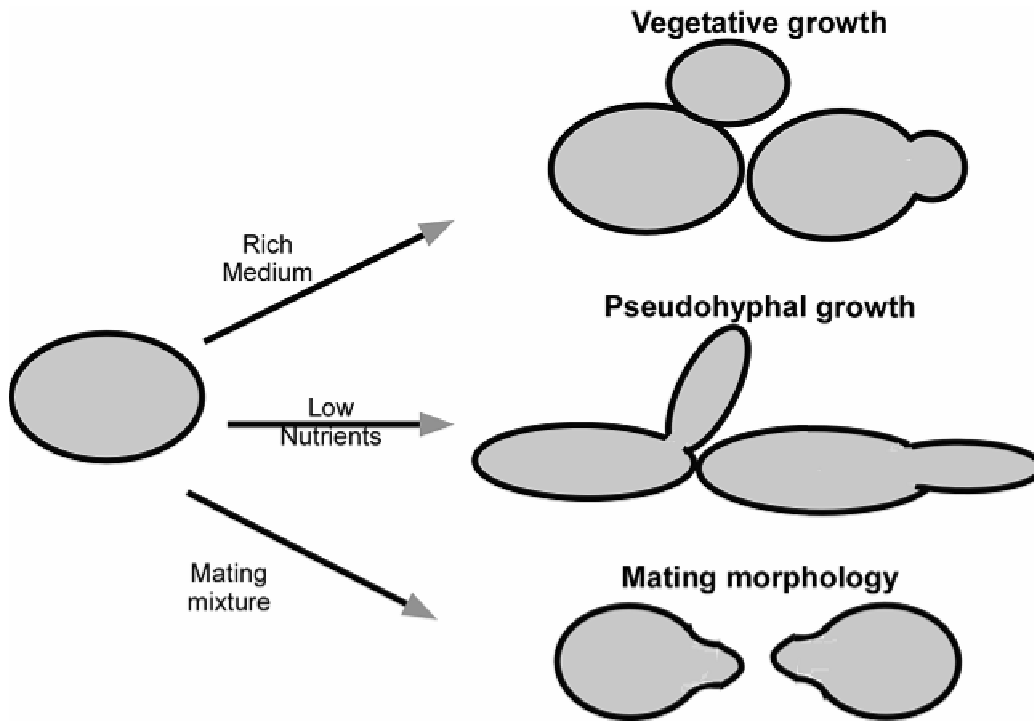


Figure 1-9: The three major polarization states in budding yeast.

The three major polarization states in budding yeast, *S.cerevisiae* are depicted (Figure 1-9). During conditions of nutrient abundance, yeast cells initiate polarized bud growth that then determines the axis of cell division [82]. Conditions of nutrient depletion elicit a second polarization state characterized by pseudohyphal growth having long filamentous processes presumably as a means to forage for nutrients. The ‘Shmoo’ morphology, another form of polarized growth is observed in mating mixtures that comprise the two opposite haploid yeast mating types and represents readiness to undergo mating. While budding and cell division are elicited through internal bud emergence cues, mating and pseudohyphal growth respond to external cues that signal the presence of a mating partner or nutrient starvation respectively. Despite the ability of yeast to tune its polarity based on specific stimuli, a common theme seems to ensue whereby a distinct site for growth on the cell surface is first chosen. Subsequently, the formation of a

polarity axis and re-alignment of the cytoskeleton coordinate trafficking of molecular cargo and membrane deposition to bring about a change in cellular structure and shape. I will now describe the basic molecular players in the formation and maintenance of polarization states using vegetative cell division as an example.

General mechanisms of generation of cell polarity

Yeast cells adopt a bipolar or an axial budding program based on their ploidy, with diploid yeast preferring the former and haploids the latter [83]. A rationale for this could be that an axial pattern in haploids facilitates the positioning of daughters in proximity and increase their chances of mating to form the more robust diploid due to a spontaneous switching of mating types. On the other hand, diploids prefer a distal site during bud site selection to extend the area of nutrient search, an extreme case of which occurs in the pseudohyphal growth mode that is adopted during starvation. A schematic of the events leading to the generation of polarity is shown in **figure 1-10**. In diploid yeast cells, Bud8p and Bud9p, cell surface transmembrane proteins define the machinery for bud assembly at the distal and the proximal poles respectively. Another cell surface protein Rax2p, required for bipolar budding over multiple generations, is positioned at both poles and is thought to stabilize Bud8p and Bud9p [84] dependent cues. On the other hand, axial budding that is the norm in haploid yeast cells relies on signals from the previous bud emergence point, specifically, a ring of septin filaments that remain associated at the bud neck throughout the cell cycle. In addition, proteins such as Axl2p/Bud10p, which is a cortical tag, protein appear also to be critical to the axial budding program, with disruption of these or any of the septin genes resulting in a reversion to the default bipolar budding pattern [82].

Establishment of an axis of polarity

Both bipolar and axial budding pathways merge to give rise to common sequence of events as shown in **figure 1-10**. Bud formation that starts after the G1/S transition involves polarization of the cytoskeleton, secretion and cell wall synthesis and is thought to occur in conjunction with bud site selection. A Ras related GTPase (Rsr1p), along with its GAP (Bud2p) and GEF (Bud5p), is recruited by spatial cues to the nascent bud emergence site, as is evidenced by the physical interaction of the cytoplasmic tail of Axl2p with Bud5p. The Rsr1 GTPase module interacts with Cdc42p, a conserved Rho GTPase whose importance towards the formation of an axis of polarity is underscored by the following. Unlike other previously mentioned proteins that were determinants of sites of polarity, an increased level of Cdc42-GTP through mutations or over-expression is alone sufficient to form an axis in conjunction with a polarized actin cytoskeleton, although this process occurs in a regulated fashion under normal conditions. Moreover, this suggests the existence of a positive feedback loop driving stochastic Cdc42p accumulation with polarization of actin filaments [85].

The centrality of Cdc42p is further emphasized by its interactions with numerous proteins that may function together in the establishment of a polarity axis. For example, the interaction of Cdc42p with the mammalian PAK protein kinase homologs, Ste20p and Cla4p, is thought to help direct its activity towards the sites of polarized cell growth. Cdc24p, that functions as the GEF for Cdc42p, and Bem1p are also positioned at the incipient bud site to direct formation of a polarization axis [86]. Similarly, proteins such as Bem3p and Rga1/2p, which are RhoGAP homologs, as well as Gic1/2p appear associated with Cdc42p at the bud tip. The control of the timing and the stochastic components associated with these events is however the subject of intense scrutiny.

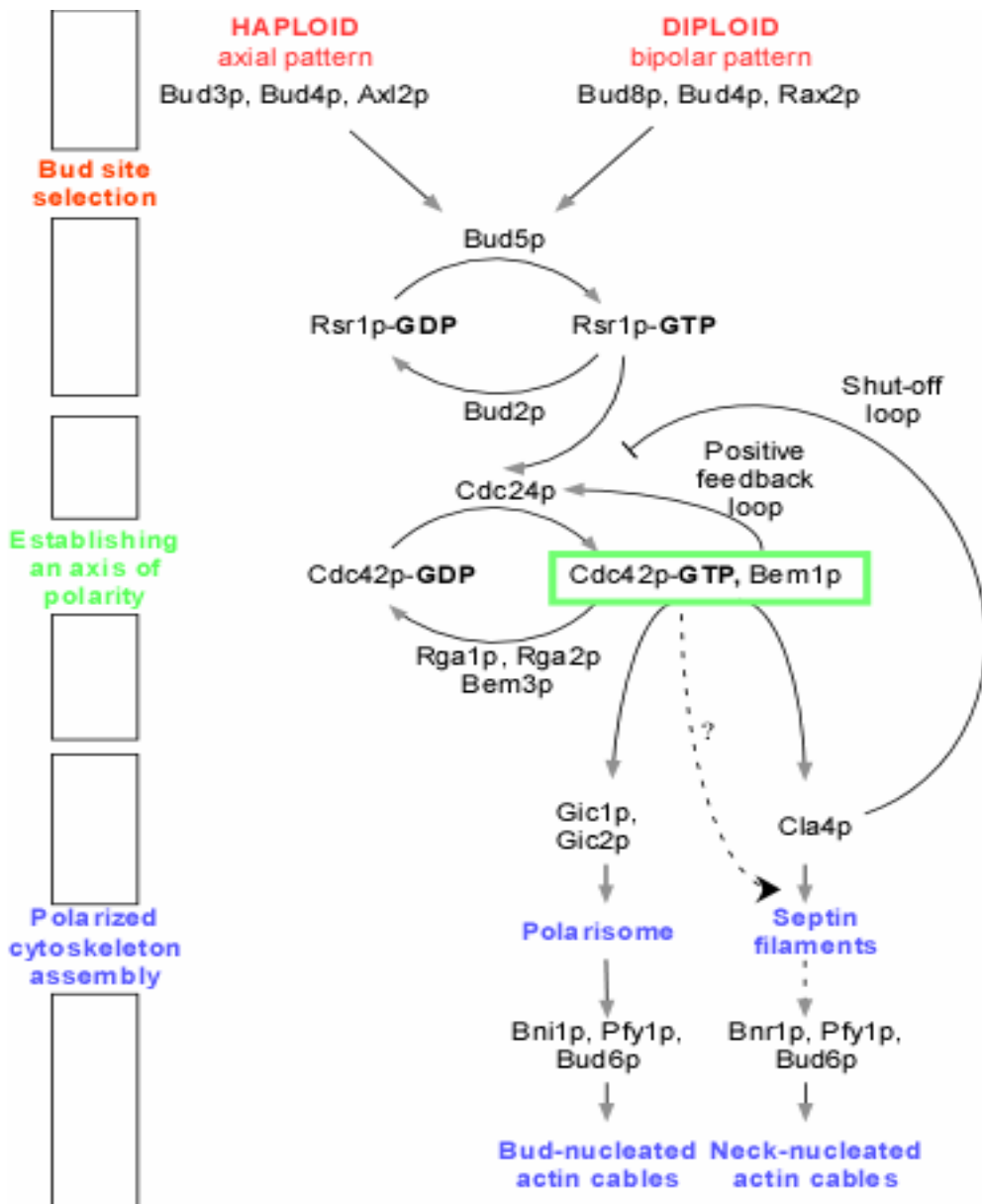


Figure 1-10: Signaling events during polarized growth in budding yeast. After budding cues are sensed, an axis of polarity is established with the activation of Cdc42-GTP. Subsequently, a polarized actin cytoskeleton is assembled culminating in successful polarized growth.

In haploids, Cdc24p is sequestered in the nucleus until G1, and is thought to preclude bud initiation before late G1 while the Cdc42p PAK, Cla4p phosphorylates and inactivates Cdc24p after bud emergence, thus limiting its window of activity. Cdc42p is

primarily responsible for initiating localization of septins and formins, which can then direct assembly of polarized actin cables.

Role of the cytoskeleton in polarity

Two of the major cytoskeletal systems, actins and septins, are critical for establishment and maintenance of cellular polarity through their interactions with a host of proteins. Actin is essential for any form of polarized growth and exists in two forms – actin patches that localize primarily at the bud and actin cables that run longitudinally along the length of the cell and often intersect actin patches at their ends [82, 86]. Actin patches may represent sites of membrane deposition and cell wall assembly, as is evidenced by cell wall defects at the restrictive temperature in strains harboring temperature-sensitive actin mutants. Dynamic actin cables representing another form of actin function as tracks along which cargo destined to the polarization tip is directed. Cables are formed by polymerization of Act1p, F-actin cross linking proteins- Fimbrin (Sac6p) and Abp140 and two tropomyosin isoforms Tpm1p and Tpm2p.

Nucleation of actin filaments is aided by another class of conserved proteins called Formins. Budding yeast formins constitute the Bni1p (Bud neck interactor) and Bnr1p (Bni1p-related) proteins, each having N-terminal Rho GTPase binding sites and the C-terminally conserved formin homology domains FH1 and FH2. These two domains are sufficient to nucleate actin filament assembly with conditional mutations in either formin protein, leading to rapid loss of actin cables. Bni1p is positioned at the bud neck by interactions with Spa2p and Bud6p, components of the polarisome complex, while Bnr1p is dependent on septin proteins for localization at the neck [82, 86]. The localization of Bni1p and the polarisome components is initially dependent on Cdc42p.

The septin ring, among the first to initiate assembly of a polarized actin cytoskeleton, is represented by five proteins that are co-expressed during vegetative growth in *S.cerevisiae*: Cdc3p, Cdc10p, Cdc11p, Cdc12p and Shs1p [87]. The septin structure at the mother-bud neck junction plays crucial roles in bud assembly and cytokinesis and is postulated to switch from a more dynamic ring state before cell cycle entry to the stable hourglass structure during bud emergence. As mentioned, Cdc42p directly and indirectly influences the localization and activation of septins and formins, in addition to other protein players, thus tying the formation of a polarization framework in time and space.

Mechanisms of transport of polarized cargo

Polarized secretion and transport of cargo, such as organelles destined to be segregated to the daughter, and cell wall constituents intended towards bud growth, is effected by an elaborate mechanism involving two classes of actin binding proteins – myosins and cofilin (**Figure 1-11**). Cofilin regulates actin depolymerization and therefore its dynamics. There are five types of myosins in yeast – Myo1p through Myo5p, of which Myo1p is involved in proper cytokinesis, while Myo3p and Myo5p are involved in proper polarization of the cytoskeleton and endocytosis [82, 86].

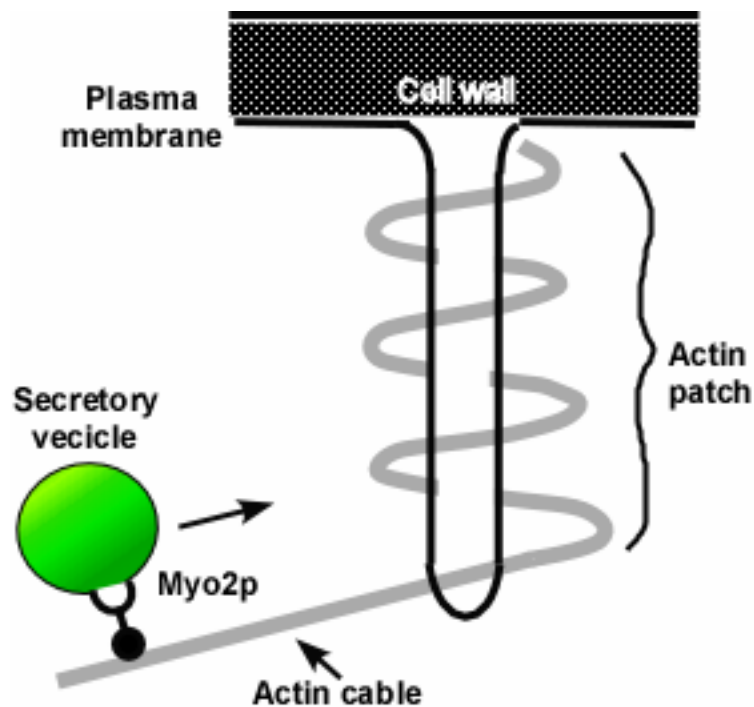


Figure 1-11: A schematic of the transport of secretory vesicles along actin cables.

Actin filaments are stabilized by tropomyosin and cross-linked by fimbrin to generate cables. Myo2p and other myosin motors may move along them and deliver cargo to actin patches that are sites of plasma membrane invaginations.

Myosin type V homologs, Myo2p and Myo4p are thought to serve as the actin-based motors that translocate secretory vesicles to growth sites. Myo2p, for example mediates polarized recruitment to the growth tip of post-golgi secretory vesicles that are ‘marked’ by Sec4p, a rab family GTPase suggesting that the Myo2p-Sec4p interaction may be important in cargo selection. Many aspects of the Myosin V function as the cargo selection of Myo2p and Myo4p and their separation in cell cycle time and space need to be understood, as well as the Myo V docking receptors for all the different organelles. Docking of the vesicles at the plasma membrane is mediated by an eight subunit protein complex called the exocyst. At least two components of the exocyst, Exo70p and Sec3p, are regulated by multiple rho proteins, including Cdc42p, further underscoring the

intimate connection established between the several components in the polarization process.

Polarized cell growth during the mating response

Pheromone sensing and signal transduction

Having seen the basic pathways that operate to lay down the polarization framework during budding, we will now examine the events involved in setting the scene during the mating process [88, 89]. One of the most fascinating morphological changes that a yeast cell undergoes occurs during the process of mating of two haploids to form a diploid. I will briefly introduce the molecular events that trigger and regulate the formation of the ‘shmoo’ morphology and the cellular events accompanying it, the subject of two chapters in my dissertation.

Axial budding cues such as Axl2p are overridden during pheromone sensing, as a result of which the cell is able to orient itself towards the pheromone gradient. This ‘erasing’ of axial bud positional information is brought about by the C-terminal region of Far1p. The N-terminal region of Far1p additionally serves to inhibit the Cln1p and Cln2p cyclin complexes that drive cell cycle through G1 phase, thereby resulting in pheromone induced growth arrest.

Upon sensing the pheromone gradient and formation of a cortical landmark adjacent to a potential mating partner, a similar although not identical sequence of events to budding occur leading to the recruitment of polarity establishment proteins at the site to initiate projection formation. Genetic and biochemical evidence suggest the formation of a multi-protein complex that coordinates signal transduction with polarized growth. Pheromone binding to the G-protein coupled receptor triggers the release of G $\beta\gamma$ (Ste4p-

Ste18p) subunits from the inhibitory G α Gpa1p subunit so that the G-protein initiated signal is then transmitted and amplified via multiple effectors that interact with the released G $\beta\gamma$ subunits (Figure 1-12).

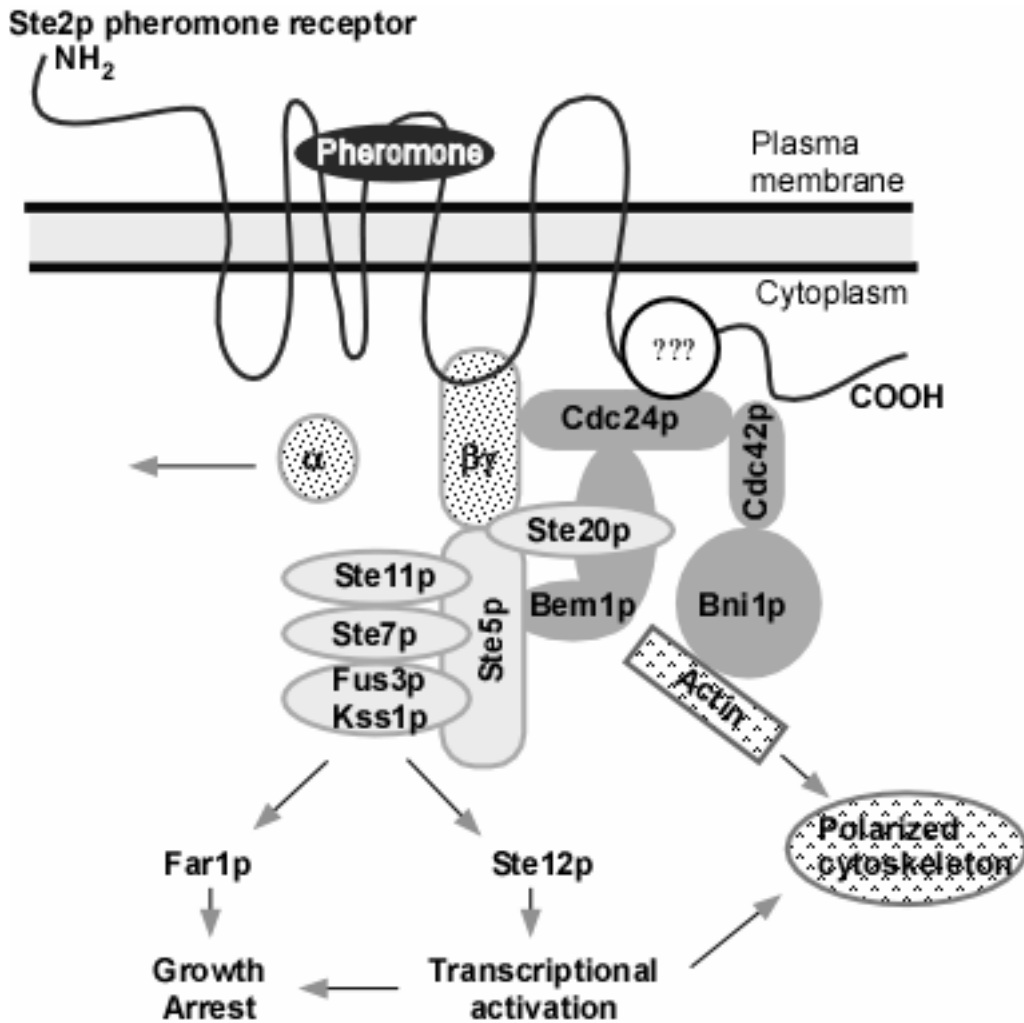


Figure 1-12: Model for the establishment of pheromone-induced polarized growth. Binding of pheromone to its receptor triggers a mitogen-activated protein kinase pathway that culminates in the transcriptional activation of several genes, cell cycle arrest and mating projection formation at the site of highest pheromone concentration. The C-terminal domain of the receptor may be involved in coupling the polarization machinery with the pheromone signaling proteins (black).

A G $\beta\gamma$ effector that is critical for mating is Cdc24p, a GEF for Cdc42p Rho GTPase also involved as described during budding. Far1p, which functions in overriding the budding cues, appears to act as the scaffold mediating the interaction of Cdc24p with G $\beta\gamma$. In the absence of pheromone, Far1p, a nucleocytoplasmic shuttle protein, sequesters Cdc24p largely in the nucleus, whereas upon pheromone exposure, nuclear export predominates causing the accumulation of Cdc24p in the cytosol [90]. Genetic and biochemical evidence implicate the pheromone dependent interaction of Ste4p with both Ste20p and Ste5p, two proteins that participate in connecting the mating MAP kinase signaling pathway with the polarization process. Ste20p functions during mating to activate the Fus3p/Kss1p MAPK signaling module in addition to its interactions with Cdc42p as a PAK.

Budding and Mating – A sharing of the polarization machinery?

It is not surprising that many components required for bud formation are also important for mating projection formation (**Figure 1-13**). Membrane vesicles and actin patches accumulate at the projection tip as happens during cell division in vegetatively growing cells. Protein such as Bem1p, Spa2p, Bni1p and Bud6p, involved in the initial polarization events, are localized at both the bud and the ‘shmoo’ tips. Mutations in actin and in the signaling proteins involved in polarization cause defects in projection formation and morphology.

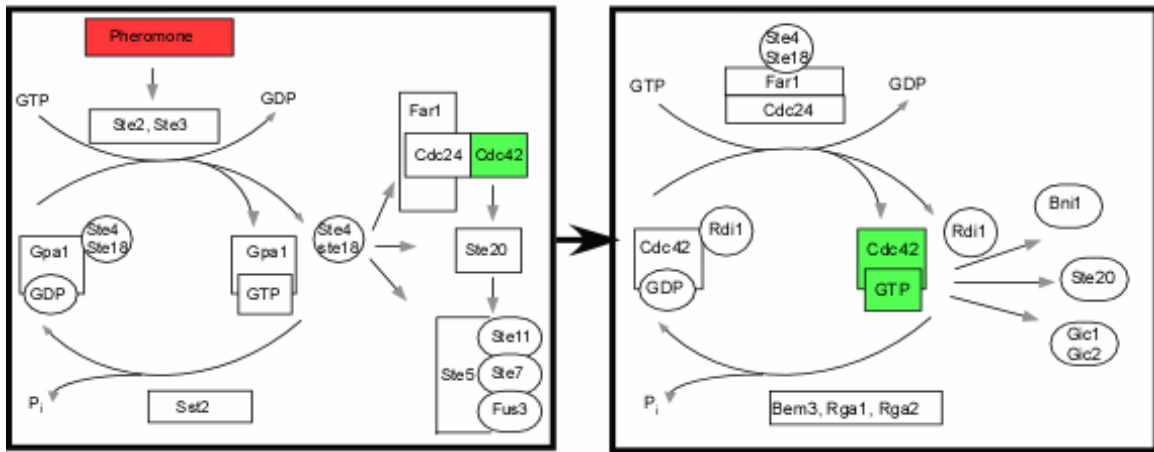


Figure 1-13: Shared signaling proteins in budding and pheromone induced ‘shmooing’. Cdc42p-GTP is a shared effector in both pheromone response and budding as indicated by the same downstream machinery involved in both processes.

A telling study conducted by Baba et al. [91] revealed large-scale organization of organelles along the polarization axis upon pheromone exposure. Three dimensional reconstructions of electron micrographs of alpha factor treated *Mat ‘a’* yeast cells showed dynamic structural reorganization of intracellular structures. For example, vesicles dispersed throughout the cell at the onset accumulated at the site of projection formation after pheromone treatment, along with a re-orientation of the golgi apparatus towards the newly formed polarization axis. Other organelles such as the nucleus and rough endoplasmic reticulum also exhibited similar changes in anticipation of mating.

SPECIFIC AIMS

We have seen that polarization is a ubiquitous phenomenon affecting several developmental events in budding yeast and therefore presents a model of choice for studying spatiotemporal dynamics. In addition, systematic high-throughput screens for

which yeast is amenable can give us a systems level understanding of cellular pathways and gene function. With these goals in mind, we propose,

- 1) To develop a high-throughput imaging technique for systematically evaluating the morphological change that accompanies pheromone treatment in a library of yeast deletions.
- 2) To apply such a technique to a library of yeast GFP tagged gene fusions and identify the complement of proteins that localize to the mating or the 'shmoo' tip.

As explained in Chapter 4, the proteome in response to nutrient deprivation presents interesting challenges. Therefore, as an extension of the high throughput imaging screen that we developed, my third specific aim, is

- 3) To study the dynamics of the stationary phase proteome in budding yeast especially as it pertains to proteins in the cytoplasm.

REFERENCES

1. Schena, M., *Genome analysis with gene expression microarrays*. Bioessays, 1996. **18**(5): p. 427-31.
2. DeRisi, J.L., V.R. Iyer, and P.O. Brown, *Exploring the metabolic and genetic control of gene expression on a genomic scale*. Science, 1997. **278**(5338): p. 680-6.
3. Duffield, G.E., *DNA microarray analyses of circadian timing: the genomic basis of biological time*. J Neuroendocrinol, 2003. **15**(10): p. 991-1002.
4. Alter, O., *Genomic signal processing: from matrix algebra to genetic networks*. Methods Mol Biol, 2007. **377**: p. 17-60.
5. Giaever, G., et al., *Chemogenomic profiling: identifying the functional interactions of small molecules in yeast*. Proc Natl Acad Sci U S A, 2004. **101**(3): p. 793-8.
6. Frayling, T.M. and M.I. McCarthy, *Genetic studies of diabetes following the advent of the genome-wide association study: where do we go from here?* Diabetologia, 2007. **50**(11): p. 2229-33.
7. Frayling, T.M., *Genome-wide association studies provide new insights into type 2 diabetes aetiology*. Nat Rev Genet, 2007. **8**(9): p. 657-62.

8. Smith, L.T., G.A. Otterson, and C. Plass, *Unraveling the epigenetic code of cancer for therapy*. Trends Genet, 2007. **23**(9): p. 449-56.
9. Bentley, D.R., *Whole-genome re-sequencing*. Curr Opin Genet Dev, 2006. **16**(6): p. 545-52.
10. Woll, D., et al., *More efficient photolithographic synthesis of DNA-chips by photosensitization*. Nucleosides Nucleotides Nucleic Acids, 2003. **22**(5-8): p. 1395-8.
11. Nuwaysir, E.F., et al., *Gene expression analysis using oligonucleotide arrays produced by maskless photolithography*. Genome Res, 2002. **12**(11): p. 1749-55.
12. Dalma-Weiszhausz, D.D., et al., *The affymetrix GeneChip platform: an overview*. Methods Enzymol, 2006. **410**: p. 3-28.
13. Birney, E., et al., *Identification and analysis of functional elements in 1% of the human genome by the ENCODE pilot project*. Nature, 2007. **447**(7146): p. 799-816.
14. Beltran, A., et al., *Interrogating genomes with combinatorial artificial transcription factor libraries: asking zinc finger questions*. Assay Drug Dev Technol, 2006. **4**(3): p. 317-31.
15. Zhu, H., M. Bilgin, and M. Snyder, *Proteomics*. Annu Rev Biochem, 2003. **72**: p. 783-812.
16. Lu, P., et al., *Absolute protein expression profiling estimates the relative contributions of transcriptional and translational regulation*. Nat Biotechnol, 2007. **25**(1): p. 117-24.
17. Mallick, P., et al., *Computational prediction of proteotypic peptides for quantitative proteomics*. Nat Biotechnol, 2007. **25**(1): p. 125-31.
18. Krogan, N.J., et al., *Global landscape of protein complexes in the yeast *Saccharomyces cerevisiae**. Nature, 2006. **440**(7084): p. 637-43.
19. Gavin, A.C., et al., *Functional organization of the yeast proteome by systematic analysis of protein complexes*. Nature, 2002. **415**(6868): p. 141-7.
20. Gavin, A.C., et al., *Proteome survey reveals modularity of the yeast cell machinery*. Nature, 2006. **440**(7084): p. 631-6.
21. Collins, S.R., et al., *Toward a comprehensive atlas of the physical interactome of *Saccharomyces cerevisiae**. Mol Cell Proteomics, 2007. **6**(3): p. 439-50.
22. Guo, Y., et al., *In silico and in vitro pharmacogenetic analysis in mice*. Proc Natl Acad Sci U S A, 2007. **104**(45): p. 17735-40.
23. Hu, S., J.A. Loo, and D.T. Wong, *Human saliva proteome analysis and disease biomarker discovery*. Expert Rev Proteomics, 2007. **4**(4): p. 531-8.
24. Bergeron, J.J. and M. Hallett, *Peptides you can count on*. Nat Biotechnol, 2007. **25**(1): p. 61-2.
25. Zhou, L., et al., *Phenotype microarray analysis of *Escherichia coli* K-12 mutants with deletions of all two-component systems*. J Bacteriol, 2003. **185**(16): p. 4956-72.
26. Bochner, B.R., *New technologies to assess genotype-phenotype relationships*. Nat Rev Genet, 2003. **4**(4): p. 309-14.

27. Fernandez-Ricaud, L., et al., *PROPHECY--a database for high-resolution phenomics*. Nucleic Acids Res, 2005. **33**(Database issue): p. D369-73.
28. Phizicky, E., et al., *Protein analysis on a proteomic scale*. Nature, 2003. **422**(6928): p. 208-15.
29. Huang, J., et al., *Finding new components of the target of rapamycin (TOR) signaling network through chemical genetics and proteome chips*. Proc Natl Acad Sci U S A, 2004. **101**(47): p. 16594-9.
30. Ray, S., et al., *Classification and prediction of clinical Alzheimer's diagnosis based on plasma signaling proteins*. Nat Med, 2007. **13**(11): p. 1359-62.
31. Ziauddin, J. and D.M. Sabatini, *Microarrays of cells expressing defined cDNAs*. Nature, 2001. **411**(6833): p. 107-10.
32. Wu, R.Z., S.N. Bailey, and D.M. Sabatini, *Cell-biological applications of transfected-cell microarrays*. Trends Cell Biol, 2002. **12**(10): p. 485-8.
33. Wheeler, D.B., A.E. Carpenter, and D.M. Sabatini, *Cell microarrays and RNA interference chip away at gene function*. Nat Genet, 2005. **37** Suppl: p. S25-30.
34. Wheeler, D.B., et al., *RNAi living-cell microarrays for loss-of-function screens in Drosophila melanogaster cells*. Nat Methods, 2004. **1**(2): p. 127-32.
35. Bailey, S.N., et al., *Microarrays of lentiviruses for gene function screens in immortalized and primary cells*. Nat Methods, 2006. **3**(2): p. 117-22.
36. Bailey, S.N., R.Z. Wu, and D.M. Sabatini, *Applications of transfected cell microarrays in high-throughput drug discovery*. Drug Discov Today, 2002. **7**(18 Suppl): p. S113-8.
37. Bailey, S.N., D.M. Sabatini, and B.R. Stockwell, *Microarrays of small molecules embedded in biodegradable polymers for use in mammalian cell-based screens*. Proc Natl Acad Sci U S A, 2004. **101**(46): p. 16144-9.
38. Harder, N., R. Eils, and K. Rohr, *Automated classification of mitotic phenotypes of human cells using fluorescent proteins*. Methods Cell Biol, 2008. **85**: p. 539-54.
39. Wollman, R. and N. Stuurman, *High throughput microscopy: from raw images to discoveries*. J Cell Sci, 2007. **120**(Pt 21): p. 3715-22.
40. Lamprecht, M.R., D.M. Sabatini, and A.E. Carpenter, *CellProfiler: free, versatile software for automated biological image analysis*. Biotechniques, 2007. **42**(1): p. 71-5.
41. Bakal, C., et al., *Quantitative morphological signatures define local signaling networks regulating cell morphology*. Science, 2007. **316**(5832): p. 1753-6.
42. Zhao, T. and R.F. Murphy, *Automated learning of generative models for subcellular location: Building blocks for systems biology*. Cytometry A, 2007. **71**(12): p. 978-90.
43. Garcia Osuna, E. and R.F. Murphy, *Automated, systematic determination of protein subcellular location using fluorescence microscopy*. Subcell Biochem, 2007. **43**: p. 263-76.
44. Chen, S.C., et al., *Automated image analysis of protein localization in budding yeast*. Bioinformatics, 2007. **23**(13): p. i66-71.
45. Huh, W.K., et al., *Global analysis of protein localization in budding yeast*. Nature, 2003. **425**(6959): p. 686-91.

46. Ghaemmaghani, S., et al., *Global analysis of protein expression in yeast*. Nature, 2003. **425**(6959): p. 737-41.
47. Giaever, G., et al., *Functional profiling of the *Saccharomyces cerevisiae* genome*. Nature, 2002. **418**(6896): p. 387-91.
48. Mnaimneh, S., et al., *Exploration of essential gene functions via titratable promoter alleles*. Cell, 2004. **118**(1): p. 31-44.
49. Ito, T., T. Chiba, and M. Yoshida, *Exploring the protein interactome using comprehensive two-hybrid projects*. Trends Biotechnol, 2001. **19**(10 Suppl): p. S23-7.
50. Cagney, G., P. Uetz, and S. Fields, *High-throughput screening for protein-protein interactions using two-hybrid assay*. Methods Enzymol, 2000. **328**: p. 3-14.
51. Tong, A.H. and C. Boone, *Synthetic genetic array analysis in *Saccharomyces cerevisiae**. Methods Mol Biol, 2006. **313**: p. 171-92.
52. Bader, G.D., et al., *Functional genomics and proteomics: charting a multidimensional map of the yeast cell*. Trends Cell Biol, 2003. **13**(7): p. 344-56.
53. Fraser, A.G. and E.M. Marcotte, *A probabilistic view of gene function*. Nat Genet, 2004. **36**(6): p. 559-64.
54. Fraser, A.G. and E.M. Marcotte, *Development through the eyes of functional genomics*. Curr Opin Genet Dev, 2004. **14**(4): p. 336-42.
55. Bork, P., et al., *Protein interaction networks from yeast to human*. Curr Opin Struct Biol, 2004. **14**(3): p. 292-9.
56. Lee, I., et al., *A probabilistic functional network of yeast genes*. Science, 2004. **306**(5701): p. 1555-8.
57. Jiang, T. and A.E. Keating, *AVID: an integrative framework for discovering functional relationships among proteins*. BMC Bioinformatics, 2005. **6**: p. 136.
58. Troyanskaya, O.G., et al., *A Bayesian framework for combining heterogeneous data sources for gene function prediction (in *Saccharomyces cerevisiae*)*. Proc Natl Acad Sci U S A, 2003. **100**(14): p. 8348-53.
59. Jansen, R., et al., *A Bayesian networks approach for predicting protein-protein interactions from genomic data*. Science, 2003. **302**(5644): p. 449-53.
60. Mellor, J.C., et al., *Predictome: a database of putative functional links between proteins*. Nucleic Acids Res, 2002. **30**(1): p. 306-9.
61. von Mering, C., et al., *STRING: known and predicted protein-protein associations, integrated and transferred across organisms*. Nucleic Acids Res, 2005. **33**(Database issue): p. D433-7.
62. Combs, D.J., et al., *Prp43p is a DEAH-box spliceosome disassembly factor essential for ribosome biogenesis*. Mol Cell Biol, 2006. **26**(2): p. 523-34.
63. Martin, A., S. Schneider, and B. Schwer, *Prp43 is an essential RNA-dependent ATPase required for release of lariat-intron from the spliceosome*. J Biol Chem, 2002. **277**(20): p. 17743-50.
64. McGary, K.L., I. Lee, and E.M. Marcotte, *Broad network-based predictability of *S. cerevisiae* gene loss-of-function phenotypes*. Genome Biol, 2007. **8**(12): p. R258.
65. Zhang, J., et al., *Genomic scale mutant hunt identifies cell size homeostasis genes in *S. cerevisiae**. Curr Biol, 2002. **12**(23): p. 1992-2001.

66. Schneider, B.L., et al., *Growth rate and cell size modulate the synthesis of, and requirement for, G1-phase cyclins at start.* Mol Cell Biol, 2004. **24**(24): p. 10802-13.
67. Jorgensen, P., et al., *The size of the nucleus increases as yeast cells grow.* Mol Biol Cell, 2007. **18**(9): p. 3523-32.
68. Cook, M. and M. Tyers, *Size control goes global.* Curr Opin Biotechnol, 2007. **18**(4): p. 341-50.
69. Fingerman, I., et al., *Sfp1 plays a key role in yeast ribosome biogenesis.* Eukaryot Cell, 2003. **2**(5): p. 1061-8.
70. Cipollina, C., et al., *Revisiting the role of yeast Sfp1 in ribosome biogenesis and cell size control: a chemostat study.* Microbiology, 2008. **154**(Pt 1): p. 337-46.
71. Saito, T.L., et al., *Data mining tools for the Saccharomyces cerevisiae morphological database.* Nucleic Acids Res, 2005. **33**(Web Server issue): p. W753-7.
72. Saito, T.L., et al., *SCMD: Saccharomyces cerevisiae Morphological Database.* Nucleic Acids Res, 2004. **32**(Database issue): p. D319-22.
73. Ohya, Y., et al., *High-dimensional and large-scale phenotyping of yeast mutants.* Proc Natl Acad Sci U S A, 2005. **102**(52): p. 19015-20.
74. Singer, R.H., *RNA localization: visualization in real-time.* Curr Biol, 2003. **13**(17): p. R673-5.
75. Kumar, A., et al., *Subcellular localization of the yeast proteome.* Genes Dev, 2002. **16**(6): p. 707-19.
76. Jarvik, J.W., et al., *In vivo functional proteomics: mammalian genome annotation using CD-tagging.* Biotechniques, 2002. **33**(4): p. 852-4, 856, 858-60 passim.
77. Hoffmann, C., et al., *A FIAsh-based FRET approach to determine G protein-coupled receptor activation in living cells.* Nat Methods, 2005. **2**(3): p. 171-6.
78. Matsuyama, A., et al., *ORFeome cloning and global analysis of protein localization in the fission yeast Schizosaccharomyces pombe.* Nat Biotechnol, 2006. **24**(7): p. 841-7.
79. Remy, I., F.X. Campbell-Valois, and S.W. Michnick, *Detection of protein-protein interactions using a simple survival protein-fragment complementation assay based on the enzyme dihydrofolate reductase.* Nat Protoc, 2007. **2**(9): p. 2120-5.
80. Drawid, A., R. Jansen, and M. Gerstein, *Genome-wide analysis relating expression level with protein subcellular localization.* Trends Genet, 2000. **16**(10): p. 426-30.
81. Drawid, A. and M. Gerstein, *A Bayesian system integrating expression data with sequence patterns for localizing proteins: comprehensive application to the yeast genome.* J Mol Biol, 2000. **301**(4): p. 1059-75.
82. Madden, K. and M. Snyder, *Cell polarity and morphogenesis in budding yeast.* Annu Rev Microbiol, 1998. **52**: p. 687-744.
83. Pruyne, D. and A. Bretscher, *Polarization of cell growth in yeast.* J Cell Sci, 2000. **113** (Pt 4): p. 571-85.
84. Fujita, A., et al., *Rax1, a protein required for the establishment of the bipolar budding pattern in yeast.* Gene, 2004. **327**(2): p. 161-9.

85. Pruyne, D. and A. Bretscher, *Polarization of cell growth in yeast. I. Establishment and maintenance of polarity states*. J Cell Sci, 2000. **113 (Pt 3)**: p. 365-75.
86. Pruyne, D., et al., *Mechanisms of polarized growth and organelle segregation in yeast*. Annu Rev Cell Dev Biol, 2004. **20**: p. 559-91.
87. Iwase, M., et al., *Role of a Cdc42p effector pathway in recruitment of the yeast septins to the presumptive bud site*. Mol Biol Cell, 2006. **17(3)**: p. 1110-25.
88. Dohlman, H.G. and J.E. Slessareva, *Pheromone signaling pathways in yeast*. Sci STKE, 2006. **2006(364)**: p. cm6.
89. Dohlman, H.G., *G proteins and pheromone signaling*. Annu Rev Physiol, 2002. **64**: p. 129-52.
90. Dohlman, H.G. and J.W. Thorner, *Regulation of G protein-initiated signal transduction in yeast: paradigms and principles*. Annu Rev Biochem, 2001. **70**: p. 703-54.
91. Baba, M., et al., *Three-dimensional analysis of morphogenesis induced by mating pheromone alpha factor in Saccharomyces cerevisiae*. J Cell Sci, 1989. **94 (Pt 2)**: p. 207-16.

Chapter 2: Systematic profiling of cellular phenotypes with spotted cell microarrays reveals new mating-pheromone response genes.

INTRODUCTION

In this chapter, we describe a technology for measuring cell morphology and subcellular localization phenotypes, applied to a model system in which yeast change morphology in response to mating pheromone [92, 93]. Wild-type haploid yeast cells, on detecting pheromone of the opposite mating type via a cell surface receptor, heterotrimeric G protein, and mitogen-activated protein (MAP) kinase-mediated signal transduction cascade, arrest their cell cycles in G1 phase and grow in a polarized fashion towards the pheromone secreting cells, forming a characteristic cell shape termed a 'shmoo' [90]. Several hundred genes change expression during this process [94]. Shmoos of opposite mating type fuse, producing a diploid organism. The pheromone-response MAP kinase cascade is broadly conserved across eukaryotes, yet characterization of even this canonical signal transduction pathway is incomplete. Here, we describe the development of spotted cell microarrays and their application in defining genes controlling the response of yeast cells to mating pheromone.

We developed spotted cell microarrays for highly parallel, high-throughput analyses of cell phenotypes, complementing efforts for assessing cell growth and morphology [25, 72, 95-99], protein expression levels [46, 96, 100, 101], and imaging of tissues [102] and single cells [103]. Spotted cell microarrays are distinct from transfected cell microarrays [31, 104, 105] or RNA interference (RNAi) microarrays [106], in which mammalian cells are cultured over a microarray spotted with defined DNAs, allowing transfection of the overgrown cells with different clones. Instead, spotted cell microarrays

are made by contact deposition of suspensions of cells from an arrayed library onto coated glass slides

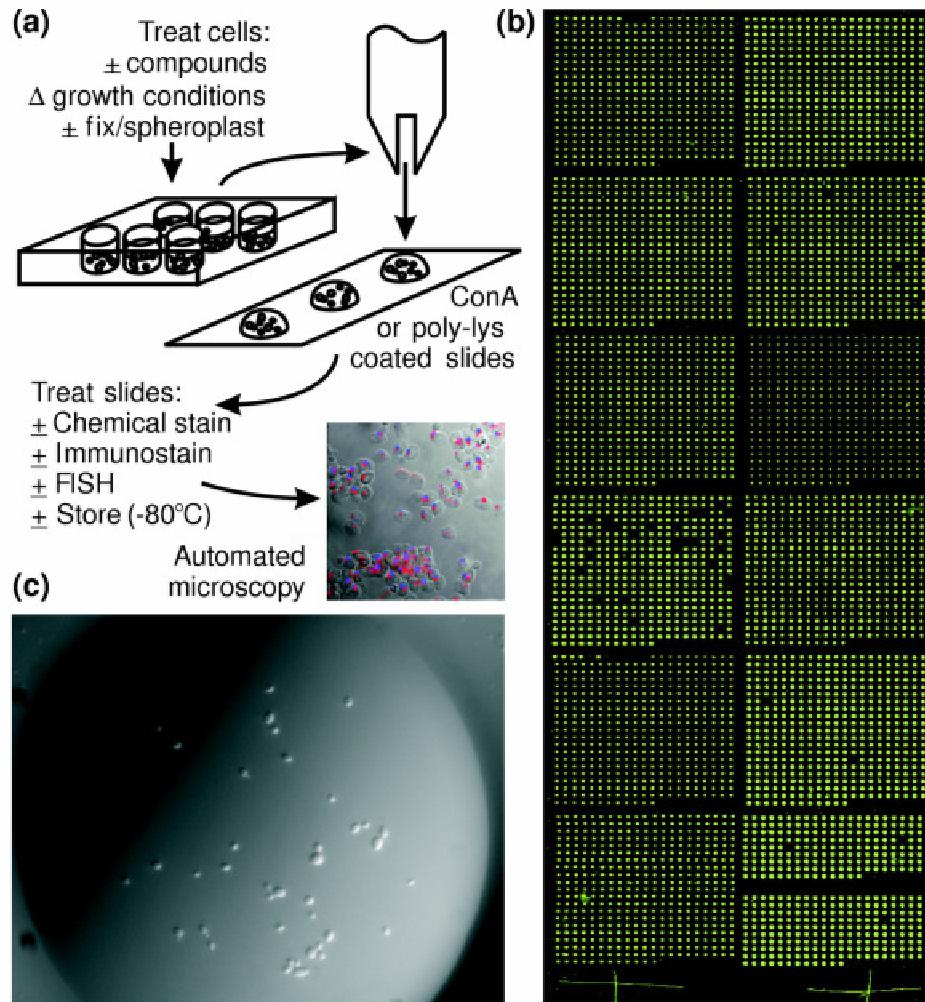


Figure 2-1 An overview of spotted cell microarrays. (a) Cell chips are constructed using slotted steel pins to print cells robotically from 96-well plates onto poly-L-lysine or Con A/Mn²⁺/Ca²⁺-coated glass slides. The sample image shows arrayed yeast cells immunostained for tubulin using fluorescein isothiocyanate (FITC)-conjugated-goat anti-rat IgG/rat anti- α -tubulin (red), overlaid on a bright field image and a DAPI-stained image (blue) of the cells' nuclei. FISH, fluorescence in situ hybridization. (b) Wide-field light scattering image of a cell microarray (approximately 2 cm \times 6 cm) containing around 4,800 viable, haploid yeast deletion strains. The bright dots arise from light scattered when scanning the array with a Genepix DNA microarray scanner. Spots are around 200 μ m in diameter, separated by 410 μ m. (c) Close-up of a typical spot from the microarray showing distinct cells at 40 \times magnification. This image was taken immediately after printing, so growth medium (YPD, 17% glycerol, 200 mg/l G418) is still visible.

using a microarray robot (**Figure 2-1**). Printing cells directly allows cells of different genetic backgrounds to be arrayed, taking advantage of strain collections such as the set of around 4,800 haploid yeast deletion strains (in which each strain lacks the coding sequence of a single gene).

High-density cell microarrays, with each spot containing cells from a distinct deletion strain and all of the strains represented on a single microscope slide, simplify automated image collection and minimize reagent use when probing the cells. With this approach, a single cellular feature can be examined in all approximately 4,800 genetic backgrounds, identifying genes contributing to that feature, associating genes with specific phenotypes, and providing information about spatial structures controlled by the genes. We have successfully created cell chips from 4,848 yeast deletion strains, automated collection of around 20,000 microscope images per cell chip, constructed the initial computational infrastructure to support the microscopy, and used cell chips to screen for genes affecting normal cellular morphology and for genes affecting the response of yeast to mating pheromone.

RESULTS

A high-throughput screen of yeast cellular morphology

Cells from each of the 4,848 distinct haploid yeast deletion strains, grown in rich media (YPD), were printed onto glass microscope slides coated with poly-L-lysine or concanavalin A (ConA) using a custom-built high-speed robotic arrayer that is normally used to manufacture DNA microarrays [2]. **Figure 2-1b** shows an image of a cell microarray printed using this methodology. Each spot normally contains around 20-40 cells from a single deletion strain, as seen in **Figure 2-1c** using a standard microscope.

Our preliminary data indicate that arrayed cells remain viable and physiologically normal after printing and washing, although cells are typically fixed for imaging purposes. A cell chip is analyzed using an automated fluorescence microscope to sequentially autofocus and image each spot.

As an initial proof-of-concept, we first performed genome-wide differential interference contrast (DIC) imaging to examine the effects of deleting each yeast gene on basic aspects of cellular morphology such as cell shape, size, budding pattern and clumping, from which we expected to find genes controlling fundamental cell growth processes. Systematic analysis of the haploid yeast deletion strain phenotypes on two slides (around 10,000 images) reveals that about 2,000 of the 4,848 strains exhibited atypical morphologies of varying degree. Two independent graders manually assigned numerical scores to phenotypes by severity, penetrance in the population, and type (large, small, elongated, round, and clumped [47], as well as polarized bud growth and pseudohyphal-like morphology). Control experiments were performed by constructing cell chips from known morphology mutants and wild-type strains, and grading these in the same grading scheme. Of these deletion strains, 381 (8%) were considered to have severe morphology defects (**Figure 2-2**) to a degree considered significant in the control experiments, with an estimated precision of 82% and recall of 26% [107].

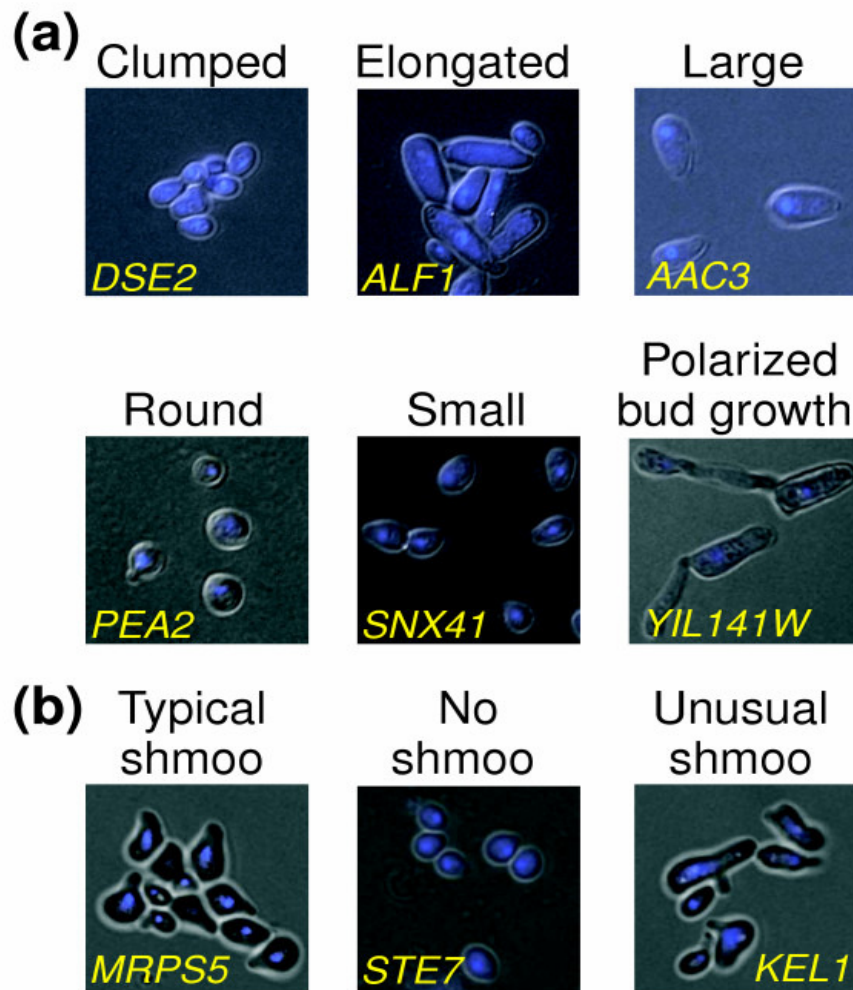


Figure 2-2: Characteristic yeast cell phenotypes observed on arrays. DIC images from cell chips were collected automatically at 60 \times magnification with DAPI-stained nuclei superimposed in blue pseudocolor. Each gene name indicates the corresponding deletion strain (for example, *dse2* Δ KanMX4). (a) Six phenotypic classes observed among the haploid yeast deletion strains. *YIL141W* overlaps the *AXL2* gene, whose disruption in the deletion strain probably provides the observed morphology. (b) Changes in cell morphology observed after treating the deletion collection with mating pheromone. Many mutants, such as the *mrps5* Δ KanMX4 deletion strain (left), form 'wild-type'-like mating projections upon adding alpha factor, while cells lacking *STE7* (middle) fail to form mating projections, and cells lacking *KEL1* (right) form mating projections of unusual morphology.

Genes deleted from strains with an observed morphology defect were often functionally diverse. Nonetheless, certain general functions were enriched, which we

evaluated by comparing the sets of strains exhibiting a given phenotype with the sets of strains previously known to exhibit characteristic cell morphologies [47] or with sets of genes associated with distinct Munich Information Center for Protein Sequences (MIPS) functions [108] or Gene Ontology [109] functions. Elongated strains were enriched ($p < 0.01$, as calculated using FunSpec [110] for genes operating in nucleic acid metabolism, cell-cycle defects, transcription, and meiosis; large strains were enriched for transporter defects; round strains for cell wall, budding, cell polarity, and cell-differentiation genes; small strains for mitochondrial, carbohydrate metabolism, and phosphate-transport genes; and strains with polarized bud growth defects for budding, cell polarity, and filament-formation genes. Large and elongated strains significantly ($p < 0.01$) overlapped strains previously identified with these phenotypes during analysis of the homozygous diploid yeast deletion strains [47, 107].

Systematic identification of genes controlling mating pheromone response

Having established the typical morphology of each haploid deletion strain, we examined the primary morphological differentiation pathway in budding yeast - the response of the cells to the mating pheromone alpha factor during sexual conjugation.

Although this pathway is well studied [90], it has yet to be analyzed to completion. We reasoned that additional genes affecting the pheromone-response pathway, either directly or indirectly could be identified by examining shmoo phenotypes when the deletion collection was treated with alpha factor. We treated the entire mating type **a** haploid yeast deletion collection with alpha factor, then constructed and imaged spotted cell microarrays from the treated and fixed cells. Two graders manually examined the cell images for the absence of shmoos, grading the images on a numerical scale. Consistency between graders was high, and no systematic grading differences were

apparent (see Additional data file 1). Defects in shmooing were found in 142 strains; these either formed no shmoo or formed barely detectable shmoo in the imaged fields of cells (**Figure 2-2b** and [107]).

These 142 strains represent a mixture of genes participating in the pathway and false-positive results in the large-scale screen, primarily arising from stochastic sampling of cells from image fields with limited penetrance of shmoo and from ambiguity in identifying cells with mating projections. In practice, we explicitly included ambiguous cases for later retesting, thereby increasing the false-positive rate of the genome-wide screen but decreasing the false-negative rate [107]. We filtered this set for reproducible shmoo defects by manually retesting the 142 strains twice via alpha factor addition (to both mid-log and late-log phase cells) and microscopic imaging; 54 of the 142 strains showed consistent shmoo defects. Of these strains, ten were previously identified as diploid or MATalpha strains in the MATa haploid strain collection (A. Tong and C. Boone, personal communication), which correctly appear insensitive to alpha factor in this screen. Removing these strains (accounting for all diploid and MATalpha contaminants) and six strains whose deletions could not be confirmed by PCR or whose phenotype failed to reproduce in a reconstructed strain [107] leaves 38 MATa haploid strains reproducibly defective in shmoo formation. Note that deletion of one of these genes, *GPAI*, is thought to be lethal except in the presence of additional pheromone pathway mutations [111], implying either strain-specific viability or additional suppressor mutations in the library strain.

Independent validation of mating-pheromone response genes

To validate the involvement of these genes in the pheromone-response pathway, we followed up the high-throughput cell-chip screen by conducting growth assays

measuring the tendency of the strains to arrest growth upon pheromone exposure. We tested the complete set of 142 deletion strains (that is, the 38 reproducibly defectively shmooing strains and the remaining strains whose defects failed to reproduce) plus 271 additional deletion strains as controls with either normal shmooing (wild-type like, as determined from the cell microarray screen) or enhanced shmooing (marked by increased frequency of shmoos in the cell population), as well as strains deleted for 28 of the 41 genes previously known to be involved in the pheromone-response pathway. The positive controls are clearly differentiated from the normally shmooing strains in this assay (**Figure 2-3**), except for those deleted for five inhibitors of the pathway that arrest growth strongly in this assay (that is, they fail to show defective growth-arrest phenotypes). These include strains deleted for *BARI*, the protease that degrades mating pheromone [112], and *DIG2*, which inhibits pheromone-responsive transcription [113].

Figure 2-3 shows that 30 of the 38 reproducible shmoo-defective strains fail to arrest growth upon exposure to alpha factor to an extent comparable to the positive controls. Lack of growth arrest agreed well with reproducible shmoo defects. These strains were defective in both shmoo formation and growth arrest, implicating the deleted genes in the pathway. An additional four MATa haploid strains first identified as shmoo defective, but not among the 38 reproducibly shmoo-defective strains, also fail to arrest growth upon exposure to alpha factor, implicating the deleted genes in the pathway [107]. Enhanced shmooing strains arrest even more strongly and appear systematically hypersensitive to the pheromone (**Figure 2-3**). Thus, the extent of growth arrest in this assay correlates well with the penetrance of shmooing across the populations of cells as measured with the cell-chip assay.

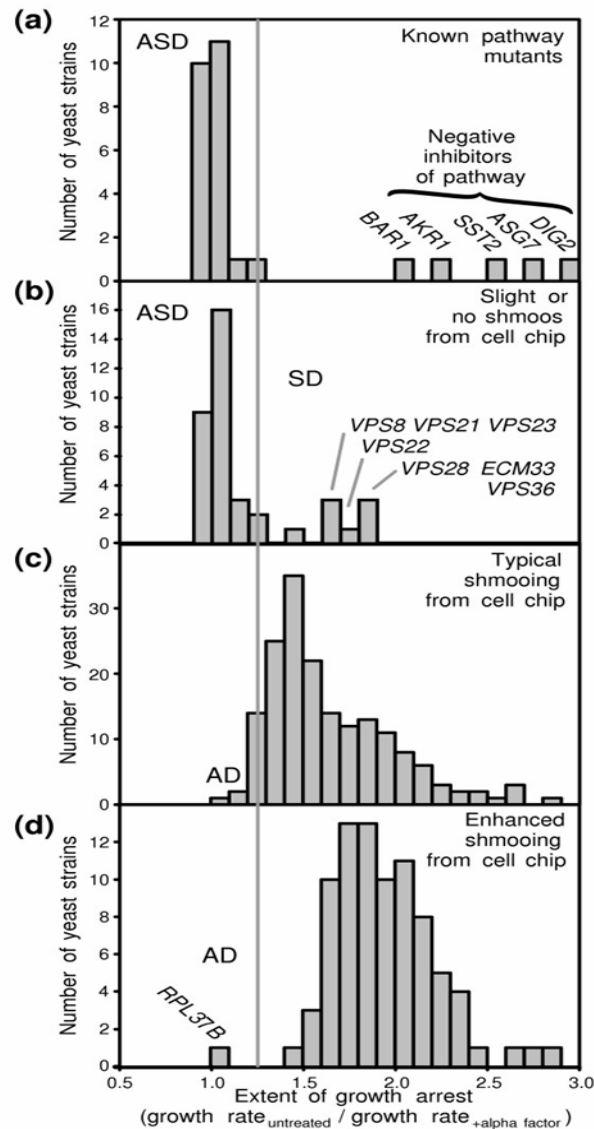


Figure 2-3: Results of a cell microarray-based genome-wide screen for genes participating in the mating-pheromone response pathway. Strains defective in the pathway fail to arrest growth when treated with alpha factor, unlike wild-type cells. The histograms report the average results of two or three replicate growth assays for (a) 28 strains containing deletions of genes known to participate in pheromone response, (b) 38 strains identified from cell microarrays as failing to shmoo properly, (c) 178 strains forming typical shmooing, and (d) 91 strains forming shmooing with a notably enhanced frequency in the cell population. The true-positive alpha factor-response pathway mutants (ASD, arrest+shmoo defective) are well separated from non-pathway mutants. Additional mutant categories identified were those defective only in the shmoo pathway (SD, shmoo defective), and those defective only in the growth arrest pathway (AD, arrest defective). Gene names indicate strains deleted for the corresponding genes.

Comparison with known pathway implicates new genes in pheromone response and shmoo formation

As two distinct, although correlated, phenotypes were assayed (growth arrest and shmoo formation), we expected to find genes defective in either or both pathways - a defect in both implicates the gene in the initial alpha-factor response pathway or in both downstream pathways, whereas a defect in only one implicates the gene in the corresponding downstream pathway (**Figure 2-4**). We first investigated mutants exhibiting both defects (termed ASD, for arrest and shmoo defective), implicated in pheromone detection and signaling.

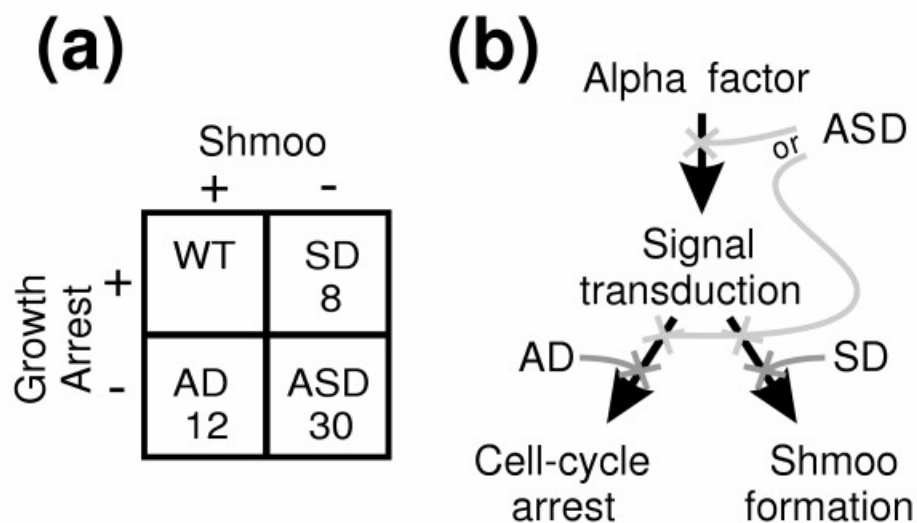


Figure 2-4: Summary of cell-chip/growth assay results. With two phenotypic screens, we expected three classes of mutants: true-positive alpha factor-response pathway mutants (ASD), those defective only in the shmoo pathway (SD), and those defective only in the growth arrest (AD). (a) The number of genes identified in each category; (b) their interpretation. Only 413 strains were tested by growth assay, so the number of strains with wild-type phenotypes (WT) is omitted.

Comparison with the known pathway (**Figure 2-5**, see also [90]) shows that of the 41 genes previously known to be in the pathway, 15 were recovered in the cell microarray experiment. Examination of the remaining genes is revealing: ten genes are not represented in the deletion library (many are essential), 13 genes are inhibitors of the

pathway and are thus not expected to be observed in either screen, as the deletion strains still shmoo, and the remaining three genes were missed for technical reasons related to image focus or low cell count. Thus, of the 31 genes expected to be found in this screen, 15 (48%) were correctly identified, including components of the receptor-coupled heterotrimeric G protein (*STE4*, *GPA1*), the MAP kinase signal transduction cascade (*STE20*, *STE11*, *STE5*, *STE7*, *FUS3*, *FAR1*, *STE50*), and silencers of mating loci (*SIR1*, *SIR2*, *SIR3*). Recognizing that negative regulators may not be found in this screen raises the recovery rate to 15/18 genes, or 83%. Interestingly, strains with deletions of certain negative regulators such as *HSL7* and *DIG1* are shmoo defective and we correctly identify them in the screen (**Figure 2-5**).

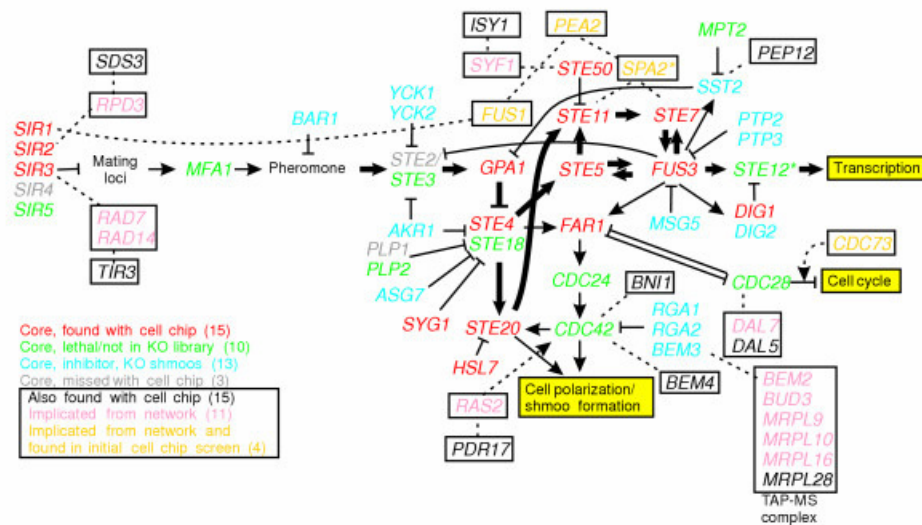


Figure 2-5: Comparison of results with the known response pathway. This comparison reveals that of the 18 known genes expected to be found in this screen, 15 were recovered (red labels); three core genes were missed (gray labels). Thirteen genes are pathway inhibitors (blue labels) whose corresponding deletion strains shmoo. Ten known pathway genes are absent from the deletion collection (green labels). Of the 15 putative additional genes found, nine (black labels, boxed) could be associated with the core pathway via protein interactions or mRNA coexpression with intermediates (pink labels, boxed). Four network-implicated intermediates (orange labels, boxed) were also found in the initial cell-chip screen, though not reconfirmed. Bold arrows mark the canonical signal transduction cascade leading to transcriptional changes. Thin black arrows indicate activation; barred lines indicate inhibition; dotted lines indicate functional linkages [56]. Genes with asterisks are also implicated in filamentous growth [114].

Beyond the known signal transduction pathway, 15 genes were found that fail to shmoo and fail to arrest growth upon exposure to alpha factor. Examples include genes with clear functions in polarized growth (*BEM4* and *BNII*), as well as regulatory functions (the histone deacetylase *SDS3* and the ubiquitin protein ligase *UBR2*). We separately validated the *BNII* and *UBR2* involvement by reconstructing and retesting the deletion strains. Other strains were PCR-confirmed for the identities of the deleted genes, but not reconstructed (see Additional data file 1), and thus should be validated by strain reconstruction before confirming the definite involvement of these genes in the pheromone-response pathway. There is a general implication of genes affecting membrane properties, including *PDR17* , which controls phospholipid synthesis/transport [115] and *LAS21*, which controls glycosylphosphatidylinositol-linked protein transport/remodeling [116]. Several genes encoding plasma-membrane transporters are identified (*QDR2* and *DAL5*), as well as a cell-wall biosynthetic enzyme (*YEA4*) and mannoprotein (*TIR3*). Loss of any of these genes disrupts pheromone response, possibly indicating membrane properties feeding back into control of mating response, consistent with the important role of plasma-membrane reorganization in shmooing [117].

Such comparisons with known and literature-associated pathway components, as well as strain reconstructions, allow us to estimate the false-positive rate of this screen. Of the 40 original genes (after removing MATalpha, diploids, and strains not verified by PCR), 15 are known pathway components, three (*BEM4*, *ISY1*, *SDS3*) can be reasonably implicated in polarized growth and pheromone response from literature, two (*BNII*, *UBR2*) were confirmed with reconstructed strains, and two were eliminated as false positives in reconstructed strains. Therefore, 20 of 40 genes were confirmed and two were false positives, placing the false positive rate at 2/22, or 9%. Not considering the three components implicated from the literature raises this to 2/19, or 11%. Nevertheless,

as with any genome-wide screen we advise reconstruction of deletion strains before unequivocally concluding that these genes are implicated in the pheromone-response pathway.

Finally, we identified strains defective in only one of the two assayed phenotypes, implicating the genes in downstream pathways. The set of strains that fail to arrest yet shmoo properly (termed AD for arrest defective) was functionally diverse as well as small (in part because only around 8% of the deletion collection was tested for growth arrest - we expect more such mutants given a complete screen for growth arrest). These strains were deleted for *FMP35*, *RPL37B*, *YHL042W*, *YDR360W*, *YGL214W*, *PUB1*, *PMT2*, *TRX2*, *SFK1*, *MUP3*, *SPL2*, and *STM1*. Conversely, eight genes were identified arresting normally yet failing to shmoo (termed SD for shmoo defective). Interestingly, six of these (*VPS8*, *VPS21*, *VPS22*, *VPS23*, *VPS28*, *VPS36*) are involved in vacuolar protein sorting, with all but *VPS8* and *VPS21* specific to class E sorting and resulting in inefficient transport out of the endosome [118], suggesting a critical role of this system in shmoo formation (that is, downstream of pheromone signaling), possibly related to plasma-membrane reorganization [117, 119]. The remaining two proteins are involved in polarized growth (*ECM33*) and transcriptional regulation (the histone acetylase *EAF3*).

DISCUSSION

We attempted to connect the 15 putative pheromone-response implicated genes (the ASD set) to the known pathway (the core set) using available functional genomics data by searching for the shortest pathways through protein interaction and mRNA coexpression networks [56] that connected the new genes to the core set. Nine of the new

genes could be reasonably connected to the core set by two interactions or fewer (**Figure 2-5**), indicating that these genes may have direct, rather than indirect roles in the pheromone response pathway. As connecting 9 of 15 genes to the core is no more than expected by random trials, these linkages serve only as hypotheses to provide a starting point for experiments validating the associations.

One gene connected in this manner is *SDS3*, a component of the Rpd3/Sin3 histone deacetylase complex implicated in gene silencing [120], and it is likely that the implication of *SDS3* in the pheromone response pathway probably stems from the action of this complex on the silencing of mating loci. Likewise, another gene implicated in the screen, the ubiquitin protein ligase *UBR2*, is an interaction partner of *DOT1*, a participant in Sir-mediated gene silencing [121], and thus a reasonable inference is that deletion of *UBR2* may also influence silencing. Another gene from the screen, *ISY1*, is pleiotropic but connected to control the cell cycle, participating in mRNA splicing and the spindle checkpoint [122]. *ISY1* exhibits some connection to polarized growth: homozygous diploid deletions of *ISY1* exhibit abnormal axial budding [123]. Although *MRPL28* can be connected to the core network in this manner, its shmoo defect might also arise by a disruption in the deletion strain of the proper functioning of the adjacent *MFA1* alpha factor mating-pheromone gene.

Cell morphology phenotypes are rich in information, and although we have focused on strains exhibiting a failure to shmoo, additional strains were identified with morphological defects in the mating projections, such as shown for the *kell* Δ *KanMX4* strain of **Figure 2-2b**. We flagged a total of 29 strains producing shmoos of aberrant morphology. These strains, listed in Additional data file 5, are deleted for genes involved in a statistically significant ($p < 0.01$ [110]) fashion in mating, especially for genes of polarized growth (*CDC10*, *KEL1* and *BUD19*), but also for genes of transcriptional and

translational regulation, including components of transcription and chromatin remodeling (*SNF6* , *SPT3* , *SPT10* , *HTL1* , and *SIN4*), translational regulation (*CBP6* , *ASC1* , and *SRO9*), and rRNA processing/ribosome biogenesis (*NSR1* , *RPP1A* , *RPL31A* , *RPS16B* , and *RAI1*). There is also some interplay between cell morphology and pheromone response phenotypes - for example, the *mrpl28* Δ *KanMX4* strain exhibits a large cell phenotype until alpha factor is added, whereupon the cell size defect is corrected, although the cells fail to shmoo [107].

Interestingly, we also find the extent of alpha factor-induced growth arrest appears largely uncorrelated with the change in expression of the corresponding genes following alpha factor treatment in wild-type cells [94], even for known genes in the core pathway [107]. Instead, the known pathway genes fall into two categories: those whose deletion strains show strong alpha factor-induced growth arrest or those that fail to arrest. The former category is exclusively composed of inhibitors of pheromone-response components. The majority of known pathway genes do not change expression following alpha factor treatment [94], nor do the majority of new genes implicated in the pathway by the combined cell chip/growth inhibition assay. Therefore, the cell chip-based screen complements the information available from DNA microarrays.

CONCLUSION

In conclusion, we describe a new genomic-scale technology for microscopy on genetically distinct cells, applied here to measuring the cell morphologies of yeast in the haploid deletion strain collection and to the mapping of genes participating in the response of yeast cells to mating pheromone. Although this paper focuses on cell morphology, cell chips have utility beyond this and can in principle be extended to any organism or cell type for which defined libraries of cells can be arrayed, such as other

easily manipulated organisms, banks of bacteria, and deletion libraries for other microorganisms. We expect that diverse collections of strains can be arrayed, such as yeast strains in which proteins are tagged with green fluorescent protein [45]. Just as it proved possible to identify pathways modulated by alpha factor, it should be possible to quickly identify mutants and pathways differentially affected by drugs. A major advantage of the cell chips is the minimal use of expensive reagents on the chips, achieved by limiting the use of antibodies and dyes to single microscope slides, as compared to the approximately 50 96-well plates required to image the complete deletion collection.

The key principle distinguishing cell chips from other approaches (such as immunoassays in 96-well plates) is, however, the separation of cell growth from imaging. Thus, we anticipate the strongest advantage of cell chips will be their use for analyzing the localization of proteins or RNAs by high-throughput *in situ* hybridization and antibody-based immunoassays. Consider the case of printing multiple identical cell chips, but probing each with a different set of dyes or antibodies. Each slide then becomes a unique assay for the dye or antibody target across the set of genetically distinct strains. In this mode, cells from the deletion strain collection are fixed, spheroplasted, and spotted onto microarrays, effectively separating the growth of the cells from the imaging process (a strategy difficult to achieve with plate assays). Around 200 cell chips can be made in a single printing session; each serves as a separate imaging assay when probed with an antibody to a distinct target, revealing the change in localization and expression of that target across the approximately 4,800 genetic backgrounds. The resulting images would indicate synthetic genetic interactions between the probe targets and the deleted genes, and the act of imaging becomes a scaleable, easily replicated assay on standardized cell chips for the high-throughput generation of synthetic interactions. Combining cell-chip

throughput with automated image processing [72, 124, 125] should provide quantitative strain- and gene-specific data. Data from such experiments will generate functional and statistical connectivities between genes [53], ultimately leading to comprehensive network analyses of genes [126].

MATERIALS AND METHODS

Cell microarray construction and imaging

All methods are described in full in Additional data file 1. In brief, cell microarrays were constructed by contact deposition of suspensions of yeast cells from the arrayed collection of *S. cerevisiae* haploid deletion strains (BY4741 genetic background; *MAT a his3 Δleu2 Δmet15 Δura3 Δ*) onto Con A [95] or poly-L-lysine-coated glass slides using a custom-built DNA microarray printing robot [2]. In about 12 h, more than 100 slides can be printed, each containing the entire deletion collection as well as the isogenic wild-type parent strain as a control. Cell arrays may be used for imaging immediately after printing or stored at 4°C or -80°C, provided that the cells are printed with glycerol. Centrifugation enhances adherence of cells to the slide, permitting washing before staining and imaging. Cell images were collected via automated microscopy, using a Nikon E800 microscope with computer-controlled *X-Y* stage and piezoelectric-positioned objective, by scanning to the position of each spot, autofocusing, and capturing the image with a Coolsnap CCD camera (Photometrics, Tucson, USA). Images were stored in a custom cell microarray image database (Cellma) for manual examination or automated image analysis. Using Perl scripts and custom MetaMorph (Universal Imaging Corporation, Sunnyvale, USA) journals, a full set of approximately 5,000 images can be

collected from a slide in bright-field mode in less than 4 hours or for fluorescent images in around 10 h.

High-throughput screen for strains unresponsive to alpha factor

To examine cell morphology after stimulation with alpha factor, each yeast deletion strain was subcultured into fresh YPD medium in 96-well Costar tissue culture plates (Corning, Corning, USA), grown for 36 hours at 30°C, centrifuged, and washed with YPD, pH 3.5, to inactivate the Bar1p protease. Alpha factor (350 µg/ml) was added to each sample well, a concentration measured by titration (as in [127]) to induce shmoo formation in around one half of the cells in the majority of deletion strains (see Additional data file 1). Cells were incubated for 4 hours at 30°C, fixed with 3.7% formaldehyde for 1 hour at room temperature, washed with YPD containing 17% (w/v) glycerol, supplemented with 20 mM CaCl₂, 20 mM MnSO₄, then spotted onto Con A-coated glass slides. Slides were stained with DAPI, imaged by automated microscopy, and manually scored by two independent graders for extent of shmooing.

Assay of alpha-factor-induced growth arrest

Four hundred and twenty-six selected deletion strains were grown overnight in YPD, centrifuged, and washed with YPD, pH 3.5. The cultures were split into replicate 96-well plates of YPD, with and without alpha factor at a final concentration of 25 µg/ml, maintaining cells at an optical density at 600 nm (OD₆₀₀) of around 0.2-0.5 [127]. Plates were incubated at 30°C for 10 h, recording OD₆₀₀ hourly from each strain. The slope of each growth curve was calculated from a plot of log (OD₆₀₀) versus time. The effect of alpha factor on the strains was obtained as the ratio of the slope from the untreated

sample to that of the alpha-factor-treated sample. Average ratios were calculated from two or three independent assays.

DETAILED EXPERIMENTAL PROTOCOLS, CONTROLS & EVALUATION OF CELL MICROARRAYS

Yeast deletion strains and growth conditions

Cell microarrays were fabricated containing all the strains of the yeast haploid deletion collection on a single microscope slide. This is a set of strains in the BY474 genetic background (MATa his3 Δ leu2 Δ met Δ ura3 Δ) generated by the International Deletion Consortium, in which each strain contains a chromosomal gene replacement cassette with a KanMX4 marker gene that confers resistance to antibiotic G418. This arrayed strain collection of 4,848 strains was obtained from Invitrogen. The frozen master plates of the library were thawed and used to inoculate 96-well costar plates with 200 μ l of YPD media containing the antibiotic G418 (200 μ g/ml) and 17% glycerol. All liquid handling operations were performed using the Biomek FX robot fitted with a 96 well pipetting head. Copies of the strain collection were incubated at 30 C and cell growth monitored by optical density measurement at 600 nm using a 96-well plate reader. Quality control for sterility and cross contamination was performed by monitoring control wells without cells in the master plates. After growth at 30 $^{\circ}$ C for 2 days, the copies were gently agitated in a plate shaker, sealed and frozen at -80 $^{\circ}$ C, with each copy thawed prior to use for printing microarrays of cells.

Slide preparation

Cell arrays were printed on pre-cleaned microscope slides coated with either poly-L-lysine or concanavlin-A. A Poly-L-lysine coating on slides promotes electrostatic

interactions with yeast cells while a Con-A coating promotes cell adherence through interactions of this lectin with mannose residues on the yeast cell wall. Poly-L-lysine coated slides were prepared with an identical protocol as for DNA microarrays essentially coating with a 0.1 w/v solution of poly-lysine (Sigma) in phosphate buffered saline (PBS) and then rinsing thoroughly with de-ionized water. Con-A coated slides were prepared by incubating slides for 15 minutes in a 0.1 mg/ml solution of ConA (Sigma) in PBS, then washing briefly with 95% ethanol. Only freshly prepared slides were used for each print. Use of ConA coated slides, also required addition of 20 mM CaCl₂ and 20 mM MnSO₄ to each well of cells (typically added to fixed cells) in order to activate the ConA for binding (**Figure 2-6**)

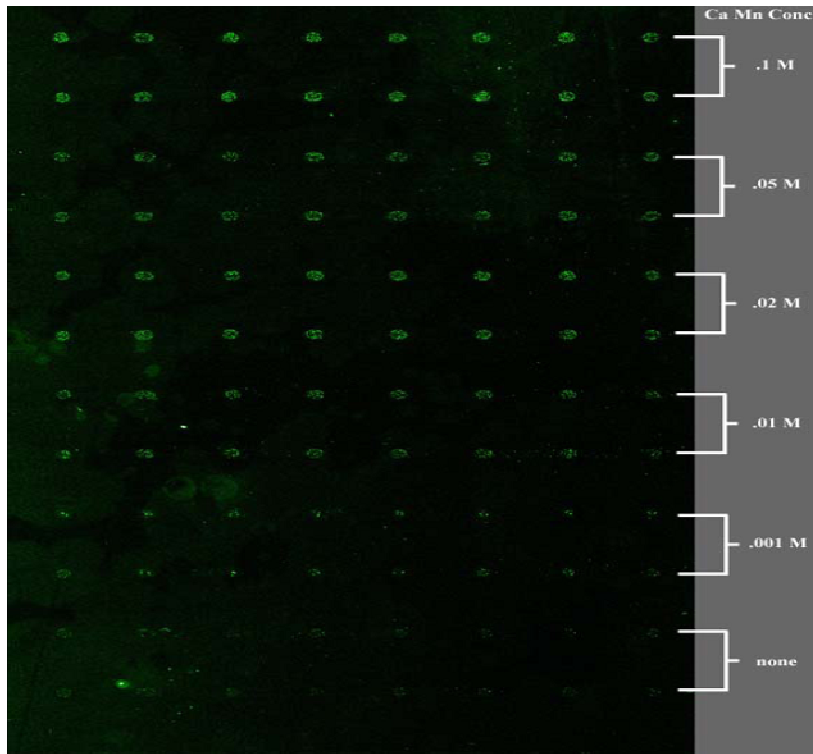


Figure 2-6: Yeast cell adherence to ConA-coated cell microarray slide surface as function of Ca/Mn concentration. Cells were spotted, then washed to test adherence.

Printing of cell microarrays

Cell microarrays were printed by contact deposition of suspension of yeast cells from the thawed arrayed strain collection onto coated glass slides using a custom-built DNA microarray printing robot (**Fig 2-7**). Printing was carried out using conically tapered 1/16 inch diameter stainless steel printing tips with 0.0015 inch slots (Majer Precision Engineering; MicroQuill 2000) that are sterilized between print runs. The resulting spots are ~200 μm in diameter, spaced 410 μm apart; spots were printed in 12 blocks, each being a 21x21 square matrix of spots. In a standard print run, upto 50 slides were printed in tandem with the tips being rinsed and vacuum dried 3 times after each loading and printing step. This is sufficient to prevent carryover of cells from one well to the next, as judged by microscopic inspection of putatively empty spots. Thawed 96-well plates from the library were placed on the printing robot after gentle agitation to resuspend cells. Plates and the array platter are kept covered at all times to prevent contamination and all surfaces are sterilized by wiping with 70% ethanol. After printing, the slides were labeled and spun down flat in a centrifuge with a swinging bucket rotor at 1,500xg for 10 mins to promote adherence. Cell microarrays can be imaged immediately at this point or can be stored at -80°C for use at a later date. In the latter case, a slide is thawed out of -80°C by immersing in 95% ethanol momentarily and spinning the slide vertically at 600xg for 5 min to drain excess ethanol.



Figure 2-7: A custom built DNA microarray printing robot.

Imaging of cell microarrays

Cell microarrays were imaged in a two step process. A freshly printed slide or a slide thawed from -80°C was first scanned using a GenePix 4000 A/B microarray scanner followed by imaging of each spot using an automated microscope. Prior to staining and imaging, each slide is marked with four reference marks using a diamond scribe. The spots of cells are detected as bright spots in the 532 nm detector channel because of light scattering by the glycerol in the print medium. In addition to serving as a cryo-protectant, the glycerol present in medium prevents evaporation of print media and enhances brightness of the spots when scanned.

A GenePix Array List (GAL) file that essentially defines each feature in the array and links a spot to a particular strain ID is then used to generate a GenePix Results format (GPR) file that contains the relative x, y positions of each spot including the reference positions. Spot coordinates can be converted from the GenePix coordinate system to the

optical coordinate system through the use of the four reference positions and an affine transformation. For typical DIC or brightfield microscopy, spots are washed with water after scanning, dried via 5 minutes of centrifugation and a few drops of mounting media containing DAPI (vector labs) added. Slides are then covered with a 24x60 mm cover slip, blotted and sealed with nail polish.

Automated microscopy was carried out using a Nikon E800 with a CF160 optical imaging system outfitted with a motorized X-Y stage with 0.1 micron resolution, a piezoelectric auto-focus device for 9.7 nm focusing resolution, Photometrix Coolsnap camera with 1392x1040x12 bit pixel resolution, filters for Differential Interference Contrast (DIC), fluorescence and visible wavelengths and Metamorph software. First, the reference marks on the slide were found and their X, Y and Z motor positions recorded using the microscope coordinate system. These positions were input into a custom affine transform PERL script that when executed converted the GPR file to a STG (stage) file consisting of the spot coordinates in the microscope coordinate system. Images were collected at each spot by executing a Metamorph 'journal' macro at each spot listed in the STG file and acquiring the DIC and DAPI image in the TIFF and JPG format. An entire slide with ~5000 spots can be imaged in ~10 hours capturing both fluorescent and DIC images.

Image annotation database

We developed an online relational database for warehousing and annotation of cell microarray images. This database called Cellma (for Cell Microarrays) centers around a suite of web pages driven by a MySQL relational database (**Figure 2-8**). The images are stored on a central server. The database administrator creates user accounts, enters information about the organisms, strains and genes studied using the web interface.

For data submission, experimenters first copy images directly to the appropriate location in the data hierarchy and then enter the details such as name, date, experimental treatment and slide number. Cellma currently supports online manual annotation of high throughput microscopy images. Although tedious, phenotypes can be reliably scored by visual inspection within reasonable timeframes.

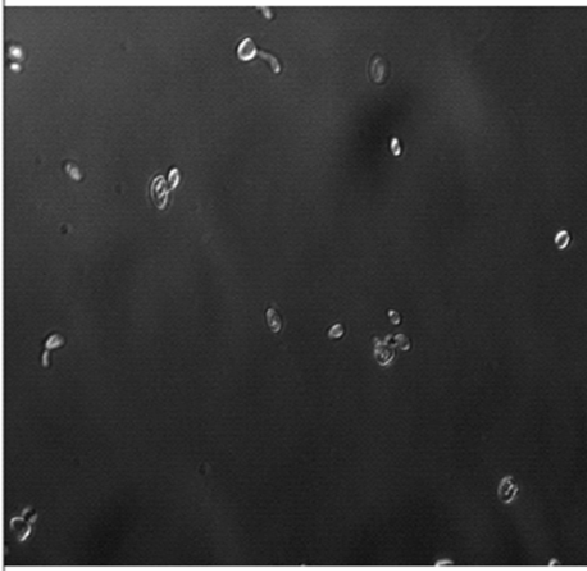
#345	Gene: YGL219C - MDM34 Slide: VH4-007 Logged in as alex	Block 1 Row 17 Column 9 OD 1.107	Index Logout	Gene: <input type="text"/> Slider: VH4-007 View: DIC <input type="button" value="Jump to Spot"/>	<input type="button" value="Save"/> <input type="button" value="Browse"/>
 <p>click to see full size image</p>				<p>Large <input type="radio"/> 0 <input type="radio"/> 1 <input type="radio"/> 2 <input type="radio"/> 3 <input type="radio"/> 4 (int) <input type="radio"/> 0 <input type="radio"/> 1 <input type="radio"/> 2 <input type="radio"/> 3 <input type="radio"/> 4 (pen)</p> <p>Small <input type="radio"/> 0 <input type="radio"/> 1 <input type="radio"/> 2 <input type="radio"/> 3 <input type="radio"/> 4 (int) <input type="radio"/> 0 <input type="radio"/> 1 <input type="radio"/> 2 <input type="radio"/> 3 <input type="radio"/> 4 (pen)</p> <p>Round <input type="radio"/> 0 <input type="radio"/> 1 <input type="radio"/> 2 <input type="radio"/> 3 <input type="radio"/> 4 (int) <input type="radio"/> 0 <input type="radio"/> 1 <input type="radio"/> 2 <input type="radio"/> 3 <input type="radio"/> 4 (pen)</p> <p>Pointed <input type="radio"/> 0 <input type="radio"/> 1 <input type="radio"/> 2 <input type="radio"/> 3 <input type="radio"/> 4 (int) <input type="radio"/> 0 <input type="radio"/> 1 <input type="radio"/> 2 <input type="radio"/> 3 <input type="radio"/> 4 (pen)</p> <p>Elongated <input type="radio"/> 0 <input type="radio"/> 1 <input type="radio"/> 2 <input type="radio"/> 3 <input type="radio"/> 4 (int) <input type="radio"/> 0 <input type="radio"/> 1 <input type="radio"/> 2 <input type="radio"/> 3 <input type="radio"/> 4 (pen)</p> <p>Pseudohyphal <input type="radio"/> 0 <input type="radio"/> 1 <input type="radio"/> 2 <input type="radio"/> 3 <input type="radio"/> 4 (int) <input type="radio"/> 0 <input type="radio"/> 1 <input type="radio"/> 2 <input type="radio"/> 3 <input type="radio"/> 4 (pen)</p> <p>Clumped <input type="radio"/> 0 <input type="radio"/> 1 <input type="radio"/> 2 <input type="radio"/> 3 <input type="radio"/> 4 (int) <input type="radio"/> 0 <input type="radio"/> 1 <input type="radio"/> 2 <input type="radio"/> 3 <input type="radio"/> 4 (pen)</p> <p>Budding <input type="radio"/> 0 <input type="radio"/> 1 <input type="radio"/> 2 <input type="radio"/> 3 <input type="radio"/> 4 (int) <input type="radio"/> 0 <input type="radio"/> 1 <input type="radio"/> 2 <input type="radio"/> 3 <input type="radio"/> 4 (pen)</p> <p>Polarized <input type="radio"/> 0 <input type="radio"/> 1 <input type="radio"/> 2 <input type="radio"/> 3 <input type="radio"/> 4 (int) <input type="radio"/> 0 <input type="radio"/> 1 <input type="radio"/> 2 <input type="radio"/> 3 <input type="radio"/> 4 (pen)</p> <p>Other <input type="radio"/> 0 <input type="radio"/> 1 <input type="radio"/> 2 <input type="radio"/> 3 <input type="radio"/> 4 (int) <input type="radio"/> 0 <input type="radio"/> 1 <input type="radio"/> 2 <input type="radio"/> 3 <input type="radio"/> 4 (pen)</p> <p>Wildtype <input type="radio"/> 0 <input type="radio"/> 1 <input type="radio"/> 2 <input type="radio"/> 3 <input type="radio"/> 4 (int) <input type="radio"/> 0 <input type="radio"/> 1 <input type="radio"/> 2 <input type="radio"/> 3 <input type="radio"/> 4 (pen)</p>	<p>Cell Count (exact)</p> <p>0 1 5 10 20 30 50 75 100 (app)</p> <p>Focus</p> <p>perfect good blurry unusable</p> <p>Problems</p> <p>empty few cells focus contamination upside other</p> <p>Comments</p>
				<p>Annotation: NO_GENE_NAME hypothetical_protein UNCLASSIFIED_PROTEINS</p>	

Figure 2-8: Screenshot of a Cellma annotation database page. Morphology phenotypes for each gene are assigned using a structured annotation scheme. Phenotypes are classified according to their severity and penetrance and are specific for a given strain in a given microarray experiment.

For scoring phenotypes,, there is a dynamically generated scoring page. Based on experiments applied to a slide and the collection fluorescent wavelengths, the page prompts the grader for several features of the image such as intensity and penetrance of the appropriate phenotype, the cell count, focus quality and problems and allows the grader to enter comments. The database supports easy navigation between genes, image

types and slides. Images can also queried in several formats such as the entire slide all at once or batch images of a gene across multiple slides and so forth.

Scoring cellular morphology phenotypes

Two graders independently evaluated the set of images from a yeast cell microarray for strains with atypical morphologies. Phenotypes were scored related to cell size (mutant phenotypes being large or small relative to wild type control strain), cell shape (mutant phenotypes being round, elongated, pointed with respect to the wild type ovoid shape) or either a pseudohyphal, clumped or polarized bud growth, or other budding defects. In each case, the intensity of a phenotype is assigned a score ranging from 0 to 4, increasing with the severity of the phenotype. The penetrance of the phenotype across the population is scored, ranging from 0 to 4, where 0 indicates absence of the phenotype while 4 indicates 100% of the cells in the field exhibiting the phenotype. In order to estimate the precision and recall achieved by this manual scoring, a control cell chip of 960 spots was constructed by randomly distributing sports of wild-type cells and known morphology mutants. This slide was scored in a fashion identical to that described above, and the accuracy of graded morphologies was calculated as function of the sum of the grader-assigned intensities and penetrances (i.e, collapsing grades from the two graders to a single score ranging from 0 to 16). **Figure 2-9** plots the recall and precision calculated from this control experiment as a function of the grader-assisted scores. Given $TP = \#$ of true positive grades, $FP = \#$ of false positive grades and $FN = \#$ False negative grades, recall is defined as $TP/(TP+FN)$ and precision is defined as $TP/(TP+FP)$.

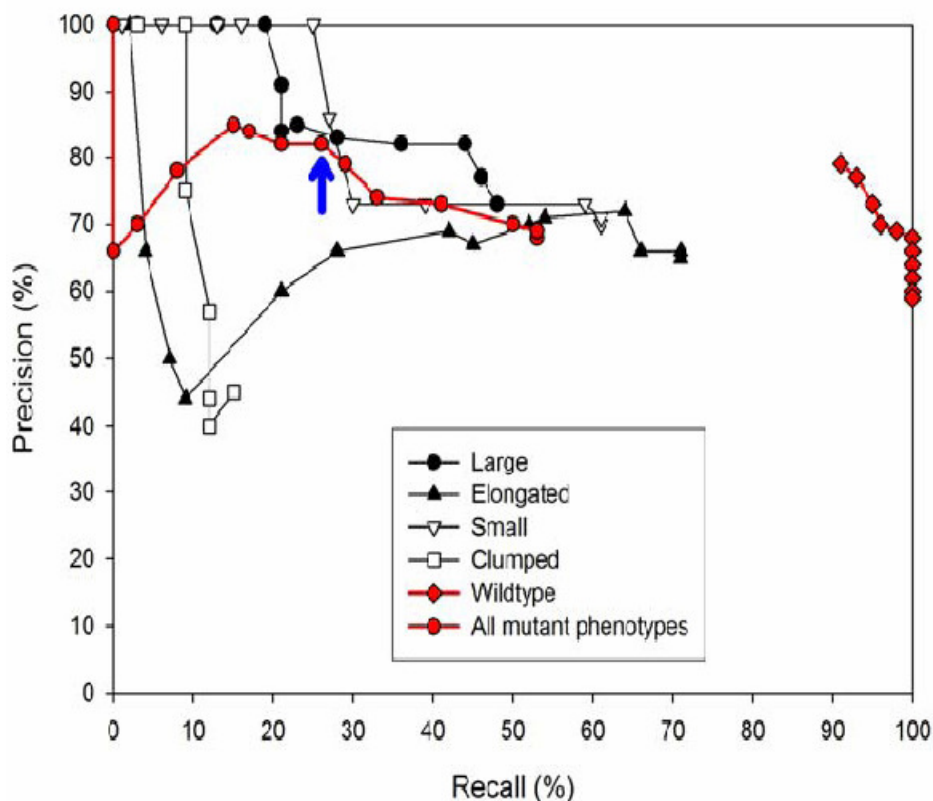


Figure 2-9: Recall/ Precision of manual grading of morphology mutant/ wild type control chip. The blue arrow represents the threshold chosen for selection of morphology mutants in the full cell chip screen.

At a minimum threshold score of 8 (typically requiring agreement by both graders as to the presence of the phenotype to an intermediate degree), the overall set of control mutant phenotypes were identified at 82% precision and 28% recall. Thus, graders were conservative at this threshold in calling mutant phenotypes, resulting in a relatively high confidence in the mutants identified at this threshold. This threshold was used for identification of morphology mutants in the full cell chip screen.

Analysis of morphology mutants

Strains exhibiting significant morphology defects as defined above were analyzed for functional trends among the deleted genes by searching for statistically significant intersections between the sets of deleted genes giving rise to a particular phenotype with the sets of genes associated with particular Gene Ontology cellular components, molecular functions and biological processes; MIPS phenotypes, protein complexes, and functional classifications; and cellular morphologies and yeast fitness data previously identified by the yeast deletion consortium. Using the program FunSpec, the probability of each intersecting set occurring at random was selected under the hypergeometric distribution [107].

Screening for genes affecting the mating pheromone response pathway

We used cell microarrays to identify genes involved in the pheromone response pathway during the mating process in yeast. Haploid yeast cells respond to mating pheromone released from neighboring cells of the opposite mating type and undergo cellular and nuclear fusion to form diploids. The pheromone response is characterized by the formation of a distinct morphological change, a mating projection called the ‘shmoo’, accompanied by cell cycle arrest thus poisoning the yeast cells to mate. We reasoned that genes that were deleted in the yeast strains that displayed anomalous shmoo morphologies could be implicated to function, either directly or indirectly, in the pheromone response pathway.

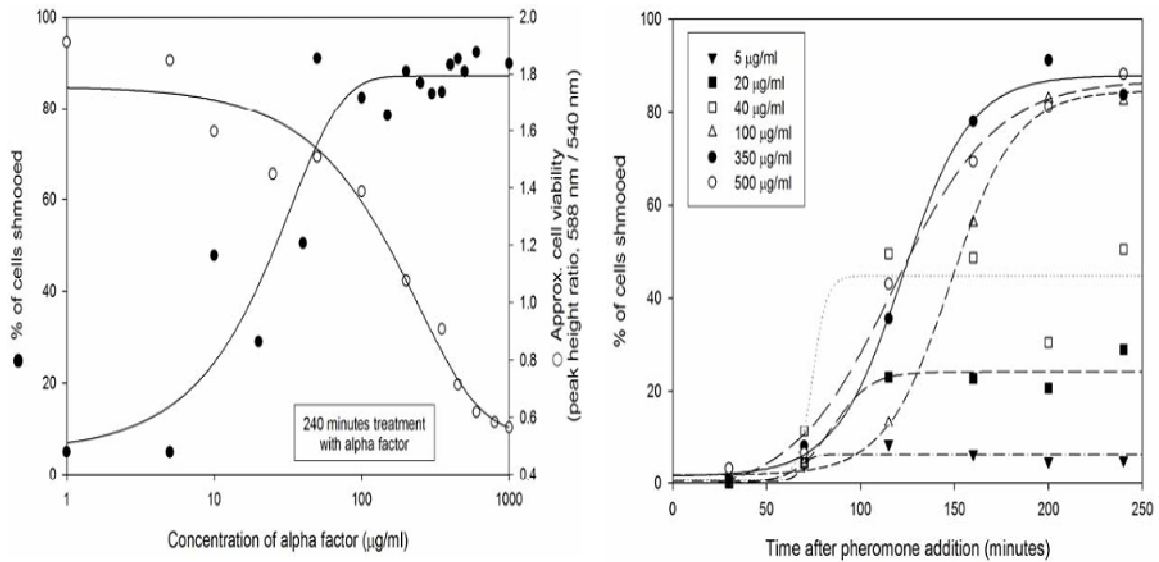


Figure 2-10: Pheromone concentration and time dependence on shmooing.

We performed our screen by treating the yeast deletion library that comprised of strains of the ‘a’ mating type with synthetic alpha factor, a 13 amino acid peptide. To do this, the yeast deletion collection was grown to saturation in 96-well plates containing. Each plate was re-inoculated into a fresh YPD plate and grown for 36 hours at 30 C without shaking. The plates were spun down and washed three times with YPD pH 3.5 to inactivate the extracellular Bar1p protease which rapidly and efficiently degrades alpha factor. The concentration of alpha factor and the time of incubation were determined empirically due to constraints on treatment duration and wash conditions critical to keeping the Bar1p protease inactive when performing the assay across the entire library comprising of 52 plates. Alpha factor titrations were done on a wild type yeast strain to estimate the percentage of cells that underwent shmooing as function of alpha factor concentration. A FUN-1 cell toxicity assay was also done in parallel to gauge the approximate cell viability. **Figure 2-10** shows the results of such an experiment. The duration of incubation was estimated at different time points ranging from 0.5-4 hrs for

alpha factor concentrations ranging from 5-500 ug/ml. Under the conditions for the full scale assay, we empirically found that alpha factor concentrations slightly higher than those suggested by the titrations were required. We used 350 ug/ml alpha factor and obtained shmoo formation in ~50% of the cells in a microscope field in the majority of deletions and wild type control strains.

Because the percentage of shmooing on the arrays was lower than expected from the titrations (50% as measured across 40 images), it appeared that the cells experienced a lower effective concentration of alpha factor than in the titration assays, probably due to less efficient washing on the full large scale assay resulting in residual activity of Bar1p protease and consequently inactivation of alpha factor. After 4 hours of treatment at 30 C, cells were fixed with 3.7% formaldehyde for 1 hour at room temperature. The plates were washed three times with YPD to remove the excess fixative and resuspended in YPD containing 17% (w/v) glycerol. At this stage, 20 mM CaCl₂ and 20 mM MnSO₄ were added to each well to promote adherence to ConA coated slides. The cells were arrayed onto both poly-L-lysine and ConA coated slides as described above. Imaging, acquisition and storage were conducted essentially as described. Control experiments were also done with hand picked deletion strains that were found to have defective morphologies in our previous screen as well as those that were known to be defective in the mating pheromone response pathway.

Manual scoring of shmoo defects

After imaging the cell microarray containing the alpha factor treated deletion strains, two independent graders visually inspected the ~5000 images and scored them for shmoo defects in the following manner. The intensity of the shmoo phenotype indicative of the degree of shmooing was graded as being 'slight', 'normal' or 'other' while the

penetrance referring to the abundance of the phenotype across the population of cells imaged was given a value from 1-4 (0-100%).

For example, images having ~50% of the cells shmooing normally, the phenotype that reflected ‘wild type like’ behavior under the assay conditions, were graded as Normal (2) and Slight (2) indicating 50% of the cells in the spot has a normal shmoo phenotype and 50% failed to shmoo. Deletion strains that were known to be shmoo defective and displayed complete absence of shmooos would lack any ‘Normal’ or ‘Other’ shmooos. A Normal(4) would indicate an enhanced fraction of normal looking shmooos in the population suggesting a hypersensitive response to alpha factor but no change in shmoo morphology.

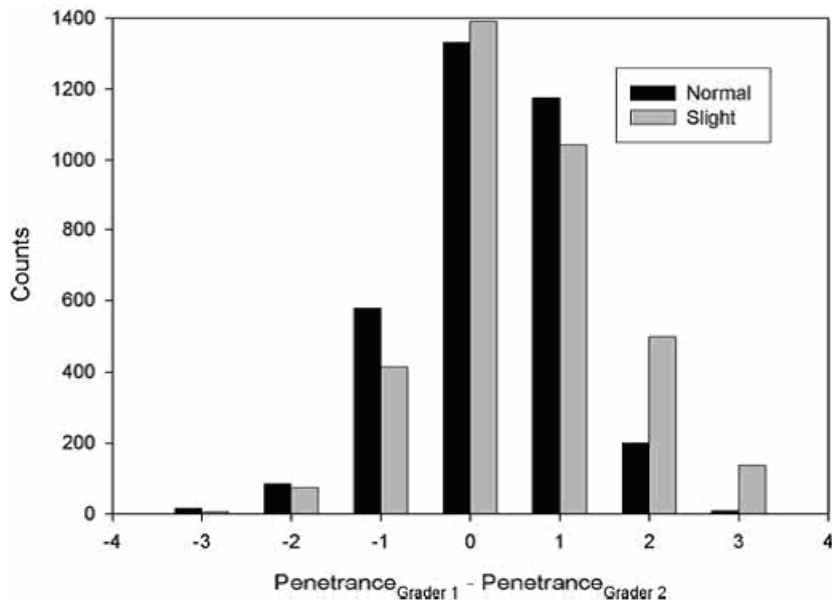


Figure 2-11: Grader agreement on shmoo phenotypes.

Some deletions that displayed abnormal looking shmooos were graded as ‘Other’ with a penetrance ranging from 1-4 based on the percentage of such shmooos in the field of cells. The ‘Other’ class of shmoo indicated unusual shmoo phenotypes (eg. *Kel1Δ*

KanMX4, fig) such as bud neck defects and other morphology defects that produced atypical shmoos. **Figure 2-11** shows a histogram of the agreement of the grades between the two graders – the Gaussian distributions indicate that the graders were largely consistent and varied from each other in a stochastic fashion with no systematic grading bias exhibiting except for an approx. $\frac{1}{2}$ unit higher penetrance on average for grader 1 relative to grader 2.

Yeast growth curves +/- alpha factor

To test if yeast strains arrested growth in the presence of alpha factor, selected strains were picked from the yeast deletion library and grown in YPD overnight until they attained log phase growth. The cultures were spun and washed with YPD pH 3.5 to inactivate Bar1p protease. The cultures were subsequently split into replicate 96 well plates, with and without alpha factor which was added to a concentration of 25 ug/ml, which keeping cells to an OD600 of 0.2 to 0.5 as recommended. The plates were incubated at 30 C for 10 hours without shaking and their absorbance recorded at 600 nm each hour. The slope of each growth curve was calculated from a plot of log OD600 VS time. The effect of alpha factor on the strains was obtained as the ratio of the slope from the untreated sample to that of the alpha factor treated sample. Average slope ratios were calculated from 2-3 independent assays. The analysis, in combination with cell microarray alpha factor treatment analysis, enabled the identification of a number of genes whose deletion affected the ability to form shmoos after alpha factor treatment. The growth curves and correct recovery of the known pheromone response pathway genes by the cell chip assay therefore provide two independent validations that identified genes are relevant to the pheromone response pathway.

False positives due to presence of diploids and MAT alpha strains

The systematic deletion strain collection used in our large scale screen was MAT a and haploid. This collection is now known to contain a few strains that are actually either diploid or MAT alpha (Boone and A.Tong, personal communication). Such contaminating strains would be expected to show up as false positives in our screen because diploid or MAT alpha strains are not sensitive to alpha factor. We removed these known diploid or MAT alpha strains from our list of genes whose deletion is known to render MATa yeast cells sterile, based on observations made during large-scale synthetic lethal analysis (C. Boone and A.Tong, personal communication). These sterile strains are incapable of mating, likely because of a defect in the mating pheromone response. Interestingly, 11 out of the 15 strains known to be MATa sterile were identified in our cell chip screen, illustrating the power of this approach to recapitulate known phenotypes.

Polymerase chain reaction (PCR) validation of deleted strains

The set of 42 deletion strains identified as SD, ASD or AD but not known to be in the core mating response pathway were validation for the identities of the deleted genes by PCR. We performed PCR validation for each of the 42 strains by using a PCR primer specific for the Kanamycin cassette with a primer specific for the region upstream of the deleted gene (using the KanB primer and 42 gene specific 'A' primers designed by the yeast deletion consortium and using the same protocol as in ref) from which we expected PCR products of approx. 400 -700 bp in size if the deletion cassette is integrated at the correct site in the genome. 38 out of the 42 strains (90%) were confirmed (**Figure 2-12**) by this approach as harboring the correct deletion.

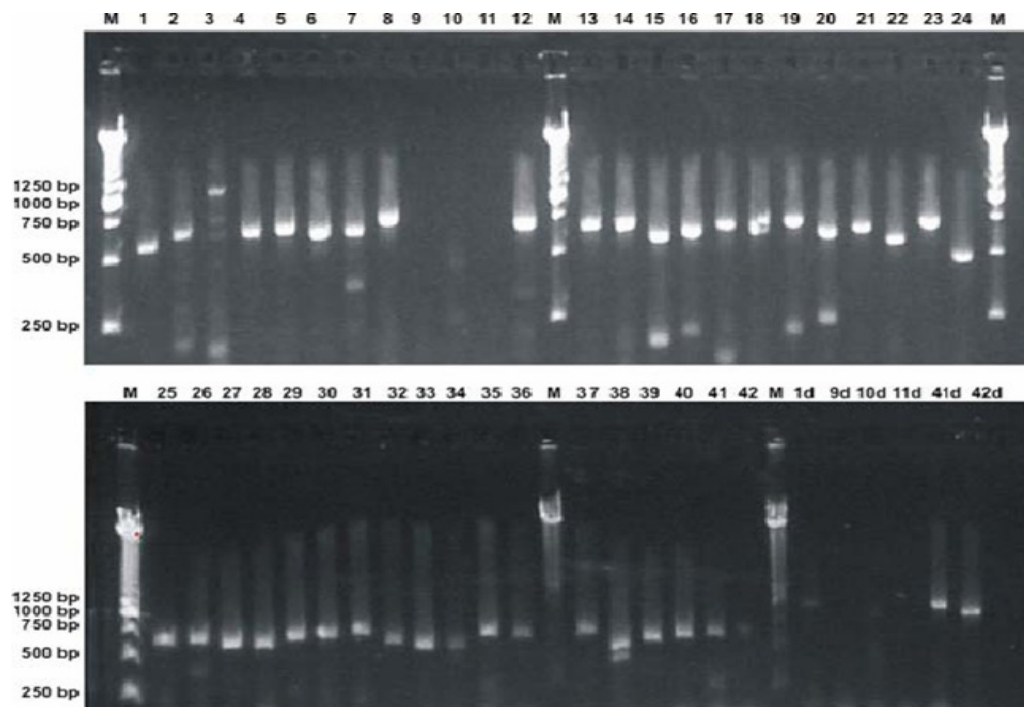


Figure 2-12: PCR validation of the identity of the gene deleted in 42 deletion strains. 38 strains were confirmed to have the correct deletion.

Three of the strains were not confirmed by either A specific primer/KanB primer pair or by PCR with the corresponding downstream (D) primer/ Kan C primer pair and thus cannot be confirmed as containing the expected deletion, while 1 strain gave a larger than expected PCR product. In addition, out of the four strains that were reconstructed by PCR amplification using the same strategy as the yeast deletion consortium, two strains displayed growth arrest phenotypes that were consistent with the corresponding deletions in the deletion collection while two 2 strain failed to reproduce the corresponding mating response defect. Thus, a total of 6 of the complete 42 strains assayed could not be validated to possess mating pathway defects and were removed from further consideration.

Deletion strain response phenotype correlate poorly with mRNA expression changes

We find that the extent of alpha factor induced growth arrest appears largely uncorrelated with the change in expression of the corresponding genes following alpha factor treatment in wild type cells even for known genes in the core pathway. Instead the known pathway genes fall into two categories: those whose deletion strains show strong alpha factor induced growth arrest and those that fail to arrest. The former category is composed exclusively of inhibitors of the pheromone response pathway components. Genes in either category may change expression following alpha factor treatment but the majority of known pathway genes do not nor do the new genes implicated in the pathway by the combined cell chip/growth arrest assay. This trend is consistent with signal transduction cascades operating at a post-transcriptional level (i.e by phosphorylation and protein interactions) and not at the transcriptional level (**Figure 2-13**).

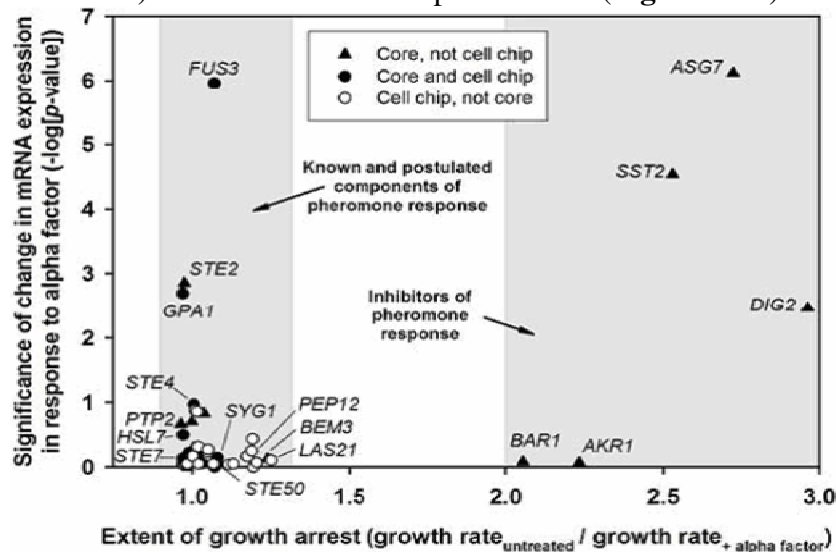


Figure 2-13: Comparison between cell chip identified pheromone responsive genes with mRNA expression. Both the Core (closed circles) and non-core (open circles) subsets identified by the cell chip did not show significant correlation with change in expression as measured by $\log(\text{probability of a significant expression change})$ plotted on the y-axis and pheromone responsiveness on the cell chip being determined by the growth arrest ratio plotted on the x-axis. A subset of genes of both the primary pathway components (growth arrest ratios ~ 1) and pathway inhibitors (growth arrest ratio > 2) show a change in expression while many of them also do not.

REFERENCES

1. Schena, M., *Genome analysis with gene expression microarrays*. Bioessays, 1996. **18**(5): p. 427-31.
2. DeRisi, J.L., V.R. Iyer, and P.O. Brown, *Exploring the metabolic and genetic control of gene expression on a genomic scale*. Science, 1997. **278**(5338): p. 680-6.
3. Duffield, G.E., *DNA microarray analyses of circadian timing: the genomic basis of biological time*. J Neuroendocrinol, 2003. **15**(10): p. 991-1002.
4. Alter, O., *Genomic signal processing: from matrix algebra to genetic networks*. Methods Mol Biol, 2007. **377**: p. 17-60.
5. Giaever, G., et al., *Chemogenomic profiling: identifying the functional interactions of small molecules in yeast*. Proc Natl Acad Sci U S A, 2004. **101**(3): p. 793-8.
6. Frayling, T.M. and M.I. McCarthy, *Genetic studies of diabetes following the advent of the genome-wide association study: where do we go from here?* Diabetologia, 2007. **50**(11): p. 2229-33.
7. Frayling, T.M., *Genome-wide association studies provide new insights into type 2 diabetes aetiology*. Nat Rev Genet, 2007. **8**(9): p. 657-62.
8. Smith, L.T., G.A. Otterson, and C. Plass, *Unraveling the epigenetic code of cancer for therapy*. Trends Genet, 2007. **23**(9): p. 449-56.
9. Bentley, D.R., *Whole-genome re-sequencing*. Curr Opin Genet Dev, 2006. **16**(6): p. 545-52.
10. Woll, D., et al., *More efficient photolithographic synthesis of DNA-chips by photosensitization*. Nucleosides Nucleotides Nucleic Acids, 2003. **22**(5-8): p. 1395-8.
11. Nuwaysir, E.F., et al., *Gene expression analysis using oligonucleotide arrays produced by maskless photolithography*. Genome Res, 2002. **12**(11): p. 1749-55.
12. Dalma-Weiszhausz, D.D., et al., *The affymetrix GeneChip platform: an overview*. Methods Enzymol, 2006. **410**: p. 3-28.
13. Birney, E., et al., *Identification and analysis of functional elements in 1% of the human genome by the ENCODE pilot project*. Nature, 2007. **447**(7146): p. 799-816.
14. Beltran, A., et al., *Interrogating genomes with combinatorial artificial transcription factor libraries: asking zinc finger questions*. Assay Drug Dev Technol, 2006. **4**(3): p. 317-31.
15. Zhu, H., M. Bilgin, and M. Snyder, *Proteomics*. Annu Rev Biochem, 2003. **72**: p. 783-812.
16. Lu, P., et al., *Absolute protein expression profiling estimates the relative contributions of transcriptional and translational regulation*. Nat Biotechnol, 2007. **25**(1): p. 117-24.
17. Mallick, P., et al., *Computational prediction of proteotypic peptides for quantitative proteomics*. Nat Biotechnol, 2007. **25**(1): p. 125-31.

18. Krogan, N.J., et al., *Global landscape of protein complexes in the yeast *Saccharomyces cerevisiae**. Nature, 2006. **440**(7084): p. 637-43.
19. Gavin, A.C., et al., *Functional organization of the yeast proteome by systematic analysis of protein complexes*. Nature, 2002. **415**(6868): p. 141-7.
20. Gavin, A.C., et al., *Proteome survey reveals modularity of the yeast cell machinery*. Nature, 2006. **440**(7084): p. 631-6.
21. Collins, S.R., et al., *Toward a comprehensive atlas of the physical interactome of *Saccharomyces cerevisiae**. Mol Cell Proteomics, 2007. **6**(3): p. 439-50.
22. Guo, Y., et al., *In silico and in vitro pharmacogenetic analysis in mice*. Proc Natl Acad Sci U S A, 2007. **104**(45): p. 17735-40.
23. Hu, S., J.A. Loo, and D.T. Wong, *Human saliva proteome analysis and disease biomarker discovery*. Expert Rev Proteomics, 2007. **4**(4): p. 531-8.
24. Bergeron, J.J. and M. Hallett, *Peptides you can count on*. Nat Biotechnol, 2007. **25**(1): p. 61-2.
25. Zhou, L., et al., *Phenotype microarray analysis of *Escherichia coli* K-12 mutants with deletions of all two-component systems*. J Bacteriol, 2003. **185**(16): p. 4956-72.
26. Bochner, B.R., *New technologies to assess genotype-phenotype relationships*. Nat Rev Genet, 2003. **4**(4): p. 309-14.
27. Fernandez-Ricaud, L., et al., *PROPHECY--a database for high-resolution phenomics*. Nucleic Acids Res, 2005. **33**(Database issue): p. D369-73.
28. Phizicky, E., et al., *Protein analysis on a proteomic scale*. Nature, 2003. **422**(6928): p. 208-15.
29. Huang, J., et al., *Finding new components of the target of rapamycin (TOR) signaling network through chemical genetics and proteome chips*. Proc Natl Acad Sci U S A, 2004. **101**(47): p. 16594-9.
30. Ray, S., et al., *Classification and prediction of clinical Alzheimer's diagnosis based on plasma signaling proteins*. Nat Med, 2007. **13**(11): p. 1359-62.
31. Ziauddin, J. and D.M. Sabatini, *Microarrays of cells expressing defined cDNAs*. Nature, 2001. **411**(6833): p. 107-10.
32. Wu, R.Z., S.N. Bailey, and D.M. Sabatini, *Cell-biological applications of transfected-cell microarrays*. Trends Cell Biol, 2002. **12**(10): p. 485-8.
33. Wheeler, D.B., A.E. Carpenter, and D.M. Sabatini, *Cell microarrays and RNA interference chip away at gene function*. Nat Genet, 2005. **37** Suppl: p. S25-30.
34. Wheeler, D.B., et al., *RNAi living-cell microarrays for loss-of-function screens in *Drosophila melanogaster* cells*. Nat Methods, 2004. **1**(2): p. 127-32.
35. Bailey, S.N., et al., *Microarrays of lentiviruses for gene function screens in immortalized and primary cells*. Nat Methods, 2006. **3**(2): p. 117-22.
36. Bailey, S.N., R.Z. Wu, and D.M. Sabatini, *Applications of transfected cell microarrays in high-throughput drug discovery*. Drug Discov Today, 2002. **7**(18 Suppl): p. S113-8.
37. Bailey, S.N., D.M. Sabatini, and B.R. Stockwell, *Microarrays of small molecules embedded in biodegradable polymers for use in mammalian cell-based screens*. Proc Natl Acad Sci U S A, 2004. **101**(46): p. 16144-9.

38. Harder, N., R. Eils, and K. Rohr, *Automated classification of mitotic phenotypes of human cells using fluorescent proteins*. *Methods Cell Biol*, 2008. **85**: p. 539-54.
39. Wollman, R. and N. Stuurman, *High throughput microscopy: from raw images to discoveries*. *J Cell Sci*, 2007. **120**(Pt 21): p. 3715-22.
40. Lamprecht, M.R., D.M. Sabatini, and A.E. Carpenter, *CellProfiler: free, versatile software for automated biological image analysis*. *Biotechniques*, 2007. **42**(1): p. 71-5.
41. Bakal, C., et al., *Quantitative morphological signatures define local signaling networks regulating cell morphology*. *Science*, 2007. **316**(5832): p. 1753-6.
42. Zhao, T. and R.F. Murphy, *Automated learning of generative models for subcellular location: Building blocks for systems biology*. *Cytometry A*, 2007. **71**(12): p. 978-90.
43. Garcia Osuna, E. and R.F. Murphy, *Automated, systematic determination of protein subcellular location using fluorescence microscopy*. *Subcell Biochem*, 2007. **43**: p. 263-76.
44. Chen, S.C., et al., *Automated image analysis of protein localization in budding yeast*. *Bioinformatics*, 2007. **23**(13): p. i66-71.
45. Huh, W.K., et al., *Global analysis of protein localization in budding yeast*. *Nature*, 2003. **425**(6959): p. 686-91.
46. Ghaemmaghami, S., et al., *Global analysis of protein expression in yeast*. *Nature*, 2003. **425**(6959): p. 737-41.
47. Giaever, G., et al., *Functional profiling of the *Saccharomyces cerevisiae* genome*. *Nature*, 2002. **418**(6896): p. 387-91.
48. Mnaimneh, S., et al., *Exploration of essential gene functions via titratable promoter alleles*. *Cell*, 2004. **118**(1): p. 31-44.
49. Ito, T., T. Chiba, and M. Yoshida, *Exploring the protein interactome using comprehensive two-hybrid projects*. *Trends Biotechnol*, 2001. **19**(10 Suppl): p. S23-7.
50. Cagney, G., P. Uetz, and S. Fields, *High-throughput screening for protein-protein interactions using two-hybrid assay*. *Methods Enzymol*, 2000. **328**: p. 3-14.
51. Tong, A.H. and C. Boone, *Synthetic genetic array analysis in *Saccharomyces cerevisiae**. *Methods Mol Biol*, 2006. **313**: p. 171-92.
52. Bader, G.D., et al., *Functional genomics and proteomics: charting a multidimensional map of the yeast cell*. *Trends Cell Biol*, 2003. **13**(7): p. 344-56.
53. Fraser, A.G. and E.M. Marcotte, *A probabilistic view of gene function*. *Nat Genet*, 2004. **36**(6): p. 559-64.
54. Fraser, A.G. and E.M. Marcotte, *Development through the eyes of functional genomics*. *Curr Opin Genet Dev*, 2004. **14**(4): p. 336-42.
55. Bork, P., et al., *Protein interaction networks from yeast to human*. *Curr Opin Struct Biol*, 2004. **14**(3): p. 292-9.
56. Lee, I., et al., *A probabilistic functional network of yeast genes*. *Science*, 2004. **306**(5701): p. 1555-8.
57. Jiang, T. and A.E. Keating, *AVID: an integrative framework for discovering functional relationships among proteins*. *BMC Bioinformatics*, 2005. **6**: p. 136.

58. Troyanskaya, O.G., et al., *A Bayesian framework for combining heterogeneous data sources for gene function prediction (in Saccharomyces cerevisiae)*. Proc Natl Acad Sci U S A, 2003. **100**(14): p. 8348-53.
59. Jansen, R., et al., *A Bayesian networks approach for predicting protein-protein interactions from genomic data*. Science, 2003. **302**(5644): p. 449-53.
60. Mellor, J.C., et al., *Predictome: a database of putative functional links between proteins*. Nucleic Acids Res, 2002. **30**(1): p. 306-9.
61. von Mering, C., et al., *STRING: known and predicted protein-protein associations, integrated and transferred across organisms*. Nucleic Acids Res, 2005. **33**(Database issue): p. D433-7.
62. Combs, D.J., et al., *Prp43p is a DEAH-box spliceosome disassembly factor essential for ribosome biogenesis*. Mol Cell Biol, 2006. **26**(2): p. 523-34.
63. Martin, A., S. Schneider, and B. Schwer, *Prp43 is an essential RNA-dependent ATPase required for release of lariat-intron from the spliceosome*. J Biol Chem, 2002. **277**(20): p. 17743-50.
64. McGary, K.L., I. Lee, and E.M. Marcotte, *Broad network-based predictability of S. cerevisiae gene loss-of-function phenotypes*. Genome Biol, 2007. **8**(12): p. R258.
65. Zhang, J., et al., *Genomic scale mutant hunt identifies cell size homeostasis genes in S. cerevisiae*. Curr Biol, 2002. **12**(23): p. 1992-2001.
66. Schneider, B.L., et al., *Growth rate and cell size modulate the synthesis of, and requirement for, G1-phase cyclins at start*. Mol Cell Biol, 2004. **24**(24): p. 10802-13.
67. Jorgensen, P., et al., *The size of the nucleus increases as yeast cells grow*. Mol Biol Cell, 2007. **18**(9): p. 3523-32.
68. Cook, M. and M. Tyers, *Size control goes global*. Curr Opin Biotechnol, 2007. **18**(4): p. 341-50.
69. Fingerman, I., et al., *Sfp1 plays a key role in yeast ribosome biogenesis*. Eukaryot Cell, 2003. **2**(5): p. 1061-8.
70. Cipollina, C., et al., *Revisiting the role of yeast Sfp1 in ribosome biogenesis and cell size control: a chemostat study*. Microbiology, 2008. **154**(Pt 1): p. 337-46.
71. Saito, T.L., et al., *Data mining tools for the Saccharomyces cerevisiae morphological database*. Nucleic Acids Res, 2005. **33**(Web Server issue): p. W753-7.
72. Saito, T.L., et al., *SCMD: Saccharomyces cerevisiae Morphological Database*. Nucleic Acids Res, 2004. **32**(Database issue): p. D319-22.
73. Ohya, Y., et al., *High-dimensional and large-scale phenotyping of yeast mutants*. Proc Natl Acad Sci U S A, 2005. **102**(52): p. 19015-20.
74. Singer, R.H., *RNA localization: visualization in real-time*. Curr Biol, 2003. **13**(17): p. R673-5.
75. Kumar, A., et al., *Subcellular localization of the yeast proteome*. Genes Dev, 2002. **16**(6): p. 707-19.
76. Jarvik, J.W., et al., *In vivo functional proteomics: mammalian genome annotation using CD-tagging*. Biotechniques, 2002. **33**(4): p. 852-4, 856, 858-60 passim.

77. Hoffmann, C., et al., *A FIAsh-based FRET approach to determine G protein-coupled receptor activation in living cells*. *Nat Methods*, 2005. **2**(3): p. 171-6.
78. Matsuyama, A., et al., *ORFeome cloning and global analysis of protein localization in the fission yeast Schizosaccharomyces pombe*. *Nat Biotechnol*, 2006. **24**(7): p. 841-7.
79. Remy, I., F.X. Campbell-Valois, and S.W. Michnick, *Detection of protein-protein interactions using a simple survival protein-fragment complementation assay based on the enzyme dihydrofolate reductase*. *Nat Protoc*, 2007. **2**(9): p. 2120-5.
80. Drawid, A., R. Jansen, and M. Gerstein, *Genome-wide analysis relating expression level with protein subcellular localization*. *Trends Genet*, 2000. **16**(10): p. 426-30.
81. Drawid, A. and M. Gerstein, *A Bayesian system integrating expression data with sequence patterns for localizing proteins: comprehensive application to the yeast genome*. *J Mol Biol*, 2000. **301**(4): p. 1059-75.
82. Madden, K. and M. Snyder, *Cell polarity and morphogenesis in budding yeast*. *Annu Rev Microbiol*, 1998. **52**: p. 687-744.
83. Pruyne, D. and A. Bretscher, *Polarization of cell growth in yeast*. *J Cell Sci*, 2000. **113** (Pt 4): p. 571-85.
84. Fujita, A., et al., *Rax1, a protein required for the establishment of the bipolar budding pattern in yeast*. *Gene*, 2004. **327**(2): p. 161-9.
85. Pruyne, D. and A. Bretscher, *Polarization of cell growth in yeast. I. Establishment and maintenance of polarity states*. *J Cell Sci*, 2000. **113** (Pt 3): p. 365-75.
86. Pruyne, D., et al., *Mechanisms of polarized growth and organelle segregation in yeast*. *Annu Rev Cell Dev Biol*, 2004. **20**: p. 559-91.
87. Iwase, M., et al., *Role of a Cdc42p effector pathway in recruitment of the yeast septins to the presumptive bud site*. *Mol Biol Cell*, 2006. **17**(3): p. 1110-25.
88. Dohlman, H.G. and J.E. Slessareva, *Pheromone signaling pathways in yeast*. *Sci STKE*, 2006. **2006**(364): p. cm6.
89. Dohlman, H.G., *G proteins and pheromone signaling*. *Annu Rev Physiol*, 2002. **64**: p. 129-52.
90. Dohlman, H.G. and J.W. Thorner, *Regulation of G protein-initiated signal transduction in yeast: paradigms and principles*. *Annu Rev Biochem*, 2001. **70**: p. 703-54.
91. Baba, M., et al., *Three-dimensional analysis of morphogenesis induced by mating pheromone alpha factor in Saccharomyces cerevisiae*. *J Cell Sci*, 1989. **94** (Pt 2): p. 207-16.
92. Elion, E.A., *Pheromone response, mating and cell biology*. *Curr Opin Microbiol*, 2000. **3**(6): p. 573-81.
93. Fields, S., *Pheromone response in yeast*. *Trends Biochem Sci*, 1990. **15**(7): p. 270-3.
94. Roberts, C.J., et al., *Signaling and circuitry of multiple MAPK pathways revealed by a matrix of global gene expression profiles*. *Science*, 2000. **287**(5454): p. 873-80.

95. Bochner, B.R., P. Gadzinski, and E. Panomitros, *Phenotype microarrays for high-throughput phenotypic testing and assay of gene function*. *Genome Res*, 2001. **11**(7): p. 1246-55.
96. Nishizuka, S., et al., *Diagnostic markers that distinguish colon and ovarian adenocarcinomas: identification by genomic, proteomic, and tissue array profiling*. *Cancer Res*, 2003. **63**(17): p. 5243-50.
97. Warringer, J., et al., *High-resolution yeast phenomics resolves different physiological features in the saline response*. *Proc Natl Acad Sci U S A*, 2003. **100**(26): p. 15724-9.
98. Xu, C.W., *High-density cell microarrays for parallel functional determinations*. *Genome Res*, 2002. **12**(3): p. 482-6.
99. Howitz, K.T., et al., *Small molecule activators of sirtuins extend *Saccharomyces cerevisiae* lifespan*. *Nature*, 2003. **425**(6954): p. 191-6.
100. Schwenk, J.M., et al., *Cell microarrays: an emerging technology for the characterization of antibodies*. *Biotechniques*, 2002. **Suppl**: p. 54-61.
101. Espina, V., et al., *Laser-capture microdissection*. *Nat Protoc*, 2006. **1**(2): p. 586-603.
102. Kononen, J., et al., *Tissue microarrays for high-throughput molecular profiling of tumor specimens*. *Nat Med*, 1998. **4**(7): p. 844-7.
103. Biran, I., et al., *Optical imaging fiber-based live bacterial cell array biosensor*. *Anal Biochem*, 2003. **315**(1): p. 106-13.
104. Blagoev, B. and A. Pandey, *Microarrays go live--new prospects for proteomics*. *Trends Biochem Sci*, 2001. **26**(11): p. 639-41.
105. Conrad, C., et al., *Automatic identification of subcellular phenotypes on human cell arrays*. *Genome Res*, 2004. **14**(6): p. 1130-6.
106. Silva, J.M., et al., *RNA interference microarrays: high-throughput loss-of-function genetics in mammalian cells*. *Proc Natl Acad Sci U S A*, 2004. **101**(17): p. 6548-52.
107. Narayanaswamy, R., et al., *Systematic profiling of cellular phenotypes with spotted cell microarrays reveals mating-pheromone response genes*. *Genome Biol*, 2006. **7**(1): p. R6.
108. Mewes, H.W., et al., *MIPS: analysis and annotation of proteins from whole genomes*. *Nucleic Acids Res*, 2004. **32**(Database issue): p. D41-4.
109. Dwight, S.S., et al., **Saccharomyces Genome Database (SGD)* provides secondary gene annotation using the Gene Ontology (GO)*. *Nucleic Acids Res*, 2002. **30**(1): p. 69-72.
110. Robinson, M.D., et al., *FunSpec: a web-based cluster interpreter for yeast*. *BMC Bioinformatics*, 2002. **3**: p. 35.
111. Wu, Y.L., et al., *Dominant-negative inhibition of pheromone receptor signaling by a single point mutation in the G protein alpha subunit*. *J Biol Chem*, 2004. **279**(34): p. 35287-97.
112. Ballensiefen, W. and H.D. Schmitt, *Periplasmic Bar1 protease of *Saccharomyces cerevisiae* is active before reaching its extracellular destination*. *Eur J Biochem*, 1997. **247**(1): p. 142-7.

113. Olson, K.A., et al., *Two regulators of Ste12p inhibit pheromone-responsive transcription by separate mechanisms*. Mol Cell Biol, 2000. **20**(12): p. 4199-209.
114. Mosch, H.U. and G.R. Fink, *Dissection of filamentous growth by transposon mutagenesis in Saccharomyces cerevisiae*. Genetics, 1997. **145**(3): p. 671-84.
115. van den Hazel, H.B., et al., *PDR16 and PDR17, two homologous genes of Saccharomyces cerevisiae, affect lipid biosynthesis and resistance to multiple drugs*. J Biol Chem, 1999. **274**(4): p. 1934-41.
116. Benachour, A., et al., *Deletion of GPI7, a yeast gene required for addition of a side chain to the glycosylphosphatidylinositol (GPI) core structure, affects GPI protein transport, remodeling, and cell wall integrity*. J Biol Chem, 1999. **274**(21): p. 15251-61.
117. Bagnat, M. and K. Simons, *Lipid rafts in protein sorting and cell polarity in budding yeast Saccharomyces cerevisiae*. Biol Chem, 2002. **383**(10): p. 1475-80.
118. Katzmann, D.J., G. Odorizzi, and S.D. Emr, *Receptor downregulation and multivesicular-body sorting*. Nat Rev Mol Cell Biol, 2002. **3**(12): p. 893-905.
119. Dulic, V. and H. Riezman, *Saccharomyces cerevisiae mutants lacking a functional vacuole are defective for aspects of the pheromone response*. J Cell Sci, 1990. **97** (Pt 3): p. 517-25.
120. Grosshans, B.L., et al., *TEDS site phosphorylation of the yeast myosins I is required for ligand-induced but not for constitutive endocytosis of the G protein-coupled receptor Ste2p*. J Biol Chem, 2006. **281**(16): p. 11104-14.
121. San-Segundo, P.A. and G.S. Roeder, *Role for the silencing protein Dot1 in meiotic checkpoint control*. Mol Biol Cell, 2000. **11**(10): p. 3601-15.
122. Dahan, O. and M. Kupiec, *Mutations in genes of Saccharomyces cerevisiae encoding pre-mRNA splicing factors cause cell cycle arrest through activation of the spindle checkpoint*. Nucleic Acids Res, 2002. **30**(20): p. 4361-70.
123. Ni, L. and M. Snyder, *A genomic study of the bipolar bud site selection pattern in Saccharomyces cerevisiae*. Mol Biol Cell, 2001. **12**(7): p. 2147-70.
124. Boland, M.V. and R.F. Murphy, *A neural network classifier capable of recognizing the patterns of all major subcellular structures in fluorescence microscope images of HeLa cells*. Bioinformatics, 2001. **17**(12): p. 1213-23.
125. Perlman, Z.E., et al., *Multidimensional drug profiling by automated microscopy*. Science, 2004. **306**(5699): p. 1194-8.
126. Prinz, S., et al., *Control of Signaling in a MAP-kinase Pathway by an RNA-Binding Protein*. PLoS ONE, 2007. **2**: p. e249.
127. Moore, S.A., *Comparison of dose-response curves for alpha factor-induced cell division arrest, agglutination, and projection formation of yeast cells. Implication for the mechanism of alpha factor action*. J Biol Chem, 1983. **258**(22): p. 13849-56.
128. Arimura, N. and K. Kaibuchi, *Neuronal polarity: from extracellular signals to intracellular mechanisms*. Nat Rev Neurosci, 2007. **8**(3): p. 194-205.
129. Krummel, M.F. and I. Macara, *Maintenance and modulation of T cell polarity*. Nat Immunol, 2006. **7**(11): p. 1143-9.
130. Gaziova, I. and K.M. Bhat, *Generating asymmetry: with and without self-renewal*. Prog Mol Subcell Biol, 2007. **45**: p. 143-78.

131. Proszynski, T.J., et al., *Plasma membrane polarization during mating in yeast cells*. J Cell Biol, 2006. **173**(6): p. 861-6.
132. Casolari, J.M., et al., *Developmentally induced changes in transcriptional program alter spatial organization across chromosomes*. Genes Dev, 2005. **19**(10): p. 1188-98.
133. Newpher, T.M., et al., *In vivo dynamics of clathrin and its adaptor-dependent recruitment to the actin-based endocytic machinery in yeast*. Dev Cell, 2005. **9**(1): p. 87-98.
134. Bagnat, M. and K. Simons, *Cell surface polarization during yeast mating*. Proc Natl Acad Sci U S A, 2002. **99**(22): p. 14183-8.
135. Bidlingmaier, S. and M. Snyder, *Large-scale identification of genes important for apical growth in Saccharomyces cerevisiae by directed allele replacement technology (DART) screening*. Funct Integr Genomics, 2002. **1**(6): p. 345-56.
136. Gehrung, S. and M. Snyder, *The SPA2 gene of Saccharomyces cerevisiae is important for pheromone-induced morphogenesis and efficient mating*. J Cell Biol, 1990. **111**(4): p. 1451-64.
137. Changwei, Z., X. Mingyong, and W. Ranran, *Afr1p has a role in regulating the localization of Mpk1p at the shmoo tip in Saccharomyces cerevisiae*. FEBS Lett, 2007. **581**(14): p. 2670-4.
138. Kumar, A., et al., *High-throughput methods for the large-scale analysis of gene function by transposon tagging*. Methods Enzymol, 2000. **328**: p. 550-74.
139. Lee, I., Z. Li, and E.M. Marcotte, *An Improved, Bias-Reduced Probabilistic Functional Gene Network of Baker's Yeast, Saccharomyces cerevisiae*. PLoS ONE, 2007. **2**(10): p. e988.
140. He, B., et al., *Exo70 interacts with phospholipids and mediates the targeting of the exocyst to the plasma membrane*. Embo J, 2007. **26**(18): p. 4053-65.
141. Wiederkehr, A., et al., *Sec3p is needed for the spatial regulation of secretion and for the inheritance of the cortical endoplasmic reticulum*. Mol Biol Cell, 2003. **14**(12): p. 4770-82.
142. Huckaba, T.M., et al., *Live cell imaging of the assembly, disassembly, and actin cable-dependent movement of endosomes and actin patches in the budding yeast, Saccharomyces cerevisiae*. J Cell Biol, 2004. **167**(3): p. 519-30.
143. Palmgren, S., et al., *Interactions with PIP2, ADP-actin monomers, and capping protein regulate the activity and localization of yeast twinfilin*. J Cell Biol, 2001. **155**(2): p. 251-60.
144. Clark, M.G., et al., *A genetic dissection of Aip1p's interactions leads to a model for Aip1p-cofilin cooperative activities*. Mol Biol Cell, 2006. **17**(4): p. 1971-84.
145. Cope, M.J., et al., *Novel protein kinases Ark1p and Prk1p associate with and regulate the cortical actin cytoskeleton in budding yeast*. J Cell Biol, 1999. **144**(6): p. 1203-18.
146. Smythe, E. and K.R. Ayscough, *The Ark1/Prk1 family of protein kinases. Regulators of endocytosis and the actin skeleton*. EMBO Rep, 2003. **4**(3): p. 246-51.
147. Tang, H.Y., J. Xu, and M. Cai, *Pan1p, End3p, and Sla1p, three yeast proteins required for normal cortical actin cytoskeleton organization, associate with each*

- other and play essential roles in cell wall morphogenesis. Mol Cell Biol, 2000. 20(1): p. 12-25.*
148. Dewar, H., et al., *Novel proteins linking the actin cytoskeleton to the endocytic machinery in Saccharomyces cerevisiae. Mol Biol Cell, 2002. 13(10): p. 3646-61.*
 149. Gourlay, C.W., et al., *A role for the actin cytoskeleton in cell death and aging in yeast. J Cell Biol, 2004. 164(6): p. 803-9.*
 150. Gilstring, C.F., M. Melin-Larsson, and P.O. Ljungdahl, *Shr3p mediates specific COPII coatomer-cargo interactions required for the packaging of amino acid permeases into ER-derived transport vesicles. Mol Biol Cell, 1999. 10(11): p. 3549-65.*
 151. Peng, R., A. De Antoni, and D. Gallwitz, *Evidence for overlapping and distinct functions in protein transport of coat protein Sec24p family members. J Biol Chem, 2000. 275(15): p. 11521-8.*
 152. Grote, E., C.M. Carr, and P.J. Novick, *Ordering the final events in yeast exocytosis. J Cell Biol, 2000. 151(2): p. 439-52.*
 153. Wicky, S., S. Frischmuth, and B. Singer-Kruger, *Bsp1p/Ypr171p is an adapter that directly links some synaptojanin family members to the cortical actin cytoskeleton in yeast. FEBS Lett, 2003. 537(1-3): p. 35-41.*
 154. Pashkova, N., et al., *Myosin V attachment to cargo requires the tight association of two functional subdomains. J Cell Biol, 2005. 168(3): p. 359-64.*
 155. Medkova, M., et al., *The rab exchange factor Sec2p reversibly associates with the exocyst. Mol Biol Cell, 2006. 17(6): p. 2757-69.*
 156. Walther, T.C., et al., *Eisosomes mark static sites of endocytosis. Nature, 2006. 439(7079): p. 998-1003.*
 157. Fleischer, T.C., et al., *Systematic identification and functional screens of uncharacterized proteins associated with eukaryotic ribosomal complexes. Genes Dev, 2006. 20(10): p. 1294-307.*
 158. Buttery, S.M., S. Yoshida, and D. Pellman, *Yeast formins Bni1 and Bnr1 utilize different modes of cortical interaction during the assembly of actin cables. Mol Biol Cell, 2007. 18(5): p. 1826-38.*
 159. Buehrer, B.M. and B. Errede, *Coordination of the mating and cell integrity mitogen-activated protein kinase pathways in Saccharomyces cerevisiae. Mol Cell Biol, 1997. 17(11): p. 6517-25.*
 160. Ono, T., et al., *The MID2 gene encodes a putative integral membrane protein with a Ca(2+)-binding domain and shows mating pheromone-stimulated expression in Saccharomyces cerevisiae. Gene, 1994. 151(1-2): p. 203-8.*
 161. Lommel, M., M. Bagnat, and S. Strahl, *Aberrant processing of the WSC family and Mid2p cell surface sensors results in cell death of Saccharomyces cerevisiae O-mannosylation mutants. Mol Cell Biol, 2004. 24(1): p. 46-57.*
 162. Cooper, T.G., et al., *Addition of basic amino acids prevents G-1 arrest of nitrogen-starved cultures of Saccharomyces cerevisiae. J Bacteriol, 1979. 137(3): p. 1447-8.*
 163. Marco, E., et al., *Endocytosis optimizes the dynamic localization of membrane proteins that regulate cortical polarity. Cell, 2007. 129(2): p. 411-22.*

164. Takizawa, P.A., et al., *Actin-dependent localization of an RNA encoding a cell-fate determinant in yeast*. Nature, 1997. **389**(6646): p. 90-3.
165. Werner-Washburne, M., et al., *Stationary phase in the yeast Saccharomyces cerevisiae*. Microbiol Rev, 1993. **57**(2): p. 383-401.
166. Gray, J.V., et al., *"Sleeping beauty": quiescence in Saccharomyces cerevisiae*. Microbiol Mol Biol Rev, 2004. **68**(2): p. 187-206.
167. Allen, C., et al., *Isolation of quiescent and nonquiescent cells from yeast stationary-phase cultures*. J Cell Biol, 2006. **174**(1): p. 89-100.
168. Pinon, R., *Folded chromosomes in non-cycling yeast cells: evidence for a characteristic g0 form*. Chromosoma, 1978. **67**(3): p. 263-74.
169. Choder, M., *A general topoisomerase I-dependent transcriptional repression in the stationary phase in yeast*. Genes Dev, 1991. **5**(12A): p. 2315-26.
170. Fuge, E.K., E.L. Braun, and M. Werner-Washburne, *Protein synthesis in long-term stationary-phase cultures of Saccharomyces cerevisiae*. J Bacteriol, 1994. **176**(18): p. 5802-13.
171. Ashrafi, K., et al., *Passage through stationary phase advances replicative aging in Saccharomyces cerevisiae*. Proc Natl Acad Sci U S A, 1999. **96**(16): p. 9100-5.
172. Martinez, M.J., et al., *Genomic analysis of stationary-phase and exit in Saccharomyces cerevisiae: gene expression and identification of novel essential genes*. Mol Biol Cell, 2004. **15**(12): p. 5295-305.
173. Broach, J.R., *RAS genes in Saccharomyces cerevisiae: signal transduction in search of a pathway*. Trends Genet, 1991. **7**(1): p. 28-33.
174. Schmelzle, T. and M.N. Hall, *TOR, a central controller of cell growth*. Cell, 2000. **103**(2): p. 253-62.
175. Raught, B., A.C. Gingras, and N. Sonenberg, *The target of rapamycin (TOR) proteins*. Proc Natl Acad Sci U S A, 2001. **98**(13): p. 7037-44.
176. Reinders, A., et al., *Saccharomyces cerevisiae cAMP-dependent protein kinase controls entry into stationary phase through the Rim15p protein kinase*. Genes Dev, 1998. **12**(18): p. 2943-55.
177. Patturajan, M., et al., *Growth-related changes in phosphorylation of yeast RNA polymerase II*. J Biol Chem, 1998. **273**(8): p. 4689-94.
178. Krause, S.A. and J.V. Gray, *The protein kinase C pathway is required for viability in quiescence in Saccharomyces cerevisiae*. Curr Biol, 2002. **12**(7): p. 588-93.
179. Torres, J., et al., *Regulation of the cell integrity pathway by rapamycin-sensitive TOR function in budding yeast*. J Biol Chem, 2002. **277**(45): p. 43495-504.
180. Kamada, Y., et al., *Tor-mediated induction of autophagy via an Apg1 protein kinase complex*. J Cell Biol, 2000. **150**(6): p. 1507-13.
181. Klionsky, D.J. and Y. Ohsumi, *Vacuolar import of proteins and organelles from the cytoplasm*. Annu Rev Cell Dev Biol, 1999. **15**: p. 1-32.
182. Paz, I., L. Abramovitz, and M. Choder, *Starved Saccharomyces cerevisiae cells have the capacity to support internal initiation of translation*. J Biol Chem, 1999. **274**(31): p. 21741-5.
183. Paz, I. and M. Choder, *Eukaryotic translation initiation factor 4E-dependent translation is not essential for survival of starved yeast cells*. J Bacteriol, 2001. **183**(15): p. 4477-83.

184. Longo, V.D., E.B. Gralla, and J.S. Valentine, *Superoxide dismutase activity is essential for stationary phase survival in Saccharomyces cerevisiae. Mitochondrial production of toxic oxygen species in vivo.* J Biol Chem, 1996. **271**(21): p. 12275-80.
185. Sobering, A.K., et al., *Yeast Rpi1 is a putative transcriptional regulator that contributes to preparation for stationary phase.* Eukaryot Cell, 2002. **1**(1): p. 56-65.
186. Gasch, A.P. and M. Werner-Washburne, *The genomics of yeast responses to environmental stress and starvation.* Funct Integr Genomics, 2002. **2**(4-5): p. 181-92.
187. Radonjic, M., et al., *Genome-wide analyses reveal RNA polymerase II located upstream of genes poised for rapid response upon S. cerevisiae stationary phase exit.* Mol Cell, 2005. **18**(2): p. 171-83.
188. Brengues, M., D. Teixeira, and R. Parker, *Movement of eukaryotic mRNAs between polysomes and cytoplasmic processing bodies.* Science, 2005. **310**(5747): p. 486-9.
189. Sinclair, D., K. Mills, and L. Guarente, *Aging in Saccharomyces cerevisiae.* Annu Rev Microbiol, 1998. **52**: p. 533-60.
190. Tissenbaum, H.A. and L. Guarente, *Model organisms as a guide to mammalian aging.* Dev Cell, 2002. **2**(1): p. 9-19.
191. Longo, V.D., *Mutations in signal transduction proteins increase stress resistance and longevity in yeast, nematodes, fruit flies, and mammalian neuronal cells.* Neurobiol Aging, 1999. **20**(5): p. 479-86.
192. Fabrizio, P. and V.D. Longo, *The chronological life span of Saccharomyces cerevisiae.* Methods Mol Biol, 2007. **371**: p. 89-95.
193. Fabrizio, P., et al., *Regulation of longevity and stress resistance by Sch9 in yeast.* Science, 2001. **292**(5515): p. 288-90.
194. Kaerberlein, M., C.R. Burtner, and B.K. Kennedy, *Recent developments in yeast aging.* PLoS Genet, 2007. **3**(5): p. e84.
195. Chen, Q., Q. Ding, and J.N. Keller, *The stationary phase model of aging in yeast for the study of oxidative stress and age-related neurodegeneration.* Biogerontology, 2005. **6**(1): p. 1-13.
196. Chen, Q., J. Thorpe, and J.N. Keller, *Alpha-synuclein alters proteasome function, protein synthesis, and stationary phase viability.* J Biol Chem, 2005. **280**(34): p. 30009-17.
197. Vernace, V.A., T. Schmidt-Glenewinkel, and M.E. Figueiredo-Pereira, *Aging and regulated protein degradation: who has the UPPer hand?* Aging Cell, 2007. **6**(5): p. 599-606.
198. Aguilaniu, H., et al., *Asymmetric inheritance of oxidatively damaged proteins during cytokinesis.* Science, 2003. **299**(5613): p. 1751-3.
199. Erjavec, N., et al., *Accelerated aging and failure to segregate damaged proteins in Sir2 mutants can be suppressed by overproducing the protein aggregation-remodeling factor Hsp104p.* Genes Dev, 2007. **21**(19): p. 2410-21.
200. Sagot, I., et al., *Actin bodies in yeast quiescent cells: an immediately available actin reserve?* Mol Biol Cell, 2006. **17**(11): p. 4645-55.

201. Wang, L., et al., *Inorganic polyphosphate stimulates mammalian TOR, a kinase involved in the proliferation of mammary cancer cells*. Proc Natl Acad Sci U S A, 2003. **100**(20): p. 11249-54.

Chapter 3: Systematic definition of protein constituents along the major polarization axis reveals an adaptive re-use of the polarization machinery in pheromone treated budding yeast

INTRODUCTION

Polarizing cells undergo extensive molecular rearrangements in a spatially and temporally concerted manner, reorganizing cellular components along the major cellular polarized growth axis. Polarization mechanisms are important for both basic cell division and specialized growth processes, such as formation of neuronal processes [128], cell motility [129] and asymmetric stem cell differentiation [130]. The resultant coordinated asymmetry affects major developmental, cell division, and metabolic programs in the cell. The budding yeast, *S. cerevisiae*, has proved an excellent model system for studying polarized growth, as it restructures the cell differentially in vegetative growth, mating and filamentous growth [82]. Each of these developmental fates is characterized by a distinct morphology, with the stimulus and outcomes of each differentiation pathway being unique. For example, internal bud cues from the previous bud site drive the cycle of bud emergence and cytokinesis. External cues such as mating pheromone and nutrient starvation trigger signal transduction pathways that induce formation of a mating projection or the filamentous ‘foraging’ phenotype, respectively. These changes in cellular morphology are accompanied by dynamic changes in the cellular proteome that function in setting up the polarization axis and orchestrating specific activities required for the appropriate response.

Wild type yeast cells, upon treatment with pheromone from the opposite mating type, undergo a differentiation program typified by the formation of a mating projection (the ‘shmoo’) accompanied by cell cycle arrest in the G1 phase. Many proteins are re-

distributed to different subcellular locations culminating in the formation of a highly structured polarization axis oriented towards the shmoo tip. Although similar polarization mechanisms dominate the formation of bud and a mating projection, there are obvious differences underlying the two processes. While budding is pre-ordained by location of the previous budding landmark, mating projection formation appears to be a dynamic process that relies on a directional pheromone gradient. Mating-competent cells can therefore continuously sense pheromone gradients and alter the site of projection formation accordingly, and in some instances even form multiple ‘shmoos’[82]. The shape and structure of mating projections also differ from buds, with the conspicuous constriction that marks buds being largely absent at the base of the ‘shmoos’. This region contains the septins, chitin, and pheromone induced proteins such as Afr1p that interact with the septins. It is therefore likely that an altered set of protein interactions during the mating process determines the shape and morphology of the projection and distinguishes it from bud formation during vegetative growth. This is more evident when one analyzes finer details such as the growth dynamics of a bud relative to a shmoo. Bud growth becomes isotropic after the apical growth phase while a shmoo displays more unidirectional growth dynamics, possibly because of differential rates of recruitment of proteins that deposit cell wall constituents. These differences arise due to the distinct functional goals that each process seeks to achieve – bud formation, nuclear segregation to the daughter and cytokinesis during vegetative growth as opposed to cell fusion and karyogamy during mating [82].

In this study, we have attempted to map the changes in localization of the yeast proteome upon formation of a mating projection. Although individual proteins that localize to the shmoo tip have been characterized (e.g., the shmoo tip marker Fus1 [131]), proteome-wide screens have not been performed to measure such localization changes

due to their expensive and cumbersome nature. We developed and implemented a novel cell microarray-based imaging assay for measuring the spatial redistribution of a large fraction of the yeast proteome, and applied this assay to identify proteins localized along the mating projection following pheromone treatment. By further incorporating information about known yeast gene associations and about protein localization during vegetative growth, we trained a machine learning algorithm to refine the cell imaging screen, resulting in a total of 74 proteins identified that specifically localize to mating projection. Functional analysis of these proteins, coupled with analyses of individual organelle movements during shmoo formation, suggests a model in which the basic machinery for cell polarization is generally conserved between processes forming the bud and the shmoo, with a distinct subset of proteins used only for shmoo formation. The net effect is a defined ordering of major organelles along the polarization axis, with specific proteins implicated at the proximal growth tip.

RESULTS

I. Organellar movement during pheromone-induced polarized growth

It has been previously observed that organelles move during the pheromone-induced, polarized growth of yeast [91]. In order to establish conditions for screening for genes involved in polarized growth we used light microscopy to identify reproducible trends in organellar movements. We systematically measured the subcellular localization of 9 major organelles via organelle-specific fluorescent protein fusion markers. For each organelle, we constructed a yeast strain expressing both a RFP-tagged organelle marker and an orientation marker, a GFP-tagged shmoo tip marker, *Fus1p*. The positions of the two fluorescent protein markers and the nucleus (detected by staining with DAPI) were

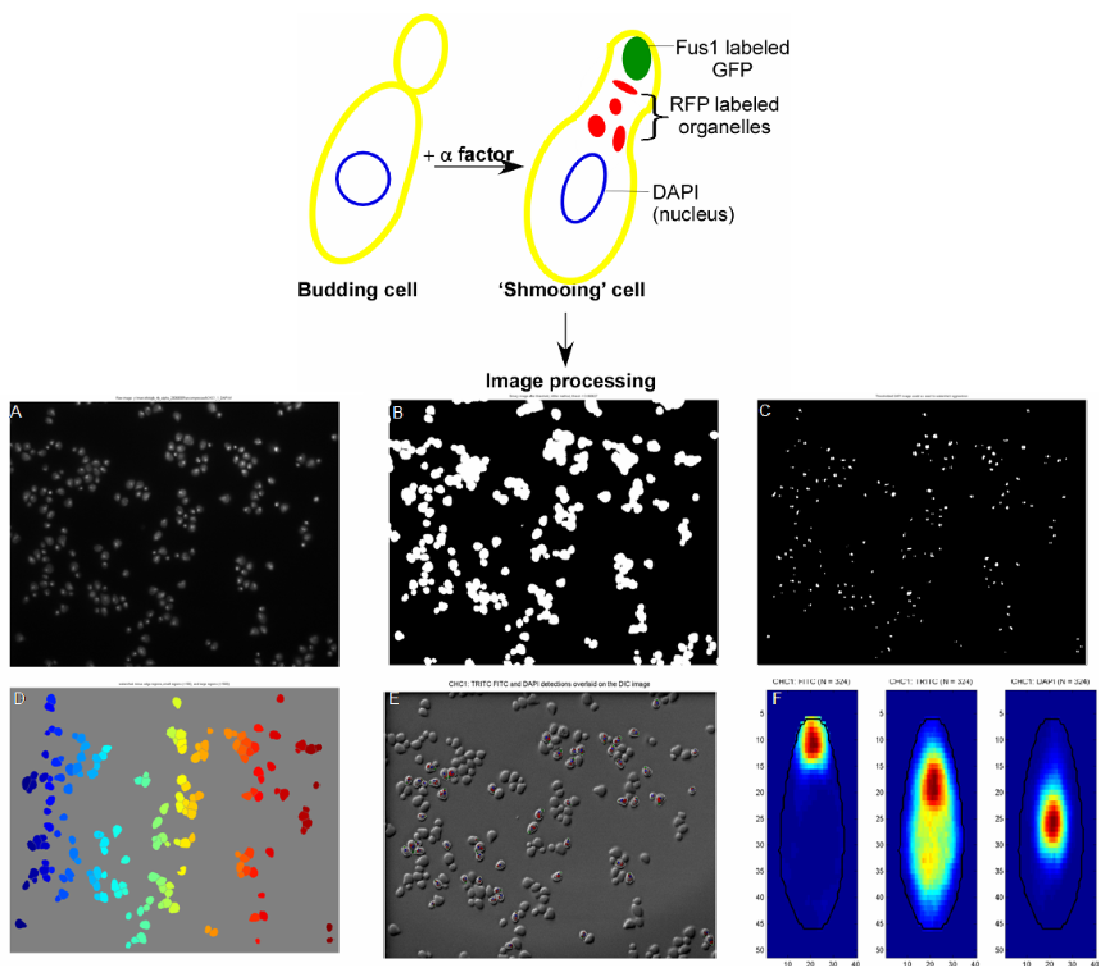


Figure 3-1: Expository figure showing the treatment and image analyses of organellar localization upon pheromone treatment. Synthetic alpha factor is added to vegetatively growing cells containing GFP tagged Fus1p and different RFP tagged organellar marker proteins. A. Image of shmoo tip marker Fus1p labeled with GFP, clathrin marker Chc1p labeled with RFP, cell nuclei stained with DAPI B. Binary thresholded image, C. Binary image of nuclei used to seed watershed segmentation, D. Result of watershed segmentation, E. Shmooring cells are identified and cell-by-cell thresholding on the FITC, TRITC, and DAPI images is overlaid on the DIC image, F. Result of rotating and overlaying thresholded fluorescent intensity distributions for all shmooring cells (n=324) from multiple still images.

determined before and after treatment with alpha factor. Image analysis was used to quantify each organelle's spatial distribution across >100 individual cells in an image (**Figure 3-1**). Organellar positions were calculated after reorienting and scaling each

individual cell in the image to a common reference frame (the axis from the nucleus to the shmoo tip).

Each organelle marker strain (**Figure 3-2**) strongly revealed the formation of an axis of polarity, presumably towards the pheromone gradient in anticipation of the mating process and subsequent cellular fusion. Several common features about organellar arrangement were evident: The nucleated actin filaments that form the actin cables were polarized towards the shmoo tip (as evidenced by Sac6-RFP fusions, the cross-linking fimbrin protein used as the marker). This was consistent with actin cables acting as ‘conduits’ for transporting organelles during vegetative growth, just as they do during mating [82]. The spindle pole body core component, Spc42 was prominent in its movement towards the shmoo tip, indicating that the tethered spindle microtubules, the nuclear envelope and the chromosomes were also re-oriented [91, 132]. In consequence, the entire nucleus was also re-oriented towards the shmoo tip, with the nucleolus being located at the opposite side of the nucleus relative to the shmoo tip. Another consequence was extensive vesicular trafficking of cargo intended for membrane deposition and new cell wall formation at the site of the shmoo projection (as evidenced by localization of clathrin protein Chc1 with Fus1-GFP). This finding was additionally corroborated by alignment towards the polarization axis of the endoplasmic reticulum marker Sec13, a component of the Nup84 nuclear pore complex and COPII complex, further indicating ongoing ER to Golgi vesicle transport. As expected, there was also a polarization of a Golgi cisternal marker, Anp1, towards the shmoo tip. While polarization was along the shmoo tip axis, transport may occur in both directions. The endosome marker, Snf7 tended to accumulate toward the shmoo tip, possibly implicating the involvement of the endocytic pathway in trafficking components between the membrane and the vacuole (for

example, the pheromone receptor Ste2 which upon pheromone binding and ubiquitination, is internalized and endocytosed into vesicles [133]).

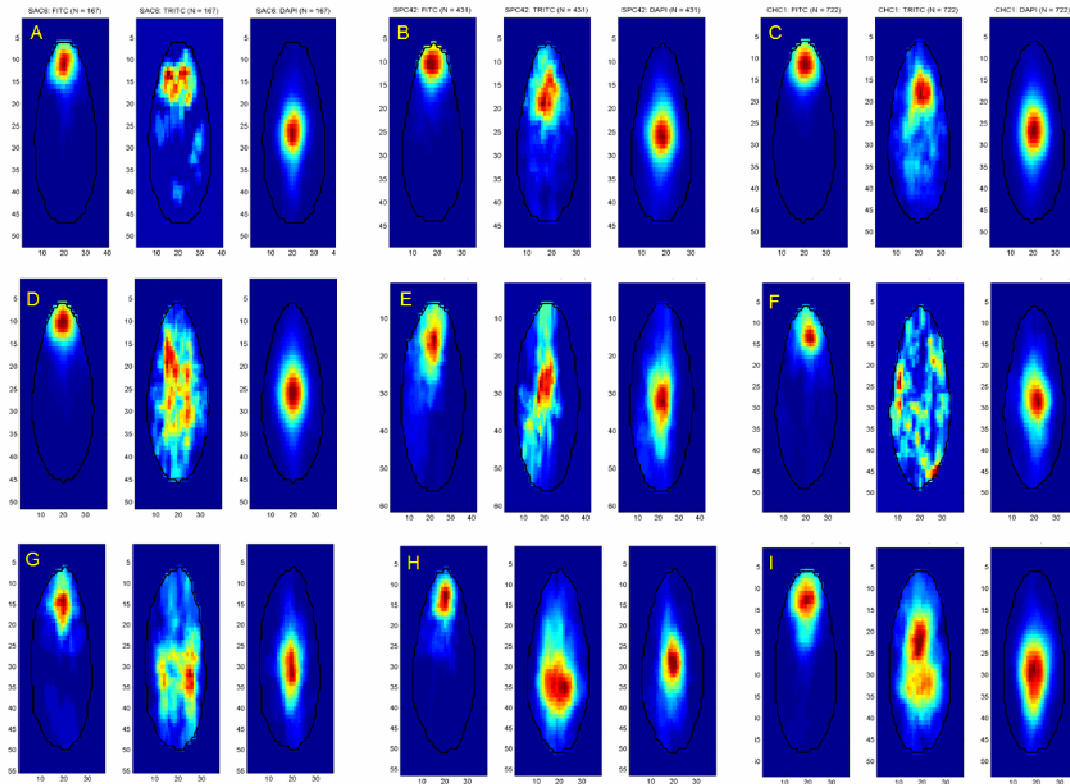


Figure 3-2: Results of rotating and overlaying thresholded fluorescent intensity distributions for all shmooing cells from multiple still images. Shmoos tip marker (FUS1) labeled with GFP, indicated organelle markers labeled with RFP, cell nuclei stained with DAPI. A. actin (SAC6), B. spindle pole (SPC42), C. clathrin (CHC1), D. golgi cis-cisterna (ANP1), E. ER/golgi (SEC13), F. peroxisome (PEX3), G. lipid particle (ERG6), H. nucleolus (SIK1), I. cytoplasm / endosomal membranes (SNF7).

Overall, our results are consistent with the establishment of an alpha factor-induced polarization axis which leads to the spatial reorganization of multiple organelles in a roughly ordered fashion from proximal to the shmoo tip to the distal end of the cell.

II. Identification of specific proteins and pathways contributing to polarized growth

Having established a reproducible cell-by-cell organellar reorganization along the polarization axis, we attempted to identify the numerous proteins and protein complexes that mediated these cell-wide changes in morphology and distribution. We therefore undertook a systematic, high-throughput analysis of alpha factor-induced changes in protein localization of GFP-tagged yeast strains. It should be noted that a comprehensive survey of proteins localized to the shmoo tip has not previously been carried out despite many studies [134-137] that have implicated key roles for individual proteins in this dynamic cellular compartment. Building on our previous success in constructing and screening yeast cell microarrays [107], we screened the collection of GFP-tagged yeast strains for pheromone-induced changes in protein localization.

a. Identifying pheromone-induced changes in protein localization using cell microarrays

An overview of the cell microarray assay is presented in **Figure 3-3**. Briefly, after treating the library of GFP-tagged fusion protein expression strains with alpha factor, we fixed and robotically printed [45] the strains on to poly-lysine-coated microscope slides [107] and imaged the fixed strains using automated microscopy. We screened for proteins showing a clear localization proximal to the shmoo tip. In all, 187 proteins were chosen from the initial screen, based on a lenient criterion that included even marginal examples. These 187 strains were then manually re-tested in the absence of fixative, which improved signal-to-noise because of reduced background fluorescence. The follow-up screen yielded 43 strains in which GFP fusion proteins were consistently localized to the shmoo tip (**Table 3-1**).

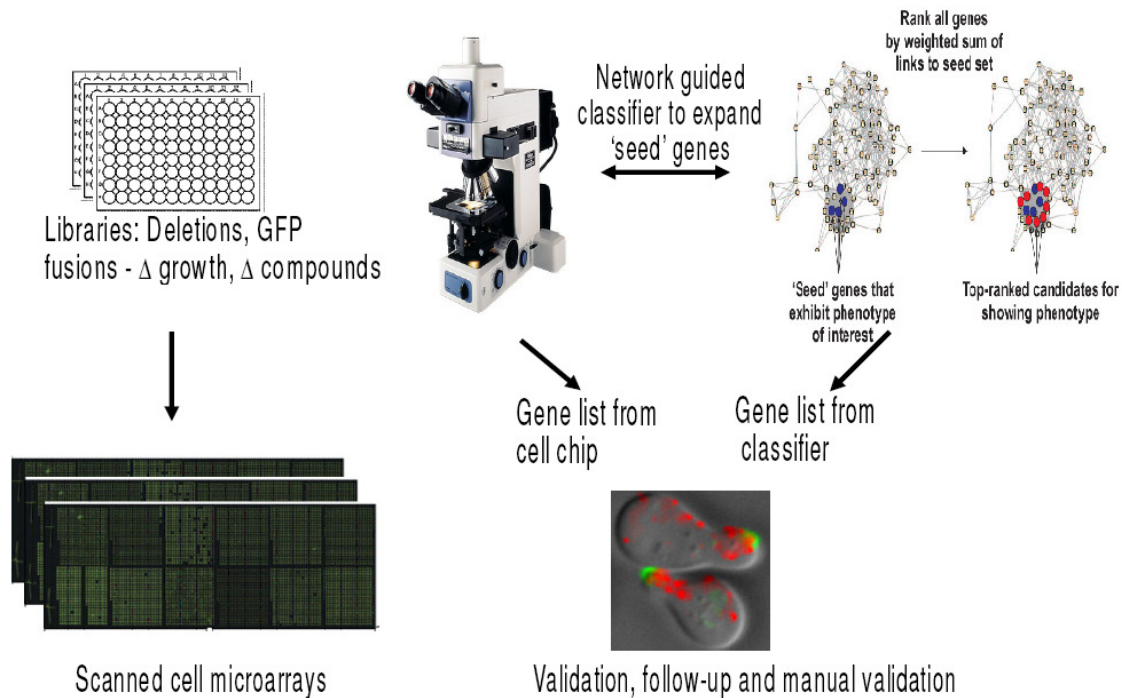


Figure 3-3: Schematic of the work flow for performing proteome-wide localization screen. Epitope tagged libraries such the GFP tagged yeast library is treated with a compound of effect a perturbation of choice. The library is then microarrayed onto a microscope slide with or without fixation. High throughput microscopy gives a list of seed genes that are then expanded using a probabilistic functional interaction network based classifier.

Statistical analysis of the cellular functions represented by these proteins [110] showed a significant enrichment for several pathways and processes, including genes involved in secretion/exocytosis, budding/cell polarity, cytoskeletal organization, and pheromone response/mating specificity. Representative examples are shown in **Figure 3-4**.

Gene name	ORF name	Gene Ontology biological process annotation
ABP1	YCR088W	establishment of cell polarity (sensu Fungi)
AIP1	YMR092C	response to osmotic stress
BEM3	YPL115C	pseudohyphal growth
CAP1	YKL007W	barbed-end actin filament capping
CAP2	YIL034C	filamentous growth
CAR1	YPL111W	arginine catabolism to ornithine
CBK1	YNL161W	regulation of exit from mitosis
CDC10	YCR002C	cell wall organization and biogenesis
CDC11	YJR076C	cell wall organization and biogenesis
CDC48	YDL126C	ubiquitin-dependent protein catabolism
COQ6	YGR255C	ubiquinone biosynthesis
COX15	YER141W	heme a biosynthesis
COX5B	YIL111W	mitochondrial electron transport, cytochrome c to oxygen
EDE1	YBL047C	endocytosis
END3	YNL084C	endocytosis
ENT1	YDL161W	endocytosis
EXO70	YJL085W	cytokinesis
EXO84	YBR102C	exocytosis
FUS1	YCL027W	conjugation with cellular fusion
INP52	YNL106C	cell wall organization and biogenesis
KEL1	YHR158C	cell morphogenesis
LSG1	YGL099W	ribosome biogenesis
MID2	YLR332W	cell wall organization and biogenesis
PEA2	YER149C	pseudohyphal growth
POP2	YNR052C	regulation of transcription from RNA polymerase II promoter
RMD9	YGL107C	biological process unknown
SEC10	YLR166C	establishment of cell polarity (sensu Fungi)
SEC18	YBR080C	ER to Golgi vesicle-mediated transport
SEC2	YNL272C	exocytosis
SEC3	YER008C	cytokinesis
SEC5	YDR166C	cytokinesis
SEC6	YIL068C	cytokinesis
SEC8	YPR055W	cytokinesis
SHM2	YLR058C	one-carbon compound metabolism
SHR3	YDL212W	ER to Golgi vesicle-mediated transport
SLA1	YBL007C	cell wall organization and biogenesis
SLG1	YOR008C	cell wall organization and biogenesis
SMY1	YKL079W	exocytosis
YCR043C	YCR043C	biological process unknown
YDR061W	YDR061W	biological process unknown
YMR295C	YMR295C	biological process unknown
YNL100W	YNL100W	biological process unknown
YOR304C-A	YOR304C-A	biological process unknown

Table 3-1: Manually verified shmoo tip localized genes identified by the cell chip.

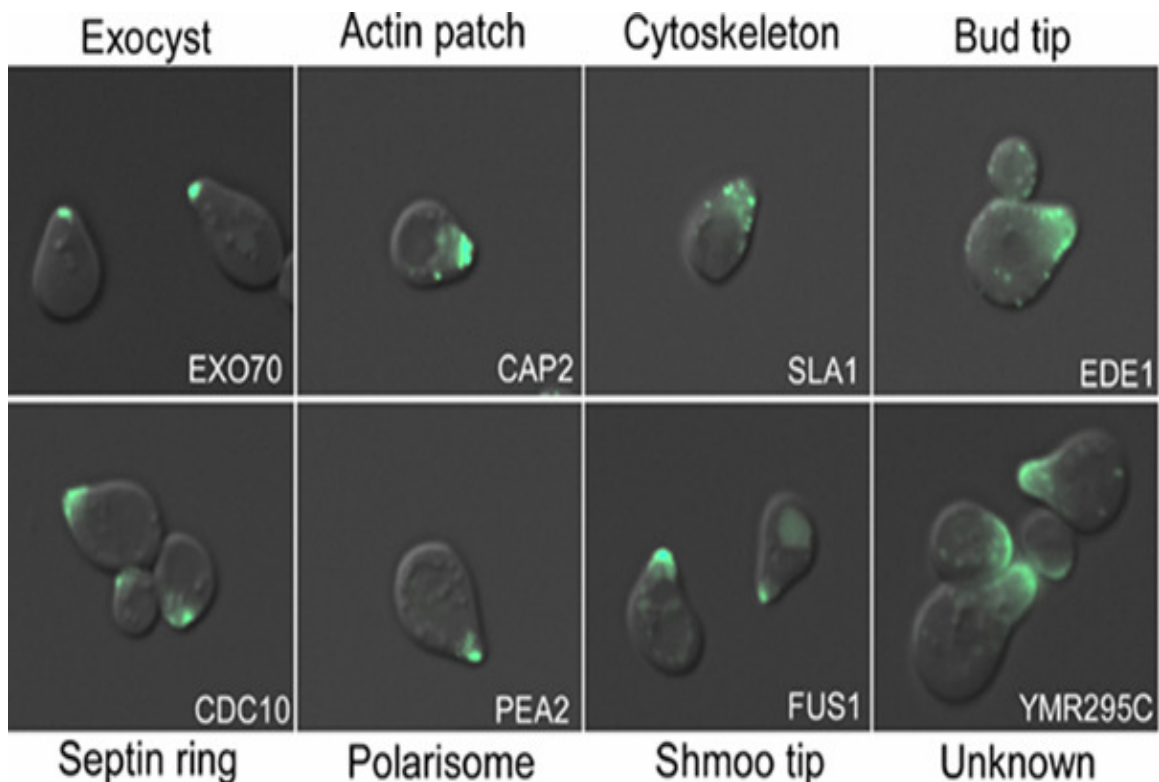


Figure 3-4: Representative components of cellular systems that were recovered from the cell chip after a round of manual validation. Each panel shows a few cells from one yeast strain expressing a GFP-tagged protein localized to the tip of the shmoo following pheromone response. With the exception of YMR295C, the proteins displayed are known components of the cellular processes labeled outside each panel.

Of the 144 proteins not confirmed by the manual follow-up imaging assay, roughly 65% were either mitochondrial proteins or proteins that were localized at the base of the shmoo neck or at the base of the shmoo tip. These classes were obviously difficult to distinguish from true proximal shmoo localization, leading to their inclusion in our initial lenient screen. The remaining 35% of the excluded proteins exhibited punctate structures not reproducibly associated with the shmoo tip (e.g., peroxisomal proteins). The high throughput survey recovered about 13% of the SGD-annotated, shmoo-localized proteins.[109]. This high false negative rate is likely due to fixation induced auto-fluorescence, which masks low abundance proteins.

b. Computational identification and confirmation of additional shmoo-localized proteins

We took advantage of near genome-wide datasets of protein localization in vegetative growing yeast cells [45, 138] and an integrated probabilistic gene network of functional genomic and proteomics data [56, 139] in order to develop a machine learning algorithm for predicting additional proteins localized to the shmoo tip (for example, proteins that had been missed because of low expression or phenotype penetrance). As detailed in the Methods section, our initial set of 37 proteins obtained from the cell chip screen was used to train a *naïve* Bayesian classifier. Application of the classifier identified 151 proteins exceeding a 50% probability score threshold. An advantage of this approach is that the delimited set of candidate genes could then be individually assayed in the absence of fixative, a task that was greatly simplified because 118 of the 151 proteins were already present in the extant GFP library. We manually re-tested each of these 118 GFP fusion strains for protein localization to the shmoo tip. From this set, 37 additional proteins (~32%), were confirmed to be shmoo-localized (**Table 3-2**).

The classifier-guided retesting strategy improved the coverage of the screen dramatically, and any remaining false negatives could be rationalized based upon low protein abundance. Of genes in the GFP library, we could identify 63% of the known shmoo tip-localized proteins that were present at >2500 molecules/cell, but less than 21% of known proteins with <2500 molecules/cell. On average, the shmoo tip proteins identified via the classifier method were less abundant than those recovered via the cell chip method lending credence to using a network guided approach to expand an initial list of seed genes. Although we were interested in specifically identifying proteins localized to the shmoo tip and therefore picked the highest confidence linkages, it must be

mentioned that this process can be iterated to potentially reveal more genes that are related to the pheromone response pathway.

Gene name	ORF name	Gene Ontology biological process annotation
ABP140	YOR239W	actin cytoskeleton organization and biogenesis
ARK1	YNL020C	protein amino acid phosphorylation
BCK1	YJL095W	protein amino acid phosphorylation
BEM1	YBR200W	establishment of cell polarity (sensu Fungi)
BNI1	YNL271C	pseudohyphal growth
BOI1	YBL085W	establishment of cell polarity (sensu Fungi)
BSP1	YPR171W	actin cortical patch distribution
BUD6	YLR319C	actin filament organization
BZZ1	YHR114W	endocytosis
CHS3	YBR023C	cytokinesis
CHS5	YLR330W	spore wall assembly (sensu Fungi)
ENT2	YLR206W	endocytosis
KEL2	YGR238C	conjugation with cellular fusion
LAS17	YOR181W	endocytosis
MYO2	YOR326W	vesicle-mediated transport
MYO5	YMR109W	cell wall organization and biogenesis
PAN1	YIR006C	endocytosis
PRK1	YIL095W	protein amino acid phosphorylation
RGD1	YBR260C	response to acid
RVS161	YCR009C	endocytosis
RVS167	YDR388W	endocytosis
SAC6	YDR129C	endocytosis
SEC15	YGL233W	cytokinesis
SEC31	YDL195W	ER to Golgi vesicle-mediated transport
SFB3	YHR098C	ER to Golgi vesicle-mediated transport
SHS1	YDL225W	establishment of cell polarity (sensu Fungi)
SLA2	YNL243W	telomere maintenance
SMI1	YGR229C	telomere maintenance
SRV2	YNL138W	pseudohyphal growth
SYP1	YCR030C	biological process unknown
TWF1	YGR080W	bipolar bud site selection
VRP1	YLR337C	endocytosis
WSC2	YNL283C	cell wall organization and biogenesis
WSC3	YOL105C	cell wall organization and biogenesis
YDR348C	YDR348C	biological process unknown
YER071C	YER071C	biological process unknown
YIR003W	YIR003W	biological process unknown

Table 3-2: Manually verified shmoo tip localized proteins identified by the classifier.

III. Adaptive re-use of polarization machinery

The 74 shmoo-tip localized proteins (37 from the cell microarray screen, 37 from computational prediction and screening) showed a marked enrichment for functional categories (with $p < 10^{-6}$ being the probability calculated using a hypergeometric distribution that the intersection of given list with any functional category occurs by chance) such as cytokinesis, budding, and formation of the cytoskeletal architecture (**Figure 3-5**). More specifically, we note that many of the proteins localized to the shmoo tip belong to protein complexes that are also involved in mediating polarized growth at the bud tip during vegetative growth (**Figure 3-6**). Thus, there appears to be broad adaptive re-use of the polarization machinery between these two processes.

Category	p-value
cytoskeletal protein binding [GO:0008092]	1.00E-14
protein binding [GO:0005515]	1.00E-14
actin binding [GO:0003779]	5.11E-12
cytoskeletal adaptor [GO:0008093]	1.15E-06
cytoskeletal regulatory protein binding [GO:0005519]	1.49E-05
binding [GO:0005488]	2.08E-05
F-actin capping [GO:0003782]	0.000134
actin cross-linking [GO:0003780]	0.000791
motor [GO:0003774]	0.000917
microfilament motor [GO:0000146]	0.001948
structural constituent of cytoskeleton [GO:0005200]	0.002417
Rho GTPase activator [GO:0005100]	0.00457

Figure 3-5: GO molecular functions enriched in the list of shmoo tip localized proteins.

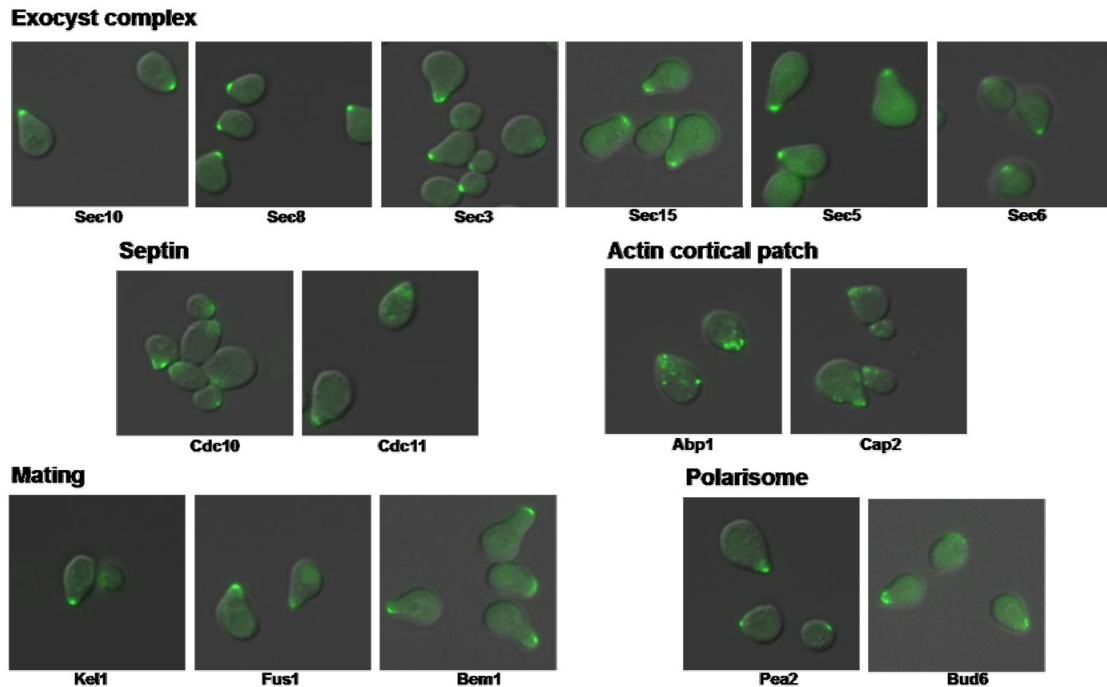


Figure 3-6: Representative components of cellular systems found localized to the shmoo tip. Components of cellular systems such as exocyst, septin, polarisome and actin cortical patch were recovered almost in their entirety (Table 3-1, 3-2). Proteins that function in signaling and fusion events such as Bem1, Fus1 and Kel1 are also represented.

The exocyst (**Figure 3-6**) is an evolutionarily conserved octameric protein complex thought to be targeted to the plasma membrane through the interaction of Exo70 with phospholipids [140] and stabilized by Sec3 [141]. One of the major functions of the exocyst is to direct docking of myosin motor driven vesicles at the bud site during vegetative growth. Although the exocyst has not been directly implicated in pheromone-induced polarization, its localization at the shmoo tip strongly suggests this role and the conservation of the polarization machinery between the two polarized growth processes.

The pentameric septin ring, a collar-like structure that is one of the first organizing components at the site of polarized growth, may also be localized at the shmoo neck [82, 86], given that a number of its component proteins (Cdc10, Cdc11 and Shs1) were recovered in our screens (**Figure 3-6**). Cdc12, another septin component,

displayed filamentous structure and orientation towards the polarization axis. However, Cdc3, the fifth component, was absent from the GFP library, and thus could not be identified by either screen.

On a larger scale, there is clearly remodeling of the actin cytoskeleton and vesicular transport (to enable membrane and cell wall deposition) during shmoo formation [142], and these proteins were heavily represented in our screens (**Figure 3-6; Table 3-1, Table 3-2**). Sac6, a fimbrin protein involved in bundling actin monomers to filaments was localized at the shmoo tip, as was the twinfilin Twf1, a protein that assists in actin monomer localization to sites of rapid filament formation [143]. Twinfilin localization is assisted by the cap binding proteins Cap1 and Cap2 [143], which were also recovered in the screen. The dynamic nature of actin reorganization at the shmoo tip was indicated by the identification of Aip1, which is known to regulate cofilin mediated actin depolymerization [144].

The actin regulating kinases Ark1 and Prk1 were found and are known to modulate actin cortical patch components and endocytic pathways through phosphorylation cycles [145, 146]. Substrates of Ark1 and Prk1 that were recovered included Sla1, Sla2, Pan1, Ent1, and Ent2 suggesting the involvement of the Pan1-End3-Sla1p complex that is known to be required not only for actin cytoskeleton organization but also for normal cell wall morphogenesis [147]. Srv2, another tip-localized protein, binds adenylyl cyclase and ADP-actin monomers and may facilitate regulation of actin dynamics and cell morphogenesis.

Consistent with the idea that Sla1 couples proteins in the actin cortical patch with the endocytic machinery [148, 149], we observed cortical patch proteins such as Las17 (homolog of human Wiskott Aldrich syndrome protein), Vrp1 (homolog of human wasp interacting protein), Abp1 and Abp140 as well as proteins involved in endosomal vesicle

trafficking, endocytosis and exocytosis at the shmoo tip. For instance, proteins such as Sfb3, Sec31 and Shr3 [150, 151] that mediate sorting of COPII vesicles between the ER and Golgi, and Sec18 [152], which is involved in post-Golgi vesicular transport. Other endosomal pathway proteins such as Bsp1 that functions as an adaptor linking the synaptojanin protein Inp52 implicated in TGN-to-early endosome sorting to the cortical actin cytoskeleton[153] were also identified. The type V myosin, Myo2 along with its interacting partners and cargo peroxisomes sum up the vesicular transport phenomena directed at the shmoo tip. Myo2, for example interacts with Chs5 to deliver chitin synthase enzyme Chs3 and with Smy1 to transport vesicles, and organelles such as vacuole [154] towards the tip. The final step involves docking and tethering of the endosomal vesicles to the site of polarized growth. Sec2 [155], a protein that functions as the Guanine nucleotide exchange factor for the rab GTPase Sec4 mediates vesicle tethering to the exocyst and localizes at the shmoo tip. Proteins involved in cellular processes such as maintenance of cell wall integrity (Rgd1, Slg1, Wsc2, Wsc3) and in cell fusion (Kel1, Kel2 and Fus1) are tip localized as well tying polarization events and pheromone specific functions at a systemic level.

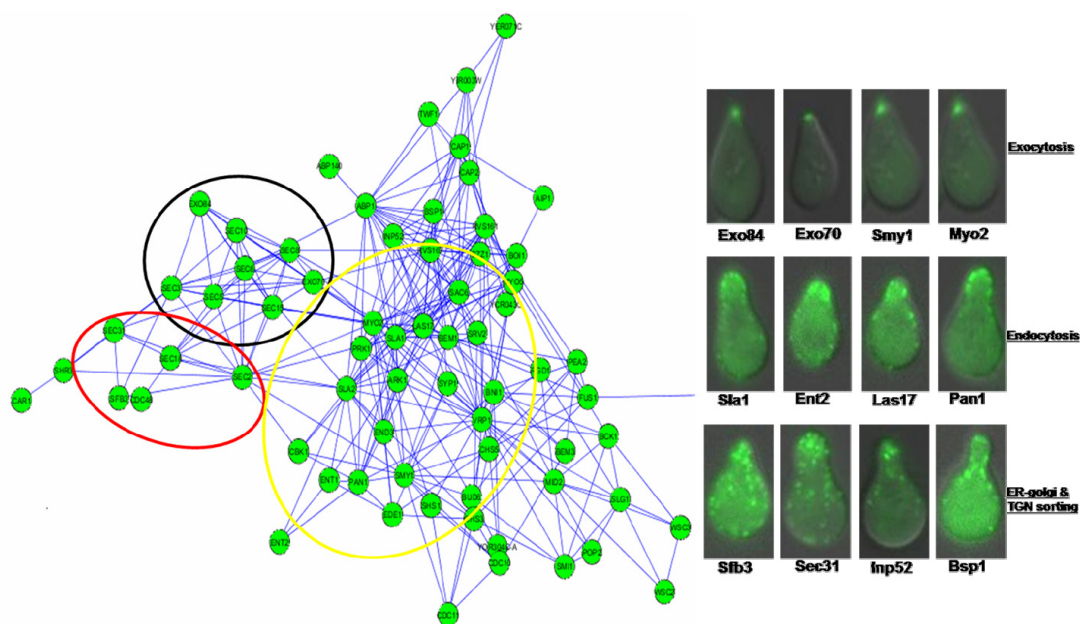


Figure 3-7: Interconnectedness of spatially related classes of proteins involved in vesicular transport. The images to the right show representatives of proteins showing similar spatial localization patterns relative to the shmoo tip involved in vesicular transport events such as exocytosis, endocytosis and vesicular sorting events. These spatially related ‘groups’ also are better inter-connected to themselves than to other shmoo tip proteins in the yeast network (Left: Black circle – exocytosis, Red circle- ER-golgi & TGN sorting, Yellow circle – endocytosis related proteins showing diffuse connectivities to members of the cortical patch and other transport related proteins).

An interesting observation made from the shmoo tip localization screen was the relative positioning of the proteins that were involved in various phases of vesicle mediated transport in our images as well as their interconnectivities in the yeast network (**Figure 3-7**). Proteins that were involved in exocytosis such as the components of the exocyst were spatially situated tightly at the shmoo tip as seen by the GFP localization signal and also showed were better interconnected amongst themselves (enclosed within black circle **Figure 3-7**) as compared to the rest of the proteins from the screen. These proteins are involved in the final stages of protein transport such as protein docking and secretion and presumably indicate regions of membrane-vesicle interactions. Another group of proteins (enclosed within red circle **Figure 3-7**) showing similar spatial

distributions of GFP localization were those involved in ER-Golgi and trans-golgi to plasma membrane vesicle trafficking showing a dynamic re-orientation of GFP signal towards the shmoo tip presumably reflecting vesicular transport. These too resulted in showing better connectivities between themselves as compared to other proteins from the imaging screen. Lastly, a more diffusely localized protein set (enclosed within yellow circle **Figure 3-7**) displaying a GFP signal spread across the area around the shmoo tip may define hot spots of endocytosis and includes proteins such as Sla1, Las17 and others. This group was more dispersed in their connectivities, showing connections with proteins involved in a broad range of functions such as the actin cortical patch, myosin transporters and other cellular systems involved in polarization. Formation of such hot spots is still an active area of research with recent discoveries being made in yeast of 'eisosomes' that appear to mark endocytic sites [156]. Clearly, the actin cytoskeleton and cortical proteins play important roles in such processes with Rvs161 interacting with eisosomal marker proteins [64]. We were therefore able to translate the spatial information reflected through similar localization patterns relative to the shmoo tip into interconnectedness in a yeast functional network.

Several unknown proteins recovered in our screen such as Ymr295c [157], Ydr348c and Yor304c-a localize to both the bud [45] and shmoo tips suggesting a role in the generic polarization machinery. Upon attempting to connect these proteins in the functional network [64] (**Figure 3-8 A**), Yor304c-connects to Bud6, a central protein in signaling polarization (recovered in the screen) and Duo1, a cytoskeletal protein. Ymr295c and Ydr348c were found linked to each other, with the former being strongly connected to glycolytic transcription factor Gcr1 and the latter being connected to cell cycle progression genes, Clb2 and Cdc28. This may implicate a role for these genes in connecting polarization with processes such as cell cycle state and metabolism.

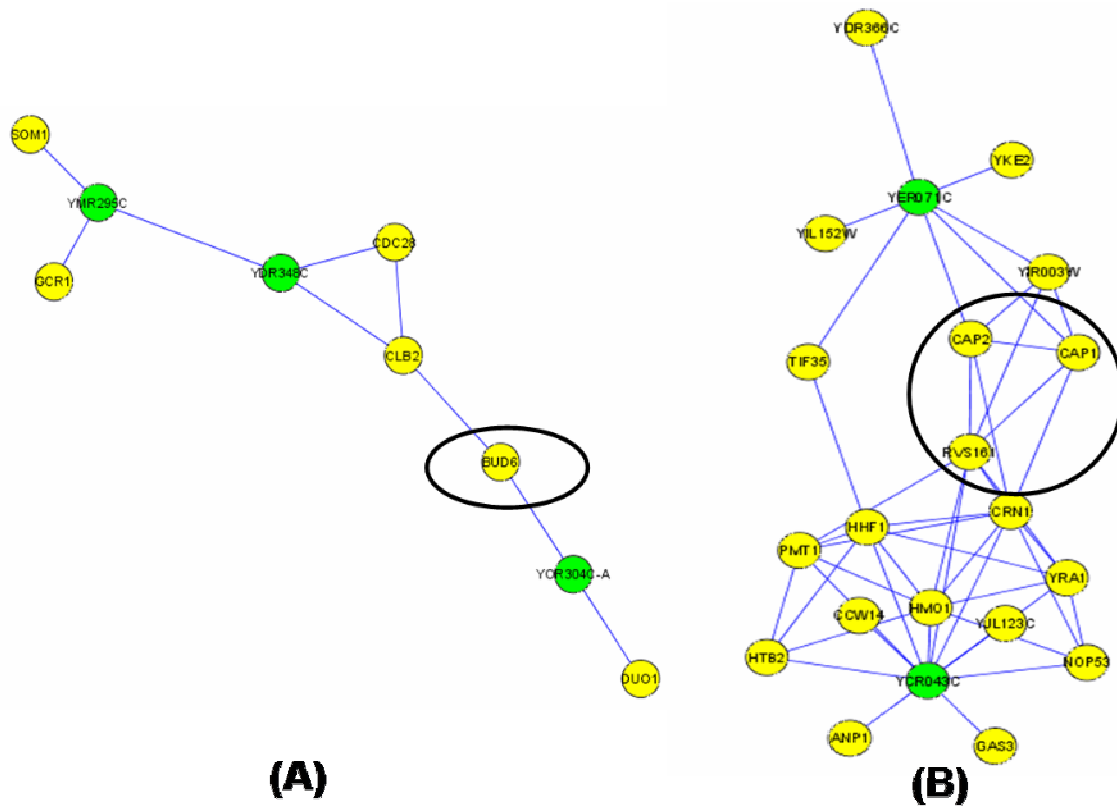


Figure 3-8: Functional linkages of unknown proteins recovered from the screen. Proteins in green circles were the unknown shmoo tip localized proteins that we tried to connect with the help of the network. Their partners are show in yellow. Black circles enclose proteins already known to be part of the shmoo tip network. A and B show two such unknown sets of proteins that connect at different points of the shmoo tip network.

IV. Proteins unique to the bud or shmoo tip

In addition to proteins playing a role in polarization during vegetative growth and mating, we identified a set of proteins that may be unique to one or the other process. Amongst the 81 false positive GFP-tagged strains predicted to be shmoo tip-localized by the classifier, several were involved in vesicular transport with 18 localizing to the bud tip. In other words, even though the computational method did not always directly predict localization to the mating tip, it predicted proteins involved in processes very similar to

and possibly mechanistically overlapping with shmoo-formation. For example, Boi2 and Bnr1 were conspicuously absent from the shmoo tip but were present at the bud tip and may reflect differential organization and positioning of the cytoskeletal architecture during pheromone induced mating as compared to vegetative buds [158].

Another distinct class of proteins appeared to be shmoo specific in their localization, an indication of differential sets of protein interactions driving the processes of mating and cell fusion. The shmoo tip marker Fus1 was recovered [131] as was Bck1, a cytosolic protein kinase in vegetative cells that appears to concentrate at the polarized shmoo tip. This is presumably due to its role in regulating cell wall integrity, a process closely connected to the mating response pathway [159]. Similarly, Mid2, a cell wall sensor normally present uniformly around the cell wall [45] shows a three fold increase in expression levels upon pheromone stimulation [160] and a biased distribution around the shmoo tip indicative of the increased occurrence of cell wall deposition at the site of polarized growth [161].

Yer071c, a protein annotated as having a punctate composite cytosolic localization and Ycr043c, a golgi annotated protein [45] were also recovered and have not been implicated to play a role in polarization. The yeast network (**Figure 3-8 B**) connects Yer071c with actin cap binding proteins Cap1 and Cap2 while Ycr043c links to Rvs161, a lipid raft protein all of which were found at the mating tip. Car1, an arginase that when deleted causes cells to undergo G1 cell cycle arrest upon starvation [162] and Lsg1, a protein involved in 60S ribosome biogenesis are two other proteins we found that were not obviously mating related. Our screen therefore adds evidence and provides putative hypotheses for the involvement of such unknown proteins in the mating polarization pathway.

Discussion

We report a large-scale imaging-based screen for proteins showing spatial localization to the growing tip of the yeast mating projection following pheromone response. A summary of our findings is presented in **figure 3-9**. Our screen has enabled us to align the proteome down to the level of individual proteins identified along the polarization axis induced by pheromone stimulation. Based upon this systematic assay, we demonstrate that the bulk of shmoo-tip localized proteins are conserved with those localized to the bud tip during vegetative growth. These data therefore support a model for the adaptive reuse of polarized growth machinery between different polarized growth processes. For example, Huh et al. [45] had shown that actin related genes are structured along the polarization axis during budding. We show that this observation is true during mating as well. This process is not automatic since the budding and mating projection sites are distinct and therefore the point of origin of cellular asymmetry is bound to be different. Although the process of establishment of cell polarity by proteins such as Cdc42, Cdc24 and Far1 are well studied, the exact molecular mechanisms towards predictive cellular models are still wanting [163]. Our efforts are a first step towards screening proteome-wide dynamics to understand precisely how biological systems spatially coordinate protein interactions and regulate their dynamics.

In our system-wide study, we observe a statistically reproducible alignment of many cellular organelles along the major growth axis. Our observations are summarized in **Figure 3-9**. Additionally, our image data reveal distinct spatial separation of protein complexes involved in different aspects of vesicular transport relative to the site of polarized growth (**Figure 3-7**).

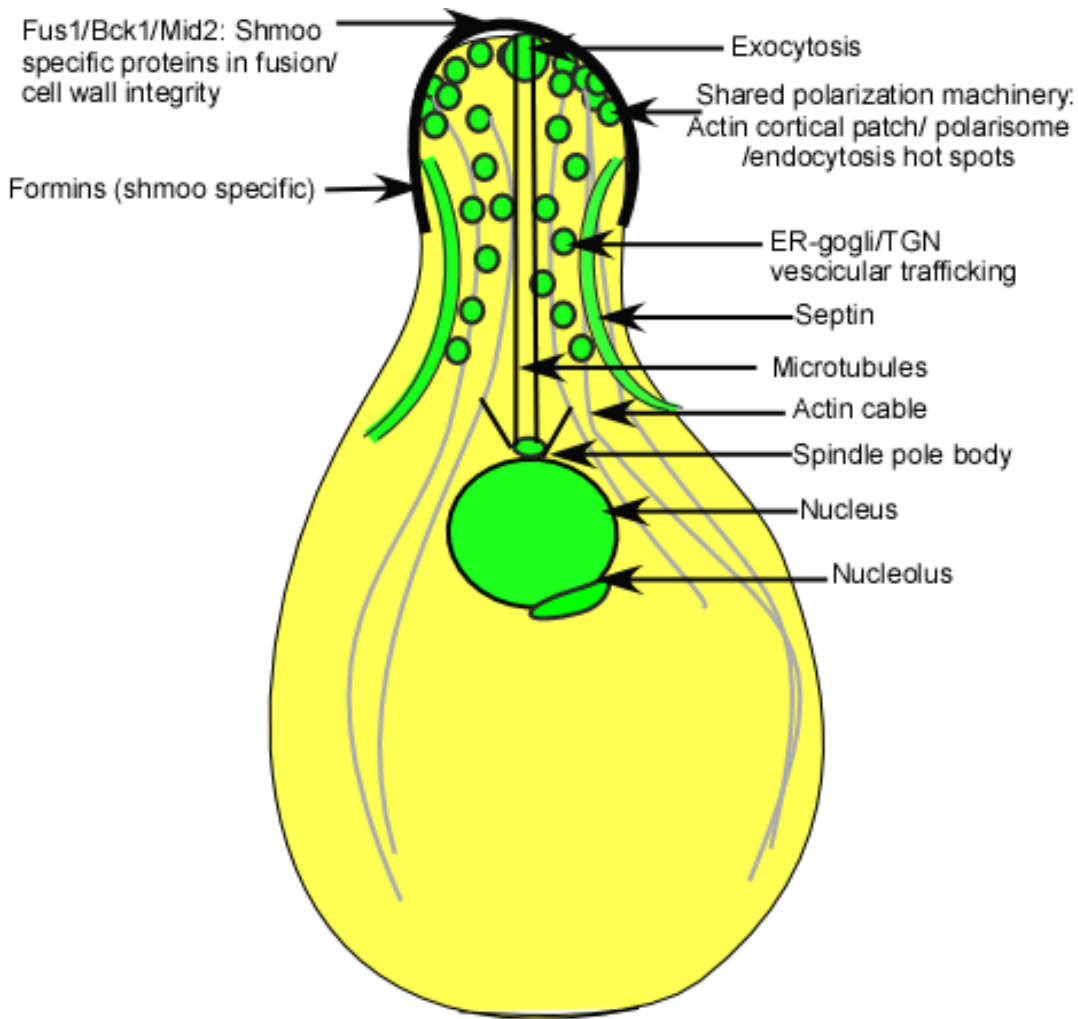


Figure 3-9: Summary of re-organization of organelles and protein complexes around the shmoo tip.

Our screen recovered in all 37 proteins from the cell chip out of 188 strains manually tested and 37 from the classifier out of 118 manually tested (Figure 3-10A) (Total strains manually tested was 306). We had an overall intersection of 13 strains with the known set from SGD. Most of the ones that we missed were low abundance signaling proteins with signals too weak to be detected by GFP alone. In the 118 strains tested as part of the classifier, there were 81 false positives that did not localize to the shmoo tip. Of these 81, 18 were annotated to be bud localized and included bud specific formins

such as Bnr1 and Boi2. Of the proteins recovered in the screen, 7 were unique to shmoo tip. This is summarized in Figure 3-10 B. These findings emphasize the involvement of a differential set of protein interactions driving each process towards their separate goals after the initial shared polarization machinery has been put in place.

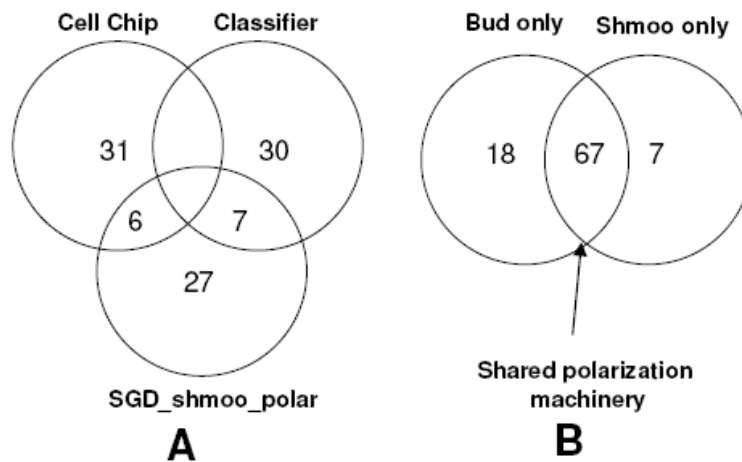


Figure 3-10: Venn diagram summarizing the proteins recovered. A: Intersection of the cell chip, classifier and known set of shmoo tip localized proteins from SGD. B: Of the 306 strains manually tested as part of the follow-ups, 18 were unique to the bud tip, 7 to the shmoo tip and 67 to both.

Finally, we have used to screen to uncover novel players in the polarization pathway, some of them completely unknown to date. For example, the shmoo tip localization of Lsg1, a protein involved in 50S ribosome biogenesis may imply spatially polarized RNA localization mechanisms operating to transport RNA molecules towards the mating projection similar to the Ash1 mRNA which has previously been found localized to the daughter bud tip [164].

Conclusions

Our data unequivocally recaptures the dynamics of the proteome under an altered polarization state. We show that there is there is a large adaptive re-use of the

polarization machinery indicative of the centrality of this process in evolution. We also discover several previously unknown proteins that function as part of the general polarization machinery as well as unique to the budding and mating specific polarization process. We attempt to rationalize the functions of these proteins using a probabilistic protein interaction network. Our high throughput screen can be used to capture temporal and spatial dynamics as more libraries become available adding valuable data dimensionality and thereby improving our understanding of gene functions.

MATERIALS AND METHODS

Yeast green fluorescent protein (GFP) tagged strains and growth conditions: Spotted cell microarrays were manufactured from the *S. cerevisiae* GFP tagged clone collection (Invitrogen), in which each of ~4200 individual strains with genetic background EY0986 (ATCC 201388: MATa his3 Δ 1 leu2 Δ 0 met15 Δ 0 ura3 Δ 0 (S288C)) was chromosomally tagged with the coding sequence of Aequorea Victoria GFP (S65T) at the C-terminal end of an open reading frame (cite). This collection was copied in 96 well plates using a Biomek FX liquid handling robot, inoculating each strain into 200 μ l of YPD containing 17% glycerol, growing at 30 C for ~ 2 days without shaking, mixed on a plate shaker, and sealed and frozen at -80 C.

Alpha factor treatment: GFP-tagged strains were treated with alpha factor in the following manner: A copy of the GFP clone collection was thawed from -80 C and a 1% inoculum used to seed a fresh copy in YPD medium. After growth to near saturation for ~36 hrs at 30 C, this intermediate copy was used at 1% to inoculate another such one in YPD. This copy (twice removed from the glycerol stock) was grown overnight at 30 C and was washed three times by serial dilution to inactivate secreted extracellular Bar1p protease that degrades alpha factor. Subsequently, alpha factor was added to each sample

well in the collection at 75 µg/ml final concentration and allowed to incubate for ~ 3 hrs at 30 C. The samples were fixed using freshly prepared 2% formaldehyde for 1 hr at 30 C and the excess fixative removed by three successive washing rounds of YPD containing 17% glycerol before re-suspension in 100 µl YPD plus 17% glycerol. These sample plates were stored at -80 C or directly printed.

Slide preparation, printing and imaging of cell microarrays: Cell microarrays were printed onto freshly treated poly-L-lysine coated slides *via* contact deposition of a suspension of yeast cells from the arrayed yeast collection using a DNA microarray spotting robot. Locations of cell spots were identified by scanning the freshly printed slides using a GenePix microarray scanner, then cells in each spot were imaged using an automated Nikon E800 fluorescence microscope and Photometrix Coolsnap CCD camera as in (cite), collecting DIC images and fluorescent images in the DAPI and GFP channels from each spot, on two replicate slides, for a total of ~26,000 microscope images. Images were stored and analyzed using the Cellma cell microarray image database software (cite). Two independent graders manually inspected the images, selecting strains in which the GFP-fusion protein showed punctate localization proximal to the shmoo tip.

Manual follow-up of shmoo-tip localized proteins

Doubly fluorescent strains for co-localization were constructed by mating and tetrad dissection. Red fluorescent protein (RFP) tagged marker strains (EY0987; ATCC 201389: MAT α his3 Δ 1 leu2 Δ 0 lys2 Δ 0 ura3 Δ 0 (S288C)) for several organelles and cellular structures (gift of the laboratory of Erin O'Shea) were mated with the FUS1-GFP strain (EY0986), and diploids selected on Lys(-) Met(-) media. After sporulation, tetrads were dissected and doubly fluorescent 'a' type yeast propagated.

Image Analysis

Quantitative image analysis was performed using custom MATLAB image processing software. Primary software features include background noise removal, cell region identification, cell boundary segmentation, and subcellular feature description. All fluorescent images underwent background noise removal which was accomplished through background image subtraction and median filtering to remove speckle noise. Yeast cells were identified by implementation of the Kittler and Illingworth automated thresholding method (cite) on composite images for each field of view. These composite images were created by stacking all fluorescent channels as well as a histogram-modified DIC image. Cell boundary segmentation was accomplished using a seeded watershed algorithm in which the cell seed was generated using a fluorescent image of the DAPI stained nuclei. When DAPI stain was not available, cell segmentation was performed manually through image annotation in ImageJ. In order to remove improperly segmented cells, automatic cell segmentation results were required to meet pre-defined minimum and maximum cell size restrictions. Subcellular feature identification was accomplished through cell-by-cell automated thresholding on each of the fluorescent channels.

The previously described methods were applied to still images as well as movies of the RFP-GFP labeled yeast as they were exposed to alpha factor mating pheromone. Several additional analyses were performed on each of these two data types. Yeast cells identified in the still images were computationally reoriented along the axis between the center of fluorescence of the DAPI stained nuclei and the GFP labeled shmoo tip. These rotated cells were then stretched or compressed so that the distance between these two points was uniform for all cells. After these transformations, each cell in the still images was overlaid so that RFP labeled organelle localization could be visualized.

Time-lapse video images of organelle localization relative to the shmoo tip over time were recorded and analyzed. Additional image processing of the movies was necessary in order to ensure good data quality. First, movies were smoothed using a sliding averaging window of five frames. This significantly reduced jitter in the movies that had been introduced by minor imprecision in the automated microscope stage. Second, cells in each frame were assessed for being in or out of focus by analyzing the standard deviation of the pixel values in the fluorescent channels. When the intensity distribution of a cell became extremely uniform in a single frame, the cell was removed from our analysis. Finally, the location of the shmoo tip was monitored for each cell. If the location of the center of fluorescence of the shmoo tip changed drastically the cell was assumed to have started a second shmoo and was also removed from the analysis for the duration of the movie. As expected, all cells appeared to have clear shmoos that extended incrementally for the first two hours of the movies but developed a second shmoo in a distant location on the cell after approximately 2 to 2 ½ hours. The data curation described above allowed us to clearly identify cells that were shmooing and enabled tracking of the RFP organelle markers with respect to the shmoo tip label.

Classifier construction:

We trained a *naïve* Bayesian classifier (implemented in Weka) to identify additional shmoo-tip localized genes on the basis of the genes identified in the high throughput screen (except six mitochondrial genes). Classifier features were aggregated from data provided by the UCSF GFP screen and the functional gene network of Lee *et al.* (cite). The features collected for each gene were: the sum of the gene's network log likelihood scores (LLS) to the set of training genes, the ratio of the sum of the gene's LLS scores to the training set genes divided by the sum of LLS scores to all other genes,

protein abundance (molecules per cell), and cell location (using primary cellular location). The classifier was applied to the set of 5,804 yeast genes, either using all genes as the training/test set or using 10-fold cross-validation (both gave similar results). After training, the classifier recovered 20 of the 37 shmoo genes (cross-validation: 19). An additional 151 (cross-validation: 153) genes not identified in the initial screen were also classified as shmoo genes using a 0.5 probability cutoff. Of the 151 genes, 118 were present in the GFP library and re-screened manually; 37 of these proved to be shmoo localized.

REFERENCES

1. Arimura, N. and K. Kaibuchi, *Neuronal polarity: from extracellular signals to intracellular mechanisms*. Nat Rev Neurosci, 2007. **8**(3): p. 194-205.
2. Krummel, M.F. and I. Macara, *Maintenance and modulation of T cell polarity*. Nat Immunol, 2006. **7**(11): p. 1143-9.
3. Gaziova, I. and K.M. Bhat, *Generating asymmetry: with and without self-renewal*. Prog Mol Subcell Biol, 2007. **45**: p. 143-78.
4. Madden, K. and M. Snyder, *Cell polarity and morphogenesis in budding yeast*. Annu Rev Microbiol, 1998. **52**: p. 687-744.
5. Proszynski, T.J., et al., *Plasma membrane polarization during mating in yeast cells*. J Cell Biol, 2006. **173**(6): p. 861-6.
6. Baba, M., et al., *Three-dimensional analysis of morphogenesis induced by mating pheromone alpha factor in Saccharomyces cerevisiae*. J Cell Sci, 1989. **94** (Pt 2): p. 207-16.
7. Casolari, J.M., et al., *Developmentally induced changes in transcriptional program alter spatial organization across chromosomes*. Genes Dev, 2005. **19**(10): p. 1188-98.
8. Newpher, T.M., et al., *In vivo dynamics of clathrin and its adaptor-dependent recruitment to the actin-based endocytic machinery in yeast*. Dev Cell, 2005. **9**(1): p. 87-98.
9. Bagnat, M. and K. Simons, *Cell surface polarization during yeast mating*. Proc Natl Acad Sci U S A, 2002. **99**(22): p. 14183-8.

10. Bidlingmaier, S. and M. Snyder, Large-scale identification of genes important for apical growth in *Saccharomyces cerevisiae* by directed allele replacement technology (DART) screening. *Funct Integr Genomics*, 2002. **1**(6): p. 345-56.
11. Gehrung, S. and M. Snyder, *The SPA2 gene of Saccharomyces cerevisiae is important for pheromone-induced morphogenesis and efficient mating*. *J Cell Biol*, 1990. **111**(4): p. 1451-64.
12. Changwei, Z., X. Mingyong, and W. Ranran, *Afr1p has a role in regulating the localization of Mpk1p at the shmoo tip in Saccharomyces cerevisiae*. *FEBS Lett*, 2007. **581**(14): p. 2670-4.
13. Narayanaswamy, R., et al., *Systematic profiling of cellular phenotypes with spotted cell microarrays reveals mating-pheromone response genes*. *Genome Biol*, 2006. **7**(1): p. R6.
14. Huh, W.K., et al., *Global analysis of protein localization in budding yeast*. *Nature*, 2003. **425**(6959): p. 686-91.
15. Robinson, M.D., et al., *FunSpec: a web-based cluster interpreter for yeast*. *BMC Bioinformatics*, 2002. **3**: p. 35.
16. Dwight, S.S., et al., *Saccharomyces Genome Database (SGD) provides secondary gene annotation using the Gene Ontology (GO)*. *Nucleic Acids Res*, 2002. **30**(1): p. 69-72.
17. Kumar, A., et al., *High-throughput methods for the large-scale analysis of gene function by transposon tagging*. *Methods Enzymol*, 2000. **328**: p. 550-74.
18. Lee, I., et al., *A probabilistic functional network of yeast genes*. *Science*, 2004. **306**(5701): p. 1555-8.
19. Lee, I., Z. Li, and E.M. Marcotte, *An Improved, Bias-Reduced Probabilistic Functional Gene Network of Baker's Yeast, Saccharomyces cerevisiae*. *PLoS ONE*, 2007. **2**(10): p. e988.
20. He, B., et al., *Exo70 interacts with phospholipids and mediates the targeting of the exocyst to the plasma membrane*. *Embo J*, 2007. **26**(18): p. 4053-65.
21. Wiederkehr, A., et al., *Sec3p is needed for the spatial regulation of secretion and for the inheritance of the cortical endoplasmic reticulum*. *Mol Biol Cell*, 2003. **14**(12): p. 4770-82.
22. Pruyne, D., et al., *Mechanisms of polarized growth and organelle segregation in yeast*. *Annu Rev Cell Dev Biol*, 2004. **20**: p. 559-91.
23. Huckaba, T.M., et al., *Live cell imaging of the assembly, disassembly, and actin cable-dependent movement of endosomes and actin patches in the budding yeast, Saccharomyces cerevisiae*. *J Cell Biol*, 2004. **167**(3): p. 519-30.
24. Palmgren, S., et al., *Interactions with PIP2, ADP-actin monomers, and capping protein regulate the activity and localization of yeast twinfilin*. *J Cell Biol*, 2001. **155**(2): p. 251-60.
25. Clark, M.G., et al., *A genetic dissection of Aip1p's interactions leads to a model for Aip1p-cofilin cooperative activities*. *Mol Biol Cell*, 2006. **17**(4): p. 1971-84.

26. Cope, M.J., et al., *Novel protein kinases Ark1p and Prk1p associate with and regulate the cortical actin cytoskeleton in budding yeast.* J Cell Biol, 1999. **144**(6): p. 1203-18.
27. Smythe, E. and K.R. Ayscough, *The Ark1/Prk1 family of protein kinases. Regulators of endocytosis and the actin skeleton.* EMBO Rep, 2003. **4**(3): p. 246-51.
28. Tang, H.Y., J. Xu, and M. Cai, *Pan1p, End3p, and Sla1p, three yeast proteins required for normal cortical actin cytoskeleton organization, associate with each other and play essential roles in cell wall morphogenesis.* Mol Cell Biol, 2000. **20**(1): p. 12-25.
29. Dewar, H., et al., *Novel proteins linking the actin cytoskeleton to the endocytic machinery in Saccharomyces cerevisiae.* Mol Biol Cell, 2002. **13**(10): p. 3646-61.
30. Gourlay, C.W., et al., *A role for the actin cytoskeleton in cell death and aging in yeast.* J Cell Biol, 2004. **164**(6): p. 803-9.
31. Gilstrig, C.F., M. Melin-Larsson, and P.O. Ljungdahl, *Shr3p mediates specific COPII coatomer-cargo interactions required for the packaging of amino acid permeases into ER-derived transport vesicles.* Mol Biol Cell, 1999. **10**(11): p. 3549-65.
32. Peng, R., A. De Antoni, and D. Gallwitz, *Evidence for overlapping and distinct functions in protein transport of coat protein Sec24p family members.* J Biol Chem, 2000. **275**(15): p. 11521-8.
33. Grote, E., C.M. Carr, and P.J. Novick, *Ordering the final events in yeast exocytosis.* J Cell Biol, 2000. **151**(2): p. 439-52.
34. Wicky, S., S. Frischmuth, and B. Singer-Kruger, *Bsp1p/Ypr171p is an adapter that directly links some synaptojanin family members to the cortical actin cytoskeleton in yeast.* FEBS Lett, 2003. **537**(1-3): p. 35-41.
35. Pashkova, N., et al., *Myosin V attachment to cargo requires the tight association of two functional subdomains.* J Cell Biol, 2005. **168**(3): p. 359-64.
36. Medkova, M., et al., *The rab exchange factor Sec2p reversibly associates with the exocyst.* Mol Biol Cell, 2006. **17**(6): p. 2757-69.
37. Walther, T.C., et al., *Eisosomes mark static sites of endocytosis.* Nature, 2006. **439**(7079): p. 998-1003.
38. McGary, K.L., I. Lee, and E.M. Marcotte, *Broad network-based predictability of S. cerevisiae gene loss-of-function phenotypes.* Genome Biol, 2007. **8**(12): p. R258.
39. Fleischer, T.C., et al., *Systematic identification and functional screens of uncharacterized proteins associated with eukaryotic ribosomal complexes.* Genes Dev, 2006. **20**(10): p. 1294-307.
40. Buttery, S.M., S. Yoshida, and D. Pellman, *Yeast formins Bni1 and Bnr1 utilize different modes of cortical interaction during the assembly of actin cables.* Mol Biol Cell, 2007. **18**(5): p. 1826-38.
41. Buehrer, B.M. and B. Errede, *Coordination of the mating and cell integrity mitogen-activated protein kinase pathways in Saccharomyces cerevisiae.* Mol Cell Biol, 1997. **17**(11): p. 6517-25.

42. Ono, T., et al., The MID2 gene encodes a putative integral membrane protein with a Ca(2+)-binding domain and shows mating pheromone-stimulated expression in *Saccharomyces cerevisiae*. *Gene*, 1994. **151**(1-2): p. 203-8.
43. Lommel, M., M. Bagnat, and S. Strahl, *Aberrant processing of the WSC family and Mid2p cell surface sensors results in cell death of Saccharomyces cerevisiae O-mannosylation mutants*. *Mol Cell Biol*, 2004. **24**(1): p. 46-57.
44. Cooper, T.G., et al., *Addition of basic amino acids prevents G-1 arrest of nitrogen-starved cultures of Saccharomyces cerevisiae*. *J Bacteriol*, 1979. **137**(3): p. 1447-8.
45. Marco, E., et al., *Endocytosis optimizes the dynamic localization of membrane proteins that regulate cortical polarity*. *Cell*, 2007. **129**(2): p. 411-22.
46. Takizawa, P.A., et al., *Actin-dependent localization of an RNA encoding a cell-fate determinant in yeast*. *Nature*, 1997. **389**(6646): p. 90-3.

Chapter 4: Extensive formation of punctate foci by metabolic proteins under nutrient depleted conditions in budding yeast

INTRODUCTION

All living cells proliferate through normal mitotic division but are also capable of entering an alternate resting or quiescent state when nutrients become limiting. A defining quality of quiescent cells of both prokaryotic and eukaryotic organisms is their ability to survive for extended periods of time [165]. It is therefore imperative to study this very important phase in order grasp the conserved mechanisms underlying entry into, survival in and exit out from quiescence as this may implicitly lead to development of novel therapies against cancer, aging and neurodegenerative diseases. However, historically, quiescence has been a poorly studied subject due to low biochemical activity of cells in this phase. Indeed, the holy grail of researchers working on quiescence is to identify a core regulatory program that allows cells to survive and sustain themselves when nutrients are limiting and transition them back rapidly into cell cycle when conditions become favorable again. Given that quiescence is a poorly studied phenomenon, budding yeast represents a favorable model system for many of the previously articulated reasons. These include tractability of *S. cerevisiae* to all kinds of experiments and the ready availability of libraries, the presence of orthologs of several yeast regulators in mammals such as TOR (Target of Rapamycin) and the similarity in the phenotypes exhibited by both quiescent mammalian and quiescent yeast cells. I will focus the rest of this section enunciating the salient features of this interesting phase from the perspective of using yeast as a model system for its study.

Stationary phase in budding yeast – salient features

Figure 4-1 shows the growth phase typical of yeast cells cultured in glucose rich media. During the initial logarithmic phase, fermentative growth occurs with an average doubling time of ~90 minutes by utilization of glucose. As glucose starts to become limiting, the cells transiently display ‘diauxic’ shifted metabolism where they re-adjust their energy production to a respiratory mode and utilize the remaining non-fermentable carbon sources still present in the medium. In the post-diauxic phase, cells in the culture undergo 1-2 doublings very slowly and use the ethanol produced in the fermentative phase for energy before finally entering true stationary phase at ~4-5 days. This final phase represents a period of cessation of proliferation and exhaustion of non-fermentable carbon sources and ethanol [166].

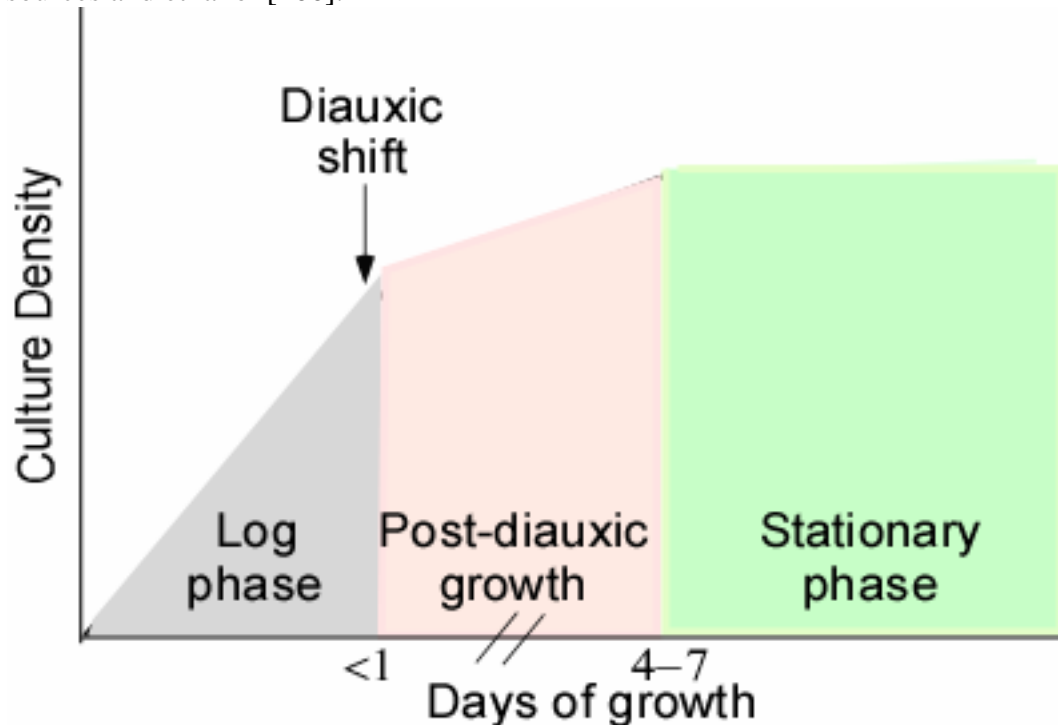


Figure 4-1: Growth phases of a yeast culture. As carbon sources become limiting, there is a transition from fermentative to respiratory metabolism with stationary phase onset occurring at around 4 days.

Gray and Werner-Washburne et al.[166] propose a nomenclature where the term 'stationary phase' refers to the saturated yeast culture grown in rich media usually for 4 to 7 days and the term 'quiescence', to the state of the constituent cells in such as saturated culture. Subsequently, work from the Werner-Washburne lab[167] has shown that a quiescent sub-population can be isolated from stationary phase yeast cultures based on their dense, un-budded nature and ability to re-enter mitotic cell cycle compared to a more heterogenous, senescent and less dense population of non-quiescent cells.

Nonetheless, a comparison of yeast cells in stationary phase cultures with those in exponentially growing cultures reveals starkly different characteristics several of them being associated with quiescence in general. Firstly, they cease to proliferate or increase in mass and volume and arrest as un-budded cells. Secondly, some of the obvious cellular changes include the formation of a thickened cell wall making them more osmotolerant and thermotolerant than proliferating cells, condensed chromosomes [168], decreased metabolic rate and accumulation of molecules such as trehalose and glycogen which may serve in storage and protective roles against oxidative damage and other stresses [165]. Additionally, the rates of transcription [169] are reduced by about three to five times and the rate of translation by about 300 fold [170] as compared to exponential phase. Given the large scale remodeling of cellular processes, it has been proposed that entry into, survival in and exit out of quiescence can be regarded as a distinct developmental process termed as the cell quiescence cycle [166]. As with the mitotic cell cycle, each turn of the cell quiescence cycle also ages the cell resulting in a reduced replicative capacity but without a doubling in cell number [171]. In support of this hypothesis, mutants have been recovered that are defective only in exit from quiescence but normally enter and stay viable in stationary phase [166]. In addition, microarray analysis of cells exiting from stationary phase revealed a dramatic increase in the levels of > 1800 mRNAs [172]

within 5-10 minutes of re-feeding and recovered 32 genes essential for stationary phase survival enriched in mitochondrial function and protection from oxidative stress.

Signaling pathways regulating stationary phase biology

A brief description of the cellular mechanisms operating during quiescence and the signaling pathways known to be involved in quiescence entry and exit is worth mentioning at this point. **Figure 4-2** gives an overview of some of the important events that mark quiescence. Quiescence entry is regulated by the Ras and Tor signal transduction pathways, both of which are critical modulators of cell growth [173, 174], with the inactivation of either of these pathways resulting in a stationary phase-like arrest.

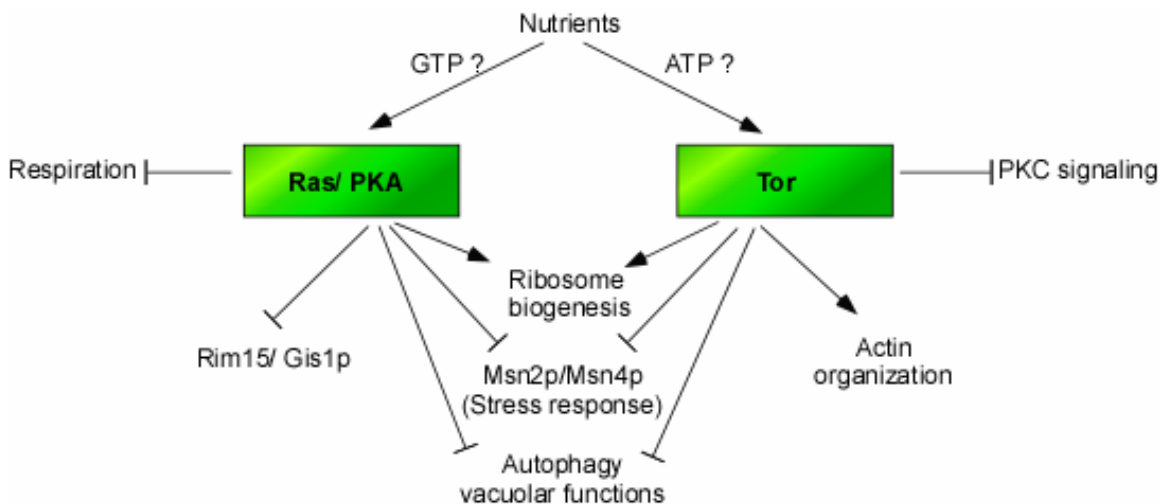


Figure 4-2: Overview of nutrient sensing and metabolic pathways during quiescence.

The *S. cerevisiae* Ras1 and Ras2 comprise small GTP binding proteins that activate the cAMP-dependent-protein kinase PKA, and together with the evolutionarily conserved serine/threonine protein kinases Tor1 and Tor2 appear to be involved in

regulating the cell's energy balance [173-175]. Both pathways may be central components of a growth checkpoint in *S. cerevisiae* [174], positively regulating protein translation, ribosome biogenesis and other cell proliferative activities, while at the same time inhibiting processes like autophagy that are refractory to growth. For example, Protein kinase A has been implicated in regulating stationary phase entry in response to nutrient availability through the regulation of its targets such as the Rim15 protein kinase [176] and by controlling the phosphorylation status of the C-terminal domain of RNA polymerase II (Rbp1 CTD) although the exact mechanism remains unclear [177]. On the other hand, the protein kinase C homolog Pkc1, a remodeler of cell wall integrity and the actin cytoskeleton has been found to be both required for stationary phase survival and inhibited by the activity of the Tor pathway [178, 179]. Although several possibilities have been proposed, the exact mechanism of inhibition of these pathways that signal entry into stationary phase has not been established. In the next section, I will introduce some of the recently discovered events that are critical for an understanding of stationary phase biology before outlining the aims and results of my experiment.

Important cellular mechanisms operating in stationary phase

Mechanisms for Stationary phase survival

Several mechanisms are important to maintain survival in stationary phase. Firstly, inhibition of Tor activity triggers autophagy, a membrane trafficking pathway essential for stationary phase survival that recycles bulk protein, organelles and other cytoplasmic components by carrying them to the vacuole for degradation [180, 181]. Specifically, the Tor activity was found to reduce the affinity of Apg1, a protein essential for autophagy, for its substrate Apg13. Secondly, the dramatic reduction in translation

rates upon entry into stationary phase is also essential for stationary phase survival [165]. Unexpectedly however, the initiation of residual translation appears to occur through a cap-independent pathway presumably via still uncharacterized internal ribosome entry sites [182, 183]. Thirdly, the importance of oxidative damage as a contributor to stationary phase cell death is underlined by the sensitivity to oxidative stress of mutants lacking in *TRX1* and *TRX2*, genes encoding the cytoplasmic thioredoxins [184]. Finally, mutants in inorganic polyphosphate metabolism also possess stationary phase survival defects [109, 185].

Stationary phase – A poised state for cell cycle re-entry?

In *S. cerevisiae*, the transition from quiescence to proliferation when nutrients become available requires a rapid, large-scale re-programming of the metabolic and replication machinery in order to successfully re-enter cell cycle. In support of a distinct regulatory program operating in stationary phase, DNA microarray analyses have shown that whereas most genes are down regulated upon entry into quiescence, the transcription of certain transcripts is induced in quiescent cells [186, 187]. At a cellular level, a thickening of cell wall, chromosome condensation and development of increased tolerance to temperature, osmotic or chemical stress mark the onset of quiescence. However, recent studies have shown the establishment of ‘pools’ of critical cellular components that may serve as a reserve for re-entry into cell cycle when nutrients are made available. Work done by the Parker lab [188] has shown that mRNAs reciprocally exchange between polysomes and cytoplasmic processing bodies called P-bodies. Stationary phase yeast have large P-bodies containing mRNAs that re-enter translation when growth resumes, a process akin to maternal mRNA storage granules in higher organisms. Another interesting study [187] found surprising results upon performing a chromatin immunoprecipitation (ChIP on chip) experiment on RNA polymerase II in

stationary phase yeast cells. Despite global repression of transcription, this genome-wide location analysis revealed that RNA polymerase II was maintained upstream of hundreds of genes that were induced upon exit indicating that the general transcription machinery could be held in a poised state during quiescence. Finally, other cellular structures such as the actin cytoskeleton also seem to undergo a quiescent phase specific transformation, whereby the highly polarized and dynamic F-actin network is re-organized into immobile, static, depolarized ‘actin bodies’. Actin bodies are seen to reassemble into F-actin upon re-feeding even in the absence of de novo protein synthesis, suggesting a readily immobilizable reserve that can be utilized for actin patch and cable formation for cell-cycle re-entry.

Yeast stationary phase as a model to study aging

Aging in *S. cerevisiae* has been studied from two different perspectives (**Figure 4-3**). ‘Replicative aging’ refers to the number of cell divisions a particular yeast cell has undergone [189, 190]. Chronological aging pertains to the total time a cell spends in normal mitotic cell cycle and in the cell quiescence cycle. It therefore takes into consideration the time spent in quiescence (stationary phase) as well [191] and has therefore been considered analogous to the biology of post-mitotic cells in higher organisms. Since a substantial portion of this time is that spent in stationary phase, several groups have used stationary phase survival as a measure of chronological aging in yeast cultures [192, 193]. A screen for long lived mutants in non-dividing yeast cells identified Sch9, a homolog of the mammalian Akt/ Protein kinase B that increases resistance to oxidation. Moreover, it was found to operate through the conserved Msn2/ Msn4 family of stress induced transcription factors [193, 194], the nutrient sensing TOR pathway and other pathways such as autophagy, going to show that mechanisms of

longevity operating through increased investment of maintenance, persist in both yeast and higher organisms.

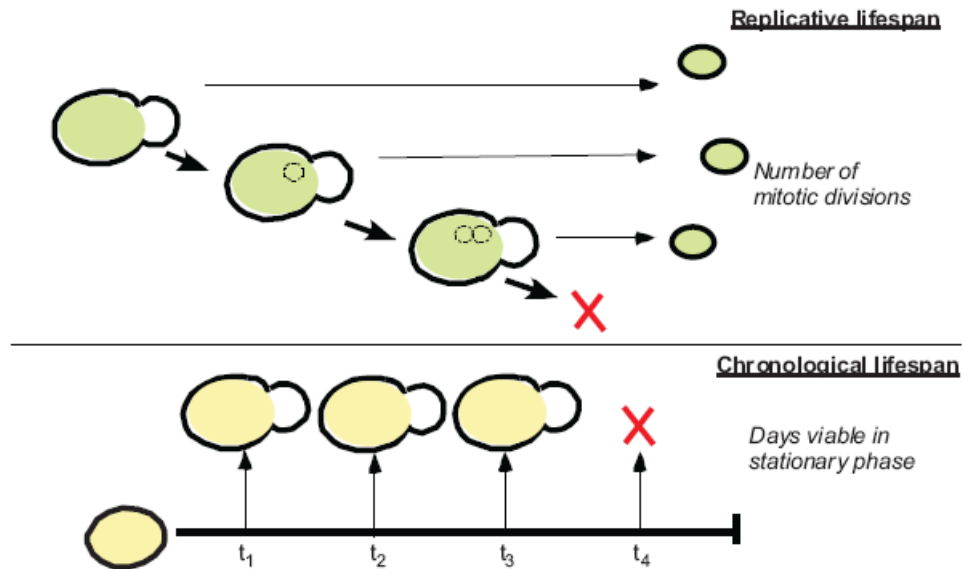


Figure 4-3 shows the models used to study yeast aging. Replicative life is indicative of the time spent in mitotic cell cycle while chronological lifespan also takes into consideration the time in cell quiescence cycle or stationary phase. Dotted circles represent bud scars.

Interestingly, the replicative life span paradigm which is akin to ‘mitotic age’ is also directly affected by the time spent by a cell in stationary phase or in other words, its chronological age [171]. Historically studied from the perspective of Silent information regulator 2 (Sir2), a family of conserved histone deacetylases (Sirtuins), replicative lifespan was found to increase upon Sir2 overexpression and decrease in a Sir2 deletion background. Sir2 appears to exert its effect by repressing the generation of extrachromosomal ribosomal DNA circles (ERCs) that accelerate replicative senescence although this has remained controversial [194]. It was found that cells that had been passaged through stationary phase exhibited a shortage in replicative lifespan than those that had never been starved [171]. An unknown factor has been implicated that builds up

during stationary phase leading to a decreased replicative potential by these cells [171]. Several other interesting observations have been made such as caloric restriction being implicated toward increasing replicative lifespan in yeast and higher organisms although its pathway of action has remained unknown.

Evolution of asymmetry as a means of damage segregation?

Having seen the inter-relatedness between the yeast aging models, it is noteworthy to look at recent reports on protein degradation, oxidation and turnover in aged yeast cultures. As alluded to earlier, protein re-cycling through autophagy plays a crucial role in the maintenance of cell viability in stationary phase. Concomitantly, chronological aging alters both the expression and composition of proteasome subunits with many studies indicating an impairment in its function with the onset of stationary phase [195-197]. This proteasomal impairment may stem from reduced ATP levels, a key feature also seen in aging post-mitotic cells and neurodegenerative conditions in higher organisms. Although causality is not clear, protein oxidation is another consequence of aging and is thought to stem from a shift to respiratory metabolism, a source of mitochondrially derived reactive oxygen species (ROS). A summary of the events proposed to affect this process is presented in **Figure 4-4**.

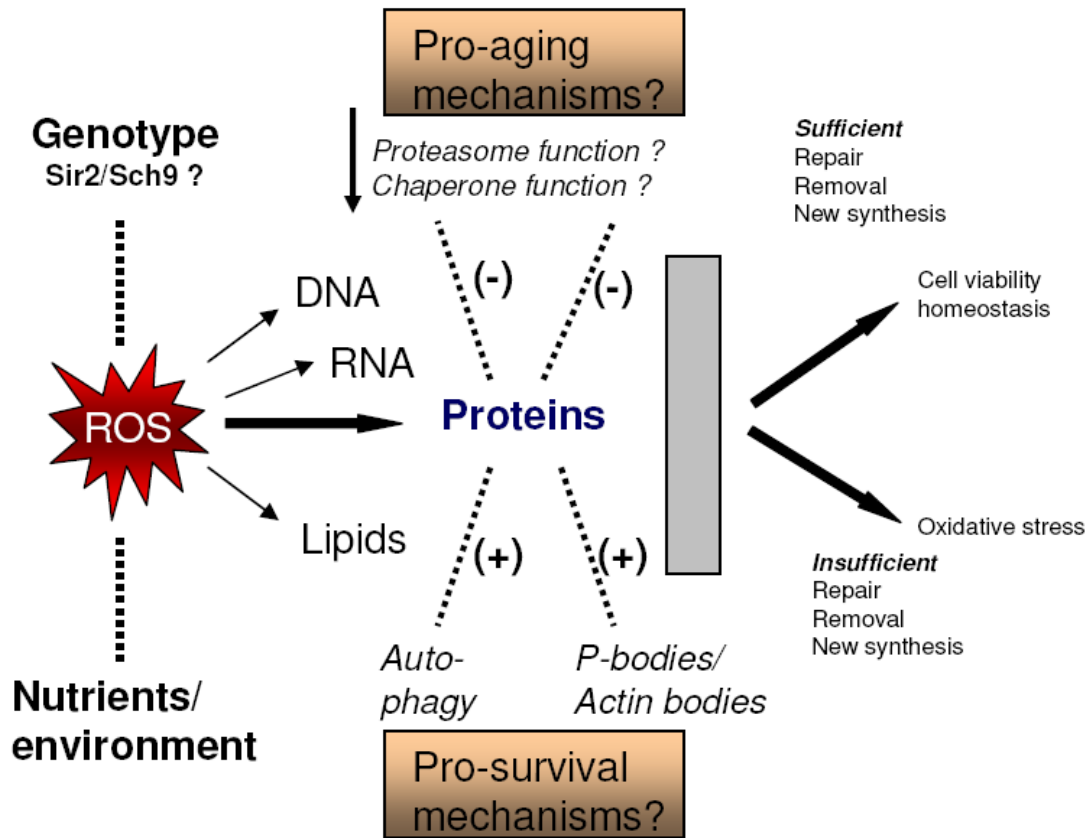


Figure 4-4: A summary of processes affecting aging in yeast and possibly higher organisms. Reactive oxygen species (ROS) build up over time as an unavoidable consequence of changes in metabolism, genotype, nutrient intake and the environment. If damages are repaired, the cell is viable or else it ages and dies. During this phase, processes such as autophagy and mRNA storage bodies may sustain and poise the cells for cell cycle re-entry upon nutrient availability. On the other hand, decreased chaperone and proteasome functions may further aging through aggregation and other mechanisms.

Protein oxidation appears to be an unavoidable consequence of aging with protein carbonylation being one example of such a modification. Recent work in *S.cerevisiae* has shown that [198, 199] yeast and higher organisms may have evolved a Sir2 dependent system that segregates carbonylated proteins during mitotic cytokinesis, ensuring low levels of oxidative damage in the progeny. Erjavec et al. [199] demonstrate the formation

of cytosolic foci comprised of an in vivo aggregate of carbonylated proteins. Curiously, members of the protein quality control system, specifically, the Hsp104 chaperone protein is found to co-localize with this aggregate. Additionally, deficiency of Hsp104 protein results in a failure to segregate carbonylated proteins resulting in a reduced replicative potential of ensuing daughter cells. Finally, Sir2 Δ cells were diminished in their ability to segregate such oxidatively damaged proteins and also possess reduced Hsp104 activity with an overexpression of Hsp104 rescuing this defect. Earlier studies had also shown the involvement of the actin cytoskeleton with Sir2 Δ cells displaying aberrant actin cable formation, reduced actin dynamics and increased ROS production [149]. Although, the mechanism by which a nuclear deacetylase influences protein quality control and the actin cytoskeleton in the cytoplasm is still unknown, it is now proposed that chaperones such as Hsp104 may provide a bridge between carbonylated aggregates and the cytoskeleton that not only prevents proteo-toxicity but also inheritance of damaged proteins by the progeny [199].

In the work presented here, I have used the high-throughput imaging screen developed in our laboratory to identify localization changes in cytosolic proteins effected upon conditions of nutrient deprivation. I comprehensively imaged the yeast GFP tagged strain collection grown to stationary phase and find there to be extensive formation of punctate foci by several cytoplasmic proteins. We rule out the possibility that our observations might be due to a GFP tag artifact by using an orthogonal mass spectrometry based analytical technique. I further go on to show the response of two specific proteins, Ade4, a protein in the purine biosynthetic pathway and Gln1, a protein in nitrogen metabolism in yeast towards differential nutrient deprivation. This work is ongoing and further experiments are currently in progress.

RESULTS AND DISCUSSION

Stationary phase imaging screen

We used the cell microarray technique [107] developed and optimized in our lab for conducting a screen of the yeast the GFP tagged yeast collection [45] grown to stationary phase. Briefly, the near complete collection of GFP tagged strains were grown for 5 days in YPD media at 30 C without shaking, fixed with 1% formaldehyde, washed and arrayed onto poly-lysine coated glass slides. They were imaged using the protocol for cell microarrays generating images for all the strains in the collection in stationary phase. From this set of images, we decided to focus on the cytosolic protein subset in order to examine changes in localization that may have occurred under such nutrient depleted conditions (**Figure 4-5**). It is important to point out that cell viability was maintained at ~90% before the fixation process as tested by us and other groups [167].

An examination of the ~800 strains containing GFP tagged cytosolic proteins grown to stationary phase revealed surprising results. A substantial number of the strains examined from the cell chip showed an increased tendency to form punctate localization foci. This was judged by the transition of the GFP signal of the tagged protein from a diffuse cytosolic distribution to one or multiple foci within the stationary phase cell. The degree of the punctate phenotype was manually graded for all the 800 strains as being 'good', 'medium' or 'doubtful' by inspecting the images for each strain from 4 replicate cell microarray experiments in a subjective manner. The strain count was 42 in 'good', 98 in 'medium' and 118 in the doubtful categories. To start with, manual re-testing of the 42 strains in the 'good' category was performed. The strains were grown in duplicate in YPD for 5 days (a direct validation of the cell chip assay) and in synthetic dextrose overnight. The latter culture was spun down and re-suspended in synthetic minimal media and in water and allowed to incubate at 30 C for 1 hour before imaging.

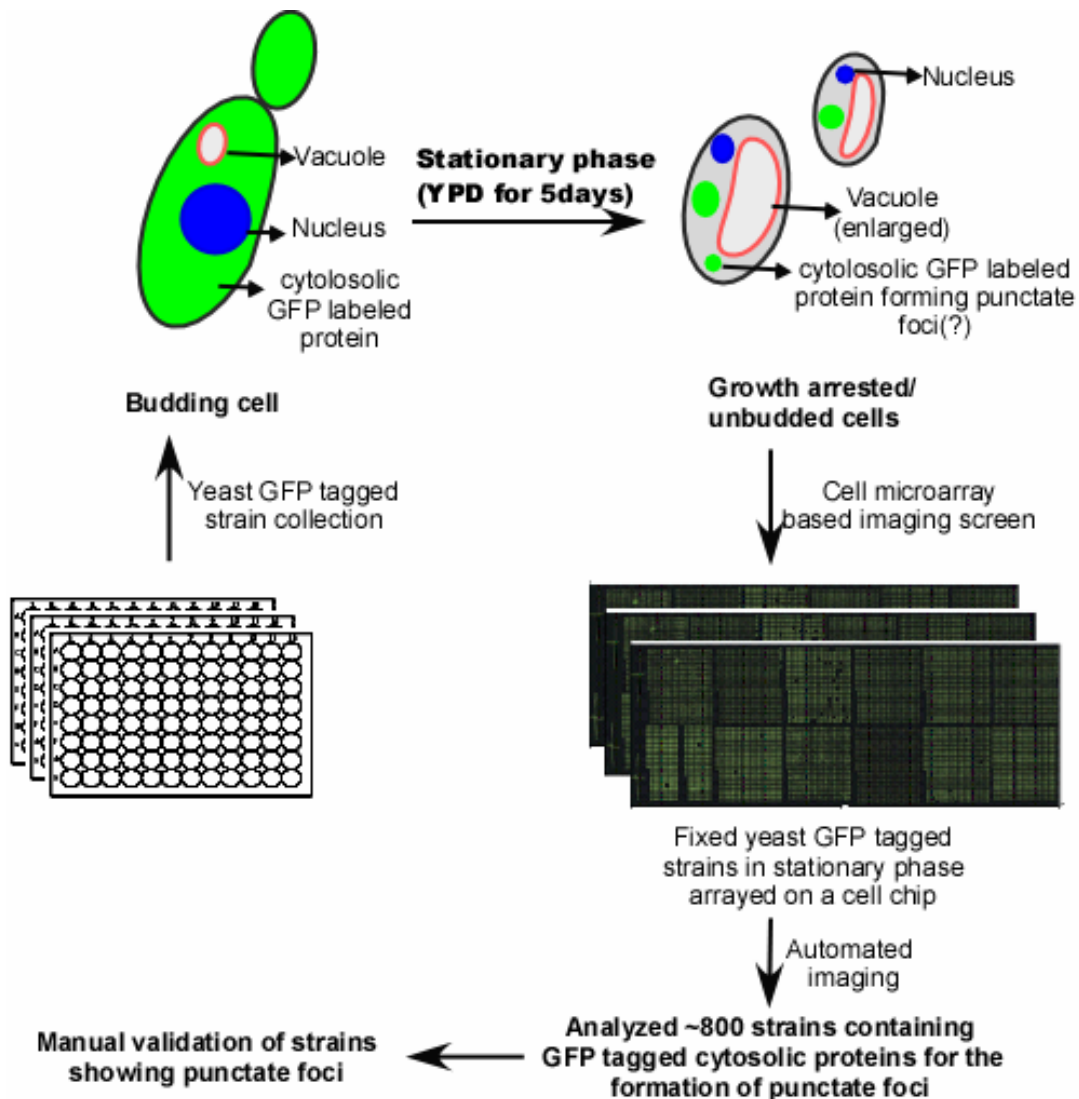


Figure 4-5: A schematic of the cell microarray experiment conducted for imaging stationary phase protein localizations. Images of cytoplasmic proteins were examined for a change in the GFP localization from a cytosolic, diffuse phenotype to a punctate phenotype.

Out of 42 strains imaged, 20 showed a clearly discernible punctate phenotype in one or more of the media conditions tested. Representative images are shown (**Figure 4-6**) for Asn2-GFP and Hsp42-GFP strains. It was apparent that many of the strains reacted

to different extents under the different types of nutrient depletions tested but overall seemed to show a tendency to form a punctate phenotype.

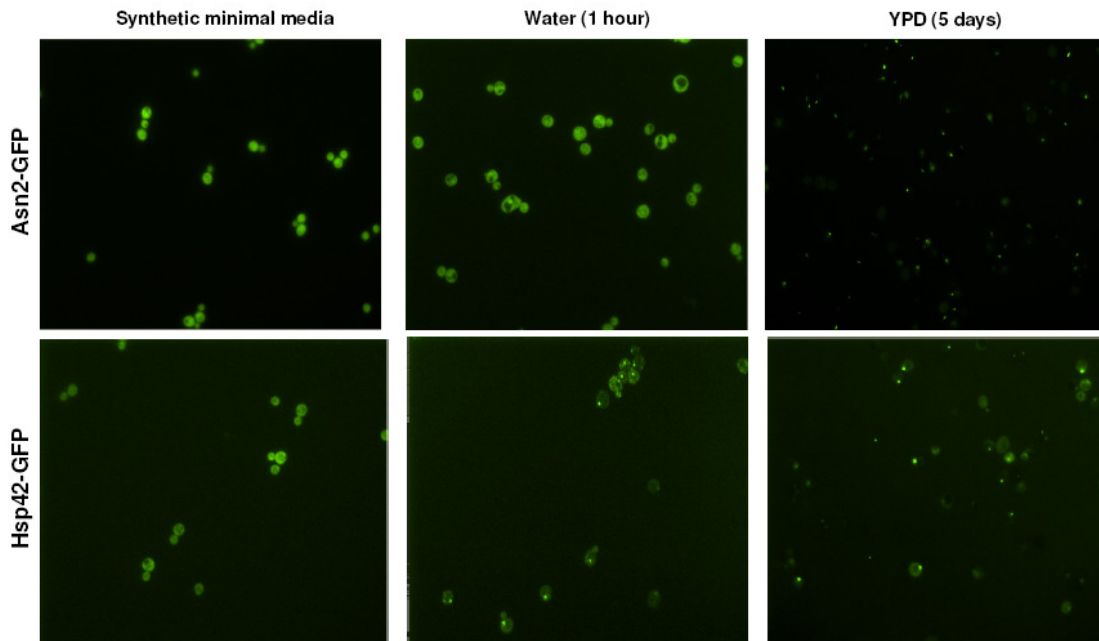


Figure 4-6: Representative strains showing formation of punctate foci of cytosolic proteins under nutrient depletion. The Asn2-GFP and the Hsp42-GFP tagged strains grown in YPD for 5 days (last panel) show a punctate phenotype. Replicate cultures grown overnight in SD were re-suspended in water for 1hour (middle panel) and in minimal media with essential nutrients (left panel). Water induces punctate foci in Hsp42-GFP and to a lesser extent in Asn2-GFP. Minimal media produces a diffuse cytosolic phenotype.

Subsequently, we manually re-tested the union of the strains graded as producing ‘good’, ‘medium’ and ‘doubtful’ punctate phenotypes. In all, 256 GFP tagged strains were grown to 48 hours in SD, a condition observed as sufficient to induce the punctate phenotype in a small test subset before being imaged. Approximately 180 proteins showed at least some degree of punctate formation with several categories of protein function being represented. These including amino acid biosynthesis, heat shock/ stress chaperones and nucleic acid biosynthesis (**Figure 4-7**) in addition to other categories like

mRNA metabolism (Lsm1, Puf3, Nmd4) and fatty acid biosynthesis (Fas1, Fas2). Metabolic proteins and stress related proteins were a dominant category although proteins in other functional classes cannot be ruled out at this point.

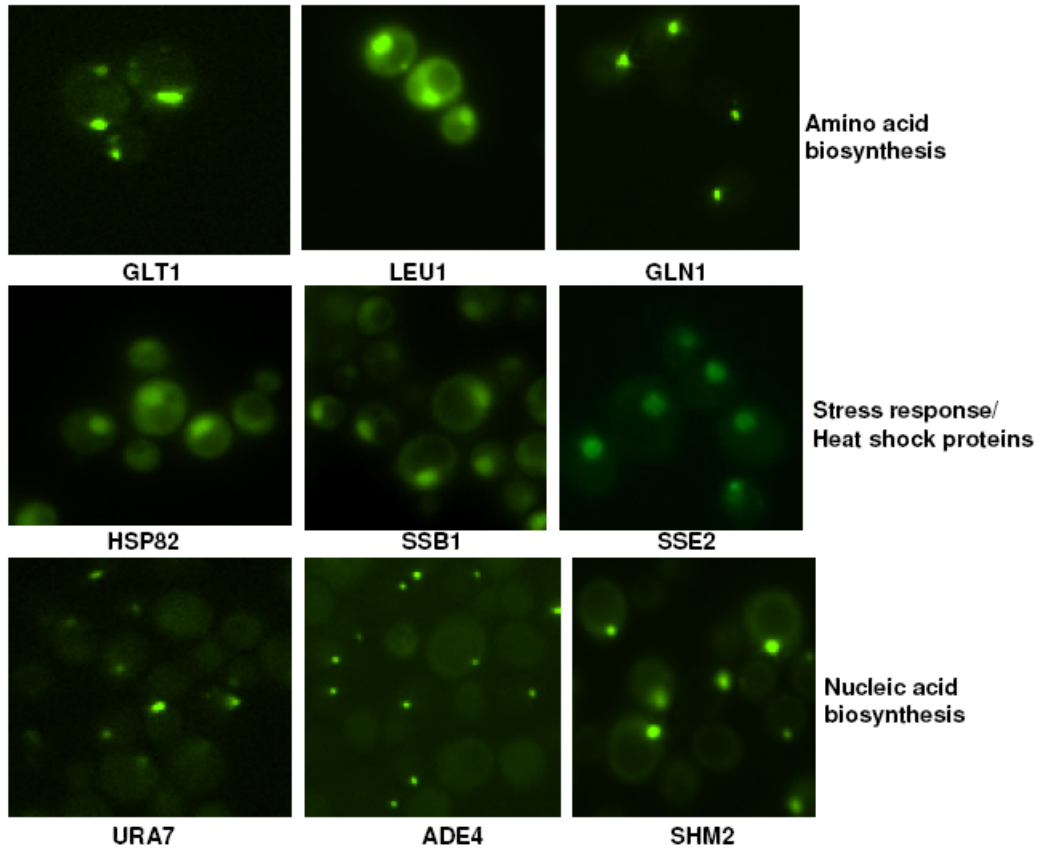


Figure 4-7: Functional categories enriched for proteins forming punctate foci in stationary phase. Proteins fall under several categories [110] with a hypergeometric probability better than intersecting by random chance. Examples include amino acid biosynthesis, stress chaperones and nucleic acid biosynthesis.

A comprehensive table containing all the strains has not been shown considering that our cell chip screen might have had a significant false-negative rate owing to low cell counts and fixation induced auto-fluorescence resulting in non-recovery of low abundance proteins. We are currently in the process of expanding this list through bioinformatics approaches. Nonetheless, our list encompasses a set of > 100 cytosolic

proteins that shows a punctate phenotype upon growth to stationary phase with an over-representation of proteins involved in stress response and in amino acid, nucleic acid and lipid biosynthesis. As alluded to in later sections of this work, nutrient depletion is carried out in YPD or in SD for 2-3 days to induce the formation of punctate structures. I refer to this phase as stationary phase although the cells are actually in diauxic or post-diauxic shifted conditions.

Reversibility of the punctate phenotype

An interesting aspect about several of the strains tested as showing a punctate phenotype was their reversibility to the ‘normal’, cytosolically diffuse form upon addition of fresh media. In all, 4 strains from the metabolic category were tested – Ade4, Gln1, Ura7 and Shm2 GFP tagged strains. These were tested because of their robust production of a punctate phenotype in stationary phase. All of them could be grown to stationary phase in YPD for 48 hours to form the punctate state., spun down to remove the spent media and recovered to form the cytosolic, diffuse state upon re-addition of fresh YPD or SD media (chosen to reduce background autofluorescence). A representative figure from a time lapse experiment is shown (**Figure 4-8**) for the Gln1-GFP strain. The time scales of recovery were of the order of 1-2 hours. By the end of two hours, the punctate foci are almost completely dissolved. It must also be noted that some of the cells in the field appear to start budding and dividing at about this time, possibly indicating an exit from quiescence and entry into cell cycle. However, at this point, we do not have statistical evidence to show a good correlation between dissolution of the punctate structures with cell division, an area that we plan on investigating further. Additionally, even though all our stationary experiments are done with cultures grown between 2 and 3 days, a rigorous establishment of both the robustness of the punctate GFP signal after incubation for

longer periods in stationary phase (> 5 days) and their respective recovery times as a function of time spent in this phase (cell quiescence cycle) still needs testing.

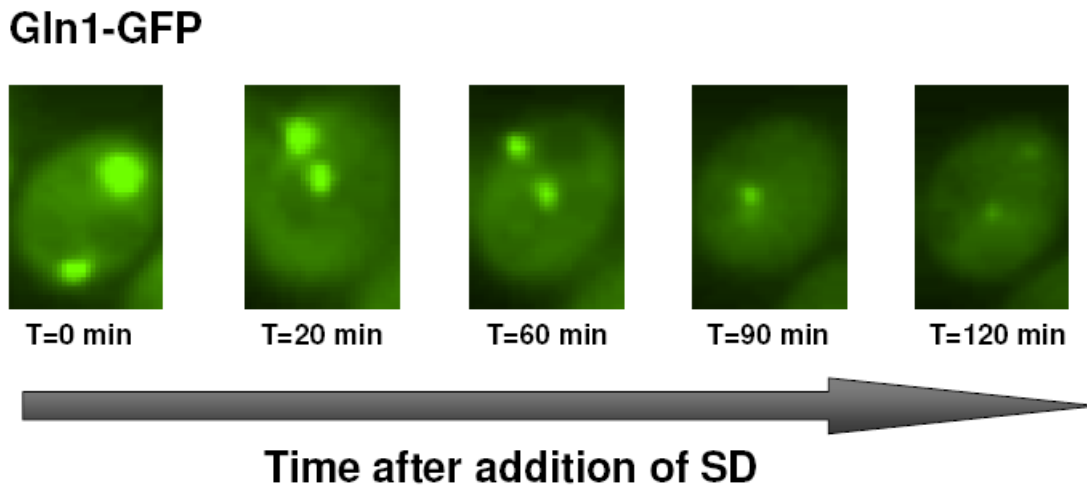


Figure 4-8: Reversibility of Gln1-GFP punctates grown in YPD for 48 hours with SD media. Gln1-GFP cultures were grown to 48 hours in YPD, spun down and treated with SD complete media before time lapse imaging on a SD agar pad for 3 hours. By 120 mins, the punctate foci are almost completely dissolved.

Biochemical enrichment of Gln1-GFP punctates

The formation and reversibility of the punctate state suggested the possibility of an altered set of protein interactions existing in stationary phase as compared to a state of nutrient abundance. With the goal of enriching for the punctate bodies by immunoprecipitation and performing mass spectrometry to identify such protein interactions, we performed a sucrose gradient polysome fractionation (7-47%) on representative GFP tagged strains known to show a punctate phenotype from the screen. The analysis was performed in duplicate on a set of strains grown to stationary phase (YPD for 3 days) with one set being recovered by fresh YPD addition for 2 hours (hence causing dissolution of the punctate bodies). Fractions were collected based on density and

a dot blot performed with anti-GFP antibody. Our assumption was that punctate bodies that appeared as dense structures within the cell would be enriched in denser fractions in the stationary phase samples as compared to the respective ones that were recovered by re-addition of fresh YPD. We however failed to see such an enrichment of the GFP protein signal, on comparison of the respective stationary and recovered states in any of the strains (data not shown). Therefore, it was concluded that the punctate structures were unstable and had gotten disrupted during lysis or were lost in the insoluble pellet fraction. An important observation from this experiment was the polysome profile itself that showed appearance of polysomes after YPD addition as compared to the complete absence of any in the stationary phase profile. This phenomenon lends credence to the fact that re-entry into cell cycle upon nutrient availability is accompanied by large-scale re-organization of protein complexes.

To test if the punctates could be recovered in any other manner, the Gln1-GFP strain was grown in YPD for 48 hours to induce formation of the punctate phenotype. Cells were lysed with glass beads and the lysate was centrifuged at 13,000 x g in a microcentrifuge for 10 minutes. The supernatant was removed and clarified by an additional centrifugation step and the clarified supernatant and the lysate pellet were imaged for GFP signal (**Figure 4-9**). As shown, the punctate GFP signal was minimal in the clarified supernatant explaining the earlier observation that a polysome profile of the soluble fraction of the lysate failed to yield significant enrichment. Much of the punctate Gln1-GFP signal is associated with the clarified lysate pellet fraction. This suggested that the punctate structures were either denser than the range of sizes separable by a sucrose gradient analysis or that there is a non-specific aggregation or association with insoluble membrane fractions. Regardless, we show that a soluble cytosolic protein such as Gln1, normally found in the soluble phase in log phase under conditions of nutrient abundance

(controls done but data not shown) transitioned to the insoluble pellet phase upon depletion of nutrients in stationary phase and this transition was reversible (**Figure 4-8**). Attempts to perform immunoprecipitation on the pellet fraction are ongoing and conditions for optimal solubilization are being established.

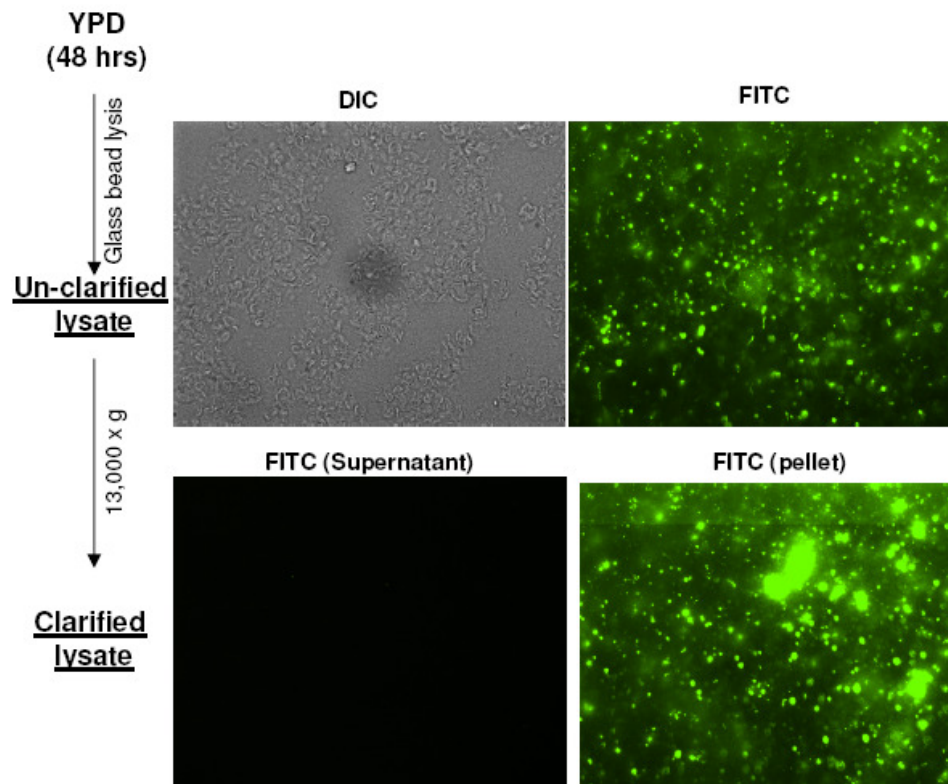


Figure 4-9: Biochemical enrichment of Gln1-GFP punctates. Gln1-GFP grown to stationary phase was lysed by glass beads and the lysate clarified by centrifugation at 13,000xg. The GFP protein signal is found highly enriched in the pellet.

We subsequently checked the conditions for dissolution of the Gln1-GFP punctate structures isolated in the pellet fraction of the lysate (**Figure 4-10**). RNase A, YPD, SDS, proteinase K and rapigest (an acid-labile detergent) were tested by direct addition to the clarified and washed stationary pellet (in lysis buffer) and incubating at 37 C for 30 mins

before imaging. Neither YPD nor RNase A was sufficient to dissolve these structures in such an in vitro complementation experiment indicating that dissolution with nutrients required additional cytoplasmic factors and that RNA was not required for maintaining the assembled punctate structure. However, addition of SDS, rapigest or proteinase K resulted in dissolution of the punctate structures clearly revealing that removal of the associated proteins disrupts them.

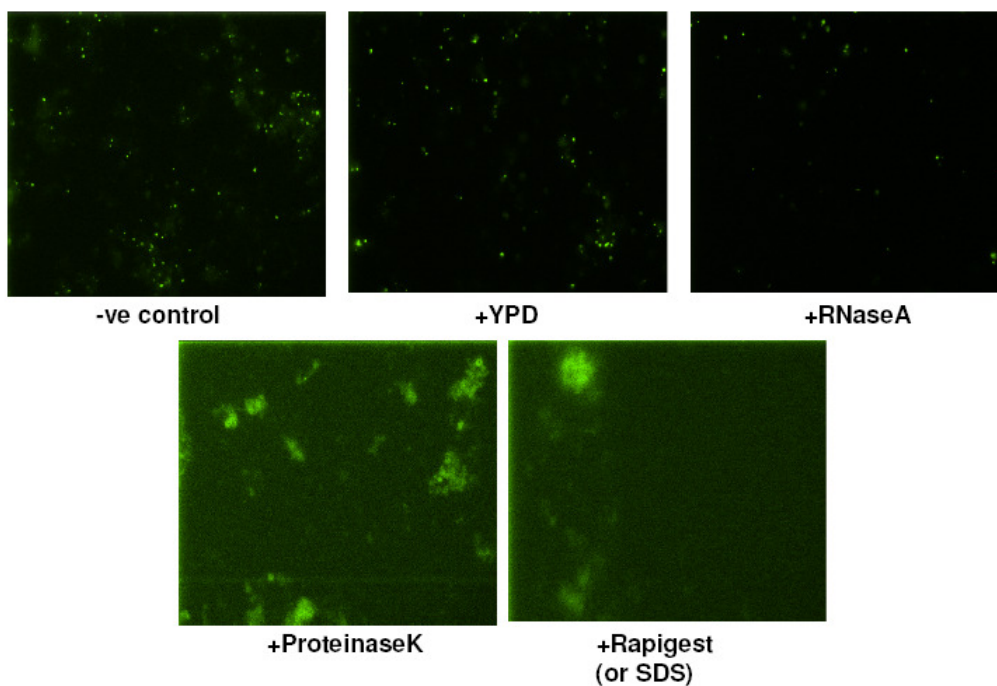


Figure 4-10: In vitro analysis of Gln1-GFP punctates. Pellet enriched Gln1-GFP punctates (-ve control) were complemented with YPD, RNaseA and protease reagents. Only proteinase K and protein detergents (rapigest, SDS) were able to disassemble the punctate bodies significantly.

Analysis of formation of punctates by mass spectrometry-based shotgun proteomics

The observation that GFP tagged cytosolic proteins reversibly transitioned to a punctate state upon nutrient depletion led us to the question whether this phenomenon would also occur with untagged native proteins. A possibility that the GFP tag, despite

being the standard for tagging proteins in cells could be an artifact was not inconceivable. Since the GFP tagged library is comprised of proteins tagged at the C-terminal end, one of the controls that we are in the process of doing is to recapitulate the punctate transition in a strain with an N-terminally tagged GFP fusion protein. However, we also wanted to validate our observations by conducting a proteome-wide measurement using an unrelated analytical technique. Towards this, we grew cultures of BY4741, the untagged parent strain for the GFP fusion collection, in duplicate, to stationary phase (YPD for 3 days). One of the cultures was spun down and 'recovered' with fresh YPD for 2 hours by shaking at 30 C. Both the stationary phase and the recovered cultures were lysed with glass beads and clarified to obtain their respective pellets and supernatants. All four fractions were treated with rapigest, an acid labile detergent, digested with trypsin, quantified and analyzed by two dimensional LC-MS/MS using a LTQ-Orbitrap mass spectrometer (**Figure 4-11**).

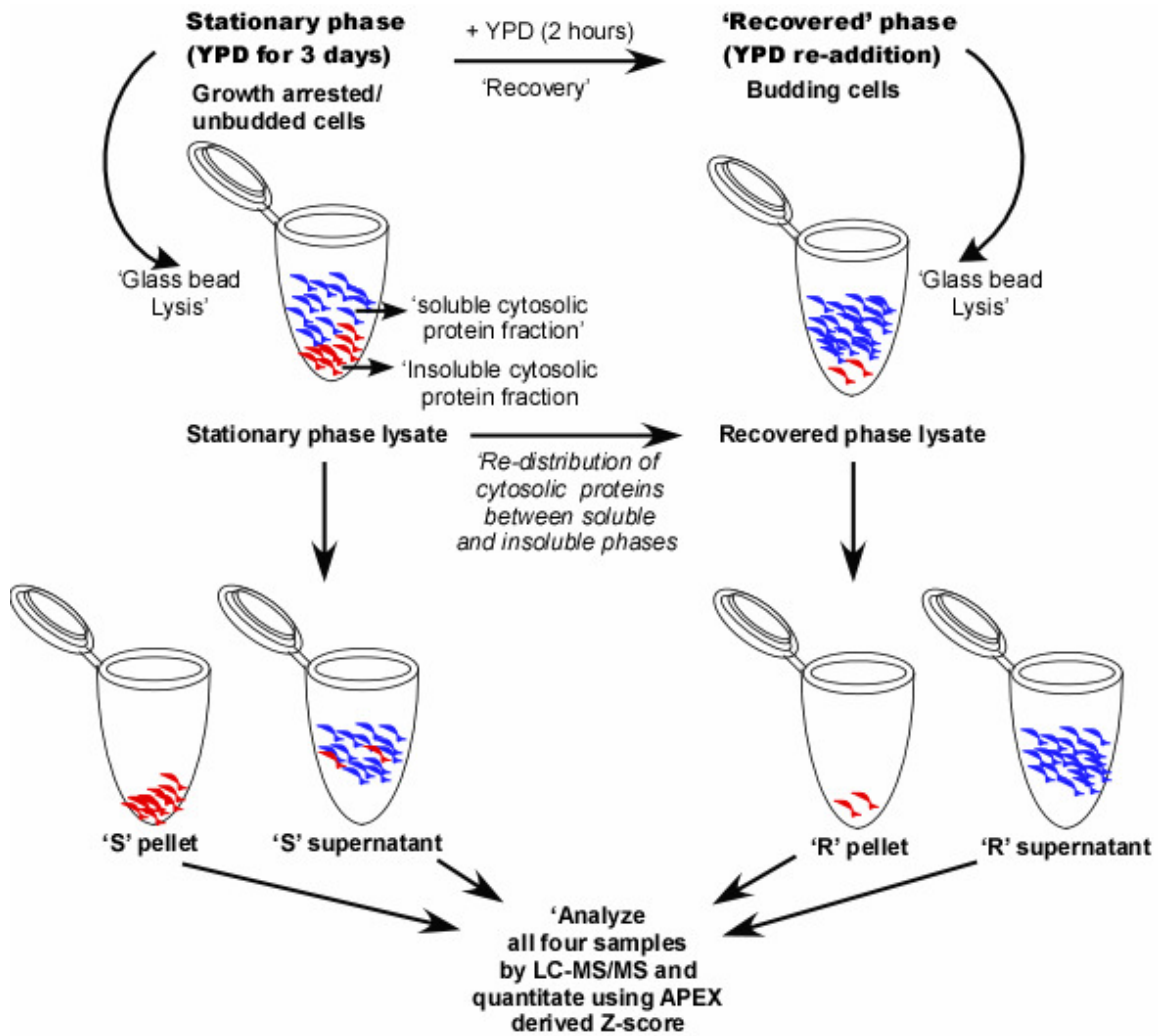
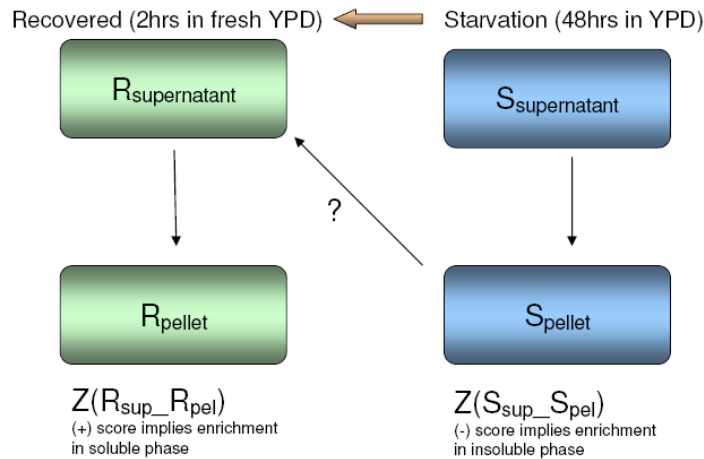


Figure 4-11: Schematic of mass spectrometric shotgun proteomic analysis of stationary phase yeast. Two BY4741 cultures were grown to stationary phase and lysed with one being recovered by fresh YPD before lysis. Their respective supernatants and pellet fractions were analyzed by 2D-LC-MS/MS. Red and blue colors represent insoluble and soluble cytosolic protein fractions respectively.

Sequest analysis of peptide counts were done by imposing a 95% confidence threshold and the corresponding protein hits recovered from a database of yeast proteins. APEX analysis was performed according to Lu et al. [16] for the four fractions and Z-scores of transition of individual proteins from soluble to insoluble fractions in both the

stationary and recovered phases were calculated. A summary of the procedure followed for performing these calculations is shown in **Figure 4-12**.



Calculate test statistic for each transition. The difference between the two Z-scores represents the deviation between the two distributions.

Figure 4-12: Calculation of Z-scores as a metric for protein transitions between fractions. The recovered and the stationary phase supernatant and pellet fractions can transition with each other and this Z-score can be calculated as shown. The real question being addressed is represented by the diagonal arrow which is whether cytosolic proteins in the stationary phase pellet transition to the supernatant in the recovered phase (please refer text).

We performed two kinds of analysis. First, we tried to group the proteins enriched in the four fractions by their functional categories by taking advantage of their Z-scores of transition. If the Z-score for a protein was such that $Z(R_{sup_R_{pel}})$ was positive, that protein was likely to exist in the soluble fraction in the recovered phase while a negative score implied an enrichment in the insoluble fraction. A similar analogy works with the $Z(S_{sup_S_{pel}})$ for finding the probability of such a transition in stationary phase. We grouped the proteins having a positive $Z(R_{sup_R_{pel}})$, negative $Z(R_{sup_R_{pel}})$, positive $Z(S_{sup_S_{pel}})$ and negative $Z(S_{sup_S_{pel}})$ into significant functional categories using the FUNSPEC program [110]. All the proteins selected passed a 95% confidence threshold. As expected for soluble proteins, cytoplasmic proteins were significantly enriched in the

supernatant of the recovered phase while the respective pellet showed an enrichment for transport vesicles. This validated our mass spectrometry-based approach for analyzing protein transitions between supernatant and pellet fractions since cytosolic proteins are largely soluble and transport vesicles are largely insoluble. On the other hand, both the supernatant and the pellet fractions of the stationary phase were significantly enriched for cytosolic proteins (Figure 4-13). This corroborated our image data that cytoplasmic proteins tended to accumulate in the pellet of stationary phase cell lysates.

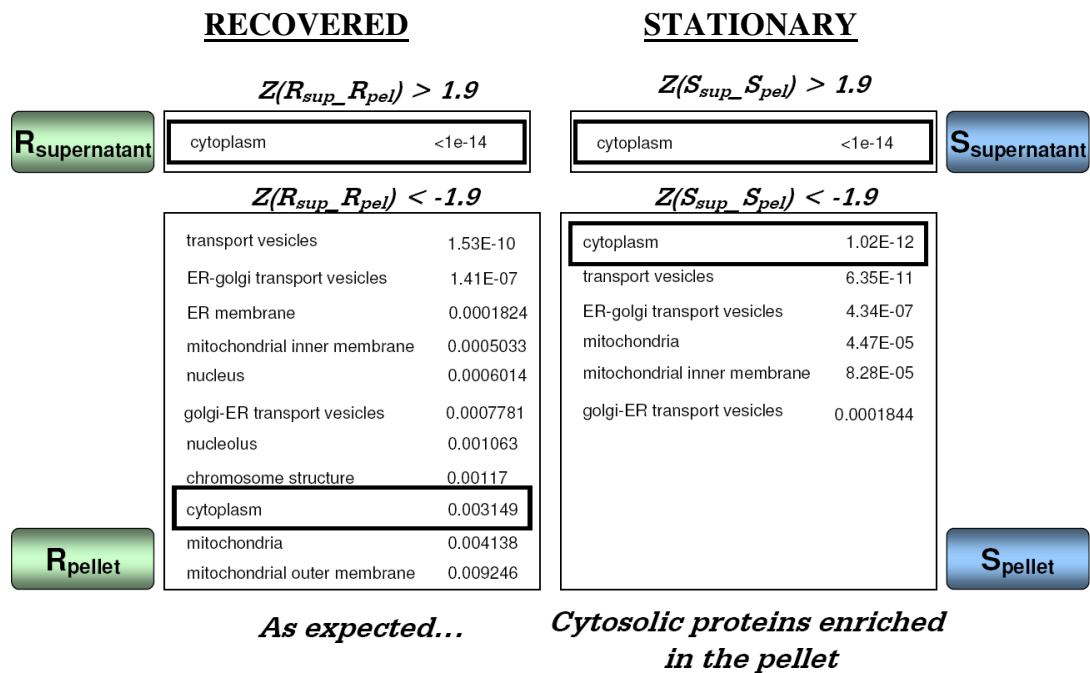


Figure 4-13: Protein functions enriched for supernatant to pellet transitions and vice versa for the two phases. Cytosolic enrichment is evident for the supernatant fraction of the recovered phase lysate but not such for the pellet. However, the stationary phase lysate displayed strong enrichment for cytosolic functions in both fractions.

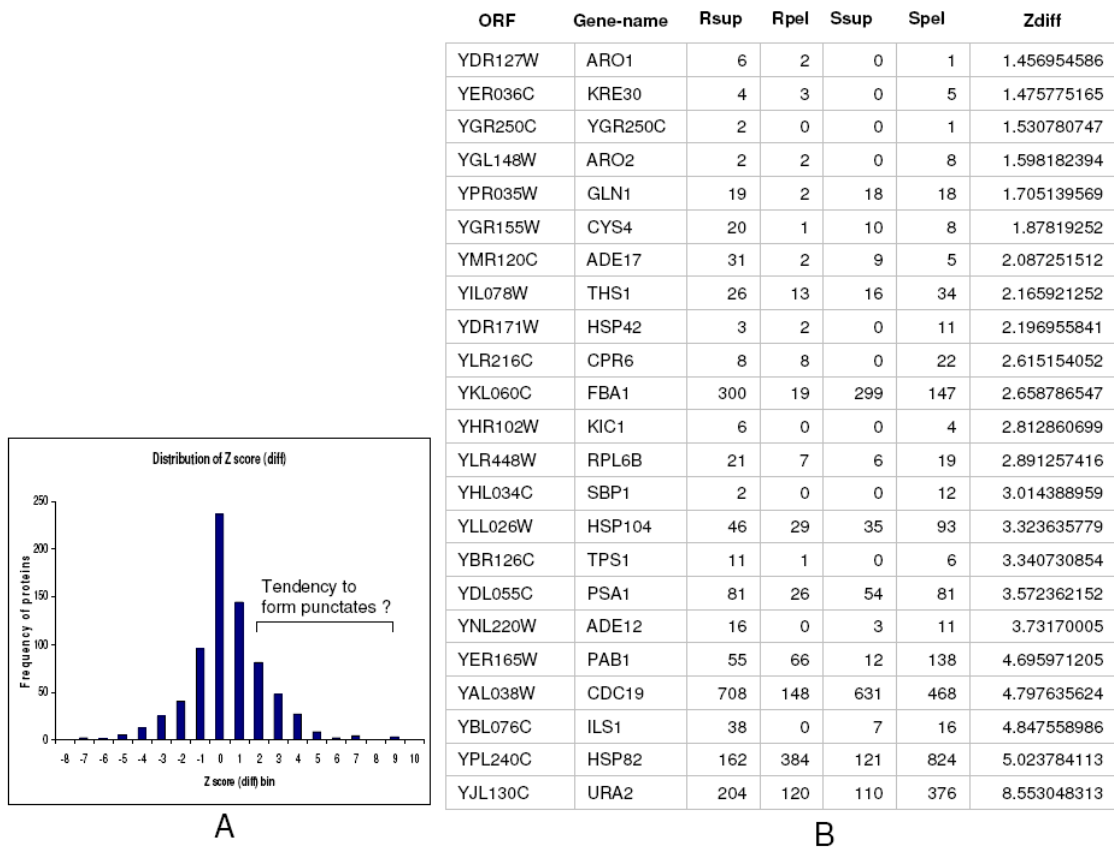


Figure 4-14: Proteins that are most likely to form stationary phase punctates as determined by mass spectrometry and the cell chip. A: A histogram of the Z-score differences with those passing the 95% cut-off being most likely to form punctates in stationary phase. B: The intersection between the mass spectrometry derived and the cell chip derived list of proteins likely to form such punctates.

In our second analysis, we addressed the issue of whether cytoplasmic proteins found enriched in the stationary phase pellet reversibly transitioned to the supernatant in the recovered phase. If $Z(R_{sup_R_{pel}})$ was greater than $Z(S_{sup_S_{pel}})$ or $Z(R_{sup_R_{pel}}) - Z(S_{sup_S_{pel}}) > 0$, then the probability for a transition from supernatant to pellet would be greater in the stationary phase as compared to the recovered phase. This would identify the list of proteins that preferentially get enriched in the stationary phase pellet as compared to that of the recovered phase. Using the difference in the two Z-scores as a metric (divided by $\sqrt{2}$ to correct for normality), we generated a list of proteins that

satisfied the above criterion and was above a ~95% confidence cut-off. We found many of the proteins in this list to be enriched for proteins found to display a punctate phenotype from the cell microarray screen. A representative set is shown. (**Figure 4-14**).

Figure 4-14 A shows a histogram of Z-score differences, of which the significant set that might be undergoing the transition are highlighted. Preliminarily, ~25 proteins (**Figure 4-14 B**) were recovered as passing this cut-off and being identified from the cell chip screen. We think that the low intersection between the two sets may be due to factors such as instability of the punctate structure, protein-abundance related bias in the mass spectrometry experiment and a false negative rate from the cell chip screen. We are in the process of testing some of the non-intersecting proteins passing the cut-off in the mass spectrometry experiment for the formation of punctates with the ultimate goal of finding out how extensive this phenomenon might be. However, a clear trend for cytosolic proteins to be enriched in the pellet of a stationary phase lysate as compared to the recovered phase (**Figure 4-13**) is seen, an overall confirmation of the trend observed from the cell chip screen.

Analysis of nutrient specificities towards induction and dissolution of punctates

Conditions for induction

Until this point, we have shown, using two independent analytical techniques that a large fraction of the cytosolic proteome displayed a previously uncharacterized dynamic upon nutrient depletion - a transition from a soluble, diffuse localization state to an insoluble, punctate state. We also show that this phenomenon is reversible by re-addition of fresh media. We subsequently wished to test for any nutrient specific induction of the punctate state. Two strains were chosen for this purpose- the Gln1-GFP

strain where Gln1 encodes for Glutamine synthetase involved in nitrogen fixation and the Ade4-GFP strain where Ade4 encodes for PRPP aminotransferase and catalyzes the first committed step in purine biosynthesis. Although we chose these strains because of the interesting behavior they displayed, we anticipate other strains to also show similar idiosyncrasies. Briefly, we grew both the Ade4 GFP and Gln1 GFP strains in YPD to log phase (OD ~ 0.5). They were then spun at low speeds (2000 x g), re-suspended in media lacking different nutrients and incubated them for 2 hours at 30 C before imaging (**Figure 4-15 and Figure 4-16**).

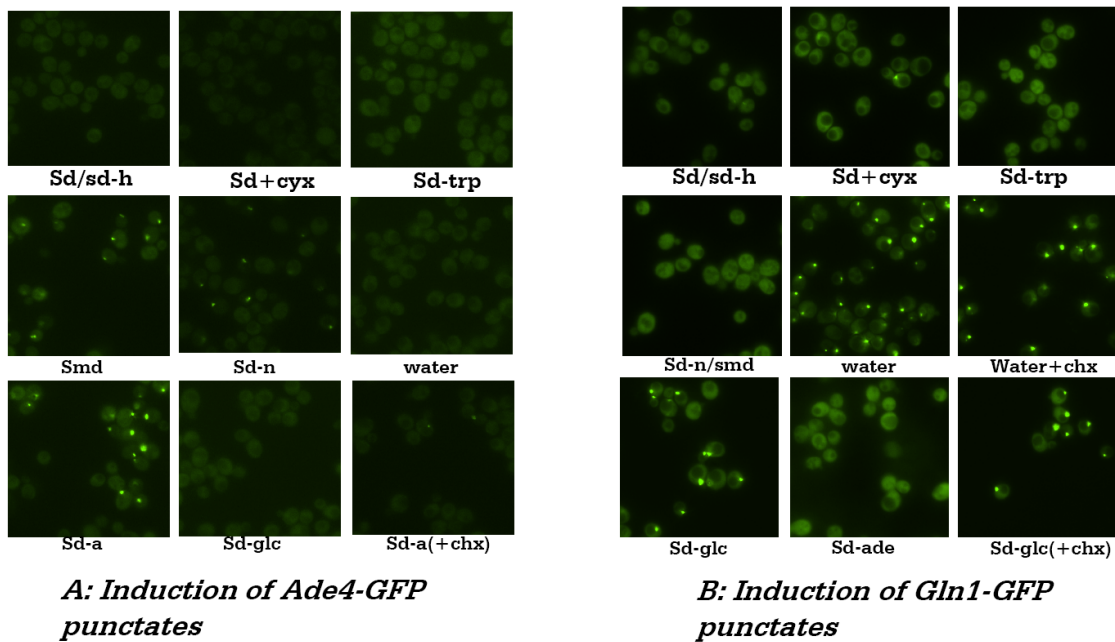
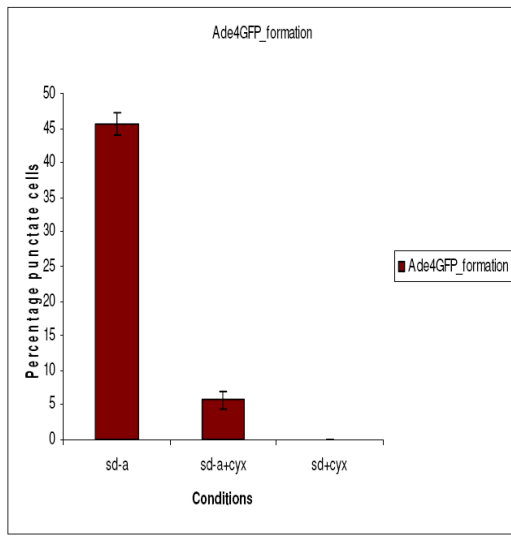
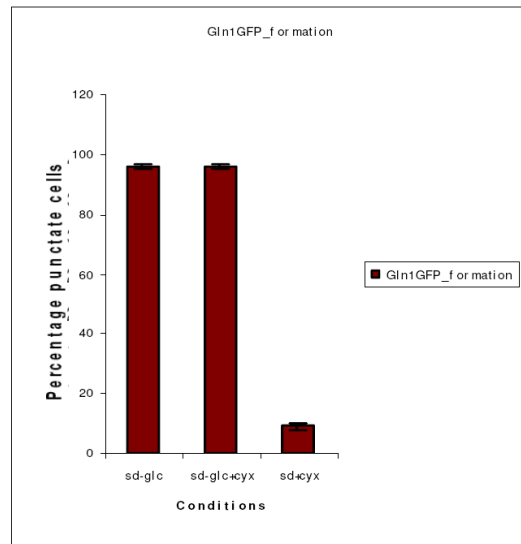


Figure 4-15: Conditions for induction of Ade4 and Gln1 GFP punctates. Ade4 and Gln1-GFP strains were grown to log phase before re-suspension in different media for 2hours and imaging. A: removal of adenine is necessary and sufficient to induce formation of Ade4-GFP punctates as seen by the punctates formed in the SD-Ade panel. However, adenine drop-out in the presence of cycloheximide (sd-ade(+chx)) does not produce robust punctates. B: Removal of glucose is necessary and sufficient for induction of Gln1-GFP punctates with cycloheximide not affecting this transition.



A: Induction of Ade4-GFP punctates



B. Induction of Gln1-GFP punctates

Figure 4-16: Summary of punctate induction in Ade4 and Gln1-GFP strains.

Percentage of cells having punctates (from three replicate images) was plotted as a function of media conditions tested. As shown in A, Ade4-GFP punctates are induced upon adenine removal and are sensitive to cycloheximide. As in B, Gln1-GFP punctates are induced upon glucose removal and are insensitive to cycloheximide treatment.

We detected specific nutrient dependencies in the induction of punctates for the two strains tested systematically (**Figure 4-15**). Each strain was subject to depletions such as carbon source, nitrogen source, amino acid and total starvation in the form of water re-suspension. Ade4-GFP appears to transition into a punctate state in SD-Ade (adenine dropped out), SMD (minimal media lacking adenine) and in SD-N (nitrogen dropped out from minimal media and therefore lacking adenine). This suggested that adenine, when dropped out, is sufficient to stimulate a change to the punctate state in Ade4-GFP. Interestingly, water re-suspension, despite lacking adenine, did not show this induction. In the case of Gln1-GFP, we see that carbon starvation in the form of glucose removal or total nutrient depletion in the form of water re-suspension caused the formation of robust punctates leading us to believe that carbon source depletion is

sufficient for this process to occur in Gln1-GFP. The effect of protein synthesis was also tested and produced interesting results. While adenine drop-out media induced Ade4-GFP to go punctate, this transition was heavily undermined by the addition of cycloheximide. Gln1-GFP showed no such effect in response to cycloheximide addition accompanying a glucose drop-out. This suggests a requirement for continued protein synthesis for the induction of Ade4-GFP punctates in the absence of adenine while the induction of Gln1-GFP punctates appear refractory to overall protein synthesis as long as glucose is made limiting. The results are summarized in **Figure 4-16**.

Conditions for dissolution

The induced punctates also showed nutrient specific reversibility. A similar experiment was performed with both the strains where punctates were induced by adenine removal (for Ade4-GFP) and glucose removal (for Gln1-GFP). Cells in the punctate state were then subject to re-addition of different nutrients (**Figure 4-17**), and incubated for 2 hours at 30C before imaging. While an unrelated amino acid such as histidine was not able to dissolve the Ade4 punctate, adenine and the related nucleotide hypoxanthine dissolved the punctate bodies in Ade4-GFP cells. Similarly, glucose was sufficient to dissolve the Gln1-GFP punctate bodies formed by glucose depletion. Interestingly however, both the strains differed in their behavior to cycloheximide as could be hinted from the induction experiments. Dissolution of the Ade4 punctate occurred by simply inhibiting overall protein synthesis by addition of cycloheximide reiterating that continued protein synthesis is necessary to not only form but also maintain this punctate state. However, Gln1-GFP was not affected by the addition of cycloheximide alone although, when added along with glucose, there is reduced efficiency of punctate dissolution (**Figure 4-18**). We also tested the effect of PMSF, a

serine protease inhibitor that is known to inhibit vacuolar proteases and would therefore inhibit degradation of proteins destined for the vacuole. If this were the case, a longer lasting and more stable punctate state would be expected to result. Ade4-GFP punctates, when treated with PMSF and cycloheximide show a slightly greater degree of punctates per cell when compared to treatment with cycloheximide only. However, Gln1-GFP appeared to be insensitive to the addition of PMSF (Summarized in **figure 4-18**).

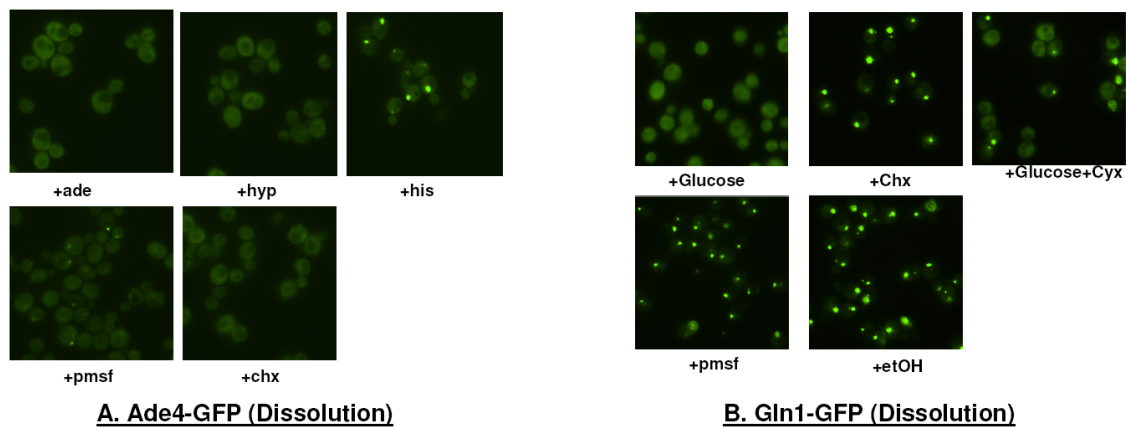


Figure 4-17: Nutrient specific dissolution of Ade4-GFP and Gln1-GFP punctates. Reversibility of punctate formation by re-addition of adenine (or metabolically related hypoxanthine) and glucose is displayed for Ade4-GFP and Gln1-GFP strains respectively. However, the reversal is sensitive to cycloheximide for Ade4-GFP and only partially so for Gln1-GFP.

These observations argue towards a dynamic process regulating the Ade4-GFP punctate formation and dissolution as opposed to the Gln1-GFP punctates which appear to be more static affected by only carbon source depletion and largely independent of overall protein synthesis and degradation. Involvement of vacuolar protein degradation is also seen as a possibility.

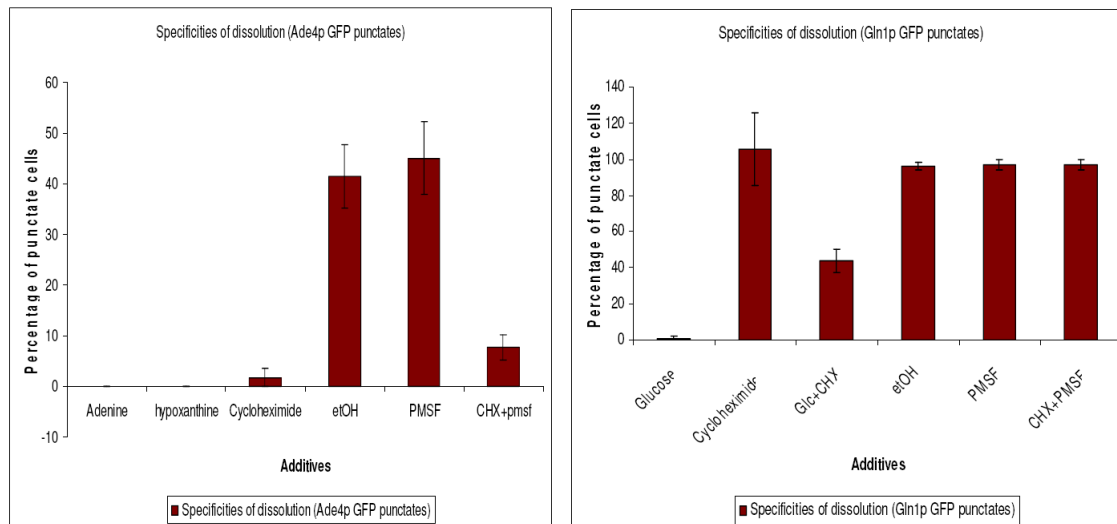


Figure 4-18: Summary of nutrient specific dissolution of Ade4-GFP and Gln1-GFP punctates. Adenine and Glucose re-addition completely dissolves Ade4 and Gln1 GFP punctates respectively (three replicates). As shown in A, however, this dissolution is sensitive to cycloheximide (chx) addition. Addition of chx with PMSF rescues this effect to a small extent. In B, Gln1-GFP punctate dissolution is partially sensitive to cycloheximide as seen from the Glucose+chx panel while PMSF showed no effect.

Conclusions, models and future directions

We show evidence that suggests an extensive transition of cytoplasmic proteins to an insoluble, punctate state under conditions of nutrient depletion in stationary phase grown yeast cultures. This observation is supported by two genome-wide experiments in the form of a high-throughput cell microarray-based imaging method and a mass spectrometry-based shotgun proteomics method. The orthogonality of the two methods precludes the notion that the phenomenon might have been a solely GFP-tag-derived artifact. We further go on to show for two specific strains that had their Ade4 and Gln1 genes tagged with GFP, a nutrient specific induction and dissociation of a punctate state from log phase grown cultures. While Ade4-GFP punctates show cycloheximide-sensitive reversible induction and dissociation to adenine or the related hypoxanthine, Gln1-GFP

punctates display such reversible behavior in response to a carbon source like glucose in a largely cycloheximide independent manner. In our attempts to rationalize these observations based on phenomena that are known to operate in quiescence, we propose the following possible models and future experiments that may be performed to address each of them (Summarized in **Figure 4-19**).

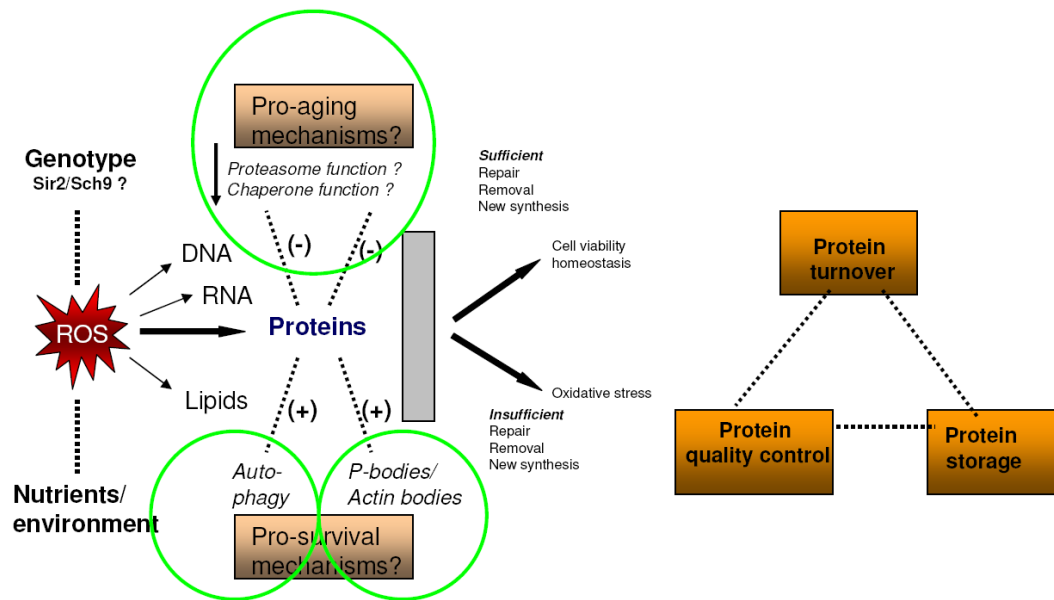


Figure 4-19: Recapitulation of mechanisms that may be involved in the formation of punctates. Green circles represent the pathways in question. All three suggested mechanisms may also be systemically inter-connected as depicted.

Protein re-cycling by autophagy

Autophagy is the predominant protein re-cycling mechanism that operates under nutrient depleted conditions. Traditionally, autophagy is stimulated by nitrogen starvation and autophagosome vesicles marked by proteins such as Atg2 and other proteins are observed to go punctate [180]. Autophagocytic vesicles carry cytosolic cargo such as proteins and organelles to the vacuole for re-cycling. In support of this model, the

punctates seen in our work are produced during stationary phase although not specifically under nitrogen depletion. A vacuolar involvement is also seen in the case of Ade4-GFP punctates which appear to be stabilized two to three fold in the presence of PMSF and cycloheximide (**Figure 4-18 A**). We therefore tested Gln1-GFP and Ade4-GFP protein localizations in strain backgrounds containing deletions in *ATG2* (Autophagy defective) and *VPS33* (Vacuole minus) (**Figure 4-20**).

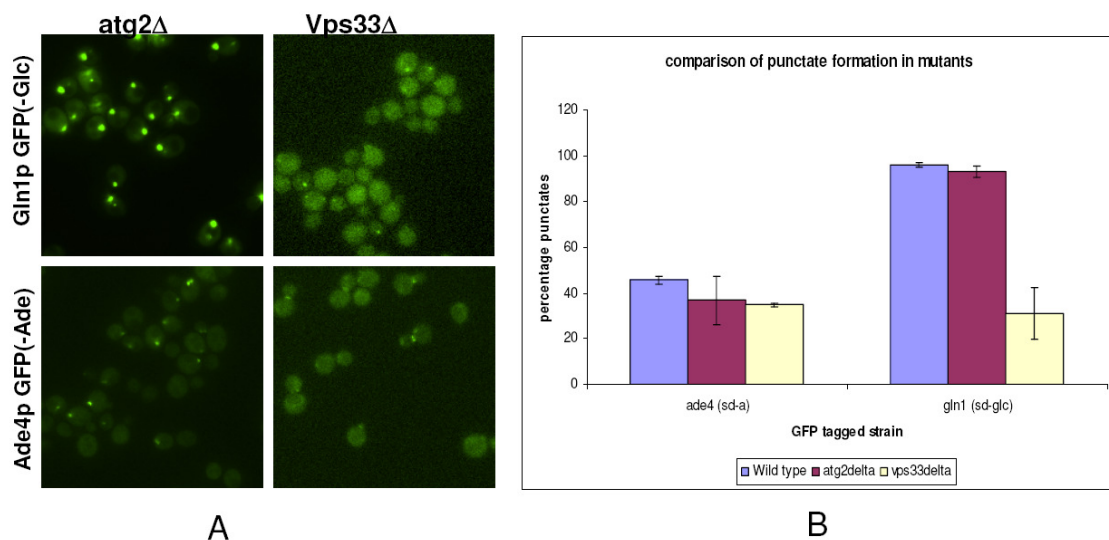


Figure 4-20: Punctate localization tests in autophagy and vacuole defective strains.

A: Gln1 and Ade4GFP punctates appear un-affected by a deletion in *atg2* that produces an autophagy defect. *Vps33* deletion that results in vacuole minus cells severely impairs Gln1-GFP punctates and appears to produce Ade4-GFP punctates that are proximal to the bud tip. B: graphical summary of the observations done in three replicates.

Our results showed that an autophagy defect did not appear to affect punctate formation in both strains tested. However, a vacuolar defect severely impairs Gln1-GFP punctate formation and restricts Ade4-GFP punctates to the bud tip, an event that was an aberration as compared to the wild type background. These results are consistent with the important role played by the vacuole under nutrient depleted conditions in protein

turnover. However, specific mechanisms about the punctates are not explained by this experiment.

A protein storage mechanism for keeping cells in a poised state

As previously mentioned, there may exist cellular depots in quiescent cells such as P-bodies for mRNA storage [188], actin bodies [200]) and genomic positioning of transcription factors [187] which appear to keep cells in a poised state for cell cycle re-entry upon availability of nutrients. Co-localization with P-body marker proteins revealed no significant co-localization with either Gln1-GFP or Ade4-GFP punctates (data not shown). Co-localizations with actin bodies remain to be tested.

Our observation that many cytoplasmic proteins transition to a punctate form suggests that a similar storage mechanism may operate at the protein level. In favor of this, we see that punctate foci persist for several of the proteins tested for weeks (up to 2 weeks tested) in stationary phase. The fact that stress response and biosynthetic proteins are enriched may also imply that the biosynthetic machinery is poised for nutrient availability to facilitate rapid re-entry into the cell cycle. This is supported by rapid polysome synthesis and actin re-polarization when cells exit quiescence. In order to prove such a model, an experiment such as pulse-chase labeling of a specific protein in a punctate form would have to be attempted. Any result that shows that the proteins in the punctate structure is re-used by the cell but not degraded upon availability of nutrients will support this model favorably.

Aggregation due to compromised protein-quality-control

Currently, this model seems to be a favorable one since it explains most of our observations. It is thought that proteasome and chaperone functions may be compromised under conditions of nutrient depletion. This may happen because of low ATP availability

and the high demand for ATP for these processes to function effectively. As a result, highly expressed cytosolic proteins that have a propensity to aggregate may not undergo proper quality control causing them to form aggregates in stationary phase. The observation that Gln1-GFP forms punctates upon glucose removal is explained well by this model because removal of the major carbon source depletes energy and therefore, presumably, ATP content in a cell. The concomitant decrease in chaperone activity may cause Gln1 to aggregate forming punctates. A useful experiment to support this would be to look at co-localization with inorganic poly-phosphate stores that likely serve as P_i reserves of ATP synthesis [201]. The observation that Gln1-GFP punctates dissolve before the cells bud upon re-addition of media may also suggest that such aggregates function as a cell cycle checkpoint. Hsp104 and Sir2 have already been implicated in damage segregation by facilitating cellular asymmetry during budding [199]. An experiment where punctate formation is tested in a strain over-expressing or deleted in heat shock protein genes or longevity related genes such as Sir2 may lend support towards this model. A chronological lifespan assay could also be conducted to see if sequential starvation and re-feeding of Gln1-GFP cells results in a severely aged population thereby implicating such aggregates to reducing their replicative potential. Other experiments that detect oxidative damage such as carbonylation of proteins in the punctate structures will also lend credence to this model.

The observation that Ade4-GFP goes punctate upon adenine removal could result from an over-expression of Ade4 protein under this condition (since adenine removal is known to up-regulate Ade4) that may overwhelm the protein quality control mechanism being performed by heat shock proteins. Re-addition of adenine may lower it back to normal levels which can undergo effective quality control. Sensitivity to cycloheximide is also consistent with this model since a continued synthesis of Ade4 protein is required for

this over-expression to occur in order to overwhelm the protein quality control system. Bioinformatic approaches to detect systematic biases towards factors such as expression levels and aggregation propensities of proteins are currently underway in an attempt to rationalize the punctate set obtained in our experiments. An understanding of the proteome dynamics in this interesting phase promises to have implications in comprehending the evolution of cellular pathways operating in aging, post-mitotic states and quiescence.

MATERIALS AND METHODS

Media, deletions, GFP tagging and imaging

All YPD experiments were performed in Yeast extract (1%), Peptone (2%) and Glucose (2%) purchased from Difco. SD was made by mixing 1x YNB (Difco), Drop-out aminoacid mix and essential nutrients (Sigma), supplementing dropped-out amino acids from lab stocks (Sigma) using protocols and recipes from Yeast protocols in Genetics (Cold Spring Harbor press). Manual follow-ups of the chip screen were done by growing in SD for 48 hrs and imaging without fixation. All deletions were obtained from the Invitrogen BY4741 haploid deletion library and grown in G418 antibiotic to pick single colonies before any manipulation. All tagged strains generated for imaging in deletion backgrounds were done following standard PCR tagging strategies using a C-terminal GFP tagging plasmid kindly provided by Arlen Jonhson, Makunni Jayaram and Zhihua Li. Tagged strains were verified by colony PCR after growth in selection media. All imaging protocols were identical to those followed in earlier work.

Biochemical fractionation, sample preparation and mass spectrometry

Biochemical fractionation for isolation of Gln1-GFP punctates were done by glass bead lysis of cultures grown to 48 hrs in YPD. Cultures were spun down, washed in lysis buffer (50mM Tris pH 7.6, 150 mM KCl, 1mM β -mercaptoethanol and 1x Roche EDTA free protease inhibitor cocktail) and lysed after adding glass beads in a bead beater for 5x 1 minute cycles with 2 minute pauses on ice. Clarification was done by spinning at 13,000 x g in a microcentrifuge.

For mass spectrometry, samples (roughly equal cells) were separated into the pellet and supernatant fraction after clarification (and washing the pellet in lysis buffer). No detergents were added. All the samples (four samples- pellet and supernatant fractions from stationary and recovered phases) were treated with the acid-labile rapigest (Waters Inc) following company protocols to facilitate mild denaturation . Roughly equal protein was then subject to trypsin digestion overnight at 37 C with trypsin concentration being 10-fold higher to protein concentration. Peptides were modified by iodoacetamide to block free sulfhydryl groups and purified on a gel filtration column before performing a 2D LC-MS/MS experiment on a LTQ Orbitrap mass spectrometer.

REFERENCES

1. Werner-Washburne, M., et al., *Stationary phase in the yeast Saccharomyces cerevisiae*. Microbiol Rev, 1993. **57**(2): p. 383-401.
2. Gray, J.V., et al., "*Sleeping beauty*": *quiescence in Saccharomyces cerevisiae*. Microbiol Mol Biol Rev, 2004. **68**(2): p. 187-206.
3. Allen, C., et al., *Isolation of quiescent and nonquiescent cells from yeast stationary-phase cultures*. J Cell Biol, 2006. **174**(1): p. 89-100.
4. Pinon, R., *Folded chromosomes in non-cycling yeast cells: evidence for a characteristic g0 form*. Chromosoma, 1978. **67**(3): p. 263-74.
5. Choder, M., *A general topoisomerase I-dependent transcriptional repression in the stationary phase in yeast*. Genes Dev, 1991. **5**(12A): p. 2315-26.

6. Fuge, E.K., E.L. Braun, and M. Werner-Washburne, *Protein synthesis in long-term stationary-phase cultures of Saccharomyces cerevisiae*. J Bacteriol, 1994. **176**(18): p. 5802-13.
7. Ashrafi, K., et al., *Passage through stationary phase advances replicative aging in Saccharomyces cerevisiae*. Proc Natl Acad Sci U S A, 1999. **96**(16): p. 9100-5.
8. Martinez, M.J., et al., *Genomic analysis of stationary-phase and exit in Saccharomyces cerevisiae: gene expression and identification of novel essential genes*. Mol Biol Cell, 2004. **15**(12): p. 5295-305.
9. Broach, J.R., *RAS genes in Saccharomyces cerevisiae: signal transduction in search of a pathway*. Trends Genet, 1991. **7**(1): p. 28-33.
10. Schmelzle, T. and M.N. Hall, *TOR, a central controller of cell growth*. Cell, 2000. **103**(2): p. 253-62.
11. Raught, B., A.C. Gingras, and N. Sonenberg, *The target of rapamycin (TOR) proteins*. Proc Natl Acad Sci U S A, 2001. **98**(13): p. 7037-44.
12. Reinders, A., et al., *Saccharomyces cerevisiae cAMP-dependent protein kinase controls entry into stationary phase through the Rim15p protein kinase*. Genes Dev, 1998. **12**(18): p. 2943-55.
13. Patturajan, M., et al., *Growth-related changes in phosphorylation of yeast RNA polymerase II*. J Biol Chem, 1998. **273**(8): p. 4689-94.
14. Krause, S.A. and J.V. Gray, *The protein kinase C pathway is required for viability in quiescence in Saccharomyces cerevisiae*. Curr Biol, 2002. **12**(7): p. 588-93.
15. Torres, J., et al., *Regulation of the cell integrity pathway by rapamycin-sensitive TOR function in budding yeast*. J Biol Chem, 2002. **277**(45): p. 43495-504.
16. Kamada, Y., et al., *Tor-mediated induction of autophagy via an Apg1 protein kinase complex*. J Cell Biol, 2000. **150**(6): p. 1507-13.
17. Klionsky, D.J. and Y. Ohsumi, *Vacuolar import of proteins and organelles from the cytoplasm*. Annu Rev Cell Dev Biol, 1999. **15**: p. 1-32.
18. Paz, I., L. Abramovitz, and M. Choder, *Starved Saccharomyces cerevisiae cells have the capacity to support internal initiation of translation*. J Biol Chem, 1999. **274**(31): p. 21741-5.
19. Paz, I. and M. Choder, *Eukaryotic translation initiation factor 4E-dependent translation is not essential for survival of starved yeast cells*. J Bacteriol, 2001. **183**(15): p. 4477-83.
20. Longo, V.D., E.B. Gralla, and J.S. Valentine, *Superoxide dismutase activity is essential for stationary phase survival in Saccharomyces cerevisiae. Mitochondrial production of toxic oxygen species in vivo*. J Biol Chem, 1996. **271**(21): p. 12275-80.
21. Sethuraman, A., N.N. Rao, and A. Kornberg, *The endopolyphosphatase gene: essential in Saccharomyces cerevisiae*. Proc Natl Acad Sci U S A, 2001. **98**(15): p. 8542-7.
22. Sobering, A.K., et al., *Yeast Rpi1 is a putative transcriptional regulator that contributes to preparation for stationary phase*. Eukaryot Cell, 2002. **1**(1): p. 56-65.
23. Gasch, A.P., et al., *Genomic expression programs in the response of yeast cells to environmental changes*. Mol Biol Cell, 2000. **11**(12): p. 4241-57.

24. Radonjic, M., et al., *Genome-wide analyses reveal RNA polymerase II located upstream of genes poised for rapid response upon S. cerevisiae stationary phase exit*. Mol Cell, 2005. **18**(2): p. 171-83.
25. Brengues, M., D. Teixeira, and R. Parker, *Movement of eukaryotic mRNAs between polysomes and cytoplasmic processing bodies*. Science, 2005. **310**(5747): p. 486-9.
26. Sinclair, D., K. Mills, and L. Guarente, *Aging in Saccharomyces cerevisiae*. Annu Rev Microbiol, 1998. **52**: p. 533-60.
27. Tissenbaum, H.A. and L. Guarente, *Model organisms as a guide to mammalian aging*. Dev Cell, 2002. **2**(1): p. 9-19.
28. Longo, V.D., *Mutations in signal transduction proteins increase stress resistance and longevity in yeast, nematodes, fruit flies, and mammalian neuronal cells*. Neurobiol Aging, 1999. **20**(5): p. 479-86.
29. Fabrizio, P. and V.D. Longo, *The chronological life span of Saccharomyces cerevisiae*. Methods Mol Biol, 2007. **371**: p. 89-95.
30. Fabrizio, P., et al., *Regulation of longevity and stress resistance by Sch9 in yeast*. Science, 2001. **292**(5515): p. 288-90.
31. Kaerberlein, M., C.R. Burtner, and B.K. Kennedy, *Recent developments in yeast aging*. PLoS Genet, 2007. **3**(5): p. e84.
32. Chen, Q., Q. Ding, and J.N. Keller, *The stationary phase model of aging in yeast for the study of oxidative stress and age-related neurodegeneration*. Biogerontology, 2005. **6**(1): p. 1-13.
33. Chen, Q., J. Thorpe, and J.N. Keller, *Alpha-synuclein alters proteasome function, protein synthesis, and stationary phase viability*. J Biol Chem, 2005. **280**(34): p. 30009-17.
34. Vernace, V.A., T. Schmidt-Glenewinkel, and M.E. Figueiredo-Pereira, *Aging and regulated protein degradation: who has the UPPer hand?* Aging Cell, 2007. **6**(5): p. 599-606.
35. Aguilaniu, H., et al., *Asymmetric inheritance of oxidatively damaged proteins during cytokinesis*. Science, 2003. **299**(5613): p. 1751-3.
36. Erjavec, N., et al., *Accelerated aging and failure to segregate damaged proteins in Sir2 mutants can be suppressed by overproducing the protein aggregation-remodeling factor Hsp104p*. Genes Dev, 2007. **21**(19): p. 2410-21.
37. Gourlay, C.W., et al., *A role for the actin cytoskeleton in cell death and aging in yeast*. J Cell Biol, 2004. **164**(6): p. 803-9.
38. Narayanaswamy, R., et al., *Systematic profiling of cellular phenotypes with spotted cell microarrays reveals mating-pheromone response genes*. Genome Biol, 2006. **7**(1): p. R6.
39. Huh, W.K., et al., *Global analysis of protein localization in budding yeast*. Nature, 2003. **425**(6959): p. 686-91.
40. Robinson, M.D., et al., *FunSpec: a web-based cluster interpreter for yeast*. BMC Bioinformatics, 2002. **3**: p. 35.
41. Lu, P., et al., *Absolute protein expression profiling estimates the relative contributions of transcriptional and translational regulation*. Nat Biotechnol, 2007. **25**(1): p. 117-24.

42. Sagot, I., et al., *Actin bodies in yeast quiescent cells: an immediately available actin reserve?* Mol Biol Cell, 2006. **17**(11): p. 4645-55.
43. Wang, L., et al., *Inorganic polyphosphate stimulates mammalian TOR, a kinase involved in the proliferation of mammary cancer cells.* Proc Natl Acad Sci U S A, 2003. **100**(20): p. 11249-54.

References

1. Aguilaniu, H., et al., Asymmetric inheritance of oxidatively damaged proteins during cytokinesis. *Science*, 2003. **299**(5613): p. 1751-3.
2. Allen, C., et al., Isolation of quiescent and nonquiescent cells from yeast stationary-phase cultures. *J Cell Biol*, 2006. **174**(1): p. 89-100.
3. Alter, O., Genomic signal processing: from matrix algebra to genetic networks. *Methods Mol Biol*, 2007. **377**: p. 17-60.
4. Aragon, A.D., et al., Release of extraction-resistant mRNA in stationary phase *Saccharomyces cerevisiae* produces a massive increase in transcript abundance in response to stress. *Genome Biol*, 2006. **7**(2): p. R9.
5. Ashrafi, K., et al., Passage through stationary phase advances replicative aging in *Saccharomyces cerevisiae*. *Proc Natl Acad Sci U S A*, 1999. **96**(16): p. 9100-5.
6. Baba, M., et al., Three-dimensional analysis of morphogenesis induced by mating pheromone alpha factor in *Saccharomyces cerevisiae*. *J Cell Sci*, 1989. **94** (Pt 2): p. 207-16.
7. Babst, M., et al., Escrt-III: an endosome-associated heterooligomeric protein complex required for mvb sorting. *Dev Cell*, 2002. **3**(2): p. 271-82.
8. Babst, M., et al., Endosome-associated complex, ESCRT-II, recruits transport machinery for protein sorting at the multivesicular body. *Dev Cell*, 2002. **3**(2): p. 283-9.
9. Bader, G.D., et al., Functional genomics and proteomics: charting a multidimensional map of the yeast cell. *Trends Cell Biol*, 2003. **13**(7): p. 344-56.
10. Bagnat, M. and K. Simons, Cell surface polarization during yeast mating. *Proc Natl Acad Sci U S A*, 2002. **99**(22): p. 14183-8.

11. Bagnat, M. and K. Simons, Lipid rafts in protein sorting and cell polarity in budding yeast *Saccharomyces cerevisiae*. *Biol Chem*, 2002. **383**(10): p. 1475-80.
12. Bailey, S.N., R.Z. Wu, and D.M. Sabatini, Applications of transfected cell microarrays in high-throughput drug discovery. *Drug Discov Today*, 2002. **7**(18 Suppl): p. S113-8.
13. Bakal, C., et al., Quantitative morphological signatures define local signaling networks regulating cell morphology. *Science*, 2007. **316**(5832): p. 1753-6.
14. Bergeron, J.J. and M. Hallett, Peptides you can count on. *Nat Biotechnol*, 2007. **25**(1): p. 61-2.
15. Bidlingmaier, S. and M. Snyder, Large-scale identification of genes important for apical growth in *Saccharomyces cerevisiae* by directed allele replacement technology (DART) screening. *Funct Integr Genomics*, 2002. **1**(6): p. 345-56.
16. Biran, I., et al., Optical imaging fiber-based live bacterial cell array biosensor. *Anal Biochem*, 2003. **315**(1): p. 106-13.
17. Birney, E., et al., Identification and analysis of functional elements in 1% of the human genome by the ENCODE pilot project. *Nature*, 2007. **447**(7146): p. 799-816.
18. Bitterman, K.J., O. Medvedik, and D.A. Sinclair, Longevity regulation in *Saccharomyces cerevisiae*: linking metabolism, genome stability, and heterochromatin. *Microbiol Mol Biol Rev*, 2003. **67**(3): p. 376-99, table of contents.
19. Bochner, B.R., New technologies to assess genotype-phenotype relationships. *Nat Rev Genet*, 2003. **4**(4): p. 309-14.
20. Bochner, B.R., P. Gadzinski, and E. Panomitros, Phenotype microarrays for high-throughput phenotypic testing and assay of gene function. *Genome Res*, 2001. **11**(7): p. 1246-55.

21. Boyd, C., et al., Vesicles carry most exocyst subunits to exocytic sites marked by the remaining two subunits, Sec3p and Exo70p. *J Cell Biol*, 2004. **167**(5): p. 889-901.
22. Brengues, M., D. Teixeira, and R. Parker, Movement of eukaryotic mRNAs between polysomes and cytoplasmic processing bodies. *Science*, 2005. **310**(5747): p. 486-9.
23. Buttery, S.M., S. Yoshida, and D. Pellman, Yeast formins Bni1 and Bnr1 utilize different modes of cortical interaction during the assembly of actin cables. *Mol Biol Cell*, 2007. **18**(5): p. 1826-38.
24. Cagney, G., P. Uetz, and S. Fields, High-throughput screening for protein-protein interactions using two-hybrid assay. *Methods Enzymol*, 2000. **328**: p. 3-14.
25. Caviston, J.P., et al., The role of Cdc42p GTPase-activating proteins in assembly of the septin ring in yeast. *Mol Biol Cell*, 2003. **14**(10): p. 4051-66.
26. Chen, Q., Q. Ding, and J.N. Keller, The stationary phase model of aging in yeast for the study of oxidative stress and age-related neurodegeneration. *Biogerontology*, 2005. **6**(1): p. 1-13.
27. Chen, Q., et al., Proteasome synthesis and assembly are required for survival during stationary phase. *Free Radic Biol Med*, 2004. **37**(6): p. 859-68.
28. Chen, S.C., et al., Automated image analysis of protein localization in budding yeast. *Bioinformatics*, 2007. **23**(13): p. i66-71.
29. Chughtai, Z.S., et al., Starvation promotes nuclear accumulation of the hsp70 Ssa4p in yeast cells. *J Biol Chem*, 2001. **276**(23): p. 20261-6.
30. Cipollina, C., et al., Revisiting the role of yeast Sfp1 in ribosome biogenesis and cell size control: a chemostat study. *Microbiology*, 2008. **154**(Pt 1): p. 337-46.
31. Clayton, T.A., et al., Pharmaco-metabonomic phenotyping and personalized drug treatment. *Nature*, 2006. **440**(7087): p. 1073-7.

32. Collins, F.S., et al., A vision for the future of genomics research. *Nature*, 2003. **422**(6934): p. 835-47.
33. Colman-Lerner, A., et al., Regulated cell-to-cell variation in a cell-fate decision system. *Nature*, 2005. **437**(7059): p. 699-706.
34. Conrad, C., et al., Automatic identification of subcellular phenotypes on human cell arrays. *Genome Res*, 2004. **14**(6): p. 1130-6.
35. Cook, M. and M. Tyers, Size control goes global. *Curr Opin Biotechnol*, 2007. **18**(4): p. 341-50.
36. Dalma-Weiszhausz, D.D., et al., The affymetrix GeneChip platform: an overview. *Methods Enzymol*, 2006. **410**: p. 3-28.
37. Date, S.V. and E.M. Marcotte, Protein function prediction using the Protein Link EXplorer (PLEX). *Bioinformatics*, 2005. **21**(10): p. 2558-9.
38. Dennis, P.B., et al., Mammalian TOR: a homeostatic ATP sensor. *Science*, 2001. **294**(5544): p. 1102-5.
39. DeRisi, J.L. and V.R. Iyer, Genomics and array technology. *Curr Opin Oncol*, 1999. **11**(1): p. 76-9.
40. Dewar, H., et al., Novel proteins linking the actin cytoskeleton to the endocytic machinery in *Saccharomyces cerevisiae*. *Mol Biol Cell*, 2002. **13**(10): p. 3646-61.
41. Dohlman, H.G., G proteins and pheromone signaling. *Annu Rev Physiol*, 2002. **64**: p. 129-52.
42. Dohlman, H.G. and J.E. Slessareva, Pheromone signaling pathways in yeast. *Sci STKE*, 2006. **2006**(364): p. cm6.
43. Dohlman, H.G. and J.W. Thorner, Regulation of G protein-initiated signal transduction in yeast: paradigms and principles. *Annu Rev Biochem*, 2001. **70**: p. 703-54.

44. Domon, B. and R. Aebersold, Mass spectrometry and protein analysis. *Science*, 2006. **312**(5771): p. 212-7.
45. Drawid, A. and M. Gerstein, A Bayesian system integrating expression data with sequence patterns for localizing proteins: comprehensive application to the yeast genome. *J Mol Biol*, 2000. **301**(4): p. 1059-75.
46. Dwight, S.S., et al., Saccharomyces Genome Database (SGD) provides secondary gene annotation using the Gene Ontology (GO). *Nucleic Acids Res*, 2002. **30**(1): p. 69-72.
47. Echeverri, C.J., et al., Minimizing the risk of reporting false positives in large-scale RNAi screens. *Nat Methods*, 2006. **3**(10): p. 777-9.
48. Elion, E.A., Pheromone response, mating and cell biology. *Curr Opin Microbiol*, 2000. **3**(6): p. 573-81.
49. Erdman, S., et al., Pheromone-regulated genes required for yeast mating differentiation. *J Cell Biol*, 1998. **140**(3): p. 461-83.
50. Erjavec, N., et al., Accelerated aging and failure to segregate damaged proteins in Sir2 mutants can be suppressed by overproducing the protein aggregation-remodeling factor Hsp104p. *Genes Dev*, 2007. **21**(19): p. 2410-21.
51. Fabrizio, P., L. Li, and V.D. Longo, Analysis of gene expression profile in yeast aging chronologically. *Mech Ageing Dev*, 2005. **126**(1): p. 11-6.
52. Fabrizio, P. and V.D. Longo, The chronological life span of *Saccharomyces cerevisiae*. *Methods Mol Biol*, 2007. **371**: p. 89-95.
53. Fagarasanu, M., A. Fagarasanu, and R.A. Rachubinski, Sharing the wealth: peroxisome inheritance in budding yeast. *Biochim Biophys Acta*, 2006. **1763**(12): p. 1669-77.

54. Fernandez-Ricaud, L., et al., PROPHECY--a yeast phenome database, update 2006. *Nucleic Acids Res*, 2007. **35**(Database issue): p. D463-7.
55. Fleischer, T.C., et al., Systematic identification and functional screens of uncharacterized proteins associated with eukaryotic ribosomal complexes. *Genes Dev*, 2006. **20**(10): p. 1294-307.
56. Fraser, A.G. and E.M. Marcotte, A probabilistic view of gene function. *Nat Genet*, 2004. **36**(6): p. 559-64.
57. Fraser, A.G. and E.M. Marcotte, Development through the eyes of functional genomics. *Curr Opin Genet Dev*, 2004. **14**(4): p. 336-42.
58. Frayling, T.M., Genome-wide association studies provide new insights into type 2 diabetes aetiology. *Nat Rev Genet*, 2007. **8**(9): p. 657-62.
59. Fuge, E.K., E.L. Braun, and M. Werner-Washburne, Protein synthesis in long-term stationary-phase cultures of *Saccharomyces cerevisiae*. *J Bacteriol*, 1994. **176**(18): p. 5802-13.
60. Gasch, A.P. and M. Werner-Washburne, The genomics of yeast responses to environmental stress and starvation. *Funct Integr Genomics*, 2002. **2**(4-5): p. 181-92.
61. Gavin, A.C., et al., Proteome survey reveals modularity of the yeast cell machinery. *Nature*, 2006. **440**(7084): p. 631-6.
62. Gavin, A.C., et al., Functional organization of the yeast proteome by systematic analysis of protein complexes. *Nature*, 2002. **415**(6868): p. 141-7.
63. Gaziova, I. and K.M. Bhat, Generating asymmetry: with and without self-renewal. *Prog Mol Subcell Biol*, 2007. **45**: p. 143-78.
64. Gerstein, M., Tools needed to navigate landscape of the genome. *Nature*, 2006. **440**(7085): p. 740.

65. Ghaemmaghami, S., et al., Global analysis of protein expression in yeast. *Nature*, 2003. **425**(6959): p. 737-41.
66. Giaever, G., et al., Functional profiling of the *Saccharomyces cerevisiae* genome. *Nature*, 2002. **418**(6896): p. 387-91.
67. Giaever, G., et al., Chemogenomic profiling: identifying the functional interactions of small molecules in yeast. *Proc Natl Acad Sci U S A*, 2004. **101**(3): p. 793-8.
68. Gourlay, C.W., et al., A role for the actin cytoskeleton in cell death and aging in yeast. *J Cell Biol*, 2004. **164**(6): p. 803-9.
69. Gray, J.V., et al., "Sleeping beauty": quiescence in *Saccharomyces cerevisiae*. *Microbiol Mol Biol Rev*, 2004. **68**(2): p. 187-206.
70. Grote, E., C.M. Carr, and P.J. Novick, Ordering the final events in yeast exocytosis. *J Cell Biol*, 2000. **151**(2): p. 439-52.
71. Harder, N., R. Eils, and K. Rohr, Automated classification of mitotic phenotypes of human cells using fluorescent proteins. *Methods Cell Biol*, 2008. **85**: p. 539-54.
72. He, B., et al., Exo70 interacts with phospholipids and mediates the targeting of the exocyst to the plasma membrane. *Embo J*, 2007. **26**(18): p. 4053-65.
73. Herman, P.K., Stationary phase in yeast. *Curr Opin Microbiol*, 2002. **5**(6): p. 602-7.
74. Hoffmann, C., et al., A FIAsh-based FRET approach to determine G protein-coupled receptor activation in living cells. *Nat Methods*, 2005. **2**(3): p. 171-6.
75. Howitz, K.T., et al., Small molecule activators of sirtuins extend *Saccharomyces cerevisiae* lifespan. *Nature*, 2003. **425**(6954): p. 191-6.
76. Hu, Z., et al., Towards zoomable multidimensional maps of the cell. *Nat Biotechnol*, 2007. **25**(5): p. 547-54.

77. Hu, Z., et al., VisANT 3.0: new modules for pathway visualization, editing, prediction and construction. *Nucleic Acids Res*, 2007. **35**(Web Server issue): p. W625-32.
78. Huckaba, T.M., et al., Live cell imaging of the assembly, disassembly, and actin cable-dependent movement of endosomes and actin patches in the budding yeast, *Saccharomyces cerevisiae*. *J Cell Biol*, 2004. **167**(3): p. 519-30.
79. Hughes, T.R., et al., Functional discovery via a compendium of expression profiles. *Cell*, 2000. **102**(1): p. 109-26.
80. Hughes, T.R., et al., The promise of functional genomics: completing the encyclopedia of a cell. *Curr Opin Microbiol*, 2004. **7**(5): p. 546-54.
81. Huh, W.K., et al., Global analysis of protein localization in budding yeast. *Nature*, 2003. **425**(6959): p. 686-91.
82. Ideker, T., T. Galitski, and L. Hood, A new approach to decoding life: systems biology. *Annu Rev Genomics Hum Genet*, 2001. **2**: p. 343-72.
83. Iwase, M., et al., Role of a Cdc42p effector pathway in recruitment of the yeast septins to the presumptive bud site. *Mol Biol Cell*, 2006. **17**(3): p. 1110-25.
84. Jansen, R. and M. Gerstein, Analyzing protein function on a genomic scale: the importance of gold-standard positives and negatives for network prediction. *Curr Opin Microbiol*, 2004. **7**(5): p. 535-45.
85. Jansen, R., et al., A Bayesian networks approach for predicting protein-protein interactions from genomic data. *Science*, 2003. **302**(5644): p. 449-53.
86. Jarvik, J.W., et al., In vivo functional proteomics: mammalian genome annotation using CD-tagging. *Biotechniques*, 2002. **33**(4): p. 852-4, 856, 858-60 passim.
87. Jiang, T. and A.E. Keating, AVID: an integrative framework for discovering functional relationships among proteins. *BMC Bioinformatics*, 2005. **6**: p. 136.

88. Jorgensen, P., et al., The size of the nucleus increases as yeast cells grow. *Mol Biol Cell*, 2007. **18**(9): p. 3523-32.
89. Kaerberlein, M., C.R. Burtner, and B.K. Kennedy, Recent developments in yeast aging. *PLoS Genet*, 2007. **3**(5): p. e84.
90. Kolkman, A., et al., Proteome analysis of yeast response to various nutrient limitations. *Mol Syst Biol*, 2006. **2**: p. 2006 0026.
91. Kononen, J., et al., Tissue microarrays for high-throughput molecular profiling of tumor specimens. *Nat Med*, 1998. **4**(7): p. 844-7.
92. Krogan, N.J., et al., Global landscape of protein complexes in the yeast *Saccharomyces cerevisiae*. *Nature*, 2006. **440**(7084): p. 637-43.
93. Kumar, A., et al., Subcellular localization of the yeast proteome. *Genes Dev*, 2002. **16**(6): p. 707-19.
94. Lamprecht, M.R., D.M. Sabatini, and A.E. Carpenter, CellProfiler: free, versatile software for automated biological image analysis. *Biotechniques*, 2007. **42**(1): p. 71-5.
95. Lee, I., et al., A probabilistic functional network of yeast genes. *Science*, 2004. **306**(5701): p. 1555-8.
96. Lee, I., Z. Li, and E.M. Marcotte, An Improved, Bias-Reduced Probabilistic Functional Gene Network of Baker's Yeast, *Saccharomyces cerevisiae*. *PLoS ONE*, 2007. **2**(10): p. e988.
97. Lehner, B., et al., Systematic mapping of genetic interactions in *Caenorhabditis elegans* identifies common modifiers of diverse signaling pathways. *Nat Genet*, 2006. **38**(8): p. 896-903.
98. Lockhart, D.J. and E.A. Winzeler, Genomics, gene expression and DNA arrays. *Nature*, 2000. **405**(6788): p. 827-36.

99. Longo, V.D. and P. Fabrizio, Regulation of longevity and stress resistance: a molecular strategy conserved from yeast to humans? *Cell Mol Life Sci*, 2002. **59**(6): p. 903-8.
100. Longtine, M.S. and E. Bi, Regulation of septin organization and function in yeast. *Trends Cell Biol*, 2003. **13**(8): p. 403-9.
101. Lu, P., et al., Absolute protein expression profiling estimates the relative contributions of transcriptional and translational regulation. *Nat Biotechnol*, 2007. **25**(1): p. 117-24.
102. Madden, K. and M. Snyder, Cell polarity and morphogenesis in budding yeast. *Annu Rev Microbiol*, 1998. **52**: p. 687-744.
103. Mann, M., et al., Analysis of protein phosphorylation using mass spectrometry: deciphering the phosphoproteome. *Trends Biotechnol*, 2002. **20**(6): p. 261-8.
104. Martin, A., S. Schneider, and B. Schwer, Prp43 is an essential RNA-dependent ATPase required for release of lariat-intron from the spliceosome. *J Biol Chem*, 2002. **277**(20): p. 17743-50.
105. Martinez, M.J., et al., Genomic analysis of stationary-phase and exit in *Saccharomyces cerevisiae*: gene expression and identification of novel essential genes. *Mol Biol Cell*, 2004. **15**(12): p. 5295-305.
106. Matheos, D., et al., Pheromone-induced polarization is dependent on the Fus3p MAPK acting through the formin Bni1p. *J Cell Biol*, 2004. **165**(1): p. 99-109.
107. McGary, K.L., I. Lee, and E.M. Marcotte, Broad network-based predictability of *S. cerevisiae* gene loss-of-function phenotypes. *Genome Biol*, 2007. **8**(12): p. R258.
108. Mewes, H.W., et al., MIPS: analysis and annotation of proteins from whole genomes. *Nucleic Acids Res*, 2004. **32**(Database issue): p. D41-4.

109. Mosch, H.U. and G.R. Fink, Dissection of filamentous growth by transposon mutagenesis in *Saccharomyces cerevisiae*. *Genetics*, 1997. **145**(3): p. 671-84.
110. Munson, M. and P. Novick, The exocyst defrocked, a framework of rods revealed. *Nat Struct Mol Biol*, 2006. **13**(7): p. 577-81.
111. Narayanaswamy, R., et al., Systematic profiling of cellular phenotypes with spotted cell microarrays reveals mating-pheromone response genes. *Genome Biol*, 2006. **7**(1): p. R6.
112. Nern, A. and R.A. Arkowitz, Nucleocytoplasmic shuttling of the Cdc42p exchange factor Cdc24p. *J Cell Biol*, 2000. **148**(6): p. 1115-22.
113. Nishizuka, S., et al., Diagnostic markers that distinguish colon and ovarian adenocarcinomas: identification by genomic, proteomic, and tissue array profiling. *Cancer Res*, 2003. **63**(17): p. 5243-50.
114. Nuwaysir, E.F., et al., Gene expression analysis using oligonucleotide arrays produced by maskless photolithography. *Genome Res*, 2002. **12**(11): p. 1749-55.
115. Ohya, Y., et al., High-dimensional and large-scale phenotyping of yeast mutants. *Proc Natl Acad Sci U S A*, 2005. **102**(52): p. 19015-20.
116. Pandey, A., J.S. Andersen, and M. Mann, Use of mass spectrometry to study signaling pathways. *Sci STKE*, 2000. **2000**(37): p. PL1.
117. Parker, R. and U. Sheth, P bodies and the control of mRNA translation and degradation. *Mol Cell*, 2007. **25**(5): p. 635-46.
118. Perlman, Z.E., et al., Multidimensional drug profiling by automated microscopy. *Science*, 2004. **306**(5699): p. 1194-8.
119. Pinon, R., Folded chromosomes in non-cycling yeast cells: evidence for a characteristic g0 form. *Chromosoma*, 1978. **67**(3): p. 263-74.

120. Poetz, O., et al., Protein microarrays for antibody profiling: specificity and affinity determination on a chip. *Proteomics*, 2005. **5**(9): p. 2402-11.
121. Poetz, O., et al., Protein microarrays: catching the proteome. *Mech Ageing Dev*, 2005. **126**(1): p. 161-70.
122. Porter, D., J. Yao, and K. Polyak, SAGE and related approaches for cancer target identification. *Drug Discov Today*, 2006. **11**(3-4): p. 110-8.
123. Prinz, S., et al., Control of Signaling in a MAP-kinase Pathway by an RNA-Binding Protein. *PLoS ONE*, 2007. **2**: p. e249.
124. Proszynski, T.J., et al., Plasma membrane polarization during mating in yeast cells. *J Cell Biol*, 2006. **173**(6): p. 861-6.
125. Pruyne, D. and A. Bretscher, Polarization of cell growth in yeast. I. Establishment and maintenance of polarity states. *J Cell Sci*, 2000. **113** (Pt 3): p. 365-75.
126. Pruyne, D. and A. Bretscher, Polarization of cell growth in yeast. *J Cell Sci*, 2000. **113** (Pt 4): p. 571-85.
127. Pruyne, D., et al., Mechanisms of polarized growth and organelle segregation in yeast. *Annu Rev Cell Dev Biol*, 2004. **20**: p. 559-91.
128. Radonjic, M., et al., Genome-wide analyses reveal RNA polymerase II located upstream of genes poised for rapid response upon *S. cerevisiae* stationary phase exit. *Mol Cell*, 2005. **18**(2): p. 171-83.
129. Raught, B., A.C. Gingras, and N. Sonenberg, The target of rapamycin (TOR) proteins. *Proc Natl Acad Sci U S A*, 2001. **98**(13): p. 7037-44.
130. Reinders, A., et al., *Saccharomyces cerevisiae* cAMP-dependent protein kinase controls entry into stationary phase through the Rim15p protein kinase. *Genes Dev*, 1998. **12**(18): p. 2943-55.

131. Robinson, M.D., et al., FunSpec: a web-based cluster interpreter for yeast. *BMC Bioinformatics*, 2002. **3**: p. 35.
132. Saghatelian, A. and B.F. Cravatt, Global strategies to integrate the proteome and metabolome. *Curr Opin Chem Biol*, 2005. **9**(1): p. 62-8.
133. Sagot, I., S.K. Klee, and D. Pellman, Yeast formins regulate cell polarity by controlling the assembly of actin cables. *Nat Cell Biol*, 2002. **4**(1): p. 42-50.
134. Sagot, I., et al., Actin bodies in yeast quiescent cells: an immediately available actin reserve? *Mol Biol Cell*, 2006. **17**(11): p. 4645-55.
135. Saito, T.L., et al., SCMD: *Saccharomyces cerevisiae* Morphological Database. *Nucleic Acids Res*, 2004. **32**(Database issue): p. D319-22.
136. Saito, T.L., et al., Data mining tools for the *Saccharomyces cerevisiae* morphological database. *Nucleic Acids Res*, 2005. **33**(Web Server issue): p. W753-7.
137. Schneider, B.L., et al., Growth rate and cell size modulate the synthesis of, and requirement for, G1-phase cyclins at start. *Mol Cell Biol*, 2004. **24**(24): p. 10802-13.
138. Schwenk, J.M., et al., Cell microarrays: an emerging technology for the characterization of antibodies. *Biotechniques*, 2002. **Suppl**: p. 54-61.
139. Sheth, U. and R. Parker, Targeting of aberrant mRNAs to cytoplasmic processing bodies. *Cell*, 2006. **125**(6): p. 1095-109.
140. Silva, J., et al., RNA-interference-based functional genomics in mammalian cells: reverse genetics coming of age. *Oncogene*, 2004. **23**(51): p. 8401-9.
141. Sinclair, D., K. Mills, and L. Guarente, Aging in *Saccharomyces cerevisiae*. *Annu Rev Microbiol*, 1998. **52**: p. 533-60.
142. Sinclair, D.A., Cell biology. An age of instability. *Science*, 2003. **301**(5641): p. 1859-60.

143. Sinclair, D.A. and L. Guarente, Extrachromosomal rDNA circles--a cause of aging in yeast. *Cell*, 1997. **91**(7): p. 1033-42.
144. Singer, R.H., RNA localization: visualization in real-time. *Curr Biol*, 2003. **13**(17): p. R673-5.
145. Smith, L.T., G.A. Otterson, and C. Plass, Unraveling the epigenetic code of cancer for therapy. *Trends Genet*, 2007. **23**(9): p. 449-56.
146. Smythe, E. and K.R. Ayscough, The Ark1/Prk1 family of protein kinases. Regulators of endocytosis and the actin skeleton. *EMBO Rep*, 2003. **4**(3): p. 246-51.
147. Smythe, E. and K.R. Ayscough, Actin regulation in endocytosis. *J Cell Sci*, 2006. **119**(Pt 22): p. 4589-98.
148. Takizawa, P.A., et al., Actin-dependent localization of an RNA encoding a cell-fate determinant in yeast. *Nature*, 1997. **389**(6646): p. 90-3.
149. Templin, M.F., et al., Protein microarrays: promising tools for proteomic research. *Proteomics*, 2003. **3**(11): p. 2155-66.
150. Tissenbaum, H.A. and L. Guarente, Model organisms as a guide to mammalian aging. *Dev Cell*, 2002. **2**(1): p. 9-19.
151. Tong, A.H. and C. Boone, Synthetic genetic array analysis in *Saccharomyces cerevisiae*. *Methods Mol Biol*, 2006. **313**: p. 171-92.
152. Tong, A.H., et al., Global mapping of the yeast genetic interaction network. *Science*, 2004. **303**(5659): p. 808-13.
153. Valdez-Taubas, J. and H.R. Pelham, Slow diffusion of proteins in the yeast plasma membrane allows polarity to be maintained by endocytic cycling. *Curr Biol*, 2003. **13**(18): p. 1636-40.
154. Veenstra, T.D., et al., Biomarkers: mining the biofluid proteome. *Mol Cell Proteomics*, 2005. **4**(4): p. 409-18.

155. Verhoeckx, K.C., et al., A combination of proteomics, principal component analysis and transcriptomics is a powerful tool for the identification of biomarkers for macrophage maturation in the U937 cell line. *Proteomics*, 2004. **4**(4): p. 1014-28.
156. Vernace, V.A., T. Schmidt-Glenewinkel, and M.E. Figueiredo-Pereira, Aging and regulated protein degradation: who has the UPPER hand? *Aging Cell*, 2007. **6**(5): p. 599-606.
157. von Mering, C., et al., STRING: known and predicted protein-protein associations, integrated and transferred across organisms. *Nucleic Acids Res*, 2005. **33**(Database issue): p. D433-7.
158. Walther, T.C., et al., Eisosomes mark static sites of endocytosis. *Nature*, 2006. **439**(7079): p. 998-1003.
159. Wang, L., et al., Inorganic polyphosphate stimulates mammalian TOR, a kinase involved in the proliferation of mammary cancer cells. *Proc Natl Acad Sci U S A*, 2003. **100**(20): p. 11249-54.
160. Want, E.J., B.F. Cravatt, and G. Siuzdak, The expanding role of mass spectrometry in metabolite profiling and characterization. *Chembiochem*, 2005. **6**(11): p. 1941-51.
161. Warren, D.T., et al., Sla1p couples the yeast endocytic machinery to proteins regulating actin dynamics. *J Cell Sci*, 2002. **115**(Pt 8): p. 1703-15.
162. Warringer, J., et al., High-resolution yeast phenomics resolves different physiological features in the saline response. *Proc Natl Acad Sci U S A*, 2003. **100**(26): p. 15724-9.
163. Wedlich-Soldner, R., et al., Spontaneous cell polarization through actomyosin-based delivery of the Cdc42 GTPase. *Science*, 2003. **299**(5610): p. 1231-5.

164. Werner-Washburne, M., et al., Stationary phase in the yeast *Saccharomyces cerevisiae*. *Microbiol Rev*, 1993. **57**(2): p. 383-401.
165. Werner-Washburne, M., et al., Stationary phase in *Saccharomyces cerevisiae*. *Mol Microbiol*, 1996. **19**(6): p. 1159-66.
166. West, M., et al., Embracing the complexity of genomic data for personalized medicine. *Genome Res*, 2006. **16**(5): p. 559-66.
167. Wheeler, D.B., et al., RNAi living-cell microarrays for loss-of-function screens in *Drosophila melanogaster* cells. *Nat Methods*, 2004. **1**(2): p. 127-32.
168. Woll, D., et al., More efficient photolithographic synthesis of DNA-chips by photosensitization. *Nucleosides Nucleotides Nucleic Acids*, 2003. **22**(5-8): p. 1395-8.
169. Wollman, R. and N. Stuurman, High throughput microscopy: from raw images to discoveries. *J Cell Sci*, 2007. **120**(Pt 21): p. 3715-22.
170. Wu, J., et al., ChIP-chip comes of age for genome-wide functional analysis. *Cancer Res*, 2006. **66**(14): p. 6899-902.
171. Wu, R.Z., S.N. Bailey, and D.M. Sabatini, Cell-biological applications of transfected-cell microarrays. *Trends Cell Biol*, 2002. **12**(10): p. 485-8.
172. Wu, Y.L., et al., Dominant-negative inhibition of pheromone receptor signaling by a single point mutation in the G protein alpha subunit. *J Biol Chem*, 2004. **279**(34): p. 35287-97.
173. Xia, Y., et al., Analyzing cellular biochemistry in terms of molecular networks. *Annu Rev Biochem*, 2004. **73**: p. 1051-87.
174. Xu, C.W., High-density cell microarrays for parallel functional determinations. *Genome Res*, 2002. **12**(3): p. 482-6.
175. Zhang, J., et al., The importance of being big. *J Investig Dermatol Symp Proc*, 2005. **10**(2): p. 131-41.

176. Zhang, J., et al., Genomic scale mutant hunt identifies cell size homeostasis genes in *S. cerevisiae*. *Curr Biol*, 2002. **12**(23): p. 1992-2001.
177. Zhang, X., et al., Cdc42 interacts with the exocyst and regulates polarized secretion. *J Biol Chem*, 2001. **276**(50): p. 46745-50.
178. Zhao, T. and R.F. Murphy, Automated learning of generative models for subcellular location: Building blocks for systems biology. *Cytometry A*, 2007. **71**(12): p. 978-90.
179. Zhou, L., et al., Phenotype microarray analysis of *Escherichia coli* K-12 mutants with deletions of all two-component systems. *J Bacteriol*, 2003. **185**(16): p. 4956-72.
180. Zhu, H., M. Bilgin, and M. Snyder, Proteomics. *Annu Rev Biochem*, 2003. **72**: p. 783-812.
181. Ziauddin, J. and D.M. Sabatini, Microarrays of cells expressing defined cDNAs. *Nature*, 2001. **411**(6833): p. 107-10.

Vita

Rammohan (Ram) Narayanaswamy was born April 2, 1978 in Chennai, India, to Chellammal and Narayanaswamy. After finishing his high school from the Delhi Public School, he completed his B.S (Hons) in Biochemistry from the University of Delhi in 1998. Subsequently, he entered into the Indian Institute of Science, Bangalore, where, under the guidance of Dr. M.R.S. Rao, he completed his M.S. thesis in Biological Sciences working on chromatin remodeling factors in rat spermatogenesis. In 2001, Ram was accepted into the University of Texas at Austin's graduate program in Cell and Molecular Biology where he studied under Dr. Andrew D. Ellington and Dr. Edward M. Marcotte on developing and applying tools in systems biology research. He is a recipient of the David and Mary Miller scholarship for continuing graduate students. His publications include:

- 1) Lee, I, Narayanaswamy, R and Marcotte, EM, *Bioinformatic prediction of yeast gene function*..Methods in Microbiology, 2007(36): p. 597-628.
- 2) Narayanaswamy, R., Niu, W, Scouras, A.D, Hart, TG, Davies, J, Ellington, AD, Iyer, VR and Marcotte, EM., *Systematic profiling of cellular phenotypes with spotted cell microarrays reveals mating-pheromone response genes*. Genome Biol, 2006. 7(1): p. R6.
- 3) Narayanaswamy, R. and A.D. Ellington, *Engineering RNA-based circuits*. Handb Exp Pharmacol, 2006(173): p. 423-45.

4) Narayanaswamy, R., Niu, W, Scouras, A.D, Hart, TG, Davies, J, Ellington, AD, Iyer, VR and Marcotte, EM Cell Microarray for profiling of cellular phenotypes and gene function (UTAU 1073; Patent filed).

Permanent address: 3457 Lake Austin Blvd., Apt B, Austin, TX 78703

This dissertation was typed by the author.